PRODUCTION OF MONODISPERSE, CRACK-FREE CERIUM OXIDE MICROSPHERES BY INTERNAL GELATION SOL-GEL METHODS

by

Jeffrey A. Katalenich

A dissertation submitted in partial fulfillment
of the requirements for the degree of
Doctor of Philosophy
(Nuclear Engineering and Radiological Sciences)
in the University of Michigan
2014

Doctoral Committee:

Professor Gary S. Was, Chair
Associate Professor John E. Foster
Professor John W. Halloran
Director Steven D. Howe, Center for Space Nuclear Research

© Jeffrey A. Katalenich
All Rights Reserved 2014

DEDICATION

To the good people of Roscommon, Michigan and others who helped me along my way.

ACKNOWLEDGEMENTS

This thesis work was made possible through the help and backing of many individuals and several funding agencies.

I would like to begin by thanking my mother, father, brother, and wife for their unfailing love, support, and guidance in my life. Mom, Dad, and Scott - I couldn't have done this without you. And without a doubt, I would not have finished this thesis without the patience, understanding, and encouragement of my wife, Kimberly. I also owe a debt of gratitude to my friends Gregg Neville, Ben Barber, Paul Wojey, Pete Radecki, and Jim Beinke, each of whom had a tremendous impact on my life and development as an individual.

I would like to thank my current adviser, Dr. Gary Was, for his help as I finished my research and thesis as well as my former adviser, Dr. Michael Hartman, who helped me to pursue an experimental project tailored to my interests. I am also grateful for the revisions and advice I received from my committee members Dr. John Halloran, Dr. John Foster, and Dr. Steven Howe. I would like to thank Dr. Howe and everyone at the Center for Space Nuclear Research for introducing me to space nuclear power and the research field in general. During my graduate studies, I was very thankful for the skills and experience I gained from Dr. Brad King during my undergraduate work at Michigan Tech.

My graduate work was supported by many individuals who deserve recognition. First, I would like to thank Brian Kitchen, Bruce Pierson, and Shyam Dwaraknath for their many useful conversations, ideas, and support throughout my research. Several other fellow University of

Michigan researchers and staff were helpful in the production and characterization of my microspheres, including Harald Eberhart, James Windak, Ted Huston, Pilar Herrera-Fierro, Eongyu Yi, and Xu Wang. I would also like to thank Dr. Ronald Gilgenbach, Dr. Ron Fleming, Dr. Sara Pozzi, Dr. Marek Flaska, Peggy Jo Gramer, and Ed Birdsall for the many ways they helped me while I was a student and for their dedication to the department.

This research was made with government support under and awarded by DoD, Air Force Office of Scientific Research, National Defense Science and Engineering Graduate (NDSEG) Fellowship, 32 CFR 168a.

This material is based upon work supported by the National Science Foundation Graduate Research Fellowship under Grant No. DGE 1256260. Any opinion, findings, and conclusions or recommendations expressed in this material is that of the author and does not necessarily reflect the views of the National Science Foundation.

This material is based upon work supported by the Center for Space Nuclear Research (CSNR) under the Universities Space Research Association (USRA) Subcontract 06711-003. The USRA operates the CSNR for the Idaho National Laboratory.

This research was supported by a research seed grant received from the Michigan Space Grant Consortium with matching funds from the University of Michigan Department of Nuclear Engineering and Radiological Sciences.

TABLE OF CONTENTS

LIST OF FIGURES

LIST OF TABLES

LIST OF APPENDICES

LIST OF ACRONYMS

ADU	Ammonium Diuranate
BET	Brunauer-Emmett-Teller
BJH	Barrett-Joyner-Halenda
CAN	Ceric Ammonium Nitrate
CBCF	Carbon-Bonded Carbon Fiber
CHN	Carbon, Hydrogen, Nitrogen
DIPRES	Direct Press
DOE	Department of Energy
EI-MS	Electron Impact Mass Spectroscopy
GDMS	Glow Discharge Mass Spectroscopy
GIS	Graphite Impact Shell
GPHS	General Purpose Heat Source
HMTA	Hexamethylenetetramine
ICP-MS	Inductively Coupled Plasma Mass Spectroscopy
INL	Idaho National Laboratory
IPA	Isopropyl Alcohol
IR	Infrared
LANL	Los Alamos National Laboratory
MOX	Mixed Oxide

NASA	National Aeronautics and Space Administration
Np-237	Neptunium-237
ORNL	Oak Ridge National Laboratory
Pu-238	Plutonium-238
Pu-239	Plutonium-239
PuFF	Plutonium Fuel Form Fabrication Facility
PWT	Pressurized Water Treatment
RHU	Radioisotope Heater Unit
RTG	Radioisotope Thermoelectric Generator
SOFC	Solid Oxide Fuel Cells
SRL	Savannah River Laboratory
TA-55	Technical Area 55
TCE	Trichloroethylene
TEM	Transmission Electron Microscopy
TGA	Thermal Gravimetric Analysis
XRD	X-Ray Diffraction

ABSTRACT

Traditional powder processes for fabricating plutonium-238 oxide heat source pellets used in radioisotope thermoelectric generators contaminate facilities and pose a health hazard to workers. These problems have motivated steps to validate an alternative, dust-free technique to produce equivalent pellets. Established internal gelation sol-gel methods for fabricating uranium oxide microspheres have been modified to produce monodisperse spheres of cerium dioxide with diameters less than 200 μm. A two-fluid nozzle designed to accommodate short needles in a chill-able configuration has resulted in the production of sintered cerium dioxide microspheres with an average diameter of 100.28 μm ± 2.8 μm. Final sphere diameter was controlled within the range 65 – 210 μm by adjustments to feed solution and stripping oil feed rates. Sol-gel equipment designed and constructed for this study is capable of producing enough gelling product in one day to yield 10 g of sintered cerium dioxide microspheres. Improvements were made to sphere washing techniques to prevent microsphere cracking upon drying and also reduce impurity levels. Thermogravimetric analysis indicated that spheres washed by the improved method have 4.5 times less volatile mass loss upon heating than spheres washed by a traditional process. Impurity analysis on sintered microspheres has shown carbon impurities below 30 ppm and trace element levels below specified limits for Pu-238 oxide fuels. Experimental results with a lab-scale apparatus demonstrated that 10s of grams of monodisperse cerium oxide microspheres can be produced by internal gelation methods with low impurity levels. These

findings provide motivation for additional research to demonstrate dust-free production of plutonium oxide microspheres.

Chapter 1

Introduction

"Radioisotope power systems, the day of reckoning has arrived."

- Leonard Dudzinski, Program Executive for Radioisotope Power Systems, NASA Headquarters

Space nuclear power sources based on the conversion of decay heat from plutonium-238 (Pu-238) to electricity have been used by the United States since 1961 [1]. Based on the reliability of these systems, hundreds of kilograms of Pu-238 were produced in defense reactors at the Savannah River Site until they were shut down in the late 1980s [1–4]. Plutonium-238 produced by those initiatives was used to power military satellites and National Aeronautics and Space Administration (NASA) space exploration vehicles. However, the current national inventory of Pu-238 is diminishing and missions requiring radioisotope power sources depend upon a reliable supply being re-established [2]. Additionally, the production of dimensionally stable Pu-238 oxide fuel pellets is difficult and requires ball milling of plutonium precipitates into a submicron powder, which has caused the contamination of facilities and poses an inhalation hazard to workers [5–7]. This thesis investigates the use of internal gelation sol-gel

methods to prevent plutonium oxide dust generation using an aqueous route to produce 100 µm oxide microspheres that can be subsequently pressed into pellets.

1.1 Plutonium-238

Plutonium-238 is a heat-emitting radioisotope that decays by alpha emission with a half-life of 87.7 years. Gram quantities are used in radioisotope heater units to keep critical spacecraft components warm. For power sources, kilogram quantities of Pu-238 oxide are used with thermoelectric converters to produce electricity in hostile environments. Oxide powders of Pu-238 are used due to their stability at elevated operating temperatures exceeding 1000 °C. However, submicron oxide powders generated during heat source processing are highly mobile and corrosive due to their small size and internal source of heat and oxygen.

Plutonium-238 has a combination of properties that make it a suitable power source for applications where other options cannot be used. There are hundreds of heat-emitting radioisotopes, but constraints related to half-life, physical properties, and dose rate leave only a few potentially suitable isotopes [8]. Radioisotopes including strontium-90, americium-241, and curium-244 have been considered for space power sources [1], but each of these isotopes has a characteristic that makes its use undesirable. Although it has been used for terrestrial power sources [9], strontium-90 is undesirable for space missions due to the necessary shielding mass [1]. Similarly, while curium-244 has a high specific power of 2.78 W/g, its high rate of spontaneous fission requires a significant shielding mass. While americium-241 has a long half-life of 432.7 years and emits an easily-shielded 59.5 keV gamma ray, its low specific power of 0.11 W/g makes the mass required for power sources undesirable. The combination of Pu-238's high specific power of 0.556 W/g, long half-life, stable oxide, low dose rate, and successful mission heritage make it the best option. Looking to non-nuclear alternatives, the benefit of

radioisotopes becomes clear upon comparing specific energy. Existing batteries can store on the order of 1 MJ/kg while the plutonium-238 oxide used by NASA has a specific energy exceeding 1,500,000 MJ/kg. While solar power is useful for satellites orbiting Earth and can be used to power missions as far away as Mars or Jupiter, space vehicles traveling beyond Jupiter or into high radiation fields require nuclear power sources [1]. Although compact nuclear reactors could be used for space nuclear power applications, their specific power is typically much higher than that of radioisotope thermoelectric generators in the power range typically used for space exploration vehicles [10]. Further, the United States has only launched one space nuclear reactor and does not have an established flight heritage for these systems. Therefore, radioisotope power systems provide a unique capability, but improved methods are needed to produce and process kilogram quantities of plutonium-238 oxide into power sources while mitigating risks to workers and facilities.

Based on past Pu-238 power source production, a significant problem is the generation of fine oxide powders that pose a contamination and inhalation hazard. Existing power source designs are based on the use of iridium-clad plutonium oxide pellets that are prepared beginning with precipitated powder feeds. Existing processes precipitate Pu-238 oxalate from plutonium nitrate using oxalic acid to form rosette and lathe-shaped particles that are calcined to the oxide form [11–17]. Attempts to use as-precipitated powders to press pellets resulted in failure due to excessive shrinkage, necessitating the use of a ball-milling step to normalize the powder morphology [18,19]. These ball-milled powders have average particle sizes below 1 μm, resulting in highly mobile particulates due to static electricity, air currents, and recoil motion due to alpha decay [3,20,21]. Operational experience has shown that fine Pu-238 oxide powders are dispersive, corrosive, and prone to penetrating containment barriers, causing the release of alpha-

emitting particles that pose an inhalation hazard [3,5–7,20–22]. Therefore, a method that eliminates powder generation and handling would be preferable.

At the request of the Department of Energy (DOE), a committee of consultants and scientists from the Idaho, Oak Ridge, Los Alamos, and Savannah River National Laboratories met for a week in Idaho Falls, ID in the spring of 2008 to compare historical processes for fabricating Pu-238 oxide pellets with alternative manufacturing methods to see if advances in technology could mitigate hazards, particularly the generation of respirable fines [19]. While the report recognized that sol-gel methods could produce spherical particles with minimal dust generation, concerns regarding chemical purity, microsphere cracking, and unintentional sintering of spheres during calcination predominated. Based on the potential merits of sol-gel options, this thesis explores the use of internal gelation sol-gel methods with careful attention to particle sizing, chemical purity, microsphere cracking, and sintering concerns expressed in the DOE report.

1.2 Sol-Gel Fabrication of Microspheres

The benefits of sol-gel processes for fabricating nuclear fuels have motivated its development since the 1960s. The title sol-gel broadly refers to solution/sol-based routes to produce ceramic nuclear fuels. Prevalent methods include preparing de-nitrated colloidal solutions (sols) that are dehydrated in a hot organic, external gelation of nitrate solutions with organic polymers in the presence of ammonia, and internal gelation techniques relying on hydrolysis for polymerization into a gel. In each of these methods, aqueous solutions containing the desired element, or mixture of elements, are dispersed through an orifice into a forming fluid that results in solidification of spherical particles. These microspheres can be dried and thermally treated into a pure oxide form suitable for coated-particle fuels, vibro-packed fuels, or

pressing into pure oxide or inert matrix pellets without powder processing. Additionally, monodisperse spherical fuels are easily fluidized in a gas flow for the uniform application of surface coatings, such as cracking hydrocarbons to deposit a graphite coating.

The United States has performed a great deal of research on sol-gel fabrication of microspheres for nuclear fuels. Significant programs at ORNL in the 60s focused on producing thorium, uranium, and plutonium microspheres through the dehydration of denitrated sols [23–32]. These studies supported fuel development for the high temperature gas cooled reactor and sphere-pac fuels for fast reactors [33]. Also, Pu-238 oxide microspheres were used to power six SNAP-27 radioisotope thermoelectric generators for the Apollo program [34–37]. More recent work has focused on the development of pyrolytic graphite and SiC coated uranium oxide fuel kernels produced by internal gelation, sol-gel methods known as TRISO, or tri-structural isotropic, particles. TRISO fuels have been developed to support the high temperature gas cooled reactor program and have resulted in demonstration and scale up to produce kilogram quantities of 350 μm, 425 μm, and 500 μm diameter uranium microspheres using the internal gelation process [38–40,40–43].

Internal gelation techniques are unique from other sol-gel methods in that gelation is more homogeneous and not subject to gradients resulting from a mass-transfer process. While dehydration relies on the transfer of water out of the sphere and external gelation depends on ammonia transfer into the sphere, internal gelation occurs throughout the material once it reaches a temperature sufficient to begin the reaction. Aqueous nitrate solutions containing a variety of metal elements can be converted to oxide spheres by the internal gelation process. A benefit to internal gelation is that metal oxide mixtures can be created from solutions containing the desired elements, allowing for homogenous distributions of mixed fuels, stabilizers, or burnable poisons.

The internal gelation process involves the use of hexamethylenetetramine (HMTA) to promote gelation and urea as a complexing agent. As shown in Figure 1.1, a nitrate solution containing the metal of interest is chilled separately from a concentrated solution containing HMTA and urea. Once both solutions are chilled, they are mixed and urea complexes the metal ion, preventing hydrolysis. Chilled feed solutions are dispensed from a needle into a column of hot oil. As the droplets heat in the column, urea decomplexes the metal ion, allowing for a hydrolysis reaction that is driven to completion through the protonation of HMTA. Through condensation of metal hydroxides and washing with ammonium hydroxide, hydrated metal oxides form that are converted to pure metal oxides by heat treatments.

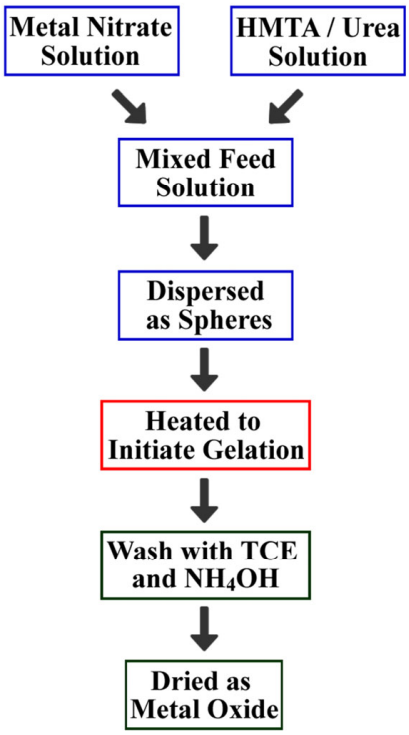

Figure 1.1: Internal gelation sol-gel processes use chilled solutions containing HMTA, urea, and a metal nitrate to provide for the temperature dependent gelation of hydrous metal oxide spheres. Gelled microspheres are washed to remove impurities and dried as a metal oxide.

Characteristics that make the internal gelation process attractive for next-generation nuclear reactor fuels are especially important for fabricating Pu-238 oxide power sources. With a half-life approximately 275 times shorter than Pu-239, the alpha decay from Pu-238 is especially hazardous if inhaled. The capability to keep Pu-238 in solution until macroscopic microspheres are created mitigates this respiratory hazard. Furthermore, the integration of internal gelation equipment into Pu-238 production and separation would preclude dissolution and precipitation steps that result in material losses and waste generation. The reduction in the number of processing steps and ease in automating also stand to simplify material processing. To realize these benefits, demonstration and scale up with Pu-238 will be necessary. However, Pu-238 is rare and very difficult to handle, so efforts for validation would benefit from preliminary work using cerium first as a non-radioactive surrogate to elucidate answers to unknown factors before proceeding.

1.3 Validation of Internal Gelation Using Cerium Dioxide

The generation and handling of Pu-238 oxide fines is a problem that must be addressed as Pu-238 production resumes in the United States. To improve safety and reduce future decontamination and decommissioning liabilities, the ball-milling step that creates these fine particles must be eliminated. This is problematic, however, because traditional precipitation techniques for Pu-238 processing do not yield particulates that can be used for pellet pressing without first being ball-milled to sub-micron sizes and formed into 44-125 μm granules. Based on the virtues of internal gelation, sol-gel methods, this thesis aims to produce sol-gel microsphere "granules" that are optimized for Pu-238 pellet fabrication while preventing dust.

Although it is believed that internal gelation, sol-gel methods can produce microspheres suitable for pressing pellets without dust generation, there are several uncertainties. First,

microspheres of Pu-238 oxide have not been made by internal gelation, nor have Pu-239 oxide microspheres. Therefore, the chemical behavior of plutonium in the internal gelation process can only be hypothesized. Second, Pu-238 fuels have specific impurity limits to prevent interactions between the fuel and cladding and limit neutron production from alpha particle interactions with light elements. Since internal gelation methods involve the use of several reagents including organics, the final carbon or other elemental levels could be too high. Third, some sol-gel microspheres have exhibited a tendency to crack upon drying in the past, introducing fine particles. Also, most previous sol-gel processes were designed to yield dense microspheres that may not have enough residual sinterability for consolidation into a homogeneous pellet. The capability to produce uniform microspheres in the desired granule size around 100 μm is also uncertain since techniques for producing spheres in this size range typically resulted in wide diameter distributions which required sieving.

Considering the potential for internal gelation methods to eliminate hazardous fine Pu-238 particles and simplify the pellet production flowsheet, this thesis addresses the uncertainties above using cerium as a non-radioactive surrogate. As will be discussed in the background section, the chemistry and material properties of cerium are analogous to plutonium in many respects and cerium is the most commonly used surrogate for plutonium. The use of cerium is expected to provide an improved basis for predicting plutonium behavior in sol-gel and ease development of equipment and methods. A validation and testing program for Pu-239 and Pu-238 sol-gel spheres would be necessary before internal gelation methods could supplant ball-milling. This thesis is aimed at determining whether those studies are worthwhile, and if so, provide a basis for development.

To establish whether internal gelation sol-gel methods can yield desirable surrogate microspheres for pellet pressing, several demonstrations and measurements were required. First, a variety of feed solution parameters were tested to find combinations that resulted in strong gels that survived washing. Second, a device was built to demonstrate that spheres with the desired size near 100 μm could be fabricated reliably. Once this was accomplished, the apparatus was scaled-up to yield multi-gram quantities for analyses such as size and monodispersity; propensity for cracking; density measurements; carbon, nitrogen, and hydrogen levels; trace element levels; and temperature-dependent mass loss. Based on these results, washing methods were modified and investigated to optimize impurity removal and eliminate cracking. Density and propensity for agglomeration was were also observed as a function of heat-treatment temperature to allow for optimization between impurity removal and residual sinterability.

Although there is a substantial literature base for the production of uranium oxide microspheres by internal gelation, very little information has been published where cerium oxide is the material of interest. Preliminary thesis work thus consisted of assessing cerium nitrate solutions and aqueous feed preparation. A systematic approach was taken to vary parameters and identify which combination of values resulted in the formation of acceptable solid gels as opposed to viscous precipitates. Multiple tradeoffs between parameters were identified and taken into consideration in the next phase of work, which was the design and construction of an apparatus to fabricate multi-gram quantities of uniform microspheres.

Two years of design, construction, and refinement resulted in an apparatus, referred to as a "sol-gel rig," which converts appropriate chilled aqueous feeds into gelled microspheres. Herein was an effort to produce monodisperse microspheres with sintered diameters near 100 μm. Equipment was iterated to provide adequate cooling, heating, bubble removal, and material

throughput. Once this was accomplished, the system's capability to produce monodisperse microspheres with sintered diameters in the range 50-250 μm was quantified and batch sizes of up to 10 g of spheres were produced for material and chemical analyses.

Factors governing microspheres' chemical purity, propensity for cracking, and undesirable bonding during heat treatments appeared to depend on the effectiveness of washing techniques employed on gelled spheres prior to drying. A variety of washing procedures were performed and compared, including traditional washing methods for uranium oxide microspheres. The apparent value of a pressurized water treatment (PWT) was also investigated. Observed bulk properties of spheres together with mass spectroscopy and impurity analyses indicated that simple modifications to baseline washing techniques resulted in microspheres with low impurity levels, minimal cracking, and minimal microsphere bonding during heat treatments.

1.4 Importance of Findings

The recommendations made by the 2008 committee on alternative Pu-238 pellet fabrication bear reconsideration given the current findings on internal gelation processes. Recent progress to re-establish Pu-238 production has limited its focus to historic methods based on the assumption that newer technologies are too uncertain. Since Pu-238 production and separation campaigns have not been performed in over 25 years, the current workforce lacks operational experience and faces the task of rebuilding capabilities based on incomplete documentation. While these hurdles can certainly be overcome, the concern remains whether historic methods for Pu-238 can be performed economically considering waste generation and contamination issues that will have to be handled differently in today's regulatory structure than it was in the 60s-80s. In a time of budget constraints, poor economics could be a bigger impediment to Pu-238 production than technical issues. For these reasons, the development and adoption of an

improved, alternative process such as internal gelation appears critical. Automated sol-gel processes stand to reduce worker dose, eliminate hazardous contamination by oxide fines, reduce and simplify waste management, diminish the likelihood of causing facility closure, and cut final decontamination and decommissioning costs. Current findings imply that these benefits are realizable.

Research efforts have shown that easily manageable modifications to existing internal gelation processes can produce the desired fuel characteristics using cerium dioxide surrogates. The lab-scale equipment constructed in this study is already within a factor of two of the anticipated desired throughput. Further, a unique capability for the degree of monodispersity in the size range of interest has been achieved. Since quality fuels depend on more than just quantity and size, in-depth analyses were performed to investigate washing methods that prevent microsphere cracking, reduce final impurities, and improve heat treatment performance. These developments, while completed with a surrogate material, provide a solid basis upon which to perform further validation studies.

Chapter 2

Background

"Personnel involved in the processing of Pu-238 have observed many unusual characteristics of the oxide. In many cases the oxide contamination appears to exhibit lifelike characteristics as it 'flies' through the air or 'walks' along pipes. In some cases, the fine particles appear to behave more like a gas than a solid."

- Dr. James W. Congdon, Senior Fellow Scientist, Westinghouse Savannah River Co.

Scientists and engineers have processed Pu-238 in the United States since work began to develop operationally deployed radioisotope thermoelectric generators around 1960 [44–48]. A variety of fuel forms were employed, including initial work with plutonium metal [47,49], Pu-238 oxide in a molybdenum cermet [49–53], plasma-torched Pu-238 oxide microspheres [37,54,55], and pure Pu-238 oxide pellets in a spherical geometry [49,53,56,57]. Since the development of the general purpose heat source beginning in the late 1970s, fuel for radioisotopic thermoelectric generators (RTGs) has been cylindrical pellets of Pu-238 oxide with a height and diameter of 2.76 cm [18,58–63]. The use of oxide fuels has dominated, largely due to its high melting point which allows for a higher operating temperature and more efficient energy conversion. However, due to a high rate of alpha decay, Pu-238 oxide powders have

unique properties that complicate handling. This chapter will provide an overview of current Pu-238 systems and processes with an emphasis on current powder processes and hazards. Solution chemistry relevant to precipitation will be presented for plutonium, uranium, and cerium. Also, accomplishments in sol-gel processing and the chemistry of internal gelation methods will be reviewed in detail.

2.1 Pu-238 Fuels

Heat produced by alpha decay can be harvested over years or decades to keep critical components warm or generate electricity in hostile environments due to the 87.7 year half-life of Pu-238. For over 50 years, radioisotope thermoelectric generators (RTGs) and radioisotopic heater units (RHUs) have been used in space to provide power and heat for missions such as Voyager, Cassini, New Horizons, and the Mars Curiosity rover [64]. Pu-238 fuels used in these applications are oxides due to their high temperature thermal stability, even with centerline temperatures around 1350-1450 °C [65–67]. In the oxide form, typical fuels have a specific power of about 0.4 W_t/g, necessitating the use of kilogram quantities for RTG applications. Since Pu-238 fuel used by NASA has a specific activity of about 12 Ci/g and a single Multi-Mission RTG has 4.8 kg of fuel, significant precautions are taken in fuel packaging to preclude release in the event of launch failure or atmospheric re-entry.

Pu-238 oxide pellets are clad in a welded iridium-alloy shell and loaded into a series of carbon-based layers called the "general purpose heat source." A general purpose heat source (GPHS) contains four Pu-238 pellets, each of which weighs about 150 g [58,63]. As shown in Figure 2.1, clad pellets are encased in a graphite impact shell (GIS), a carbon-bonded carbon fiber (CBCF) sleeve, and sealed in an aeroshell structure with a screw cap. The iridium alloy containing 0.3 weight percent tungsten and 60 parts per million (ppm) thorium was chosen as

cladding due to its high-temperature ductility, high melting point, and corrosion resistance [66,68]. Thorium in the alloy acts to prevent intergranular fracture and also prevent grain growth at its elevated operating temperature of 1200-1400 °C [68]. The multi-layer configuration and aeroshell are designed to induce desirable re-entry conditions, keep the iridium cladding below a critical temperature during re-entry, and preclude cladding rupture in the event of a high-velocity impact [60,62]. The GPHS configuration was designed and tested to withstand explosion, high temperatures, shrapnel penetration, and high-velocity impact without plutonium release [59].

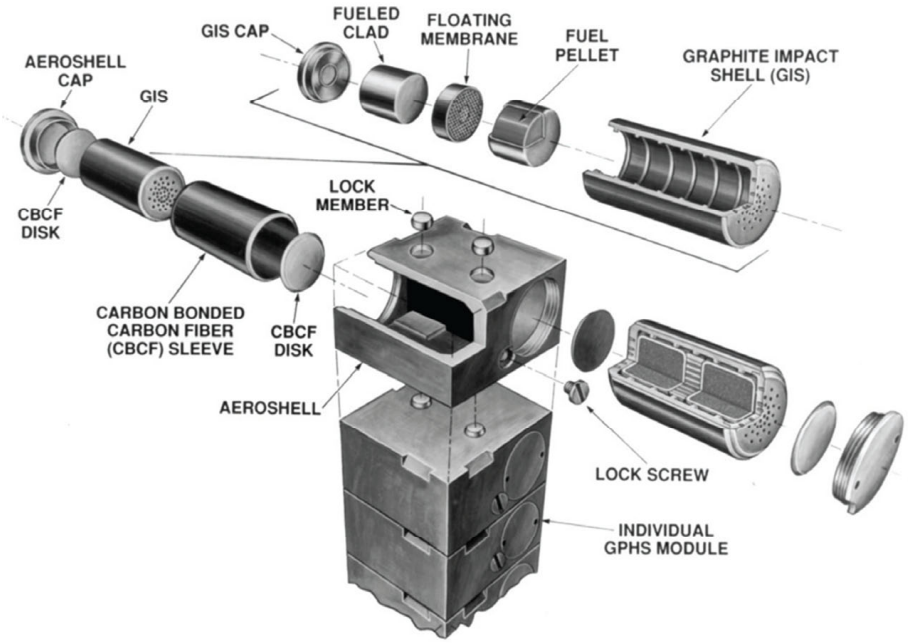

Figure 2.1: Plutonium-238 oxide pellets are encapsulated in a graphite general-purpose heat source (GPHS). Image by U.S. DOE taken from NASA MMRTG facts bulletin [69].

Pellets and their claddings must also vent helium gas to prevent pressure buildup from alpha decay. To prevent helium-induced swelling, plutonium-238 oxide fuel pellets are fabricated with 80-90% of theoretical density using granules with reduced residual sinterability [18,65,67,70]. A cladding vent is also necessary for helium release. A 450 μm hole is covered by a frit vent assembly which is electron beam welded in place at one end of the clad. The vent

assembly consists of two diffusion bonded discs sandwiching a porous, sintered iridium powder matrix which allows for helium escape but prevents the release of plutonium particulates [71]. This porous frit can become plugged due to volatile emissions from Pu-238 oxide fuels, largely due to the presence of impurities such as calcium, silicon, and aluminum [66]. Fuel impurities, such as phosphorous, iron, chromium, and nickel, are also thought to have deleterious effects on the iridium capsule or enhance plutonium migration to the frit [66]. Therefore, granules used for pellet fabrication must have low impurity levels and yield pellets that maintain their open porosity over time at elevated operating temperatures. Without ball-milling as a normalizing step, the properties of the precipitates and their impact on the pellet pressing become important.

2.2 Solution Chemistry and Powder Precipitation

Oxide powders of cerium, uranium, and plutonium are typically prepared by precipitation of insoluble species from aqueous solutions of metal salts followed by thermal treatment. While plutonium is of particular interest, practices for cerium and uranium will also be presented due to their historical use as surrogates and in the internal gelation process, respectively. Traditional oxide powder production methods will be presented to provide insight for later discussion of existing methods used for Pu-238 and internal gelation methods using cerium and uranium. Precipitation and oxide conversion details are summarized for plutonium, uranium, and cerium in Table 2.1.

Table 2.1: Summary of relevant plutonium, uranium, and cerium oxide production methods by powder precipitation

	Oxidation States in Solution	Precipitation Method from Nitrate Solutions	Precipitated Species	Oxide Conversion Temperature [°C]
Plutonium	+3 +4 +5 +6 +7	Pu(IV) Hydroxide	$Pu(OH)_4 \bullet xH_2O$	>100 [72]
		Pu(III) Oxalate	$Pu_2(C_2O_4)_3 \bullet 10H_2O$	>300 [72]
Uranium	+3 +4 +5 +6	U(VI) Hydroxide	$UO_3 \bullet xNH_3 \bullet (2\text{-}x)H_2O$	>450°C yields UO_3 >530°C yields U_3O_8 [73]
Cerium	+3 +4	Ce(III/VI) Hydroxide	$Ce(OH)_3^{\alpha}$ or $Ce(OH)_4^{\beta}$	>800$^{\gamma}$ [74,75]
		Ce(III) Carbonate	$Ce(OH)CO_3 \bullet xH_2O$	>300 [76,77]
		Ce(III) Oxalate	$Ce_2(C_2O_4)_3 \bullet xH_2O$	>300 [78]

α: $Ce(OH)_3$ can convert to $Ce(OH)_4$ in solution or upon drying in air at room temperature

β: $Ce(OH)_4$ can also be written as $CeO_2 \bullet 2H_2O$

γ: $CeO_2 \bullet 2H_2O$ dehydration occurs in stages and is complete above 800°C

2.2.1 Plutonium Chemistry and Precipitation

Plutonium chemistry is among the most complex on the periodic table. Due to the radial extent of its 5f electrons, plutonium has five oxidation states in solution, and since their oxidation potentials are all near 1V, plutonium in solution can be in four oxidation states simultaneously due to dis-proportionation and re-proportionation redox reactions in which two ions are simultaneously oxidized and reduced [79,80]. In aqueous solutions, Pu(III) exists as Pu^{3+}, Pu(IV) as Pu^{4+}, Pu(V) as PuO_2^{+}, and Pu(VI) as PuO_2^{2+}. Many complex ions are formed, with the tendency to form complexes decreasing in the order $Pu^{4+} > Pu^{3+} \approx PuO_2^{2+} > PuO_2^{+}$ [72,80,81]. Furthermore, radioactive decay of plutonium in solution results in the radiolysis of water to produce •H, •OH, •O redox agents and recombination products H_2, O_2, and H_2O_2, generally causing reduction of Pu(VI) and Pu(V) to Pu(III) and Pu(IV) over time [79,81]. In nitrate solutions, radiolysis also generates nitrogen oxides and oxygen. The presence of multiple, simultaneous species necessitates additional efforts to obtain the desired oxidation states prior to initiating chemical reactions such as precipitation. Due to unique absorption spectra of

plutonium in each oxidation state, absorption spectroscopy has been a useful tool in characterizing oxidation states of solutions and generating procedures for manipulating plutonium solutions. The use of reducing agents such as ascorbic acid, sulfamic acid, ferrous sulfamate, or hydrazine allows for reduction to Pu(IV) or Pu(III) and limits further oxidation by HNO_2 present as a result of radiolysis [80]. Precipitation reactions are typically initiated after reduction to Pu(III) or Pu(IV).

Plutonium is generally precipitated from acidic feed solutions of plutonium nitrate. Both nitric acid and hydrochloric acid solutions allow for high concentrations of plutonium, but precipitation from hydrochloric acid solutions is unattractive due to the introduction of the corrosive chlorine impurity in the product. Attractive methods for precipitating plutonium include the addition of oxalate, hydroxide, peroxide, and fluoride since good recoveries of plutonium can be obtained [80,82]. Of these methods, only oxalate and hydroxide precipitation have been used to produce Pu-238 fuels for flight applications. Pu(III) and Pu(IV) oxalates can be calcined above 300 °C, typically 500- 800 °C, for conversion into an oxide while hydroxide precipitates convert to plutonium oxide upon drying [19,82].

Precipitation of plutonium hydroxide from nitrate solutions can be achieved using a variety of bases such as ammonium hydroxide, sodium hydroxide, or potassium hydroxide. Precipitation occurs either in a "direct strike" method where hydroxide is added to the plutonium nitrate, or by "reverse strike" where plutonium nitrate is added to the hydroxide. For fuel applications, ammonium hydroxide is preferred to avoid the introduction of trace metal impurities. A major benefit of the hydroxide precipitation process is the extremely low solubility of Pu(IV) hydroxide in nitrate solution, which allows for excellent extraction of plutonium and low levels in the waste supernatant [72]. However, hydroxide precipitation does not function

well as a purification step since it is fairly non-selective and will produce hydroxides of other cationic species [19,72,80]. Additionally, plutonium hydroxide precipitates tend to be gelatinous, making it difficult to filter and process until dried. Until the mid 1970s, Mound Laboratory prepared Pu-238 powders by reverse strike hydroxide precipitation followed by vacuum drying, air-drying for oxide conversion, and crushing to form shards that could be sieved and thermally seasoned to ~89% theoretical density prior to pellet pressing [19,83]. A study of fine particles generation indicated that between 0.1-0.5% of sintered shards had effective diameters less than 5 μm prior to fuel aging [84]. A change from hydroxide precipitation to oxalate precipitation appears to have occurred when work was transferred from Mound to Savannah River since the latter already had an oxalate precipitation capability established [83,85].

Precipitation of plutonium oxalate from nitrate solutions is performed by either direct strike or reverse strike using oxalic acid, $H_2C_2O_4$. While both Pu(III) and Pu(IV) will form oxalates, Pu(III) oxalate ($Pu_2(C_2O_4)_3 \cdot 10H_2O$) is preferred since it precipitates as easily filterable crystals compared to Pu(IV) oxalate which is tacky at room temperature [80]. Oxalate precipitation also provides separation from soluble Al(III), Fe(III), and U(VI) impurities [80]. After precipitation, plutonium oxalate must be heated to evolve the waters of hydration and decompose the oxalate into an oxide. While efforts to produce Pu-238 agglomerates with sizes mostly above 10 μm by direct strike oxalate precipitation have been accomplished with varying degrees of success [11,83,85–88], all Pu-238 oxide pellets fabricated for use in general purpose heat source units were produced using reverse strike oxalate precipitation. Depending on solution concentrations and reaction temperature, particle size and morphology vary, but Pu-238 particles generated by reverse strike are typically in the range 0.7 – 55 μm [11,19]. Operational

experience pressing fuel pellets indicated that variations in the precipitate size and dimensions had significant impact on the density and microstructure of sintered fuel pellets [11,67,70], which could be overcome by ball milling the powder as a normalizing step.

2.2.2 Uranium Chemistry and Precipitation

Uranium metal is highly reactive and forms a variety of compounds with other elements, but for the present study the characteristics of uranium relevant for processing into UO_2 fuel are most important. The most common ore of uranium, pitchblende, is primarily UO_2 with some UO_3. While uranium has valence states of U(III), U(IV), U(V), and U(VI), the +4 and +6 oxidation states predominate [89]. Since U(IV) is insoluble, uranium ores must be oxidized to yield soluble U(VI) prior to dissolution [90]. Typically, sulfuric acid leaching is used to obtain aqueous uranyl sulfate, $UO_2(SO_4)_3^{4-}$. After purification of the uranium, typically by ion or solvent exchange, uranium is precipitated as yellowcake by addition of ammonium hydroxide, sodium hydroxide, or hydrogen peroxide [89]. Precipitation by H_2O_2 results in $UO_4 \bullet xH_2O$ solids that must be heated to approximately 600 °C for removal of the waters of hydration and calcination to U_3O_8 [91]. While addition of H_2O_2 yields an easy-to-handle crystalline precipitate and is more cation specific, which provides a purification step, precipitation by addition of ammonium hydroxide is most common [89,91].

Although ammonium diuranate (ADU) produced by precipitation with ammonium hydroxide is generally denoted as $(NH_4)_2U_2O_7$, it is actually a complex mixture of compounds in the $UO_3 \bullet NH_3 \bullet H_2O$ system. Examination of crystal structures of precipitates has indicated the presence of species of the form $UO_3 \bullet xNH_3 \bullet (2\text{-}x)H_2O$ where values of 0, 0.25, 0.33, 0.5, 0.66 have been observed for x [92–94]. As ammonium hydroxide concentration increases in

precipitation solutions, x values also increase. Upon exposed to water or open atmosphere, x decreases to 1/3 under ambient conditions, as shown in the equation [92]:

$$3UO_3 \bullet 2NH_3 \bullet 4H_2O \rightarrow 2UO_3 \bullet NH_3 \bullet 3H_2O \rightarrow 3UO_3 \bullet NH_3 \bullet 5H_2O\,, \qquad (1.1)$$

as ammonia is exchanged for water in the crystal. Additionally, amorphous UO_3 in the precipitate tends to convert to $UO_3 \bullet 2H_2O$ upon exposure to water [92]. As will be discussed in section 2.6, the details of these reactions become important when considering the effects on crystallite size and material properties upon heating.

Solvent extraction techniques for the separation and purification of uranium, such as in the plutonium uranium redox extraction (PUREX) and uranium extraction (UREX) flowsheets, use aqueous solutions of uranyl nitrate. Whether for spent fuel processing or advanced fuel fabrication, dissolution of UO_2 or U_3O_8 feedstock in nitric acid to produce uranyl nitrate is common. Dissolution in nitric acid can be accelerated by the addition of heat up to the melting point of uranyl nitrate at 60 °C. In aqueous solutions, U(VI) in the form of the linear uranyl ion UO_2^{2+} is the most stable entity and is produced during dissolution due to the oxidizing nature of nitric acid. The uranyl ion $(O=U=O)^{2+}$ has a linear structure and multiple bonds with oxygen atoms at either end. This structure allows many complexation reactions to occur by addition of ligands along the equatorial plane, often in the pentagonal bipyramidal configuration show in Figure 2.2 below. The formation of uranyl complexes with a variety of ligands is utilized in extraction techniques. Uranium is also a strong electron acceptor, particularly as U(IV) and U(VI). As a strong Lewis acid, coordinated uranium causes electron redistribution in its ligands, which can have significant effects on their dissociation constants and reactivity for organic species [89].

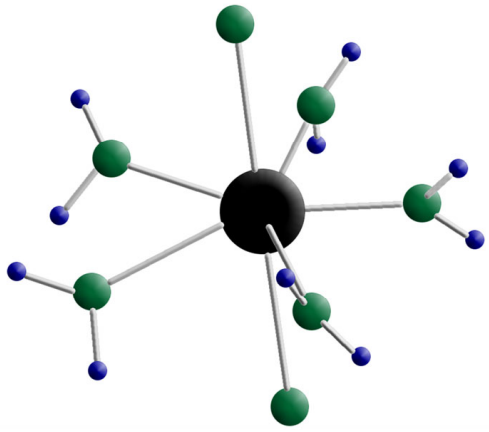

Figure 2.2: Ball-and-stick model of $UO_2(H_2O)_5^{2+}$ in the pentagonal bipyramidal configuration. Ligands generally bond with the linear uranyl ion about its equatorial plane [89].

2.2.3 Cerium Chemistry and Precipitation

Cerium is a non-radioactive, relatively non-toxic element that is used in a variety of common applications from the striker in cigarette lighters to precision polishing and carbon monoxide oxidation in catalytic converters. Cerium is most often used in the form of its oxides, Ce_2O_3 and CeO_2, in catalytic converters and is being investigated for use in solid oxide fuel cells. Automotive three-way catalysts designed to reduce NO_x to N_2 and O_2, oxidize CO to CO_2, and oxidize hydrocarbons to CO_2 and water rely on cerium as an alternating oxygen sink and source [95]. Cerium oxide is particularly suited for oxygen exchange in these converters due to its numerous intermediate O/Ce ratios between Ce_2O_3 and CeO_2 [96]. Fluorite structure ceria is also of interest in solid-oxide fuel cells since it can be heavily doped with rare earth elements for high oxygen ionic conductivity, which reduces the necessary operating temperature [97].

Unlike uranium and plutonium, cerium has only two significant oxidation states in solution and solids: Ce(III) and Ce(IV). This fact is exploited during cerium recovery from bastnasite, whereby ores are calcined to convert cerium to Ce(IV) prior to leaching with dilute

hydrochloric acid (HCl). Since Ce(IV) is insoluble in the dilute HCl, a sludge with more concentrated cerium is recovered for further processing and eventual oxalate precipitation [98]. Methods for cerium recovery by sulfur leaching from monazite ores also rely on the different chemical behavior of Ce(III) and Ce(IV) in solution. After group precipitation of rare earth hydroxides, cerium is oxidized to Ce(IV) while the remaining rare earths remain in the +3 state, allowing for selective precipitation [99].

Despite their different chemical behavior, both Ce(III) and Ce(IV) are stable in solution and are highly soluble in the form of Ce(III) trichloride ($CeCl_3$), Ce(III) nitrate ($Ce(NO_3)_3 \cdot 6H_2O$), and Ce(IV) ammonium nitrate ($(NH_4)_2Ce(NO_3)_6$). Ce(III) is primarily precipitated as $Ce(OH)_3$, $Ce(OH)CO_3 \cdot xH_2O$, or $Ce_2(C_2O_4)_3 \cdot xH_2O$ with the reagents ammonium hydroxide, ammonium carbonate, or oxalic acid, respectively [75,77,99]. $Ce(OH)_3$ oxidizes under ambient conditions to $Ce(OH)_4$, or $CeO_2 \cdot 2H_2O$, which subsequently dehydrates [75]. Hydroxide precipitation or thermal hydrolysis of Ce(IV) solutions leads to $CeO_2 \cdot 2H_2O$ [100].

As ceria-based technologies advance, there is a need for homogeneous, nanocrystalline powders for improved performance. While traditional direct strike and reverse strike precipitation methods result in irregular, micron-sized powders due to concentration gradients, hydrothermal treatments of metal-bearing solutions results in uniform precipitation of homogeneous nanopowders [75,101,102]. Thermal hydrolysis of ceric ammonium nitrate at 150-240 °C and hydrothermal treatment of ceric ammonium nitrate with urea both result in the production of CeO_2 after drying the precipitate [100]. Hydrothermal treatments of solutions containing cerous nitrate with urea or hexamethylenetetramine (HMTA) at temperatures from 150-200 °C result in the precipitation of $Ce(OH)CO_3 \cdot xH_2O$ [75,76,102,103,103–105]. The success of hydrothermal treatments in producing homogeneous powders is attributed to

temperature induced hydrolysis of cerium, which can be accomplished at lower temperatures by the introduction of ammonium from urea hydrolysis [75,100]. Hydrolysis of urea ($CO(NH_2)_2$) is also the source of CO_3^{2-} for carbonate production in solutions containing Ce(III). While cerium hydroxide converts under ambient conditions to hydrated CeO_2, cerous carbonates must be calcined at temperatures above 300 °C for oxide conversion [76,77].

Cerium is commonly used as a non-radioactive surrogate for plutonium due to its comparative ease of use and similar chemical and thermophysical properties. During sol-gel microsphere production using de-nitrated sols in the 1960s, cerium was also used as a surrogate for Pu-238 and found to be similar aside from radiolysis effects [35]. Cerium has also been used in place of plutonium for a variety of different studies. Evaluation of CeO_2 as a surrogate for PuO_2 in the fabrication of mixed oxide fuel pellets found samples containing ceria had similar compacting behavior, sintering properties, grain size, and density as well as comparable oxidation and phase behavior in the U-Ce/Pu-O system [106,107]. Geological repository studies investigating the use of cerium as a plutonium surrogate for immobilization in ceramics also found cerium to be an adequate substitute [108]. Additionally, experiments on mixed waste incineration, supercritical water oxidation, and electrorefining of plutonium indicated cerium to be the best surrogate material available [109–111]. In their analysis, these studies pointed to the similar electronic structure, specific heat, and thermodynamic stability of cerium and plutonium but noted differences in thermal conductivity, density, thermal expansion, and the strong oxidizing character of Ce(IV).

The solution chemistry of cerium and plutonium is comparable, but plutonium presents unique challenges with radiolysis, multiple oxidation states, and disproportionation / reproportionation redox reactions. As previously discussed, plutonium has oxidation states from

+3 to +7 while cerium exists as +3 and +4. However, most plutonium processing is performed once it has been adjusted to the +3 and +4 oxidation states. Unlike uranium which exists predominantly as the linear uranyl ion in solution, both cerium and plutonium typically exist as metal ions with similar ionic radii in their corresponding oxidation states. For these reasons, cerium precipitation processes, precipitation products, and calcination steps closely resemble those for plutonium.

Once calcined to the oxide form, cerium and plutonium also behave similarly. Both cerium and plutonium exist in dioxide and sesquioxide forms. PuO_2 and CeO_2 exhibit a cubic fluorite crystal structure and Ce_2O_3 and β-Pu_2O_3 are hexagonal hP5 structures [112]. In these oxide forms, plutonium and cerium share very similar values for Gibbs free energy and Gibbs free energy of formation over the range of conceivable operating and processing temperatures [113]. Although PuO_2 has a theoretical density of 11.46 g/cc compared to 7.13 g/cc for CeO_2, their behavior as a function of temperature and reactions with other elements are sufficiently similar to predict PuO_2 chemical and thermodynamic performance using CeO_2.

2.2.4 Related Cerium Sol-Gel and Hydrothermal Processes

Although not directly related to nuclear applications, a great deal of research has been performed on sol-gel preparation of cerium dioxide and mixed cerium / zirconium oxides for use as catalysts. CeO_2 and cerium mixed oxides are being developed for applications such as three-way catalysts for automotive exhaust [95,114], solid oxide fuel cells (SOFC) [115,116], and synthesis gas production by the water gas shift reaction [117,118] due to their thermal stability, oxygen mobility, and high oxygen storage capacity. While CeO_2/ZrO_2 solid solutions are traditionally produced by high-temperature firing or milling of mixed oxide powders [119], a variety of sol-gel methods have also been investigated. Fine particles of ceria–zirconia desirable

for use as catalysts have been produced from solutions using urea to catalyze hydrolysis [120] as well as from mixtures containing cerous nitrate, zirconium n-propoxide, and an alcohol [114,121]. Nanocrystalline cerium oxide structures with electrical properties suitable for electrodes used in SOFC have been produced using aged, dried gels formed from mixtures of cerium chloride, methanol, and propylene oxide as well [115]. Precipitated sols converted to gels containing samarium-doped cerium oxide for SOFC have also resulted in the generation of uniform nanoparticles that were easily sintered at 1400 °C rather than at 1600 °C, as was required for samples made using conventional techniques [116]. While many sol-gel processes use cerous nitrate hexahydrate as a cerium source, the specific process and other reagents used for sol or gel formation vary widely across studies.

Cerium sol-gel methods have also been investigated for forming a passivation layer on metal surfaces to improve corrosion resistance and replace less environmentally-friendly processes, such as chromate conversion coating [122]. It has been shown that thin CeO_2-ZrO_2 and CeO_2 coatings on steels, applied by dipping samples into a dispersed sol followed by heat treatment at 500-800 °C, resulted in improved corrosion resistance [122–124]. Similarly, 2-3 µm coatings of a cerium-loaded epoxy silicate sol-gel were bonded to an aluminum alloy used in aircraft to prevent corrosion, as a replacement for chromate-based processes [125]. In another study, CeO_2 dispersed as a sol was used to coat nickel and chromium substrates. CeO_2 crystallites deposited on these substrates were incorporated into the growth of native oxides during annealing and slowed the oxidation rate [126]. In this study it was determined that deposited ceria crystallites had a size of approximately 5 nm upon drying at room temperature, underwent rapid coarsening as temperatures exceeded roughly 400 °C, and approached a size of 25-35 nm upon heating to 800 °C.

While there has been much prior work on a variety of cerium-based sol-gel processes for a range of applications, the internal gelation process is preferred in the current research effort to produce microspheres. Catalyst-based applications for ceria typically require nanopowders to be prepared by sol-gel, which would be hazardous for the intended Pu-238 work. Alternatively, the internal gelation process allows for homogeneous precipitation of microspheres with diameters generally above 50 µm. Although hydrothermal processes for ceria also involve nanoparticles, their consideration is instructive with regard to the trends observed for a variety of treatment methods and conditions as well as the resulting effects on ceria properties, particularly on crystallite growth and sinterability.

Hydrothermal treatments have been developed for metal oxide nanopowders with the goal of controlling the particle size, size distribution, morphology, and crystal structure through the variation of parameters including temperature, pressure, and reagent concentrations [127]. Powders can either be precipitated by hydrolysis during the hydrothermal treatment, or modified by the hydrothermal treatment after precipitation. CeO_2 nanopowders have been prepared by mixing cerous nitrate with supercritical water at 450 °C [128], by direct hydrothermal treatment of ceric ammonium nitrate solutions [100,129], and from cerous nitrate and Ce(IV) sulfates by ammonia generation using urea or HMTA as an alkali source during the hydrothermal step [130,131]. Investigation of crystallite size as a function of heat treatment in the latter studies showed relatively little crystallite growth of hydrothermally-treated samples below 600 °C [130], but excellent sinterability with fully dense particles obtained at temperatures below 1300 °C [131].

Cerium dioxide can also be produced by the thermal decomposition of $CeCO_3OH$ above 300 °C, which is generated by the hydrothermal treatment of an aqueous cerium precursor, such

as cerous nitrate, mixed with an ammonia and carbon source, such as urea or HMTA, at 100-180 °C [76,77,102–105]. CeO_2 produced by oxide conversion of $CeCO_3OH$ has shown excellent sinterability with densities above 99% of theoretical upon heating to temperatures as low as 1000 °C [77].

In cases where precipitation is initiated prior to a hydrothermal step, subsequent heating in water can act to modify or grow the metal oxide crystallites [127,132]. A study investigating the hydrothermal treatment of ceria powders produced by precipitation of Ce(III) and Ce(IV) feeds using NH_4OH indicated that Ce(IV) feeds led to smaller crystallites around 3 nm, which grew during pressurized water treatments, while Ce(III) feeds produced larger crystallites around 16 nm, which did not grow significantly during hydrothermal treatment [133]. Using NaOH to initiate precipitation in cerous nitrate followed by hydrothermal treatment at 400 °C led to nanocrystals with edge lengths of 5-8 nm [134]. Alternatively, in a process where homogeneous precipitation from cerous nitrate was accomplished by cooling solutions to 5 °C and adding H_2O_2 to initiate a change in oxidation state, a hydrothermal treatment was used to convert the precipitated species to a reduced hydration state of $CeO_2 \bullet nH_2O$ [75]. In other studies, solutions were not chilled prior to mixing H_2O_2 and cerous nitrate, and NH_4OH was added to complete the precipitation of cerium hydroxide [74,135]. In these studies, crystallites less than 10 nm were formed during hydrothermal treatments at 200-250 °C [74,135] that showed little growth at temperatures up to 500 °C, but were approximately 45-50 nm after heating at 1000 °C for two hours [74]. A separate investigation of the effect of pH on crystallite growth during hydrothermal treatments found that acidic conditions promoted more rapid crystallite growth while neutral and basic solutions resulted in slower growth, even as processing temperatures were raised as high as 250 °C [136].

Cerium dioxide powders have also been produced by microwave hydrothermal treatments of ceric ammonium nitrate combined with HMTA, NH_4OH, or NaOH in a pressurized vessel to produce 2-5 nm spheres with a specific surface area of 150-250 m^2/g [137–139]. In these trials, powders prepared from ceric ammonium nitrate and sodium hydroxide had a mass loss of approximately 7% upon heating to 400 °C with minimal mass loss at higher temperatures [139].

Based on the preceding review of ceria hydrothermal processes, it is apparent that hydrothermal treatments have the potential to decompose organic species, improve the crystallinity of samples, and also result in reactive powders that densify at lower temperatures than those produced by traditional precipitation methods.

2.3 The Pu-238 Baseline Process

Plutonium-238 has been a part of the nation's science and security mission since the beginning of the 1960s. Production in the United States occurred through the 1960s, 70s, and 80s at the Savannah River Laboratory (SRL) where neptunium-237 recovered from uranium was fabricated into aluminum-matrix targets for Pu-238 production [140–143]. Fuel fabrication took place at Mound Laboratory until the mid 70s in the Special Metallurgical Building until work was transferred to building 235-F at Savannah River due to concerns about the proximity of Pu-238 work at Mound to Miamisburg, a major population center [7]. The Plutonium Fuel Form Fabrication Facility, or PuFF, at SRL contained hot cells for Pu-238 precipitation, powder processing, pressing, iridium encapsulation, and shipping [144]. As will be discussed, Pu-238 processing was moved to technical area-55 (TA-55) at Los Alamos around 1990.

Plutonium-238 is produced by neutron bombardment of neptunium-237 (Np-237) and must be chemically separated from irradiated targets. Past production campaigns occurred in heavy water moderated plutonium-production reactors in a configuration where boiling of

coolant water was intolerable. For this reason, low NpO_2 loadings in an aluminum matrix sealed in an aluminum irradiation target assembly were used to limit heat generation and maximize cooling [141–143,145]. Post-irradiation, targets were stored for a period of time to allow fission products to decay and then dissolved in either concentrated HNO_3 with mercuric nitrate and potassium fluoride catalysts or NaOH with $NaNO_3$ [140,142,146]. Dissolution is incomplete and typically a heel containing 5-15% of the initial charge, including Np and Pu in the same ratio as the initial sample, must be recycled or disposed [141,147]. Ferrous sulfamate is added to a nitrate solution containing the neptunium, plutonium, and impurities to achieve oxidation states of Np(IV) and Pu(IV) which are loaded onto an anion exchange resin [140,142,146]. At the end of column purification, Pu(IV) is eluted with dilute nitric acid. Precipitation is accomplished by addition of plutonium nitrate solution to oxalic acid and the plutonium oxalate is calcined to PuO_2 [140,142].

The fabrication flowsheet for Pu-238 oxide pellets, shown in Figure 2.3, involves a number of powder processing steps to produce feed granules suitable for pressing and sintering [18,19,142]. Stock PuO_2 is dissolved into a nitrate solution for subsequent oxalate precipitation. Oxide conversion is accomplished by heating at 735 °C for two hours. An O-16 enrichment step is performed to reduce neutron emissions caused by [α, n] reactions occurring with O-17 and O-18 from >17,000 n/s-g to less than 5,000 n/s-g [18,148,149]. Powders are then ball milled for 40-100 hours, pressed into green pellets, then pressed through a mesh screen to produce granules in the size range 44-125 μm [18,19]. The ball-milling step was included as a way to normalize the batch-to-batch variations in size and morphology of reverse strike oxalate precipitates since the generation of lathe-shaped particles caused excessive shrinkage in sintered pellets that resulted in cracking [18,19,67,70,150]. Oxalate precipitates are easily filtered, but control over

particle characteristics are sensitive to several precipitation parameters and wide variations in size and morphology have been observed [11,12,83,85,86]. While efforts have been made to produce pellets directly from rosette-shaped oxalate precipitates produced by direct-strike oxalate precipitation, it has proven difficult to consistently produce agglomerates larger than 40-50 μm without the presence of finer precipitates and lathe-shaped particles [83,85,86]. Further, ball-milled powders used directly to fabricate pellets resulted in a loss of porosity and additional sintering of the pellet at operating temperatures, which caused cracking [65]. However, granules produced by slugging a cold-pressed pellet through a 125 μm sieve yielded pellets with more uniform porosity and better intergranular contact [65]. To limit shrinkage and pellet sintering, granules are heat-treated in two fractions; 60% of the granules are heated at 1100 °C and 40% at 1600 °C. The thermally seasoned granules are then blended prior to pellet hot pressing and pellet sintering at 1600 °C [18,19,65].

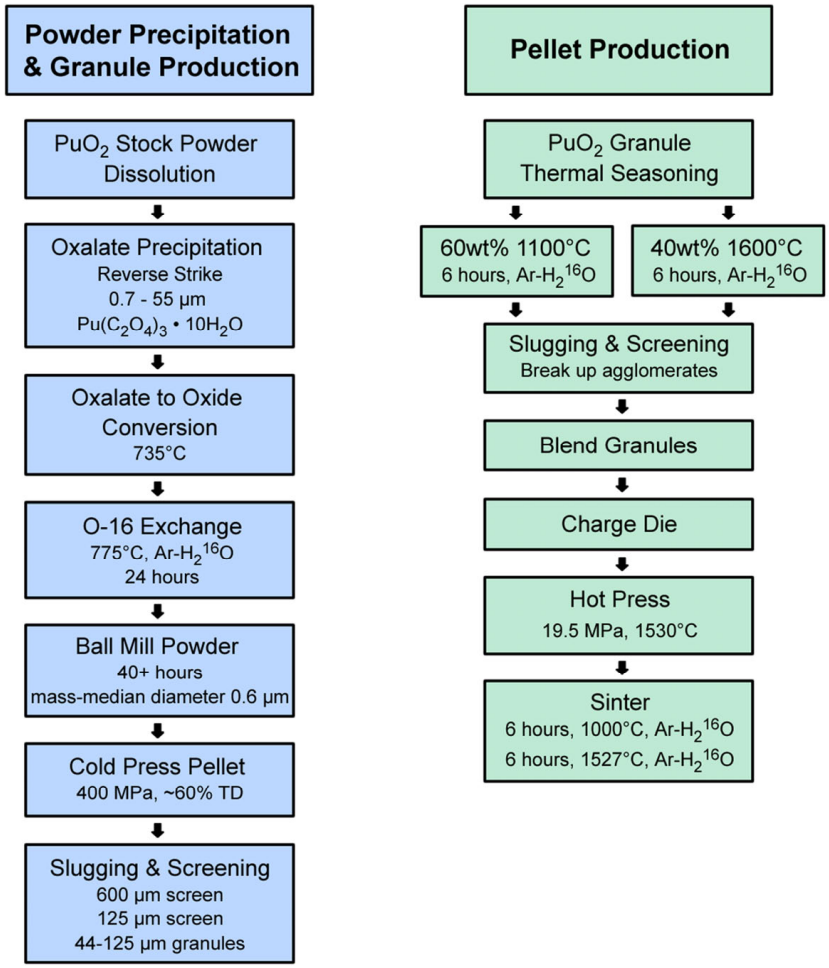

Figure 2.3: The flowsheet for Pu-238 pellet fabrication at Los Alamos involves the generation and handling of sub-micron oxide powders [18,19].

2.4 Properties of Pu-238 Oxide Powders

Submicron Pu-238 oxide powders produced by ball milling are extremely hazardous. Such fine particles are highly dispersible due to static electricity and air currents, tend not to settle, and do not appear to agglomerate during ball-milling [3,20,21]. This is especially problematic since Pu-238 oxide is very corrosive, having its own source of heat and oxygen. With an alpha activity about 275 times that of Pu-239, decay from Pu-238 presents unique problems. Empirical studies have shown that oxide particles less than 20 nm in size are prone to

movement due to alpha recoil [21]. Based on the momentum of alpha particles with an energy of 5.5 MeV, a 20 nm PuO_2 particle has a calculated recoil velocity of approximately 2.6 m/s. While a small portion of ball-milled powders may be below 20 nm initially, alpha decay occurring near particle surfaces results in the spalling of particles in this size range [3,21,151]. These small, self-mobile particles, sometimes called fleas, are the suspected mechanism for rapid glove failures in gloveboxes and the transport of Pu-238 past HEPA filters [3,21,151]. At Savannah River, workers reported that calcined oxalate precipitates originally 60% 4-20 μm and 40% >20 μm reduced in size to 54-65% <4 μm and 30-37% 4-20 μm after being stored for six months [150]. The high mobility and corrosive nature of Pu-238 oxide also lend to release through container corrosion. In the event of containment breach, Pu-238 oxide is a severe inhalation hazard. Particles under 10 μm in diameter tend to lodge in the lungs rather than in nasal passages [19] and are difficult or impossible to remove, even with chelation therapy [22]. Despite best efforts to prevent Pu-238 release, powder processing operations have resulted in significant levels of contamination and multiple instances of worker exposures.

Plutonium-238 has proven difficult to contain with releases at Mound, Savannah River, and Los Alamos. Mound Laboratory was a major facility for Pu-238 processing in the 1960s and early 70s. Although gloveboxes for Pu-238 work were maintained at a negative relative pressure and filtered through a double HEPA system, yearly releases were as high as 250 mCi out the air stack and 243 mCi for aqueous effluents [49]. During the decommissioning of the special metallurgical building used for Pu-238 processing at Mound, residual Pu-238 and contamination was found in numerous systems, including ductwork, with initial Pu-238 levels of 100,000 Ci prior to recovery and decontamination [152]. Despite this high degree of contamination, the hydroxide precipitation shard and microsphere processes used at Mound were recognized to

generate fewer fines than oxalate precipitation methods used later at Savannah River and Los Alamos [19,49].

The seriousness of the migratory and corrosive properties of Pu-238 oxide powder is evident upon consideration of the Plutonium Fuel Form Fabrication Facility (PuFF) in Building 235-F at Savannah River. Approximately 165 kg of Pu-238 was processed in PuFF hot cells from 1978 – 1983 and Pu-238 oxide spheres and pellets were produced for NASA missions. In early 1984, PuFF was placed in standby mode and decontamination was limited to areas where manipulators could reach [7,153]. Despite plans to continue production in 1986, Pu-238 program cuts and delays prevented new work in PuFF. When additional Pu-238 fuels were needed in 1990, PuFF was no longer suitable for work and responsibilities were transferred to Los Alamos. Extensive corrosion in the PuFF hot cells, particularly those where the ball-milled powders were processed, led to failure of the manipulators and concerns that Pu-238 had penetrated seals, contaminating hot cell internals [7]. Multiple grams of Pu-238 were also detected beyond the first HEPA filter [3]. Decontamination and decommissioning of PuFF still remains to be completed and has been estimated as an unfunded, $300M liability that could pose serious risks to workers at Savannah River in the event of a fire or natural disaster [7,153–155].

Accidents involving the airborne release of Pu-238 oxide powders due to the accidental pressurization of a glovebox vacuum line and the movement of a corroded Pu-238 storage canister have occurred at Los Alamos in more recent history. In 2000, Pu-238 release from a glovebox resulted in uptake in seven workers. A technician working on a Pu-238 glovebox received an estimated committed effective dose equivalent of 300 R and three other workers likely exceeded their annual limit of 5 R [5]. These four workers were subjected to chelation therapy. In 2003, two workers performing inventory disturbed a package containing Pu-238

residues and received estimated committed effective dose equivalent of 2-3 R. The accident investigation revealed that chemical, thermal, and radiolytic degradation of the inner can, PVC bag, and outer can resulted in pressure generation from helium buildup that was released upon handling [6]. In addition to the exposures, the release caused an eight-month delay in the program. Based on experiences at Mound, Savannah River, and Los Alamos, it is clear that Pu-238 oxide particulates pose a significant risk to workers, facilities, and programs.

2.5 Relevant Achievements in Sol-Gel Processing

Given the corrosive and radiological hazards of Pu-238 oxide powders, it is desirable to maintain Pu-238 in a non-dispersive form. Using internal gelation, Pu-238 would be contained in an aqueous nitrate solution until formed into macroscopic spheres for direct pressing into a pellet. Pu-238 oxide microspheres have been produced by rapid stirring, dehydration sol-gel techniques in the past, but required a difficult sol preparation step and resulted in spheres with a wide size distribution. Internal gelation sol-gel methods eliminate the sol preparation step. While a body of research exists for internal gelation of uranium microspheres, the extent of plutonium work is very limited and related to its incorporation in mixed oxide fuels. At this point, historic sol-gel technology and microsphere dispersion techniques relevant to the formation of plutonium microspheres will be reviewed.

Significant sol-gel development programs took place in the 1960s and 70s in the United States using a sol-dehydration method to produce microsphere fuels for fast breeder reactors. Based on anticipated reactor designs at the time, sol-gel microspheres were fabricated, in order of quantity, from thorium, thorium + uranium, uranium, plutonium, and plutonium + uranium [27]. Sphere formation was accomplished by dispersing droplets of an aqueous sol into an up-flowing column of 2-ethyl-1-hexanol [23,24,27,29–31,35,156–159]. The aqueous sol contained

small crystallites that coalesced into a sphere upon dehydration in the organic forming fluid. As water was extracted, spheres settled out of the up-flowing column for collection, drying, and calcining. Initial attempts to use stoichiometric nitrate sols resulted in lower-density spheres than desired. Steam de-nitration of dried metal nitrates and re-suspension in dilute nitric acid was found to form stable sols with small crystallites that resulted in dense spheres [23,24,27,31,156,157]. However, difficulties with thermal de-nitration of uranium, including the sensitivity of the extent of de-nitration to temperature and time, motivated amine nitrate extraction from sols into an organic phase as an alternative method [27,29,32,159]. Thermal de-nitration methods dominated for plutonium and cerium-surrogate work, however, with test programs producing mostly 50-250 μm diameter cerium oxide and Pu-238 oxide microspheres [35,158,160]. Pu-238 oxide microspheres were fabricated for vibropack fuel impact studies, seawater solubility experiments, and for passage through an AC plasma torch [35,158,160]. In studies with Pu-239, spheres in the size range 50-250 μm and 250-600 μm were fabricated with high densities and carbon impurities below 70 ppm [27]. During fabrication of sol-gel spheres, residual carbon from surfactants and 2-ethyl-1-hexanol in the forming column resulted in carbon impurities up to 2000-5000 ppm in cases where the firing atmosphere and temperature were not designed for carbon removal [27,156]. While modern sol-gel nuclear fuels are fabricated by internal gelation, much of the droplet-forming mechanisms still used today were assessed during work with the dehydration sol-gel process.

Monodisperse microspheres can be formed by two-fluid nozzles, vibratory nozzles, and free-fall dripping, as seen in Figure 2.4. While free-fall dripping of spheres from multiple orifices allows for high throughput, the resulting droplet sizes are larger than desired for most fuel applications [24]. When uniform spheres in the general range of 200-800 μm are desired,

two-fluid or vibratory nozzles are used. Two-fluid nozzles are generally operated at flow rates such that a jet of feed undergoes varicose breakup into droplets in a concurrent flow of an immiscible organic [24,27,29]. Assuming that the feed jet is accelerated to the velocity of the stripping fluid and that varicose droplet breakup occurs to form droplets with diameters 2.0-2.5 times that of the jet, droplet size has been estimated using [29]:

$$D = k\sqrt{\frac{4f}{\pi V}} \tag{2.1}$$

for sol flow rates of 0.5-10 mL/min through the capillary where D is the microsphere diameter, k is a dimensionless constant from 2.0-2.5, f is the feed flow rate, and V is the organic flow rate [24,27,29,161]. Using two-fluid nozzles, thorium and uranium spheres have been produced by sol dehydration at a variety of diameters from 88-590 μm with typical standard deviations of approximately 10-30% [23,27]. Pu-239 spheres have been produced with sizes ranging 50-250 μm, 250-600 μm, and 250-400 μm [24,27,160]. Similarly, Pu-238 spheres were made with diameters ranging 50-250 μm, 88-250 μm, and 50-400 μm [23,36,158]. Since spheres are made one at a time, production rates are significantly reduced as the desired sphere diameter is decreased. In general, production of spheres with diameters less than 100-300 μm was relegated to emulsification methods that yielded large batches of small spheres with a broad size distribution for applications such as vibropack fuels [23,31,35,162]. These small microspheres were made by dispersing feed into an organic in a baffled beaker with rapid stirring and the poor uniformity was overcome by sieving to obtain the desired sizes.

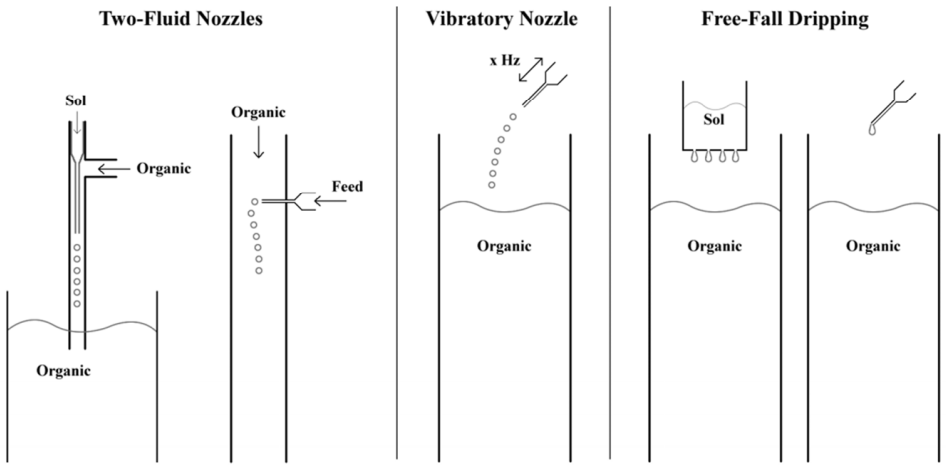

Figure 2.4: Microsphere formation can be performed with two-fluid nozzles, vibratory nozzles, or by free-fall dripping [24,27].

In an effort to improve the monodispersity of microspheres made with two-fluid nozzles at high sol flow rates, an apparatus was developed with a variable frequency vibrating plunger located above the sol capillary, as shown in Figure 2.5 [25,32]. Imparting a vibration on the sol near the natural sphere formation rate resulted in improved monodispersity. Assuming that the feed jet is accelerated to the velocity of the stripping fluid and that varicose droplet breakup occurs to form droplets with diameters approximately 2.1 times that of the jet, sphere diameters were predicted using the equation [25]:

$$D = 1.70d\sqrt{\frac{f}{V}}, \tag{2.2}$$

where D is the microsphere diameter, d is the channel inner diameter, f is the feed flow rate, and V is the organic flow rate [25,32,163]. The vibrating plunger, two-fluid nozzle resulted in standard deviations less than 2% for spheres with average diameters as small as 283 μm and 19% for spheres with an average diameter of 207 μm. Although spheres with diameters as small as 200 μm were produced, emphasis was placed on spheres in the 350-500 μm range [25,163]. Similar vibrating dispersion devices with multiple-orifices were also developed to increase throughput, but resulted in poorer size uniformity and yields due to unequal divisions of sol

between capillaries [25]. Since studies were aimed at multi-kilogram quantities for reactor applications, sphere production rates by two-fluid nozzle were considered too slow [27], and most work, including current TRISO production, focused on higher-throughput using vibratory nozzles with sphere breakup in air above the forming column.

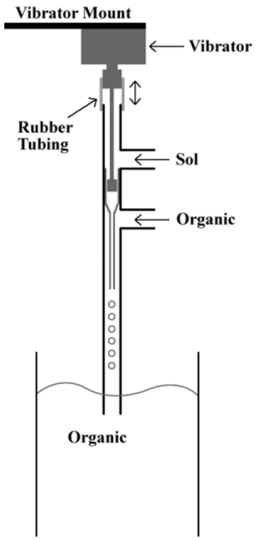

Figure 2.5: Size uniformity was improved using vibration in two-fluid nozzles at Oak Ridge National Laboratory in the 1970s [25,32].

Vibratory nozzle designs are the dominant sphere-forming technique used in modern internal gelation sol-gel work. During the sol-dehydration process development, researchers found that improved sphere uniformity could be obtained for spheres larger than 200-300 μm by coupling the dispensing capillary to a loudspeaker with variable frequency [24,27]. More recent investigations in the United States for production of internal gelation microspheres by vibratory jet breakup have focused on final sphere diameters of 350 μm, 425 μm, and 500 μm for TRISO fuels. Production campaigns at Oak Ridge and scaled-up internal gelation operations at Babcock and Wilcox for fabrication of TRISO kernels impart a vibration to the dispensing needle to impart regular breakup of feed jets [40,42,43]. Controlled vibrations near the natural frequency

of breakup also improve throughput, allowing higher feed flow rates and in some cases multiple orifices [164]. The effect of vibration near the natural frequency overcomes random disturbances that can result in off-sized spheres. Feed flow rates must be fast enough to create a jet that breaks up at regular lengths and results in sphere diameters about twice that of the jet. Thus, microsphere size can be predicted based on nozzle diameter, feed flow rate, and shrinkage factors during drying [161,164]. Electromagnetic vibrators are also used in the majority of internal gelation research studies in India for a variety of applications involving thorium, uranium, and plutonium [33,165–172]. Vibration techniques have also been employed in German external gelation sol-gel systems where acid-deficient uranyl nitrate spheres are dispensed into a column of ammonium hydroxide for precipitation [167,173]. Feed flow rates of 10-15 mL/min is typical for 350-500 μm spheres while rates as high as 20-30 mL/min have been achieved for 600-800 μm spheres [42,168,169].

While most sol-gel efforts have focused on dense microspheres for coated particle fuels or vibropack fuels, low-density microspheres have also been produced by internal gelation methods for pressing into pellets. Fabrication of homogeneous mixed-oxide (MOX) fuels for plutonium recycle motivated the sol-gel microsphere pelletization (SGMP) process in India and the direct press spheroidized (DIPRES) program in the United States [167,169,171,172,174–177]. Production of MOX pellets from internal gelation microspheres is desirable for a number of reasons including the reduction of fines, simplified processing, pour-ability of microspheres into dies, homogenous plutonium distribution, and ability to be performed remotely. Kilogram quantities of MOX microspheres were produced for studies including irradiation testing in the fast-flux test facility in the 1980s [174]. Low-density spheres were found to be desirable since pressing spheres with high crush strengths resulted in pellets with a "blackberry" structure

caused by poor particle coalescence into a homogeneous structure [167,169,171,175]. Pellets with a blackberry structure also had open porosity and theoretical densities below 85%. Early efforts to produce spheres with sufficiently low densities and crush strengths was accomplished using carbon black as a pore former, but required carbon removal by controlled oxidation during heat treatment steps. More recent work has shown that carbon black is not necessary to produce soft microspheres suitable for pressing into high density pellets if feed properties and gelation conditions are chosen carefully [167,171,175,176,178,179]. Although pellet pressing research has focused on the production of soft microspheres for high-density pellets, open porosity and 80-90% theoretical density resulting from stronger granules may be beneficial for Pu-238 oxide pellets that must accommodate helium escape [65].

2.6 Internal Gelation Chemistry

Characteristics of internal gelation microspheres depend on multiple parameters, including feed concentrations, reagent ratios, gelation temperature, and washing methods. Improving microsphere properties for a given application requires a fundamental understanding of the chemical reactions involved and their impact on the resulting gel and crystal structures. Although gel microspheres have been fabricated from a variety of non-actinide metals including aluminum, cerium, hafnium, iron, titanium, and zirconium [180–185], the process chemistry is best understood for uranium. For this reason, the chemistry of the sol-gel process will be described in terms of uranium and extrapolated to consider the anticipated behavior for cerium or plutonium.

Internal gelation uses a mixed feed of metal nitrate solution and aqueous solutions of the organic compounds urea and hexamethylenetetramine (HMTA) to delay precipitation until the feed is dispersed as microspheres. A flow diagram of the internal gelation process is provided in

Figure 2.6. Mixed feed solutions are chilled to prevent gelation and passed through a needle into a column containing a heated organic fluid. The aqueous feed breaks up into immiscible droplets in the hot organic, typically silicone oil or trichloroethylene (TCE), where the temperature increase initiates homogenous precipitation of a hydrous, gel microsphere. Gelled spheres are collected, aged in hot oil, and cooled to room temperature. Silicone oil is removed from spheres by washes with TCE or carbon tetrachloride, allowing additional washes with dilute ammonium hydroxide (NH_4OH) to complete precipitation and extract excess reactants and the reaction by-products formaldehyde and ammonium nitrate. After washing, spheres are typically dried in air prior to calcining and sintering.

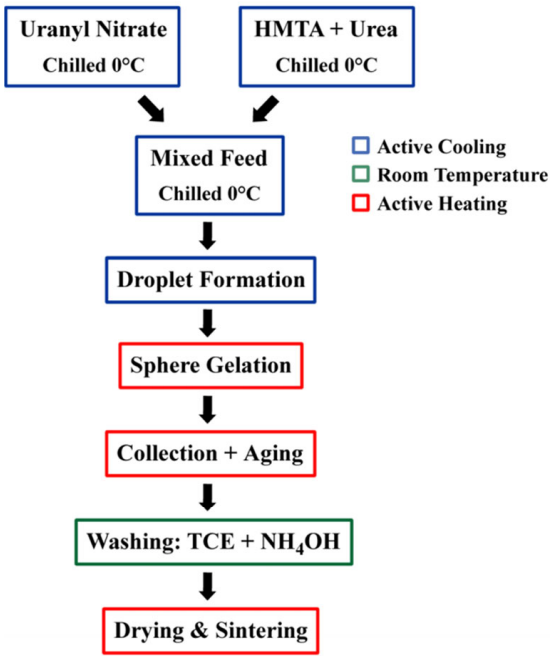

Figure 2.6: Microspheres are fabricated by internal gelation methods by temperature-induced precipitation of mixed feed solutions.

Urea ($CO(NH_2)_2$) and HMTA ($(CH_2)_6N_4$) each play a critical role in the gelation process. In chilled feed solutions, urea forms a complex with the metal ion, represented by

$$2CO(NH_2)_2\,(aq) + UO_2^{2+}\,(aq) \leftrightarrow\ UO_2[CO(NH_2)_2]_2^{2+}\,(aq), \qquad (2.3)$$

which prevents hydrolysis reactions that would otherwise lead to precipitation in the 3.3-5.7 pH range of typical mixed feed solutions [162,186,187]. Although a complex is also formed between the HMTA and uranyl ion, it is far weaker than the urea complex [162]. Urea decomplexes the uranium upon sphere heating in the forming column, allowing hydrolysis and precipitation of UO_3 according to the reactions

$$UO_2^{2+}\,(aq) + 2H_2O\,(l) \leftrightarrow UO_2(OH)_2\,(aq) + 2H^+\,(aq), \text{ and} \tag{2.4}$$

$$UO_2(OH)_2\,(aq) + H_2O\,(l) \leftrightarrow UO_2(OH)_2 \bullet H_2O\,(s) \text{ (aka } UO_3 \bullet 2H_2O). \tag{2.5}$$

HMTA in the feed droplets was originally thought to provide ammonia by thermal decomposition, according to

$$(CH_2)_6N_4\,(aq) + 6H_2O\,(l) \leftrightarrow 4NH_3\,(aq) + 6CH_2O\,(aq), \tag{2.6}$$

causing precipitation [162,186,188]. It was later shown that protonation of HMTA, or

$$(CH_2)_6N_4\,(aq) + H^+\,(aq) \leftrightarrow [(CH_2)_6N_4H]^+\,(aq), \tag{2.7}$$

occurs prior to thermal decomposition and that gelation proceeds to completion due to H^+ pickup by HMTA [177,187,189]. The HMTA decomposition reaction is promoted by urea, which reacts with formaldehyde (CH_2O) to form monomethylol urea or other urea-formaldehyde polymers [162,177,186,188]. Urea also hydrolyzes under acid conditions at elevated temperature to produce CO_2 and ammonia (NH_3), but this effect is assumed to be insignificant under sphere forming conditions [162,190].

Uranyl nitrate feed solutions are made acid deficient to NO_3^-/U ratios of 1.5-2.0 for two reasons [177,187,188]. First, uranyl nitrate solutions with higher uranium molar concentrations can be achieved with sub-stoichiometric nitrate content. Higher uranium concentrations can be understood due to hydrolysis and dimerization to $(UO_2)_2(OH)_2^{2+}$ and a high solubility of aqueous $UO_3 \bullet 2H_2O$, which can be better understood as $UO_2(OH)_2 \bullet H_2O$ [162,187,191]. Note that

precipitation of $UO_3 \cdot 2H_2O$ in uranyl nitrate solution doesn't occur unless the solution pH rises to 3.3-4.0 [187]. High reagent concentrations in the feed solutions result in less shrinkage during drying, reducing the risk of cracking. Second, removal or neutralization of nitrate in the feed solution reduces the amount of HMTA necessary to promote gelation. Acid-deficient uranyl nitrate solutions are commonly prepared by the dissolution of U_3O_8 in a sub-stoichiometric amount of nitric acid. Alternatively, the nitrate is removed by amine extraction or neutralized by addition of NH_4OH. The molar concentrations of HMTA and urea are almost always identical, allowing for the common value

$$R = \frac{[HMTA],\ [Urea]}{[Metal]}, \tag{2.8}$$

relating the organic to metal feed concentrations. Studies evaluating the effect of NO_3^-/U ratio and R value on UO_2 gel quality have found numerous formulations that produce acceptable microspheres, but approximate ratios of 1.55-1.7 for NO_3^-/U and 1.2-1.7 for R are common [42,43,170,176,177,188]. Uranium concentration in mixed feed solutions ranges from 0.7-1.85 M but is commonly 1.1-1.3 M. A major factor in the selection of feed concentrations and ratios is the tradeoff between the speed of gelation and the tendency of microspheres to crack.

Monodispersity and microsphere cracking are dependent on mixed feed parameters. Spheres with low reagent concentrations, low R values, or high NO_3^-/metal ratios take longer to gel in the forming column, causing sphere coalescence and agglomeration, and necessitating slower production rates. Alternatively, concentrated solutions, high R values, and low NO_3^- /metal ratios result in fast gelation and allow for fast production. However, fast gelation is linked to amorphous microspheres or small crystallite sizes that make the extraction of organic impurities more difficult during the washing step [43,170,176,180,186,192–194]. Residual organic impurities volatilize during subsequent heat treatments, which causes cracking. For

these reasons, intermediate values are generally selected to balance gelation time, surface erosion, and crystallite size in the production of UO_2 fuels. In other cases where oxide spheres are amorphous, impurity-related cracking must be addressed by modified washing and heat treatment steps [181–183,193,195].

Basic washing procedures for internal gelation spheres based on TCE and dilute NH_4OH have remained mostly unchanged since their introduction in the 1970s. Washes with TCE are solely for the removal of silicone oil and are not intended to have any chemical effect. Ammonia produced from NH_4OH in solution, however, serves two principal functions. First, the alkali ammonia washes complete $UO_3 \cdot 2H_2O$ precipitation. Ammonia precipitation also results in the formation of some ammonia uranates (ADU) of the form $UO_3 \cdot xNH_3 \cdot (2\text{-}x)H_2O$ [92–94,162,188,189,192]. Detection of ADU precipitates with x = 0, 0.25, and 0.5 in internal gelation gels indicated $UO_3 \cdot 2H_2O$ (x = 0) crystals were large with sizes from 1000-5000 Å while $4UO_3 \cdot NH_3 \cdot 7H_2O$ (x = 0.25) and $2UO_3 \cdot NH_3 \cdot 3H_2O$ (x = 0.5) formed predominantly small crystals in the size range <100-250 Å, particularly at high R values and low NO_3^-/U ratios where gelation was rapid [192]. This observation is supported by a general recognition that higher concentrations of ammonia in the lattice leads to significant decreases in crystallinity [93,192]. The second function of ammonia washes is to extract ammonium nitrate, urea, and HMTA from the spheres to reduce impurities and limit volatile emissions during heat treatments. Additionally, ammonia reacts with formaldehyde present as an HMTA decomposition product, resulting in the re-formation of HMTA [162]. After washing is complete, spheres are generally dried under ambient conditions prior to calcining and sintering. In some studies, cracking has been limited by techniques including additional washes, a slow drying step, slow heating ramp rates, controlled atmospheres, and low-temperature dwells [42,43,193,195].

Thermal gravimetric analysis (TGA) was used in a number of studies to determine the temperature ranges and extent of volatile emissions [42,43,183,193,196–198]. In some cases, mass or infrared (IR) spectroscopy was performed on the volatile emissions to provide insight into the temperature-dependent reactions [196–198]. TGA curves generated for expected impurities HMTA, ammonium nitrate, and urea resulted in complete mass losses by 240, 280, and 370 °C, respectively [42]. However, continuous mass losses have been observed up to at least 600 °C in air-dried microspheres [42,43,183,196]. Mass losses of 20-30% in spheres is common, of which approximately 10% is typically attributed to water evolution below 150-200 °C [42,43,183,196,197]. In the temperature range 200-400 °C, ammonia and carbon dioxide release have also been detected [196,197]. Above 400 °C, mass loss has been ascribed to carbon combustion or oxidation reactions.

2.7 Research Gap

Despite extensive development of internal gelation methods, several questions remain regarding its suitability for fabricating Pu-238 oxide pellets. These unknowns were summarized by a 2008 INL committee on the evaluation of aqueous processing techniques for Pu-238 as [19]:

1) What is the particle size distribution in the granulate that can be produced by the optimized sol-gel process?
2) What is the ceramic activity of the final granules produced by the sol-gel method?
3) Can the required chemical purity be achieved using this method?

The committee was concerned whether microspheres could be made near the 100 μm desired granule size without dust generation due to microsphere cracking. Additionally, since most microsphere work has produced dense spheres for TRISO particles and requires a calcining step to remove volatiles, it is uncertain whether enough ceramic activity remains for bonding and

production of uniform pellets. Finally, carbon impurity levels have been high in some sol-gel fuels due to organics inherent in the process. Demonstration that carbon and trace metal concentrations in sol-gel microspheres are comparable to those in current Pu-238 feed powders would be necessary. Although the committee did not highlight these issues and they will not be addressed using non-radioactive surrogates, additional unknowns include the behavior of plutonium in the sol-gel chemistry and the effects of radiolysis. Plutonium behaves differently from the uranyl ion in solution and modifications to feed preparation, mixed feed ratios, and the effects of valence stabilizers remain to be determined.

2.8 Approach

Based on the merits of internal gelation to simplify Pu-238 processing and improve safety, this thesis investigates the unknown factors listed by the 2008 INL committee. While validation with Pu-239 and Pu-238 will be necessary, these materials cannot be handled in the necessary quantities in the available university laboratory. Conveniently, non-radioactive cerium is expected to serve as a suitable surrogate for plutonium in the experiments designed to address questions 1-3 above. Although one report from Oak Ridge reviewed optimal feed parameters for the production of hydrous cerium microspheres [180] and a master's thesis from Texas A&M sought to make cerium oxide spheres by internal gelation from cerous nitrate [199], the questions previously outlined regarding sizing, cracking, heat treatments, density, and chemical purity remain unknown. Using published data on the uranium internal gelation process and equipment used for microsphere fabrication, the following tasks, outlined in Figure 2.7, were planned:

1) Find a suitable cerium feed solution and optimize feed parameters for acceptable gels.

Laboratory materials were gathered to repeat the gelation experiment published by Oak Ridge to determine if the results could be replicated. These experiments provided experience working with the relevant materials and a first-hand understanding of the methods. Additionally, first-hand observation of the gels produced allowed for further refining of parameters and selecting those that were optimal for the apparatus to be built.

2) Construct an apparatus for automatic dispersion of monodisperse microspheres in the desired size range.

Internal gelation methods require active chilling and heating in close proximity to prevent premature gelation while initiating rapid gelation of microspheres after being dispersed. Equipment was designed for automatic sphere production with reproducible control of formation parameters, including temperatures and flow rates. Many unanticipated problems with premature gelation, needle clogging, and bubble generation were overcome by modifications to equipment and procedures.

3) Scale up the sol-gel apparatus to fabricate multi-gram batches for materials analyses.

Since the original apparatus was designed primarily to determine whether spheres of the desired size could be obtained, throughput was low. Changes to the apparatus increased the daily yield tenfold to approximately 10 g/day while maintaining the desired size control.

4) Assess monodispersity and size ranges possible with dispersion technique.

Once larger quantities of spheres could be made, analysis of bulk properties became possible. To determine the size and monodispersity capabilities, spheres were collected at a variety of flow rates and needle sizes. Size was determined by optical microscopy

and digital image processing. These results indicated that the desired size and monodispersity could be attained.

5) Determine effect of washing methods on cracking and impurities.

A variety of washing techniques were investigated and those that appeared promising were compared to the baseline process. Large batches of microspheres were produced using the same reagents, feed parameters, and processing conditions but washed by different methods for comparison of volatile mass loss and residual impurities. A variety of analyses were performed including TGA to determine mass loss as a function of temperature, electron-impact mass spectroscopy (EI-MS) to identify volatile impurities, combustion carbon analysis, instrumented gas analysis for determination of hydrogen and nitrogen, and glow-discharge mass spectroscopy (GDMS) for trace element determination. The results indicated that impurity levels in sintered sol-gel spheres are well below specified limits for Pu-238 oxide fuels.

6) Measure the density of microspheres as a function of heat-treatment temperature.

A single large batch of microspheres was produced and washed by the preferred method and then heat treated to a variety of temperatures. Since impurity and TGA data provided an understanding of the necessary temperatures for microsphere processing, the density data provided insight into the expected ceramic activity after removal of volatiles for the chosen feed parameters. As a result of improved washing techniques, volatile removal could be performed at lower temperatures with little to no cracking.

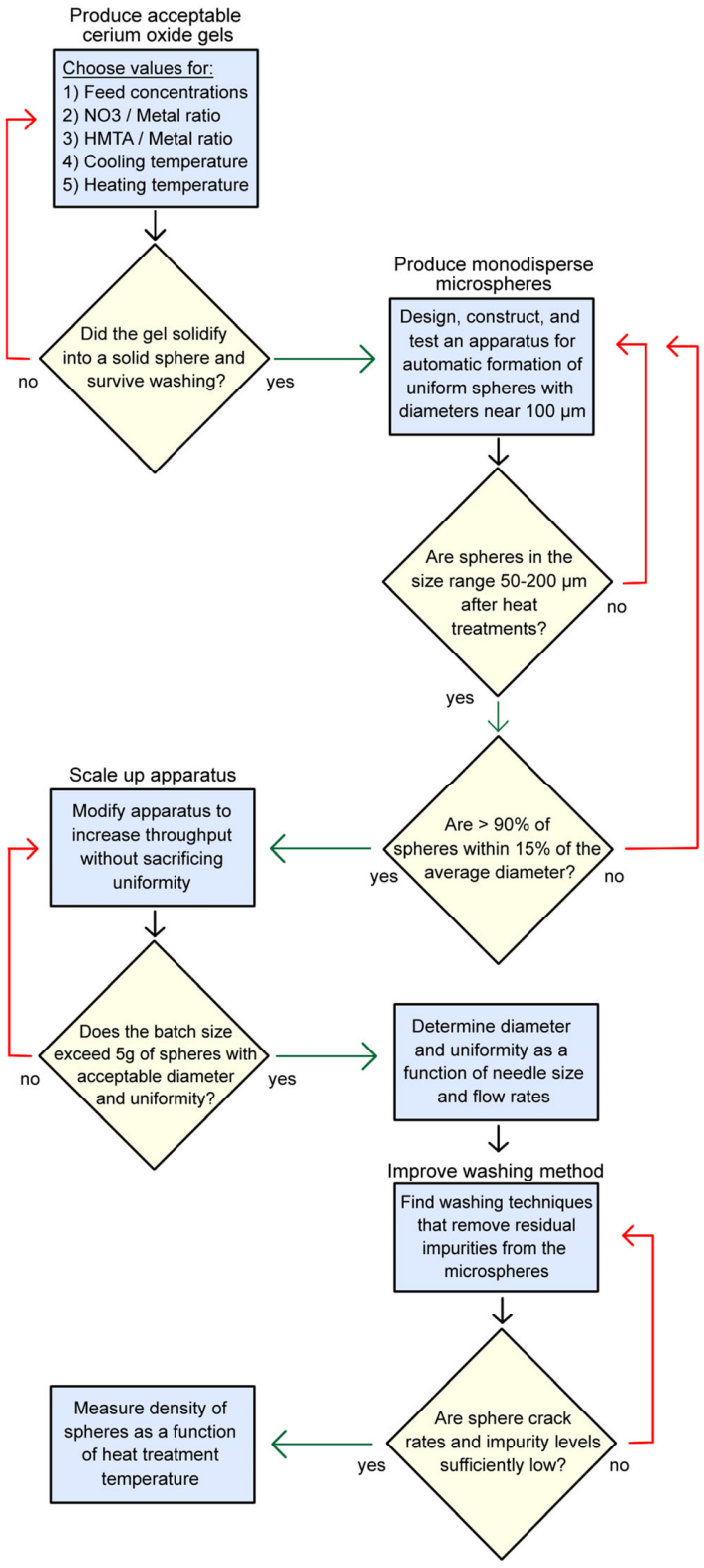

Figure 2.7: Thesis work included a variety of tasks with performance criteria

Chapter 3

Experimental Methods

"RPS technology has been a critical element in establishing and maintaining U.S. leadership in the exploration of the solar system. Continued attention to and investment in RPSs will enable the success of historic missions such as Viking and Voyager, and more recent missions such as Cassini and New Horizons, to be carried forward into the future."

- William W. Hoover, Ralph L. McNutt, Jr., Co-Chairs, Radioisotope Power Systems Committee

Development and demonstration of internal gelation sol-gel methods to produce microspheres as a replacement for powder-based granules used in Pu-238 oxide pellet fabrication is a multi-headed problem. For this reason, work with cerium surrogates encompassed a variety of tasks and experimental procedures to refine processes and equipment as well as subsequent material characterization to assess their effectiveness. The first section in this chapter will address evaluation of two cerium-based feed solutions and the optimization of reagent concentrations in mixed feed solutions to yield high-quality gels. Due to historic difficulties producing monodisperse microspheres in the desired size range, the next section overviews equipment developed for this purpose while communicating the difficulties encountered in the process and how they were overcome. The third section discusses an experiment performed to

test the capabilities of the final apparatus to produce monodisperse microspheres in the size range of interest. Since significant problems with microsphere cracking and fines generation were encountered, the fourth section presents an evaluation of a new washing technique to reduce impurities and prevent microsphere cracking. The last section discusses experiments performed to elucidate microsphere properties relevant to pressing pellets.

3.1 Cerium Gelation

To produce high-quality internal gelation microspheres, it is important to identify a suitable metal feed solution and combination of feed concentrations and ratios that cause fast gelation upon addition of heat. However, for the production of small microspheres at slow feed rates, mixed feed solutions must not gel prior to sphere formation and require active cooling. Processing parameters such as gelation times, feed ratios, and chemical concentrations also impact microsphere cracking due to their influence on crystal growth and shrinkage. Other critical values in the internal gelation process include the pH at which precipitation occurs in the metal nitrate feed solution and the pH of mixed feed solutions containing the metal nitrate, HMTA, and urea. To produce a metal oxide by internal gelation, the first step was to identify a cerium solution that did not precipitate when mixed with chilled HMTA and urea, but subsequently formed a solid gel upon heating. A metal nitrate solution was preferred to maintain similarity to established internal gelation chemistry and to prevent the addition of impurities such as chlorine or sulfur. Two cerium compounds were identified and assessed, cerium (III) nitrate and (cerous nitrate) cerium (IV) ammonium nitrate (ceric ammonium nitrate, or CAN).

3.1.1 Standard Method for Solution Preparation and Dish Washing

A standard method was developed for preparing feed solutions from stock reagents and deionized water to ensure consistency. Similarly, dishes were washed by a standard process

before experiments. Prior to handling reagents, glassware, Teflon-coated stir bars, and stainless steel tools were washed with Alconox residue-free cleaner, rinsed at least five times with deionized water for complete soap and mineral removal, dried, rinsed with acetone, and then kept dry in a glass oven at 140 °C. To prepare a solution, the necessary dishes were removed from the glass oven and allowed to cool on top of a fresh sheet of VWR International ultra-clean aluminum foil. A Mettler Toledo AL204 analytical scale with 0.1 mg resolution was calibrated using a 200 g standard mass until the scale read within 0.3 mg of 200 g. After successful calibration of the scale, a weighing boat was place on the scale and allowed to reach equilibrium before being tared. Reagents were then transferred to the weighing boat using a stainless steel spatula until the desired mass was obtained. Deionized water was added to the soluble powders in the weighing boat to facilitate pouring into a graduated cylinder without losing reagent due to static electricity. Weighing boats were rinsed 2-3 times into the beaker, which was subsequently adjusted to the desired volume using deionized water, taking care to rinse down any reagent stuck to the sides of the cylinder. A Teflon-coated stir bar was added to the graduated cylinder, which was placed on a magnetic stirrer until all reagents were fully dissolved, generally within 15 minutes. Solutions not used the same day as preparation were covered in foil for use the next day or transferred to a clean, air-tight vessel for storage.

3.1.2 Cerous Nitrate Gelation

Cerium (III) (cerous) nitrate hexahydrate dissolved in deionized water was the first cerium solution tested for suitability in the internal gelation process. It was a desirable as a feed material due to high solubility in water, commercial availability in a pure form, and since it would not introduce any additional bulk elemental impurities to the process.

Feed solution and chemicals

A 20 mL, 3 M solution of cerous nitrate was prepared by dissolution of cerous nitrate hexahydrate using the standard method for solution preparation. Cerous nitrate hexahydrate with a purity of 99.99% was obtained from Sigma Aldrich (lot # MKBF8706V). A solution with a concentration of 2.95 M in each HMTA and urea was also prepared using 99.7% urea from J.T. Baker (lot # J41628) and 99+% HMTA from Alfa Aesar (lot # 10149148). A complete listing of chemicals used for microsphere production is provided in Appendix A with their corresponding structural formulas, molecular formulas, and molar masses. The purity, supplier, and lot numbers are also provided for sol-gel feed reagents in Appendix A.

Gelation parameters

Separate samples of 3 M cerous nitrate and 2.95 M HMTA/urea in 25 mL round bottom flasks were chilled in jacketed beakers. The mixed feed vessel and jacketed beakers were all chilled with a water and ethylene glycol loop circulated by a Julabo FL601 chiller set to 0 °C. For each trial, 1 mL of chilled cerous nitrate was transferred to a cooled mixed feed vessel using a syringe and allowed to sit for a minute with stirring before adding the appropriate volume of chilled HMTA/urea solution. Trials were repeated to assess HMTA/Ce^{3+} ratios (R values) of 1.15, 1.45, 1.75, 2.05, 2.35, 2.65, 2.95, and 3.25. For each R value tested, a stopwatch was used to determine how long chilled mixed feed solutions were stable after mixing the two feed solutions. The time elapsed between mixing and a noticeable reaction was recorded. Reaction onset was recognized by a color change and increases in opacity and viscosity. Between each trial, the previously tested solution was disposed and the mixed feed vessel was cleaned by

rinsing three times with deionized water. The procedure can be summarized in the following list of steps:

1) Chill cerous nitrate and HMTA/urea solutions separately to 0 °C.
2) Use a clean syringe to transfer 1 mL chilled cerous nitrate to the mixed feed vessel with magnetic stirring.
3) Use a clean syringe to transfer the appropriate volume of HMTA/urea solution to the mixed feed vessel.
4) Start a stopwatch as soon as the HMTA/urea solution has been added.
5) Record the time a change in color begins to within 1-2 seconds.
6) Record the time the reaction stops to within 1-2 seconds.
7) Remove the mixed feed solution from the chilled vessel.
8) Rinse the mixed feed vessel and stir bar with three consecutive rinses of 25 mL deionized water.
9) Repeat procedure for the next trial and R value.

3.1.3 Ceric Ammonium Nitrate Gelation

Gelation studies were also performed using cerium (IV) (ceric) ammonium nitrate (CAN) since it also exhibits high solubility in water, is commercially available in a pure form, and does not introduce new bulk impurities to the process. Ceric ammonium nitrate was tested since it contains cerium in the +4 valence state and Ce^{4+} precipitates as a hydroxide at a pH of 2.65 in nitrate solutions, compared to Ce^{3+} which precipitates at a pH of 8.1 [200]. To assess the suitability of CAN to produce stable mixed feed solutions and solid gels, a series of gelation trials were performed to determine the effects of acid deficiency and R value. Although solutions can be made acid deficient by nitrate extraction, steam de-nitration, formic acid

addition, or ammonium hydroxide addition, the latter was chosen due to its simplicity and the pre-existence of ammonium in the cerium feed.

Feed solution and chemicals

The standard solution preparation method was used to make 100 mL of 1.675 M ceric ammonium nitrate (lot # A0331425) as well as 110 mL of 3.18 M HMTA/urea solution (from lot # SZBB2510V and lot # BCBD7141V, respectively). Ceric ammonium nitrate was divided into five, 20 mL samples and concentrated ammonium hydroxide was added to each to create varying degrees of acid deficiency, represented by OH^-/Ce^{4+} ratios of 0, 0.25, 0.5, 0.75 and 1.0. Each of the five acid-deficient CAN samples was further divided into five, 2 mL samples.

Gelation parameters

For each acid-deficient CAN solution, R values were varied from 1.5-2.5 at intervals of 0.25, resulting in 25 test cases. A summary of the trial conditions is shown in HMTA/urea solution, which was prepared using an analytical scale. Each trial was performed after rapid addition of the chilled HMTA/urea solution to the chilled cerium solution and mixing.

Table 3.1.

Gelation trials were performed in batches of five samples to accommodate chilling and sample preparation. Acid-deficient CAN samples and aliquots containing HMTA/urea were chilled to approximately 0 °C. Polypropylene centrifuge tubes with 15 mL capacity were used to hold CAN samples as well as prepared masses of HMTA/urea solution for each trial. HMTA/urea samples were cooled in an ice bath maintained at 0 °C while CAN solutions were chilled in jacketed beakers cooled by a Julabo chiller set to 0 °C. Since both OH^-/Ce^{4+} and $HMTA/Ce^{4+}$ ratios were being varied in the experiments, each trial required a unique quantity of

HMTA/urea solution, which was prepared using an analytical scale. Each trial was performed after rapid addition of the chilled HMTA/urea solution to the chilled cerium solution and mixing.

Table 3.1: Ceric ammonium nitrate gelation trials were performed by varying R values from 1.5-2.5 and OH^-/Ce^{4+} ratios from 0-1. Concentrations listed in the table represent values prior to mixing.

$HMTA/Ce^{4+}$ / OH^-/Ce^{4+}	**1.5**	**1.75**	**2**	**2.25**	**2.5**
0	[Ce] = 1.675 [OH] = 0 1.7790 g H/U V_T = 3.58 mL	[Ce] = 1.675 [OH] = 0 2.0754 g H/U V_T = 3.84 mL	[Ce] = 1.675 [OH] = 0 2.3719 g H/U V_T = 4.11 mL	[Ce] = 1.675 [OH] = 0 2.6684 g H/U V_T = 4.37 mL	[Ce] = 1.675 [OH] = 0 2.9649 g H/U V_T = 4.63 mL
0.25	[Ce] = 1.631 [OH] = 0.408 1.7317 g H/U V_T = 3.54 mL	[Ce] = 1.631 [OH] = 0.408 2.0203 g H/U V_T = 3.80 mL	[Ce] = 1.631 [OH] = 0.408 2.3090 g H/U V_T = 4.05 mL	[Ce] = 1.631 [OH] = 0.408 2.5976 g H/U V_T = 4.31 mL	[Ce] = 1.631 [OH] = 0.408 2.9649 g H/U V_T = 4.56 mL
0.5	[Ce] = 1.588 [OH] = 0.794 1.6869 g H/U V_T = 3.50 mL	[Ce] = 1.588 [OH] = 0.794 1.9681 g H/U V_T = 3.75 mL	[Ce] = 1.588 [OH] = 0.794 2.2492 g H/U V_T = 4.00 mL	[Ce] = 1.588 [OH] = 0.794 2.5304 g H/U V_T = 4.25 mL	[Ce] = 1.588 [OH] = 0.794 2.8115 g H/U V_T = 4.50 mL
0.75	[Ce] = 1.548 [OH] = 1.161 1.6444 g H/U V_T = 3.46 mL	[Ce] = 1.548 [OH] = 1.161 1.9184 g H/U V_T = 3.70 mL	[Ce] = 1.548 [OH] = 1.161 2.1925 g H/U V_T = 3.95 mL	[Ce] = 1.548 [OH] = 1.161 2.4666 g H/U V_T = 4.19 mL	[Ce] = 1.548 [OH] = 1.161 2.7406 g H/U V_T = 4.43 mL
1	[Ce] = 1.510 [OH] = 1.510 1.6039 g H/U V_T = 3.42 mL	[Ce] = 1.510 [OH] = 1.510 1.8713 g H/U V_T = 3.66 mL	[Ce] = 1.510 [OH] = 1.510 2.1386 g H/U V_T = 3.90 mL	[Ce] = 1.510 [OH] = 1.510 2.4059 g H/U V_T = 4.14 mL	[Ce] = 1.510 [OH] = 1.510 2.6732 g H/U V_T = 4.38 mL

Once mixed, samples were returned to the chiller for a minimum of 20 minutes. Stable, mixed samples were placed in an 85 °C bath containing water and ethylene glycol, shown in Figure 3.1. A stopwatch was started as soon as the sample was placed in the hot bath and the time of solidification was recorded. Samples typically reacted in under two minutes and were aged a total of ten minutes in the hot water bath before removing to a test tube rack to cool. The next

day, each sample was assessed for color, transparency, supernatant volume, pH, and rigidity. All evaluations were graded on a subjective scale except for pH, which was measured using a Thermo Scientific Orion Star A215 pH/conductivity meter calibrated with pH standards at 1.00, 4.01, 7.00, and 10.01. The procedure can be summarized in the following steps:

1) Prepare a 600mL hot water/ethylene glycol bath in a large, insulated beaker on a hot plate with the feedback thermocouple installed and set to 85 °C. Verify the temperature with an additional thermometer.
2) Place 2 mL of the appropriate acid-deficient CAN solution in each of five, 15 mL centrifuge vials and place in the jacketed beaker to cool.
3) Calibrate the analytical scale. Use the analytical scale to mass out HMTA/urea solution into five 15 mL centrifuge vials with masses corresponding to the acid deficiency and R values being tested.
4) Place the vials containing HMTA/urea in the ice bath to cool. Verify the temperature with a thermometer.
5) After all samples have cooled for at least 20 minutes, use a pipet to transfer the HMTA/urea into the corresponding acid-deficient CAN vial and agitate. Return to the chilling beaker.
6) Repeat step five for the remaining samples in the batch.
7) Once the batch of mixed samples have chilled for at least 20 minutes, remove one sample at a time and rapidly transfer to the hot water bath.
8) Start a stopwatch.
9) Hold the sample so that the liquid level in the bath and the vial are even and agitate until a color change or solidification is observed.

10) Record the times of color change and solidification.

11) Allow the sample to remain in the hot water bath for 10 minutes to cure.

12) Transfer the sample to a test tube rack to cool and tighten the screw cap for storage.

13) Repeat steps 7-12 for the remaining samples in the batch. Once a batch is complete, line up the samples and take a picture to compare color and consistency.

14) Repeat steps 2-13 for the remaining CAN solutions at different acid deficiencies.

15) The next day once all the samples have cooled and aged, make a visual assessment of the color, transparency, supernatant volume, and rigidity (using a spatula).

16) Calibrate the pH meter and obtain a pH measurement on each of the gelled samples. Rinse the pH probe clean with deionized water between each measurement.

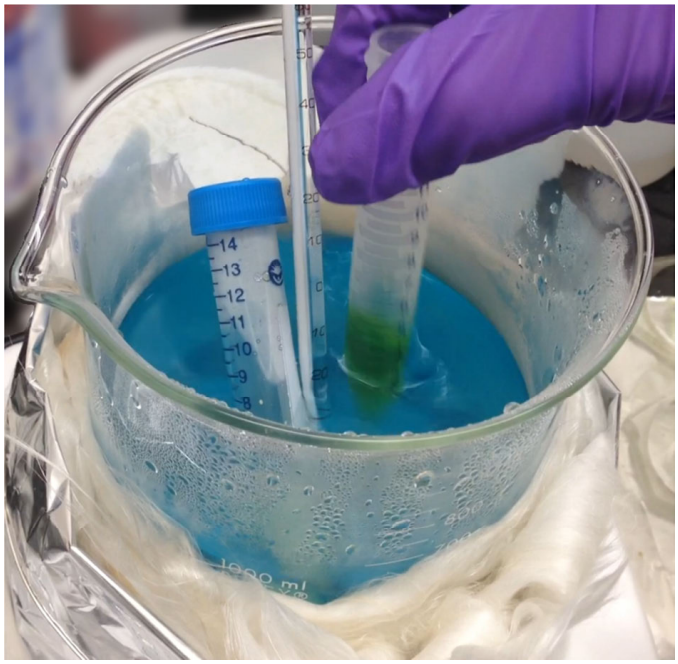

Figure 3.1: The gelation time was determined by heating freshly mixed feed solutions in an 85 °C bath with rapid agitation.

3.2 Construction and Scale-Up of a Sol-Gel Rig

A time-consuming effort was undertaken to develop an apparatus to fabricate gram-quantities of uniform cerium oxide microspheres using the optimal parameters obtained from gelation trials. Since no equipment existed at the onset of thesis work, initial efforts were very simple to test aspects of internal gelation systems described in the literature. Over time, modifications were made to prevent premature gelation, avoid needle clogging, increase throughput, and improve monodispersity.

3.2.1 Preliminary Setup

Internal gelation methods and equipment presented in the literature guided preliminary development of sol-gel hardware. To form spheres from mixed feed solutions, a long column filled with hot oil was needed. Therefore, a jacketed glass column was obtained from Chemglass and a Julabo F-25 refrigerated/heating circulator was acquired. The heater provided temperature control with a resolution of 0.1 °C and circulated Julabo Thermal C20S silicone oil for heat transfer to the jacketed column. An excess NIM electronic rack was re-fashioned to hold equipment for the sol-gel experiments, as shown in Figure 3.2. In addition to a shelf at the midpoint, a large aluminum stand was machined to accommodate the jacketed column using ring stand clamps. The jacketed column was filled with Xiameter PMX-200, 100 cS silicone oil obtained from Neely Industries LLC, which was stagnant in early work. A series of stopcocks at the bottom of the column allowed for sphere collection at the end of a run after the oil had been cooled back to room temperature.

Prior to the ceric ammonium nitrate gelation trials, initial sphere-forming runs were conducted using cerous nitrate solutions to generally assess the relationship between feed parameters, sphere size, forming column temperature, and mixed feed solution temperature. In one test, the Julabo heater was varied from 80-125 °C while maintaining a constant R value to

determine the necessary operating temperature for gelation. Another experiment compared the use of a 20 gauge needle to a 30 gauge needle using chilled and un-chilled mixed feeds. Once small batches of spheres could be produced, the effects of washing with acetone and 2M NH_4OH with subsequent drying and heating to 600 °C in a box furnace were investigated. Procedures for three preliminary, educational experiments are summarized below.

Temperature requirement:

1) Prepare separate solutions of 3 M cerous nitrate and 2.95 M HMTA/urea using the standard solution preparation procedure.
2) Fill the inner portion of the jacketed column to the top with PMX-200 silicone oil.
3) Set the Julabo heater to 80 °C, 90 °C, or 100 °C, depending on the measurement.
4) Prepare a fresh syringe with a new 30 gauge needle.
5) Once the column is at the desired temperature, mix 1-2 mL of the feed solutions with an R value = 1.8.
6) Transfer the mixed feed solution to the syringe.
7) Tap the syringe on the top of the heated column to form droplets in the column.
8) Record the height in the column where a transparent to opaque transition occurs.
9) Once 50-100 spheres have been formed, cool the oil to room temperature.
10) Extract the spheres from the column using the stopcocks to minimize oil loss.
11) Photograph the recovered spheres.
12) Repeat steps 3-11 for the remaining temperature cases.

Needle clogging:

1) Prepare separate solutions of 3 M cerous nitrate and 2.95 M HMTA/urea using the standard solution preparation procedure.
2) Fill the inner portion of the jacketed column to the top with PMX-200 silicone oil.
3) Set the Julabo heater to 100 °C.
4) Chill half of each feed solution to -2 °C.
5) Prepare two fresh syringes, one with a 20 gauge needle and the other a 30 gauge needle.
6) Mix room temperature feed solutions with an R value = 1.0 and transfer 1 mL into a syringe.
7) Using the 20 gauge needle, tap needle at the top of the column to form spheres until the feed solution gels in the syringe. Note the apparent sphere size, residence time in column, and location of opacity change.
8) Repeat steps 6-7 using the 30G needle.
9) Repeat steps 5-8 using the chilled feed solutions and note any differences in the results.

Washing and heating:

1) Prepare separate solutions of 3 M cerous nitrate and 2.95 M HMTA/urea using the standard solution preparation procedure.
2) Fill the inner portion of the jacketed column to the top with PMX-200 silicone oil.
3) Set the Julabo heater to 100 °C.
4) Chill each feed solution to 5 °C.
5) Once the oil in the column is at 100 °C, mix the chilled feed solutions with an R value = 1.8 and transfer to a fresh syringe with 30 gauge needle.

6) Tap the needle at the top of the column to produce spheres until the feed is gone or gels in the syringe.
7) Cool the silicone oil back to room temperature.
8) Extract spheres using the stopcocks and decant excess silicone oil off from the spheres.
9) Wash spheres with acetone to remove silicone oil and note effects.
10) Wash spheres with 2 M NH_4OH as a curing step and note effects.
11) Dry washed spheres with flowing nitrogen gas.
12) Heat dried spheres to 100 °C, 250 °C, and 600 °C with 2.5 hour dwells and 2 °C/min ramp rates, cooling and removing spheres after each dwell to observe the effects under an optical microscope.

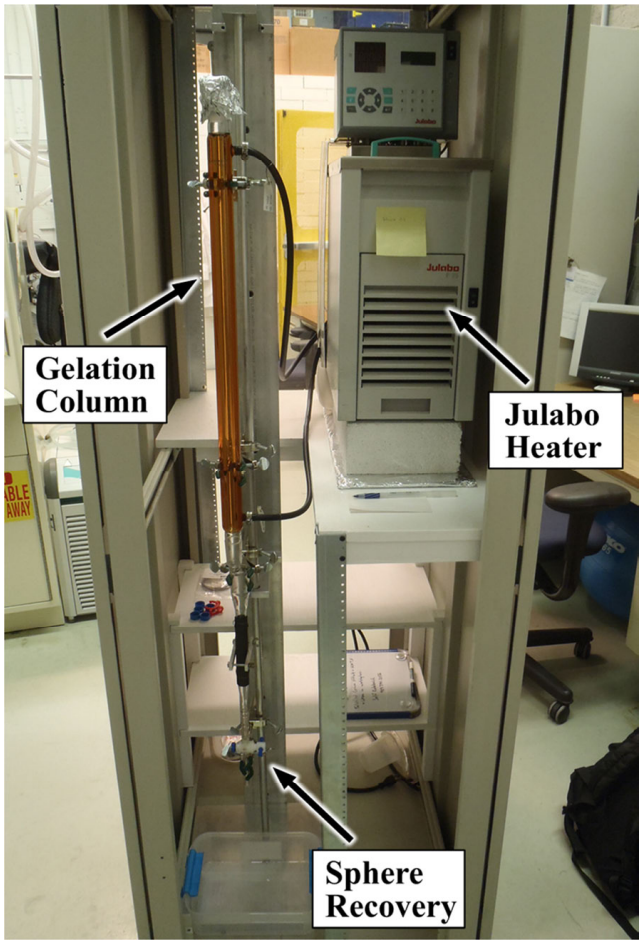

Figure 3.2: An electronics rack was reconfigured to house the sol-gel apparatus. The heater/circulator (right) and gelation column (left) are critical for microsphere gelation.

3.2.2 Automated Sphere Production

To produce gram quantities of microspheres with uniform diameters, development of an automated droplet forming device was necessary. While most systems described in the literature used vibration-assisted feed jet breakup, these systems had proven unattractive for production of microspheres in the current size range of interest. Therefore, droplet forming devices were modeled after systems published in the field of microfluidics, whereby shear forces from a viscous, continuous phase strip feed droplets off a dispensing needle as they are formed in a co-axial configuration. Such devices have been built to use emulsion or UV photopolymerization to

create spheres with diameters in the range of interest [201,202]. In addition to the development of a sphere dispersion apparatus, additions were made to the system to provide chilling of mixed feed solutions and feed transfer lines and pneumatic transfer of feed to the needle.

Development of a successful sphere forming device required several iterations before multi-gram batches could be processed without needle clogging. Initially, a co-axial two-fluid nozzle was fabricated using a quarter inch stainless steel Swagelok tee fitting. The concept was tested using water in place of feed solution in a graduated cylinder full of oil, shown in part A of Figure 3.3. While the initial demonstration device dispersed feed using $1/16^{th}$ inch stainless steel tubing, modifications were made to integrate a two-inch McMaster Carr stainless steel needle, shown in parts B and C of Figure 3.3. This setup allowed for the exchange of new needles or needles with different diameters. Using the tee apparatus, feed was dispersed from the needle into a narrow Teflon channel where silicone oil, which entered from the side of the tee, stripped off droplets. The tee device mated to the top of the column using a threaded, o-ring seal. The Teflon insert extended into a laminar region of flow in the column, away from in-flowing oil at the top of the column, to prevent microsphere agglomeration and coalescence.

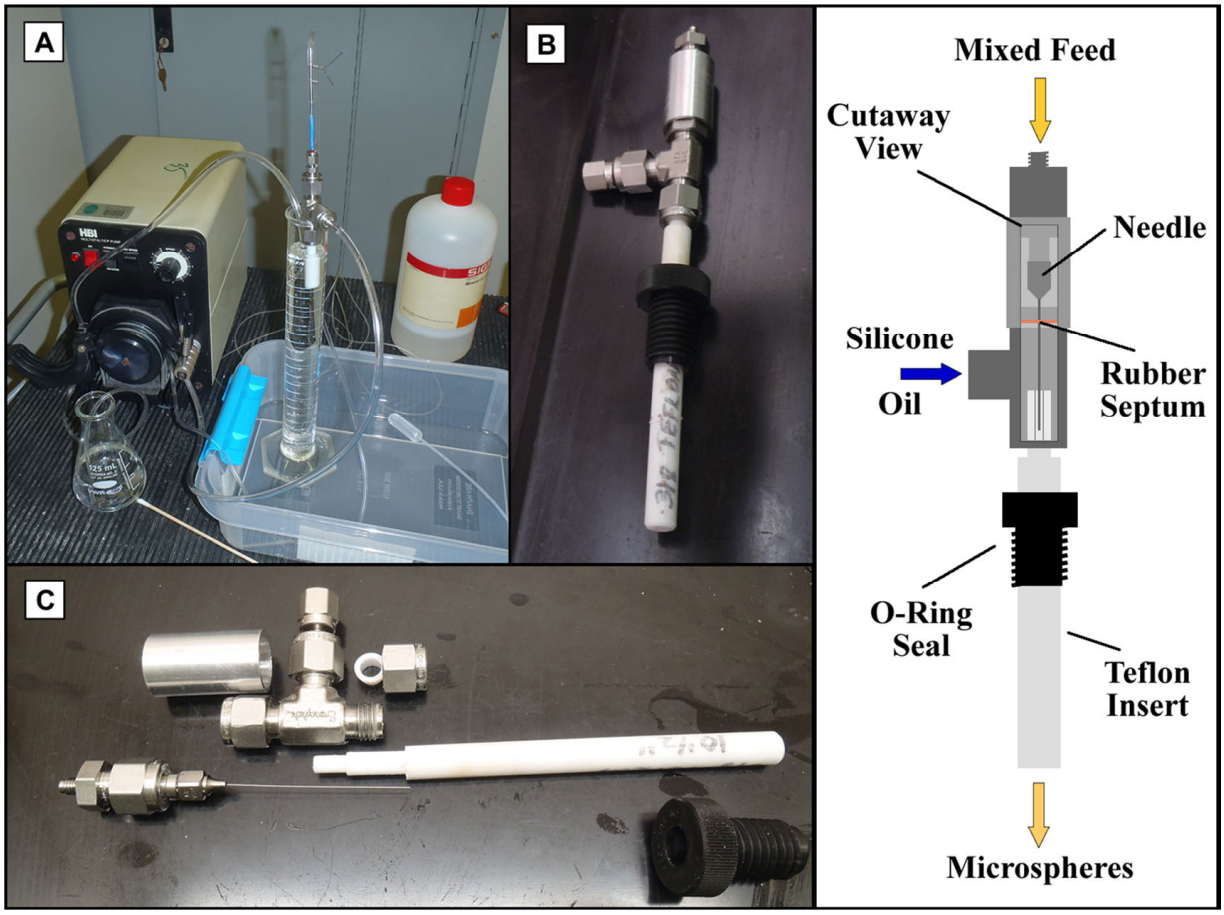

Figure 3.3: An initial microsphere dispersing device was based on a two-inch stainless steel needle, a modified Swagelok tee, and a Teflon insert.

Several additions to the sol-gel column accommodated automated microsphere production. First, a jacketed chill vessel, shown in Figure 3.4, was machined from stock acrylic, aluminum, and a Swagelok 1-inch tube adapter to straight-thread, O-ring seal. Feed-through lines for air supply, feed solution injection, and feed transfer to the needle were sealed into a machined aluminum plug, which was swaged in place. An overpressure of a few psi was applied to the mixed feed vessel using a nitrogen gas tank via a 6-foot manometer to prevent pressure spikes. A Julabo FL-601 chiller was also added to the electronics bin to chill the feed solutions and transfer lines, as shown in Figure 3.5. A schematic of the sol-gel apparatus is provided in Figure 3.6. Jacketed beakers were also installed on top of magnetic stirrers for chilling feed

solutions prior to mixing. Insulated tubing was used to complete a chill loop from the jacketed beakers to the mixed feed vessel and copper tubing was run along feed transfer lines for cooling. An impeller pump was used to transfer oil into the tee for sphere stripping and throttled using a needle valve. A peristaltic pump was also installed to transfer oil from the bottom of the column and re-introduce it at the top, creating slow, laminar flow through the column.

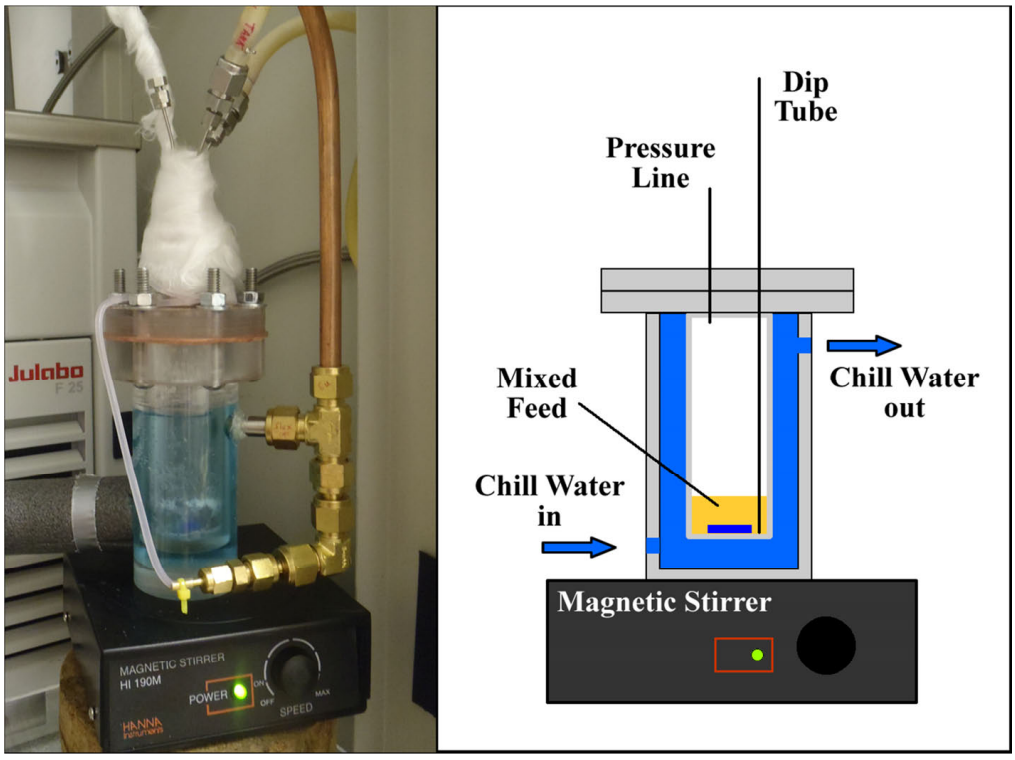

Figure 3.4: A jacketed mixed feed vessel allowed for magnetic stirring, effective chilling, and pneumatic transfer of feed to the needle.

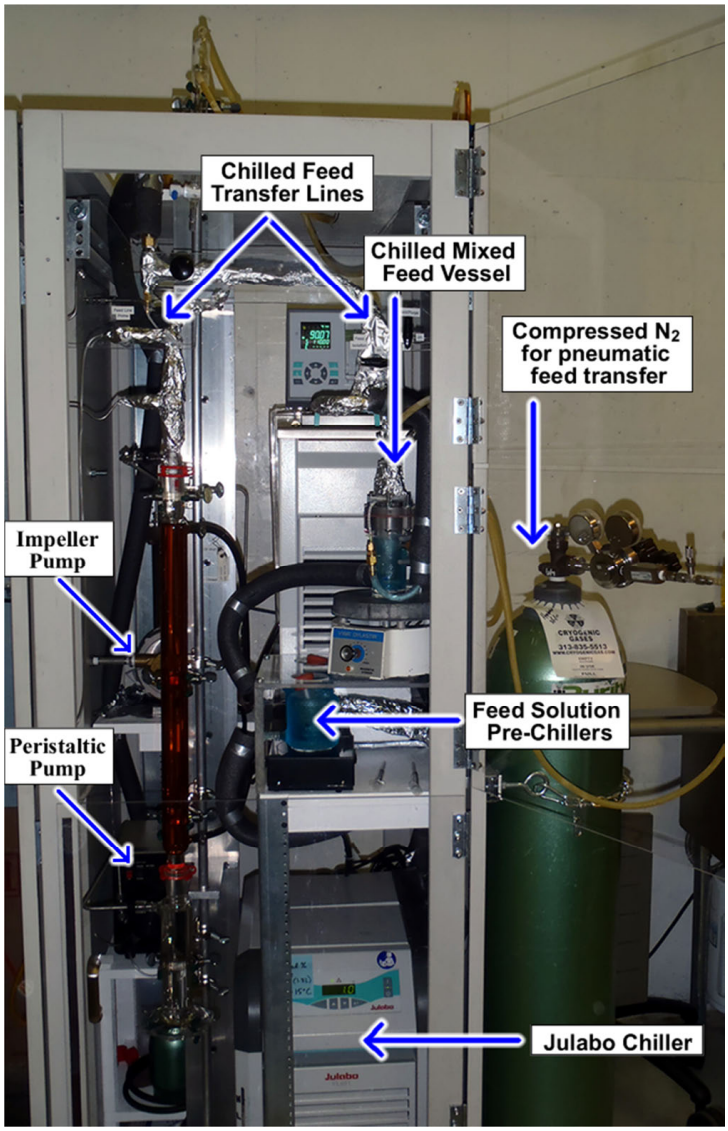

Figure 3.5: Automated sphere production was attained by the addition of chilling systems, hot oil circulation, and a pneumatic feed transfer system.

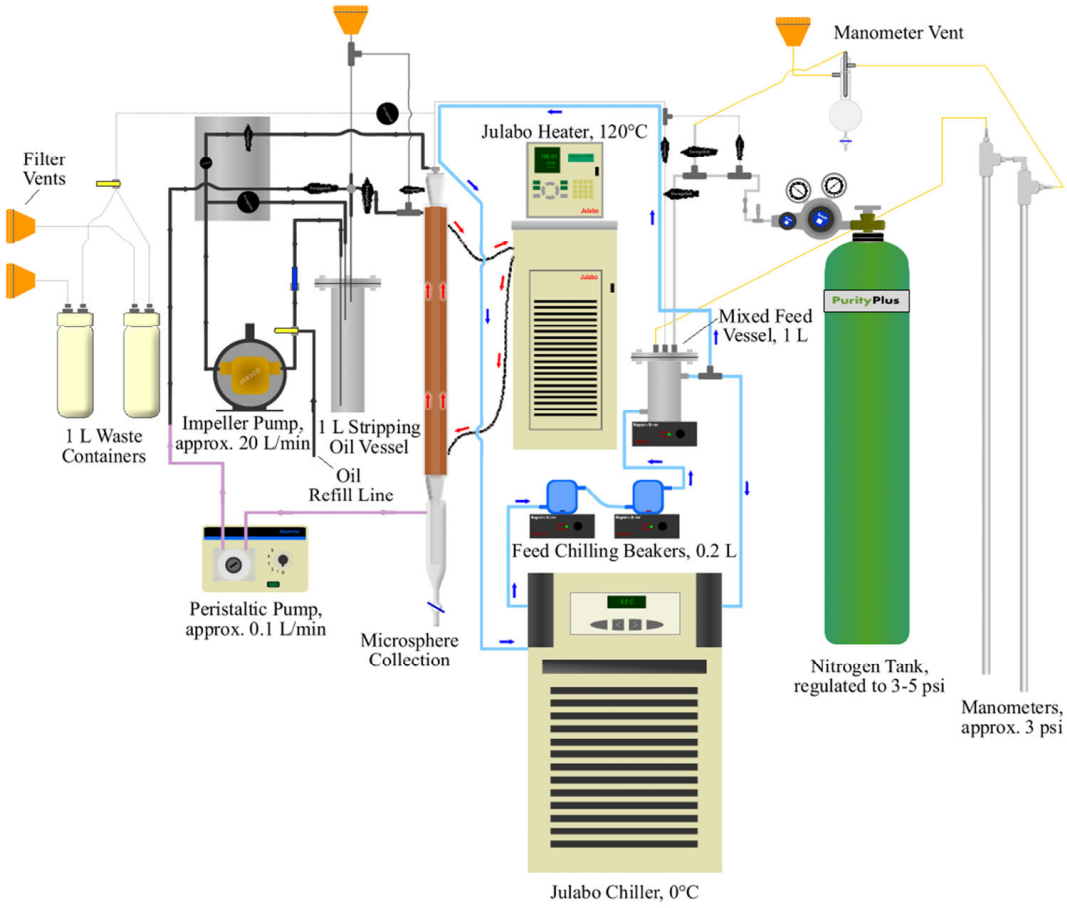

Figure 3.6: Fabrication of internal gelation microspheres required active heating and cooling, pneumatic feed solution transfer and silicone oil pumps.

With additional hardware for automated sphere production installed, experiments were performed to optimize operating parameters and procedures. To determine desirable flow rates for the feed, stripping oil, and column oil and produce a batch of spheres suitable for washing and drying experiments, the following experiment was performed:

1) Prepare 1.53 M ceric ammonium nitrate and 3 M HMTA/urea by the standard solution preparation procedure. Add concentrated ammonium hydroxide to the CAN solution for an OH^-/Ce^{4+} ratio equal to one.
2) Chill feed solutions to 0 °C.
3) Set the Julabo heater/circulator to 75 °C.

4) Heat 100 mL of silicone oil in a dish to 70 °C on a hot plate.
5) Install a 28 gauge needle in the sphere forming apparatus.
6) Start the impeller pump to begin oil flow past the needle.
7) Once chilled, mix 3 mL of acid-deficient CAN with 2.8 mL HMTA/urea solution in the mixed feed vessel corresponding to R = 2.
8) Apply pressure to the manometer (and thus the mixed feed vessel).
9) Begin sphere production by opening the feed shutoff valve.
10) Adjust the stripping oil flow rate using the needle valve to produce spheres of the desired size and record the setting.
11) Adjust the peristaltic pump flow rate to achieve laminar sphere flow with minimal microsphere spacing and record the setting.
12) Modify flow rates as necessary to improve monodispersity and limit coalescence and agglomeration.
13) Monitor progress until all the feed has been converted to microspheres.
14) Close the feed shutoff valve, depressurize the mixed feed vessel, turn off pumps, and turn off the Julabo heater.
15) Inject deionized water into the mixed feed vessel, rinse, re-pressurize, and transfer fluid to waste vial. Repeat.
16) Once oil is cool, recover spheres from the system and decant off excess silicone oil.
17) Wash microspheres:
    a. Transfer spheres to a mesh sieve held in a glass dish and wash with 40 mL 50% isopropyl alcohol, 50% 0.5 M NH_4OH for 10 minutes. Decant effluent to waste and repeat.

b. Wash with 40 mL 0.5 M NH_4OH for 30 minutes. Decant effluent to waste and repeat.
c. Wash with 40 mL 75% isopropyl alcohol, 25% deionized water for 10 minutes. Decant effluent to waste and repeat.

18) Dry spheres with flowing nitrogen gas.
19) Place spheres in a box furnace to dry at 80 °C for two hours then remove to cool and photograph.
20) Place spheres in a box furnace at 150 °C for three hours then remove to cool and photograph.
21) Replace spheres in a box furnace at 150 °C, heat to 300 °C for five hours, and remove to cool and photograph.

With additional operational experience, it became obvious that needle clogging was a primary barrier to sustained microsphere production. For this reason, additional droplet forming devices were designed to facilitate needle replacement and prevent clogging. Custom glassware was designed and built to simplify needle replacement. A prototype system is pictured in part A of Figure 3.7 while the final design is shown in part B of Figure 3.7. The glass-Teflon device provided a narrow port at the top to align the two-inch-long needle in the center of the sphere-stripping channel. Based on continued needle clogging issues, McMaster Carr stainless steel needles were discarded and custom, half-inch-long, stainless steel needles from the Hamilton Company were used in conjunction with a new, aluminum-Teflon sphere forming device shown in Figure 3.8. The aluminum-Teflon apparatus was designed to reduce the needle length from two inches to a half inch. The aluminum section allowed the needle to be cooled during

operation while the Teflon insert created a narrow region for droplet stripping. Similar to previous designs, Teflon extended down into the column to avoid exposing aqueous drops to turbulent flow.

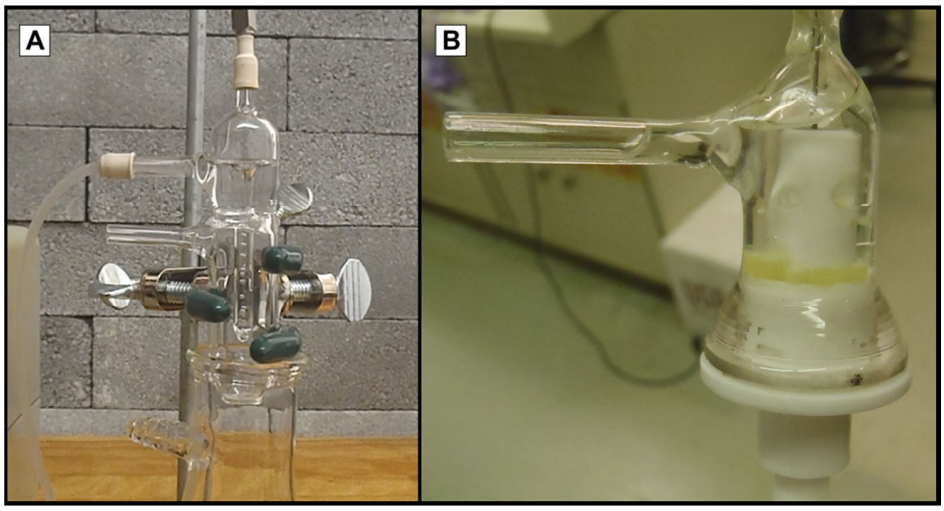

Figure 3.7: Custom glassware was designed for droplet formation to facilitate easy needle replacement and "hot-swapping" during runs.

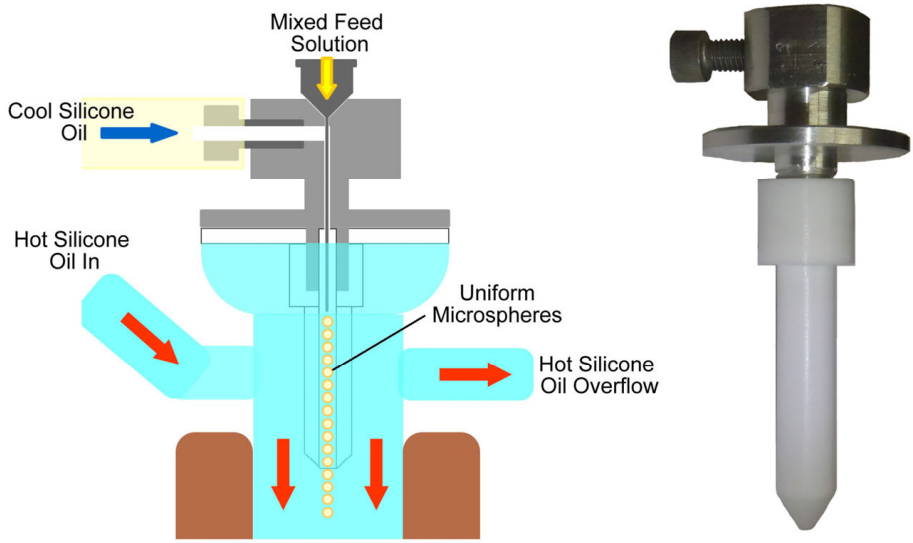

Figure 3.8: An aluminum-Teflon sphere forming apparatus allowed for much shorter needles to be used and also facilitated needle cooling.

3.2.3 Scaled-Up Production of Monodisperse Microspheres

Significant modifications were made to the sol-gel apparatus to improve throughput and microsphere monodispersity. Additionally, instruments were added to improve the control and reproducibility of experimental parameters.

Improved reproducibility:

Hardware improvements allowed optimal processing parameters to be recorded, varied, and repeated in subsequent runs. Changes included:

1) Adjustable pressure for pneumatic feed transfer with digital gauge:

   Manometers used to regulate pressure on the mixed feed solution were removed in favor of direct pressure from the nitrogen tank applied using a two-stage regulator, needle valve, and digital pressure gauge with 0.1 psi resolution. A pressure relief valve was installed in the pressurized gas line and set to 6 psi to prevent excessive pressurization of the system.

2) Chilling, pneumatic transfer, and flow rate measurement of stripping oil:

   The impeller pump providing stripping oil to the droplet forming device was removed and replaced with a sealed, stainless steel reservoir, shown in Figure 3.9. The chilling loop for the sol-gel rig was extended and passed through the stripping oil reservoir. Stripping oil was cooled before pneumatic transfer to the sphere-forming apparatus to avoid temperature-induced gelation of feed in the needle. A second regulator was attached to the compressed nitrogen tank to provide an overpressure to the stripping oil reservoir to drive flow. The stripping

oil flow rate was controlled using the nitrogen overpressure and an in-line needle valve. Flow rate measurements were obtained by calibrating a Sensirion hydrocarbon flow meter, which output a voltage to a digital display. A schematic of the gas pressure system is provided in Figure 3.10.

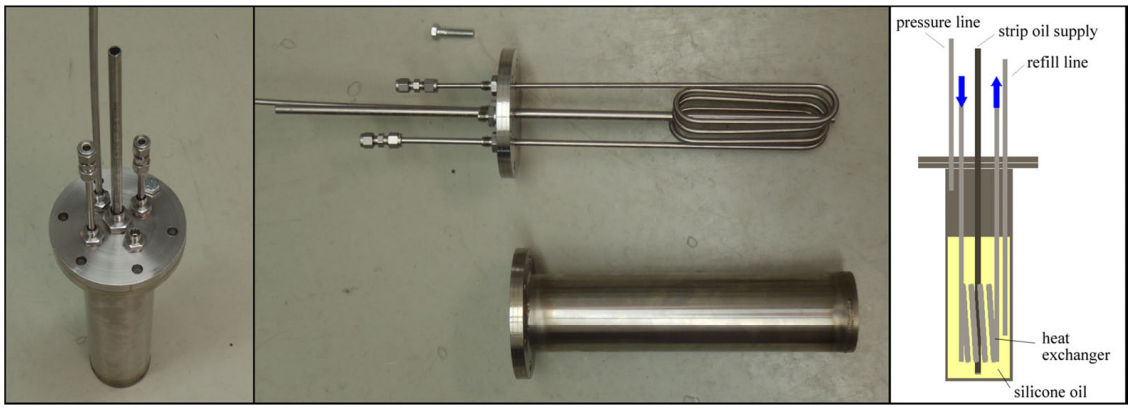

Figure 3.9: A stainless steel vessel was machined to accommodate cooling and pneumatic transfer of stripping oil.

3) Installation of thermocouples on the jacketed chill beakers, silicone oil pre-heater, and silicone oil exiting the gelation column.
4) Use of a Thermo Scientific Orion Star A215 pH/conductivity meter with an Orion four-electrode conductivity probe to monitor the conductivity of ammonium hydroxide and deionized water wash effluents.

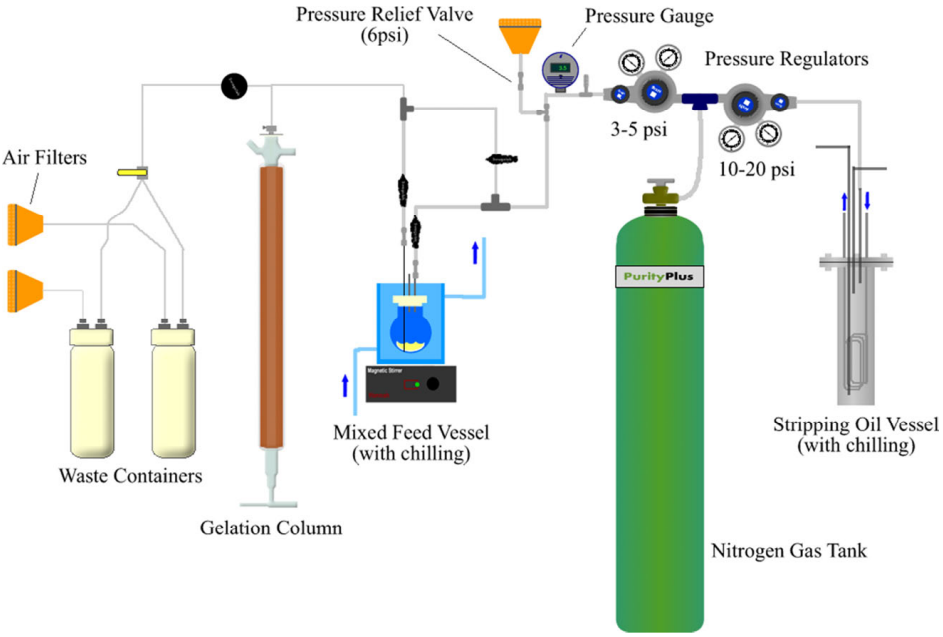

Figure 3.10: An overpressure of nitrogen gas was used to provide uniform flow of mixed feed solutions and stripping oil to the sphere forming apparatus.

Increased throughput:

As more material was processed in a single run, modifications were necessary to accommodate longer runs and prevent mixed feed solidification in transfer lines and needles. Major changes included:

1) Installation of a chilled copper block to cool feed transfer and waste transfer lines, shown in Figure 3.11.
2) Fabrication of a stainless steel mixed feed vessel for chilling large batches, also pictured in Figure 3.11.
3) Replacement of the stainless steel mixed feed vessel with glassware and Swagelok quick-connects, shown in Figure 3.12. Quick-connects allowed for easy removal for cleaning to ensure the elimination of particulates that cause needle clogging. The glass mixed feed

vessel was chilled using a 2 L jacketed beaker. The new chilling loop, copper block, and mixed feed vessel are shown in a schematic in Figure 3.13.

4) Replacement of the sphere collection glassware with serpentine tubing, a conical mesh, and glass vessel, shown in Figure 3.14.

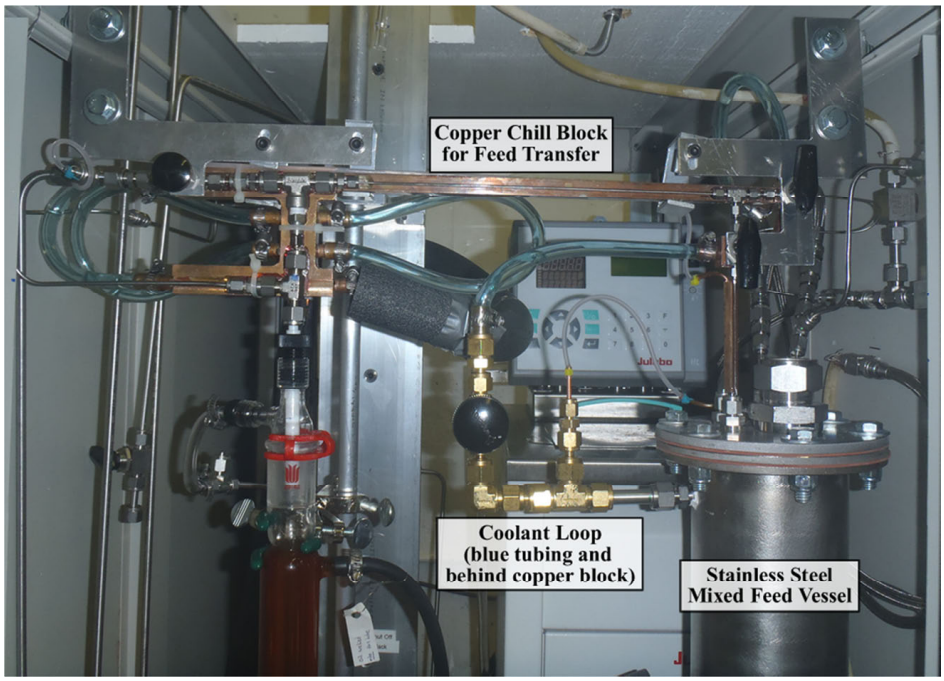

Figure 3.11: A chilled copper block was installed to prevent gelation in mixed feed transfer lines. A stainless steel mixed feed vessel was also machined for cooling large batches.

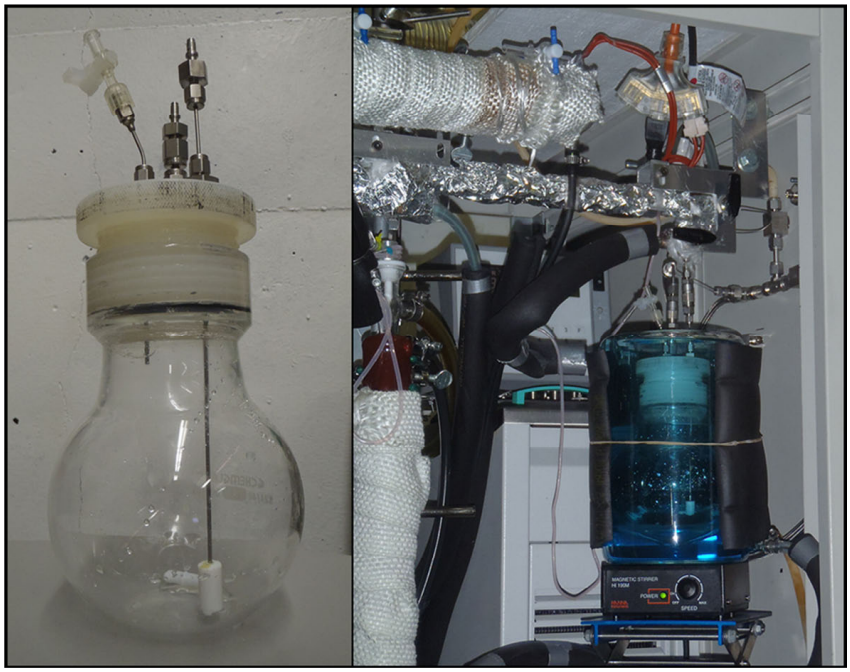

Figure 3.12: Custom glassware sealed with a nylon plug with feedthroughs was fabricated to ease removal and cleaning.

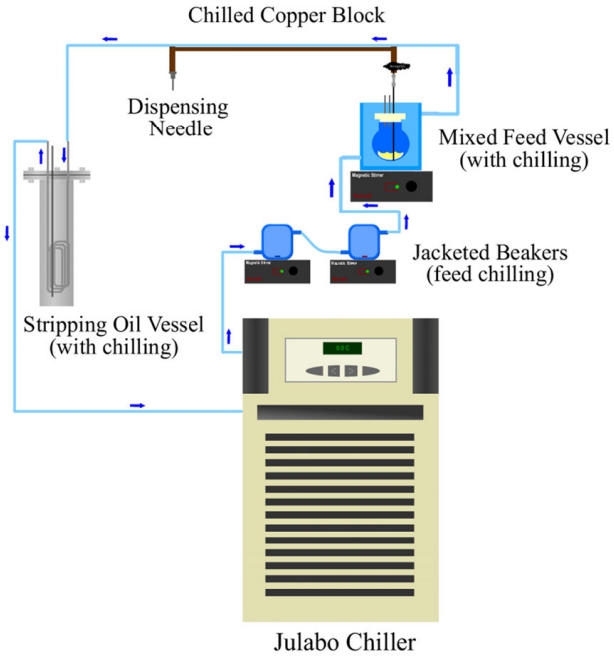

Figure 3.13: A single chilling loop was used to cool feed solutions, feed transfer lines, stripping oil, and the sphere forming apparatus.

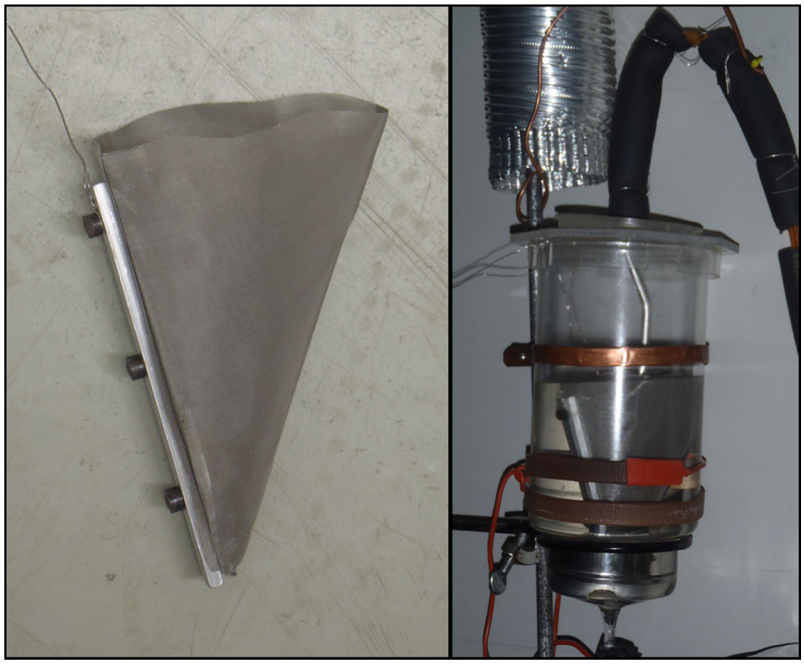

Figure 3.14: After exiting the column, microspheres pass through serpentine tubing and collect in a conical mesh basket.

Improved monodispersity:

Additional hardware revisions increased the oil temperature in the gelation column, increased the flow rate of oil through the gelation column, and prevented gas bubbles from forming in the gelation column. Modifications to improve monodispersity included:

1) Increasing the silicone oil temperature at the entrance to the gelation column where newly-formed spheres are introduced. An oil pre-heater was installed above the column, as shown in Figure 3.15.
2) Use of peristaltic pumps to circulate hot silicone oil through the gelation column and the serpentine tubing at the bottom of the column at prescribed rates.

3) Removal of dissolved gas in the silicone oil using an ultrasonic bath. A schematic showing the silicone oil flow path, oil pre-heater, microsphere collection, and ultrasonic bath is provided in Figure 3.16.

4) Replacement of long, blunt-end needles with ½ inch, tapered-end needles.

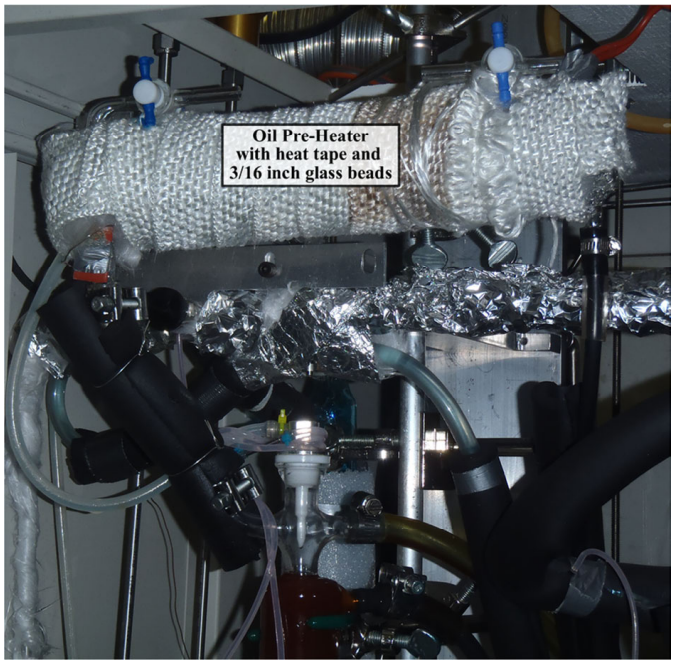

Figure 3.15: A glass tube wrapped with a 156-watt heat tape pre-heated oil before it entered the gelation column.

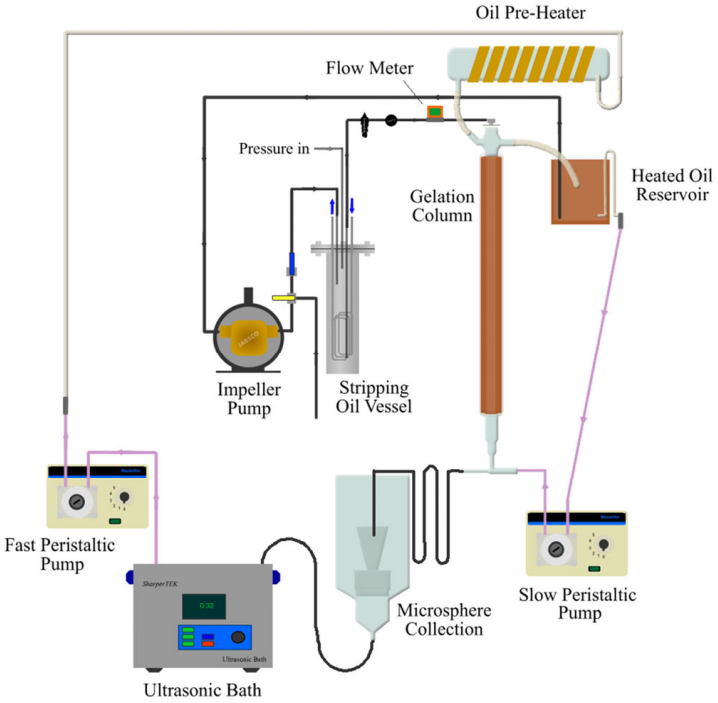

Figure 3.16: Silicone oil drained into the gelation column under the influence of gravity while pumps were used to remove spheres from the column and transfer oil from the bottom collection vessel to the oil pre-heater above the column.

With modifications to the sol-gel rig complete, a run was performed to assess the changes in throughput and monodispersity. Additionally, the system was monitored for signs of premature gelation and the formation of undesirable satellite drops along with microspheres. The process for a day-long sphere production experiment is provided below:

1) The day before an intended sol-gel production run, prepare 25 mL of 1.675 M ceric ammonium nitrate and 27 mL of 3.18 M HMTA/urea using the standard solution procedure.
2) Once the CAN is dissolved, add sufficient concentrated ammonium hydroxide to achieve an OH^-/Ce^{4+} ratio of 0.75. Break up precipitates if necessary, cover both the CAN

solution and HMTA/urea solution with foil, and continue magnetic stirring overnight in a fume hood.

3) The morning of a sol-gel run, turn the Julabo chiller on and set to -1 °C.
4) While the system is cooling, wash the glass mixed feed vessel and mesh cone via the standard washing procedure. Once dry, install the mesh cone in the sphere collection vessel and transfer the mixed feed vessel to the fume hood.
5) Transfer 25.8 mL of the acid deficient CAN into the mixed feed vessel, add a Teflon-coated stir bar, seal the nylon plug lid, and install in the sol-gel apparatus to cool.
6) Transfer the HMTA/urea solution to a clean 25 mL round bottom flask and place in a jacketed beaker to cool.
7) Once the feed solutions have been cooling for at least an hour, turn on the Julabo heater/circulator to 120 °C.
8) Turn on peristaltic pumps to begin oil circulation.
9) Turn on electric heat tapes.
10) Pressurize the stripping oil reservoir to 15 psi.
11) Use a syringe to transfer 25.1 mL HMTA/urea solution into the mixed feed vessel, adding drops slowly while mixing with a magnetic stir bar.
12) Once the silicone oil at the column outlet has reach 80 °C, pressurize the mixed feed vessel to 3.5 psi.
13) Install a new needle in the sol-gel apparatus.
14) To begin the run, open the mixed feed shutoff valve and open the stripping oil shutoff valve.

15) Once spheres begin entering the column, adjust the stripping oil to a flow rate near 4 mL/min and adjust the pressure on the mixed feed vessel to modify microsphere spacing. Record optimal operating parameters.
16) Monitor the gelation column, mixed feed pressure level, and stripping oil flow rate to avoid drift in processing parameters.
17) Add 100 mL of silicone oil to a glass dish on a hot plate set to 85 °C.
18) Once the feed solution has all been converted to microspheres, turn off the heaters, pumps, and depressurize the stripping oil reservoir and mixed feed vessel.
19) Uninstall the needle and use tubing to connect the needle port to the waste container. Examine the needle for signs of blockage or clogging.
20) Wash the mixed feed vessel and lines:
    a. Add 50 mL of 1 M nitric acid to the mixed feed vessel and apply nitrogen pressure to rinse out the feed transfer lines and needle connection.
    b. Add 50 mL of chilled deionized water to the mixed feed vessel and apply nitrogen pressure to rinse out the feed transfer lines and needle connection. Repeat.
21) Remove spheres and the mesh cone from the sol-gel apparatus and empty spheres into a stainless steel mesh submerged in the silicone oil on the hot plate.
22) Allow spheres to cure in the hot oil for 20 minutes and then remove, cover with foil, and let cool in the fume hood overnight.
23) The next day, calibrate the conductivity meter with standards at 1.413 mS/cm and 12.9 mS/cm.
24) Decant oil from the microspheres and wash with TCE, 50% isopropyl alcohol/50% 0.5 M NH_4OH, and 0.5 M NH_4OH.

25) Once the conductivity of NH_4OH effluent is below 1000 μS/cm, rinse with deionized water and transfer to an autoclave.
26) Add 110 mL deionized water to the spheres in the autoclave, record the solution conductivity, seal the autoclave, and place in a 200 °C oven for two hours. After removing, allow to cool overnight.
27) The next day, measure the conductivity of the solution in the autoclave, rinse spheres with fresh deionized water, transfer to a clean alumina dish, and loosely cover with foil to dry.

Effect of curing time

An additional experiment was performed to determine the effect of microsphere residence time in silicone oil at 85 °C. An aging step appears to have been adopted into baseline internal gelation processes as a result of an early, definitive report stating uranium oxide microspheres formed in 60 °C TCE required a minimum aging time of 20 minutes in 60 °C TCE at the end of each run to prevent cracking [42,43,188]. A later study found that curing gelled spheres in hot silicone oil results in crystallite growth and limited crystallization of amorphous material [192]. Crystallite growth would be expected to increase the pore network, reducing cracking by improved impurity extraction during washing operations and providing an escape route during heat treatments. While aging steps in the baseline process lasted 20-30 minutes, spheres produced in typical sol-gel runs for 100 μm microspheres in the current work dwell in heated silicone oil for periods of time up to four hours prior to aging 20 minutes and washing. Therefore, seven batches of spheres were collected in small mesh baskets over sequential 20

minute intervals and transferred to 85 °C oil for time periods of 0, 40, 80, 120, 160, 200, and 240 minutes.

Each batch was washed separately with fixed wash volumes. Effluents from the first and second washes with 0.5 M ammonium hydroxide were saved and their conductivity measured. As in the previously described experiment, 1.675 M ceric ammonium nitrate and 3.18 M HMTA/urea were used with an R value of 2.0 and acid deficiency ratio of 0.75. Sphere formation was completed with a feed overpressure of 3 psi and stripping oil flow rate of 4.0 mL/min. Four washes with TCE were followed by a 60-minute period for residual TCE to evaporate. Thirty-minute washes with 0.5 M ammonium hydroxide were then performed and conductivities measured in triplicate for each wash effluent. In all cases, wash volumes were 25 mL. After four ammonium hydroxide washes, spheres were stored in water overnight and air-dried in 75% isopropyl alcohol, 25% deionized water. Once dry, each batch of spheres was massed to normalize the measured conductivities to dried sphere mass for accurate comparison.

3.3 Determination of Size Uniformity

After developing a process and machinery to fabricate multi-gram batches of cerium oxide by internal gelation, additional work was performed to characterize the new system's capability to make monodisperse microspheres in the size range 50-200 μm. An experiment was designed to measure the diameters of sintered microspheres as a function of needle size and stripping oil flow rate using an optical microscope and contrast-based sizing software.

Feed solutions and chemicals

A concentrated solution of ceric ammonium nitrate (CAN) was obtained by dissolution of 99.5% CAN (lot # A0331425) in deionized water. Ceric ammonium nitrate with an initial

cerium concentration of 1.675 M was made acid deficient by the addition of concentrated ammonium hydroxide to achieve an OH^-/Ce^{4+} molar ratio of 0.75. An HMTA/urea solution with a concentration of 3.18 M was prepared by the standard method using 99.5% HMTA (lot # SZBB2510V), 99.5% urea (lot # BCBD7141V), and deionized water. After chilling to 0 °C, feed solutions were slowly mixed with an $HMTA/Ce^{4+}$ molar ratio of 2.0. Microspheres were dispersed into a column of heated, 100 cS silicone oil obtained from Neely Industries LLC. After aging, spheres were washed using Sigma Aldrich, ACS grade reagents trichloroethylene, isopropyl alcohol (IPA), and ammonium hydroxide. Ammonium hydroxide was diluted to 0.5 M for washing operations and was intended to remove excess reagents and organic reaction products.

Apparatus & gelation conditions

The sol-gel apparatus was used in the final configuration discussed in section 3.2.3 with a glass mixed feed vessel, Teflon-aluminum sphere dispersion device, pneumatic feed and stripping oil transfer, and control over mixed feed pressure, strip oil flow rate, and silicone oil temperature. Figure 3.8 provides a magnified view of the aluminum-Teflon coupler at the top of the gelation column. The coupler allowed for needle chilling, the use of a separate chilled silicone oil stream, a 0.1 cm diameter region for microsphere stripping, and introduced the unsolidified spheres into a region of laminar flow in the column. New stainless steel needles from the Hamilton Company were used in each run after cleaning with fresh aqua regia and deionized water. Prior to sizing experiments, the flow meter was calibrated over the range 0.5-8 mL/min using a stopwatch and graduated cylinders to generate a flow vs. voltage curve at the equilibrium stripping oil temperature.

Nine batches of spheres were collected using three needle sizes and three oil stripping speeds. Needles had inner diameters of 260 μm (26 G), 184 μm (28 G), and 108 μm (32 G). For each needle size, spheres were collected in separate mesh baskets at each stripping oil speed of approximately 1.5 mL/min, 4.0 mL/min, and 6.5 mL/min. Stripping oil speeds were varied from slow to intermediate to fast, corresponding to maximum, medium, and minimum sphere sizes, respectively. Change in the feed flow rate between samples was kept to a minimum and was calculated to be approximately 0.15 mL/min. Feed solutions were chilled to 0 °C, pneumatically transferred to the needle, and introduced into a column of silicone oil maintained at a temperature between 80-85 °C. Once microsphere production began and the desired stripping oil speed was set, feed pressure was tuned in the range 3-4.5 psi in order to adjust the rate of sphere formation such that inter-sphere spacing was minimal. With the desired parameters established, spheres were collected in one of several small, mesh baskets to allow for separate recovery and analysis of samples. When a sufficient quantity was produced, the mesh basket was removed from the system to a bath of silicone oil on a hot plate set to 85 °C to cure for 20 minutes. This procedure was repeated for the remaining stripping oil speeds and again for each needle. At the end of each gelation run, the mixed feed vessel and lines were washed with 1 M nitric acid followed by deionized water.

Washing & heat treatments

After cooling overnight, spheres were washed to remove silicone oil and impurities. Each mesh basket containing a unique sample was fit into a 50 mL centrifuge tube for the following wash procedure:

1) Two, 15-minute washes with 30 mL TCE to remove the bulk of silicone oil
2) Two, 15-minute washes with 30 mL 50% TCE, 50% IPA to remove residual silicone oil and water from the spheres.
3) Two, 20-minute washes with 30 mL 50% IPA, 50% 0.5 M NH_4OH
4) Three, 30-minute washes with 30 mL 0.5 M NH_4OH.

Effluents from 0.5 M NH_4OH washes were monitored for conductivity using a Thermo Scientific Orion Star A215 pH/conductivity meter calibrated at 1.413 mS/cm and 12.9 mS/cm. Spheres were washed until the effluent conductivity approached that of the stock 0.5 M NH_4OH. Spheres were then rinsed with deionized water, placed in a large beaker of deionized water heated to 85 °C for two hours and allowed to cool. After reaching room temperature, spheres were rinsed with deionized water and transferred to alumina boats to air-dry using 75% isopropyl alcohol, 25% deionized water.

After air-drying at ambient temperature for several days, spheres were heated to 150 °C, according to the profile in Figure 3.17, to allow slow evolution of remaining volatiles to avoid cracking. After dwelling at 150 °C for one hour, spheres were cooled to room temperature and transferred to a high temperature box furnace. Spheres were sintered at 1500 °C with a ramp rate of 5 °C/min, as shown in Figure 3.17.

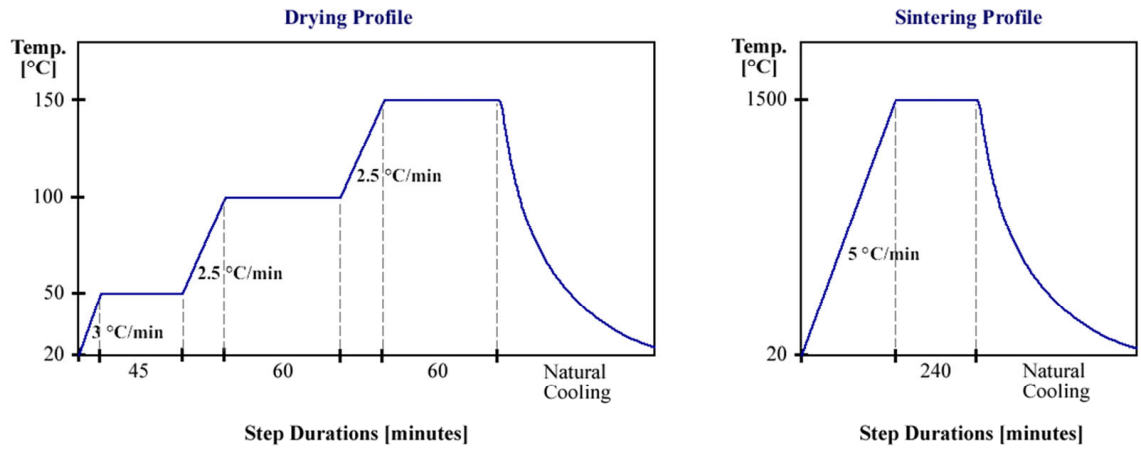

Figure 3.17: After air-drying, microspheres are first dried to 150 °C and then sintered at 1500 °C.

Sizing

After sintering, spheres were dispersed on glass microscope slides for imaging. Photoresist was applied to the glass slides as an adhesive in order to position spheres with sufficient spacing for subsequent sizing analysis and to prevent spheres from rolling off the slide and contaminating the microscope and clean room facilities. SPR 220 – 3.0 photoresist was spread at 750 rpm for 15 seconds and then spun at 2500 rpm for 30 seconds to achieve a thin layer on the slide. While the photoresist was wet, spheres were lightly distributed across the slide, which was then transferred to a 100 °C hot plate to cure for 10 minutes.

Microspheres were imaged by bright field microscopy with 5-10X magnification using an Olympus BX-51 fluorescence microscope. A motorized stage and software allowed for automated imaging of a large area by stitching many images into a single photograph of the entire slide. One slide was prepared for each of the sizing conditions, allowing size analysis of hundreds of spheres in each case. Olympus Stream micro-imaging software allowed for post-processing of images to measure the mean radius and shape factor of particles. The degree to which particles represented a perfect sphere was measured using a shape factor, defined as

$$Shape\ Factor = 4\pi \frac{area}{perimeter^2}, \quad (3.1)$$

which has a value of one for a perfect circle.

Average sphere diameters were determined using a multi-step process with the sizing software. First, the program was run with broad size constraints to include all particles sized in the analysis. This initial scan was used to generate a histogram of mean radius, which was segregated into color-coded regions corresponding to custom size windows. Particles in each size window then appeared in the image with their chosen color for visual discrimination of particle categories. Based on the color-coded results, a second analysis was run to consider both size and shape. Shape factors were obtained for particles in the desired size window and a mean radius vs. shape factor distribution plot was used to define a two-dimensional region of interest. As will be discussed in the results section, consideration of both parameters allowed for the most accurate determination of sphere size distribution by eliminating broken particles, agglomerations, and shadows that distorted contrast-based measurements.

3.4 Microsphere Washing Techniques

Since the development of the internal gelation process to fabricate uranium oxide microspheres around 1970, baseline washing procedures for spheres formed in silicone oil have consisted of a two-step process [33,42,43,179,186,195]. First, oil is removed using a solvent such as TCE, carbon tetrachloride, or hexane. Second, excess HMTA, urea, formaldehyde, and ammonium nitrate are leached from spheres into dilute ammonium hydroxide washes. After washing procedures, microspheres were dried and heated to the desired levels to remove water and carbon as well as promote densification. In the current work, modified washing processes were evaluated using cerium oxide microspheres prepared in the sol-gel apparatus.

3.4.1 Comparison of Baseline and Pressurized Water Treatment Processes

One shortcoming of the internal gelation sol-gel method is the propensity for gelled microspheres to crack upon drying or subsequent heating. Although some combinations of feed concentrations and gelation temperatures have been found to prevent cracking for some materials, these parameters are not necessarily the most desirable for a variety of other reasons. Since cracking leads to the generation of fines that would be hazardous in the case of Pu-238 oxide processing, efforts were taken to mitigate cerium oxide microsphere cracking. A 2010 investigation of yttrium-stabilized zirconium microspheres made by internal gelation indicated that a combination of pressurized water treatments and application of Dowanol PM to microspheres reduced the apparent percentage of spheres that cracked during heat treatments [193]. Considering this result, the effects of a pressurized water treatment on wet, gelled microspheres were investigated. Batches of cerium gel microspheres were produced, washed with and without pressurized water treatments, and the resulting oxide microspheres compared.

3.4.1.1 Shrinkage Comparison

Diameters of gelled microspheres typically shrink by at least 200% during the air-drying step. As gelled spheres evolve water and dry in air, they transition from soft gels to hard oxides. It seems reasonable that large dimensional changes in hardening spheres could induce stresses and promote cracking, particularly during subsequent heat treatments when volatile organics evolve. However, it was anticipated that microspheres heated to elevated temperatures in the wet, gelled state might release water soluble organic impurities and shrink without cracking. To test this theory, an experiment was conducted to determine whether shrinkage occurs as a result of elevated temperatures during a pressurized water treatment while microspheres are still soft and permeable.

Feed solutions and chemicals

A concentrated solution of ceric ammonium nitrate (CAN) was obtained by dissolution of 99.5% CAN (lot # A0331425) in deionized water. Ceric ammonium nitrate with an initial cerium concentration of 1.675 M was made acid deficient by the addition of concentrated ammonium hydroxide to achieve an OH^-/Ce^{4+} molar ratio of 0.75. An HMTA/urea solution with a concentration of 3.18 M was prepared by the standard method using 99.5% HMTA (lot # SZBB2510V), 99.5% urea (lot # BCBD7141V), and deionized water. After chilling to 0 °C, feed solutions were slowly mixed with an $HMTA/Ce^{4+}$ molar ratio of 2.0. Microspheres were dispersed into a column of heated, 100 cS silicone oil obtained from Neely Industries LLC. After aging, spheres were washed using Sigma Aldrich, ACS grade reagents trichloroethylene, isopropyl alcohol, and 0.5 M ammonium hydroxide.

Gelation conditions

Microspheres for shrinkage studies were produced in the sol-gel apparatus in its final configuration, described in section 3.2.3. Feed solutions were chilled to 0 °C before dispensing into silicone oil maintained at 80-82 °C at a rate of approximately 0.15 mL/min into stripping oil flowing at a rate of 2.5 mL/min. At the end of the run, spheres were aged in hot silicone oil on an 85 °C hot plate for 30 minutes.

Washing & sizing

After cooling overnight, silicone oil was decanted and microspheres were washed according to the procedure below:

1) Two, 15-minute washes with 70 mL TCE
2) Two, 15-minute washes with 70 mL 50% TCE, 50% IPA
3) Two, 20-minute washes with 70 mL 50% IPA, 50% 0.5 M NH_4OH
4) Eight, 30-minute washes with 70 mL 0.5 M NH_4OH, measuring the effluent conductivity at the end of each wash

At this stage, approximately half of the microspheres were transferred, using 0.5 M NH_4OH, to a clean alumina dish to air-dry. The remaining spheres were washed with deionized water and transferred into a clean autoclave with 140 mL of deionized water. The conductivity of the water containing microspheres in the autoclave was measured prior to sealing and placing the autoclave in a 200 °C oven. After a 2-hour pressurized water treatment, the autoclave was removed and allowed to cool. Upon opening the autoclave, conductivity and volume measurement were taken on the aqueous effluent. Spheres were washed with fresh deionized water, half transferred to a clean alumina dish to dry using 75% isopropyl alcohol, 25% deionized water, and half replaced in the autoclave for additional pressurized water treatment. Spheres remaining in the autoclave were subjected to an additional four hours at 200 °C. Conductivity measurements were also performed before and after the second pressurized water treatment. Microspheres subjected to a total of six hours of pressurized water treatment were also transferred to a clean alumina dish to dry using 75% isopropyl alcohol, 25% deionized water. Wet microspheres were imaged and sized at each stage of the pressurized water treatment process using a calibrated, 2-megapixel Celestron digital USB microscope. For each case, at least 40 microspheres were counted to obtain an average diameter with reasonable uncertainty.

After air-drying for at least four days, samples of microspheres air-dried in ammonium hydroxide, and those autoclaved for two and six hours were also imaged and sized.

3.4.1.2 Cracking Comparison

Dried microspheres from the previous section were also used to compare the propensity of microspheres to crack based on the use of a two-hour pressurized water treatment at 200 °C. After washing procedures were complete, spheres were allowed to air-dry for one week. Samples from the batches dried in NH_4OH and those dried in 75% isopropyl alcohol, 25% deionized water after a two-hour pressurized water treatment were compared. Each sample was added to a 150 μm sieve to eliminate any fines, massed, added to separate alumina boats, and heated according to the profile in Figure 3.18 at the same time. Once cool, samples were massed again to compare volatile mass losses. Each sample was again placed in a 150 μm sieve and the fines falling through the mesh were collected and massed. Each sample was also imaged using the Celestron digital USB microscope. Due to difficulties observing the surface features of spheres heated to 600 °C, images were also acquired using an SEM with microspheres mounted on copper tape.

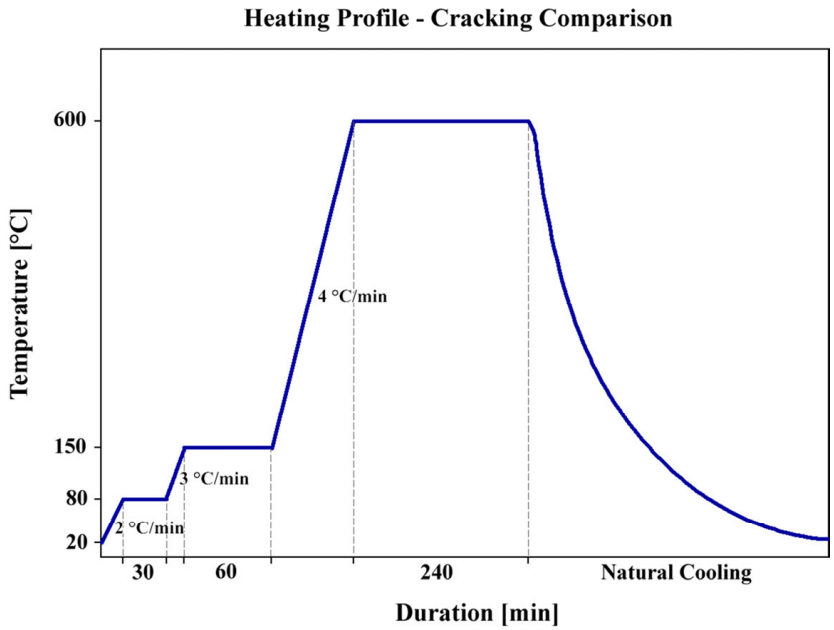

Figure 3.18: Microspheres air-dried in ammonium hydroxide and air-dried after a pressurized water treatment were slowly heated to 600 °C to compare the extent of cracking.

3.4.1.3 Crystallite Size Comparison

Microspheres produced in section 3.4.1.1 for shrinkage and cracking studies were also used to compare the crystallite size in air-dried microspheres with and without a pressurized water treatment. As a first step, crystallite size was estimated by application of the Scherrer formula to x-ray diffraction data. The Scherrer equation allows for estimation of the minimum average crystallite size based on peak broadening, and is defined according to [203]:

$$p = \frac{K\,\lambda}{b\,\cos(\theta)}\,, \tag{3.2}$$

where K is the Scherrer constant with a value near one, λ is the x-ray wavelength, θ is the Bragg angle, and b is the full-width at half-max corrected for instrumental broadening. X-ray diffraction (XRD) spectra were obtained for microspheres dried in ammonium hydroxide as well as microspheres dried after a two-hour pressurized water treatment using a Rigaku rotating anode

x-ray diffractometer. Dried microspheres were ground into a fine powder using a mortar and pestle then packed into glass sample slides using acetone. Samples were run at 1.5 degrees/min from 22-85 degrees 2θ. A lanthanum hexaboride sample was run using the same conditions for determination of instrumental broadening. Additional XRD data was obtained for 99.9% stock cerium dioxide obtained from Sigma Aldrich (lot # MKBF2924V) as a reference.

Crystallite sizes were also estimated based on images obtained by transmission electron microscopy (TEM). Finely ground powders produced with a mortar and pestle were ultrasonically dispersed in 5 mL of hexane. Dispersed powders were dripped onto copper TEM grids and allowed to dry. A JEOL 2100F corrected scanning TEM was used for observation at magnifications from 120-1200k. Crystal sizes were estimated based on pixel-to-length conversion using Adobe Fireworks.

3.4.1.4 Thermal Gravimetric Analysis Comparison

Thermal gravimetric analysis (TGA) was performed on microspheres washed by different methods to compare volatile mass losses as a function of temperature. Although many variations in washing procedures were assessed using TGA, volatile mass losses from batches subjected to a pressurized water treatment were noticeably improved and motivated additional investigation. After an initial comparison of TGA curves for spheres washed with and without a pressurized water treatment, TGA was performed for urea, HMTA, an HMTA/urea mixture, and a solid residue reduced from pressurized water treatment effluent.

Effect of pressurized water treatment on volatile mass loss

Separate batches of microspheres were prepared for TGA after washing by different methods. Each batch was prepared using a 1.675 M solution of CAN prepared by dissolution of

99.5% CAN (lot # A0331425) in deionized water and made acid deficient by the addition of concentrated ammonium hydroxide to achieve an OH^-/Ce^{4+} molar ratio of 0.75. HMTA/urea solutions with concentrations of 3.18 M were prepared by the standard method using 99.5% HMTA (lot # SZBB2510V), 99.5% urea (lot # BCBD7141V), and deionized water.

Concentrated solutions of ceric ammonium nitrate (CAN) were obtained by dissolution of 99.5% CAN (lot # A0331425) in deionized water. Ceric ammonium nitrate with an initial cerium concentration of 1.675 M was made acid deficient by the addition of concentrated ammonium hydroxide to achieve an OH^-/Ce^{4+} molar ratio of 0.75. An HMTA/urea solution with a concentration of 3.18 M was prepared by the standard method using 99.5% HMTA (lot # SZBA2210V), 99.5% urea (lot # BCBD7141V), and deionized water. After chilling to 0 °C, feed solutions were slowly mixed with an HMTA/Ce molar ratio of 2.0. Microspheres were dispersed into a column of 100 cS silicone oil heated to 85-90 °C. After aging, spheres were washed using Sigma Aldrich, ACS-grade reagents.

The first batch of microspheres were washed according to a procedure used by researchers at the Oak Ridge National Laboratory [42,43]. By this method, microspheres were first washed four times with TCE with a residence time of at least 25 minutes. Following the TCE washes, spheres were treated with 0.5 M ammonium hydroxide washes until the conductivity of the effluent was within 10% of the conductivity of the stock 0.5 M ammonium hydroxide. The second batch of microspheres were washed by the same process, but were subsequently washed in deionized water, loaded into an autoclave, and subjected to a two-hour pressurized water treatment at 200 °C. Spheres were allowed to air-dry for a minimum of five days prior to any TGA analysis.

Thermal gravimetric analysis of dried microspheres was performed using a Perkin Elmer TGA-7 with a nitrogen gas purge. Samples were heated at a rate of 10 °C/min and data was collected at a sampling frequency of 1/3 Hz. In each case, the sample mass was approximately 30 mg.

Investigation of volatile impurities

Based on the results observed from TGA and thermal treatment of air-dried microspheres, additional TGA was performed on stock urea (lot # SZBA2210V) and HMTA (lot # BCBD7141V) used to produce microspheres. Residues obtained from the pressurized water treatment effluent were also analyzed. For these measurements, a TA Instruments Q50 TGA with an air purge was used to simulate oxidizing heat treatment conditions in a standard box furnace. Samples were still heated at a rate of 10 °C/min but recorded with a frequency of 2 Hz. The TA Instruments TGA had been recently calibrated using 100 mg and 1000 mg standards and an Alumet sample that gave a Curie point within 1% of the known value.

Measurements indicating a large increase in the conductivity of the pressurized water treatment solution after heating prompted an investigation of the identity of the material extracted from the microspheres. As a first step, a solution of 3.18 M HMTA/urea was reduced to a solid on a hot plate and 8 mg used for TGA. Next, 40 mL of pressurized water treatment effluent was transferred to an evaporating dish and allowed to dry over lithium chloride until only solids remained and a stable mass was reached. A slow reduction of volume was used to prevent over-heating and premature loss of non-water volatiles. The final residue mass was obtained to determine the dissolved mass per volume in the effluent and the amount produced

per gram of microspheres. An 8 mg residue sample was used in TGA to avoid contact between bubbles formed during heating and the walls of the furnace or thermocouple.

3.4.1.5 Electron-Impact Mass Spectroscopy Comparison

A VG Analytical 70-250-S magnetic sector, double-focusing mass spectrometer with a conversion dynode, photomultiplier detector was used with electron impact ionization at 70eV to volatilize, ionize, and identify molecular species emitted from microspheres and pressurized water treatment residues as a function of temperature. The electron-impact mass spectrometer (EI-MS) was used to identify volatile species emitted from samples as a function of temperature as high as 580 °C. The instrument was calibrated using perfluorokerosene and heated to its maximum temperature of 580 °C using an empty sample to establish background peaks and levels.

Mass spectroscopy was used to compare volatile emissions between spheres washed with only TCE and ammonium hydroxide to those also subjected to a pressurized water treatment. Samples from the same batches of microspheres used for TGA in section 3.4.1.4 were used for EI-MS. Additionally, EI-MS was used to identify constituents of the pressurized water treatment residue used for TGA in the previous section. Samples were not massed precisely due to the qualitative nature of the instrument, but were between 1-5 mg. Since digital data capture from the machine was not possible, a stopwatch was used to achieve regular increases in temperature with time. After each temperature increase, peaks were identified and data was printed to record the signal at each time/temperature step.

3.4.2 Determination of Residual Impurities

One of the key questions regarding the suitability of sol-gel microspheres for replacing powder-based Pu-238 oxide granules for pellet fabrication is whether the final impurity levels

meet existing fuel specifications. To mitigate this unknown factor, emphasis was placed on determination of carbon, nitrogen, and hydrogen levels, as well as trace element analysis, due to extensive use of organic and nitrogen-bearing chemicals in the sol-gel process. A large batch of microspheres was prepared from high-purity CAN feed stock to assess whether sol-gel processing introduces any impurities that remain after sintering operations.

Feed solutions and chemicals

For impurity level experiments, Sigma Aldrich >99.99% ceric ammonium nitrate (lot # MKBL5098V) with less than 100ppm trace metals was used to produce a 1.675 M metal nitrate solution. A 3.18 M solution of HMTA/urea was prepared from Sigma Aldrich >99.5% urea (lot # BCBD7141V) and Sigma Aldrich >99.5% HMTA (lot # SZBA2210V). All solutions were prepared according to the standard solution preparation method using deionized water and a Mettler Toledo AL204 analytical scale with a resolution of 0.1 mg. The 1.675 M CAN solution was made acid deficient by addition of ACS-grade, concentrated ammonium hydroxide to achieve a OH^-/Ce^{+4} ratio of 0.75.

Particular care was taken in these experiments to clean glassware and avoid external contamination. Glassware used in the experiment was first washed by the standard process and then allowed to sit submerged in 20% nitric acid for a minimum of 24 hours. After soaking, glassware was rinsed with deionized water five times and dried in a glass oven at 140 °C. After drying, glassware and stainless steel tools were rinsed with fresh aqua regia, prepared from a 3:1 ratio of concentrated hydrochloric acid to 70% nitric acid. After cleaning with aqua regia, glassware and stainless steel tools were rinsed thoroughly with deionized water before drying in the glass oven.

Gelation conditions

Two sol-gel runs were needed to produce the necessary quantity of microspheres for impurity analysis. Although production occurred on different days, each run used feed solutions from the same preparation for consistency. In both runs, ceric ammonium nitrate and HMTA/urea solutions were individually chilled to 0°C and then mixed prior to gelation at a molar ratio of 2.0 mole HMTA to 1.0 mole cerium (R = 2). The mixtures were dispensed through a 28 gauge needle at a rate of approximately 0.15 mL/min into stripping oil flowing at a rate of 4 mL/min. Oil in the gelation column was maintained at 85-90 °C. As a normalizing step for the last spheres produced, microspheres were cured in hot oil for 20 minutes at the end of each run.

Washing procedure

One goal of the impurity determination experiment was to compare the carbon, nitrogen, and hydrogen impurity levels of microspheres washed to varying extents. Therefore, the first batch of microspheres produced was washed according to the baseline process presented in Figure 3.19. The second batch of microspheres was washed using a modified approach, using isopropyl alcohol, intended to improve silicone oil and impurity removal. Half of the microspheres washed by the modified method were subsequently subjected to a two-hour pressurized water treatment at 200 °C. Wash volumes were 70 mL in each case but durations depended on the type of wash solution. Ammonium hydroxide washes lasted 30 minutes each while TCE washes were 15 minutes and washes involving isopropyl alcohol lasted 10 minutes.

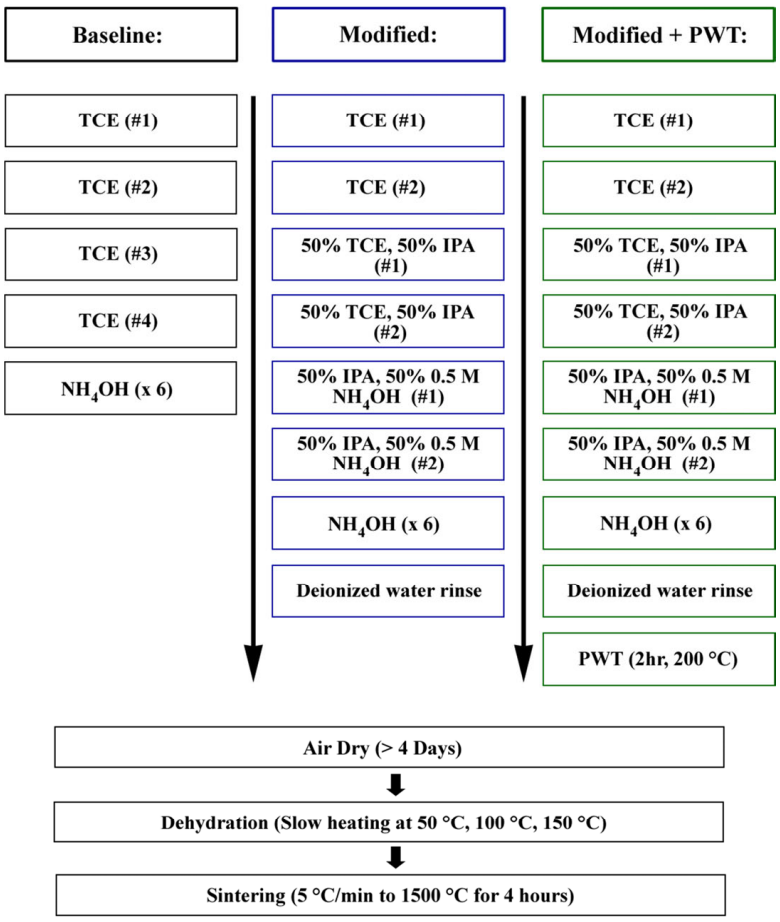

Figure 3.19: Microspheres were washed by three methods to compare final carbon, nitrogen, and hydrogen levels.

Heat treatments

After washing, spheres were allowed to air-dry at ambient temperature for a minimum of four days prior to slow heating to 150 °C in a low-temperature box furnace according to the profile in Figure 3.17. After cooling, any slight agglomerations were broken apart using light pressure above a sieve prior to transferring to a high-temperature box furnace for sintering at 1500 °C, as seen in Figure 3.17. The small box furnace was used for low-temperature treatments due to the poor sensitivity of the thermocouple in the high-temperature box furnace at low temperatures. However, the low-temperature box furnace was unable to heat to 1500 °C,

necessitating the high-temperature box furnace and a two-step heat treatment. Sintered spheres were de-agglomerated using light pressure and divided into separate samples for impurity analysis.

Impurity analysis

Sintered samples prepared for impurity analysis were shipped to Evan's Analytical Group for determination of carbon, nitrogen, hydrogen, and trace element concentrations since the desired measurement capabilities do not exist at the University of Michigan. Carbon, hydrogen, and nitrogen (CHN) analysis was performed for samples washed by each of the three methods outlined in Figure 3.19. Additionally, glow-discharge mass spectroscopy (GDMS) was performed on microspheres washed by the modified method and subjected to the pressurized water treatment since this was the preferred washing technique.

Measurements of part-per-million carbon level were accomplished using "LECO" analysis, whereby samples are combusted and gaseous products are measured using infrared absorption. Samples were combusted in an oxygen plasma at temperatures above 2000 °C in a high frequency induction furnace. Gaseous carbon monoxide and carbon dioxide were measured by four infrared absorption detectors to determine the carbon content. Quantitative measurements were obtained by calibration with standards of known carbon content. Typical detection limits were quoted as 10 ppm. Prior to analysis, microspheres were dried at 100 °C to remove moisture and then three 0.1 g samples were analyzed in sequence to determine the carbon content. If values did not agree within 15%, then two additional samples were analyzed and the average reported.

Nitrogen and hydrogen levels were determined by instrumental gas analysis with detection limits of 10 ppm. Prior to the measurement, samples were heated to 100 °C in a crucible to remove moisture followed by an inert gas purge of the chamber. Next, a high current was passed through the crucible to raise temperatures above 2500 °C. Nitrogen and hydrogen gas generated in the process was released into a flowing stream of inert gas and directed into a chamber to measure the change in thermal conductivity of the gas. Quantitative analysis of nitrogen and hydrogen levels was determined using calibration standards. Three 0.1 g samples were analyzed in sequence to determine the nitrogen/hydrogen content. If values did not agree within 15%, then two additional samples were analyzed and the average reported.

Glow-discharge mass spectroscopy was also performed on microspheres washed by the modified method and subjected to a pressurized water treatment. A VG 9000 glow-discharge mass spectrometer was used to determine trace element concentrations for 72 elements. GDMS was preferred over inductively coupled mass spectrometry or total reflection x-ray fluorescence techniques due to the comparative ease in sample preparation, ability to analyze more elements, and lower detection limits for several elements. Although GDMS has elevated detection limits for iodine, cesium, gadolinium, lead, terbium, tantalum, and uses indium as a binder, this was not expected to be problematic for the desired analysis. Detection limits for most elements was quoted to be sub-ppm with measurement uncertainties as high as 30% of the measured value.

Inductively coupled mass spectrometry (ICP-MS) was also performed on two wash effluent samples at the University of Michigan using a Thermo Finnigan Element 2 ICP-MS. Quantitative results were estimated based on comparison of sample signals to those obtained from a NIST standard with known elemental concentrations. First, a 75 μL sample of the pressurized water treatment effluent was added to 3 mL dilute nitric acid and analyzed for

sodium, calcium, aluminum, silicon and cerium levels. Second, a 150 μL sample of 0.5 M ammonium hydroxide wash effluent from the first wash in a series was diluted 20-fold in dilute nitric acid and analyzed for cerium levels. Based on previous attempts to determine the cerium concentration, measurements were taken from the vial after shaking and after allowing any solids to settle.

3.5 Heat Treatment Effects

Current concepts for dust-free Pu-238 oxide pellet fabrication involve pressing sol-gel oxide microspheres into a pellet. While this has not been demonstrated with pure cerium or plutonium, internal gelation microspheres of uranium oxide, uranium + thorium oxide, and uranium + plutonium oxide have been successfully pressed into pellets [169,171,179]. Based on correlations observed between microsphere-based pellet characteristics and microsphere properties, experiments were performed to investigate the density, specific surface area, and average crystallite size in cerium oxide microspheres as a function of temperature. A large batch of microspheres was produced and washed by the modified method described in Figure 3.19 and subjected to a pressurized water treatment. After air-drying, spheres were divided into six equal masses and heat treated to a variety of temperatures for a series of subsequent analyses. Small masses of each sample were diverted for TEM imaging while the bulk underwent nitrogen adsorption experiments followed by density measurements and x-ray diffraction analysis.

Feed solutions and chemicals

A concentrated solution of ceric ammonium nitrate (CAN) was obtained by dissolution of 99.5% CAN (lot # A0331425) in deionized water. Ceric ammonium nitrate with an initial cerium concentration of 1.675 M was made acid deficient by the addition of concentrated

ammonium hydroxide to achieve an OH^-/Ce^{4+} molar ratio of 0.75. An HMTA/urea solution with a concentration of 3.18 M was prepared by the standard method using 99.5% HMTA (lot # SZBB2510V), 99.5% urea (lot # BCBD7141V), and deionized water. Washing operations were performed using Sigma Aldrich, ACS grade reagents trichloroethylene, isopropyl alcohol, and 0.5 M ammonium hydroxide.

Gelation conditions

Microspheres for heat treatment studies were produced in the sol-gel apparatus in its final configuration. Feed solutions were chilled to 0 °C before being mixed with $HMTA/Ce^{4+} = 2.0$. The mixed feed solution was dispensed into silicone oil, maintained at 77-80 °C, at a rate of approximately 0.15 mL/min. Stripping oil maintained a flow rate of 4.0 mL/min. At the end of the run, spheres were aged in hot silicone oil on an 85 °C hot plate for 20 minutes.

Washing

After cooling overnight, silicone oil was decanted and microspheres were washed according to the procedure below:

1) Three, 20-minute washes with 50 mL TCE
2) Three, 20-minute washes with 50 mL 50% TCE, 50% IPA
3) Two, 20-minute washes with 50 mL 50% IPA, 50% 0.5 M NH_4OH
4) Eight, 30-minute washes with 50 mL 0.5 M NH_4OH, measuring the effluent conductivity at the end of each wash
5) Two deionized water rinses with a volume of approximately 1 L

At this stage, microspheres were transferred into a clean autoclave with 110 mL of deionized water and the conductivity was measured. After a two-hour pressurized water treatment at 200 °C, the autoclave was removed and allowed to cool. Upon opening the autoclave, the conductivity and volume was recorded, the effluent was saved for analysis, and spheres were rinsed with fresh deionized water. Spheres were then transferred to a clean alumina dish to air-dry using 75% isopropyl alcohol, 25% deionized water.

Heat treatment

After air-drying for several days, spheres were divided into six samples with masses between 1.6-1.7 g, corresponding to the final heat treatment conditions: air-dried, 150 °C, 450 °C, 750 °C, 1050 °C, and 1350 °C. Each sample was placed in a clean alumina boat and subjected to the drying scheme up to 150 °C shown in Figure 3.17 using the low-temperature box furnace. For samples requiring a final heat treatment of 450 °C and 750 °C, samples were heated to the final temperature at a rate of 5 °C/min after the 150 °C cycle without a cooling step. Samples heated to 1050 °C and 1350 °C were subjected to the 150 °C cycle in the low-temperature box furnace, cooled, and transferred to the high-temperature box furnace for heating at 5 °C/min to the final temperature. In all cases, the final dwell lasted four hours.

Crystallite size estimation by x-ray diffraction

The crystallite size of microspheres heated from 150-1350 °C was first estimated by application of the Scherrer formula to x-ray diffraction data. The Scherrer equation allows for estimation of the minimum average crystallite size based on peak broadening, and is defined

according to equation 3.2 [203]. X-ray diffraction (XRD) spectra were obtained using a Rigaku rotating anode X-ray diffractometer with copper $K_{\alpha 1}$ and $K_{\alpha 2}$ x-rays. To prepare powder samples, microspheres were ground into a fine powder using a mortar and pestle then packed into glass slides using acetone. Samples were run at 1.5 degrees/min from 22-85 degrees 2θ. A lanthanum hexaboride sample was run at the same conditions for determination of instrumental broadening. Additional XRD was obtained for 99.9% stock cerium dioxide obtained from Sigma Aldrich (lot # MKBF2924V) as a reference.

Transmission electron microscopy

Crystallite sizes in the heat treated samples were also estimated from images obtained by transmission electron microscopy (TEM). Finely ground powders from a mortar and pestle were ultrasonically dispersed in 5 mL of hexane. Dispersed powders were dripped onto copper TEM grids and allowed to dry. A JEOL 2100F corrected scanning TEM was used for observation at magnifications from 120-1200k. Crystal sizes were estimated based on pixel-to-length conversion using Adobe Fireworks.

Specific surface area measurements

Nitrogen adsorption techniques were used to determine the specific surface area and average pore size as a function of temperature for as many of the heat treated samples as possible. A Micromeritics ASAP 2020 (Accelerated Surface Area and Porosimetry System) sorption analyzer instrument was used to determine the surface area and pore size distribution based on the Brunauer-Emmett-Teller (BET) and Barrett-Joyner-Halenda (BJH) equations. Specific surface areas were calculated using the BET multipoint method with ten data points at

relative pressures of 0.05-0.30. Analyses were performed at -196 °C (77 K) with nitrogen gas. Since accurate measurements typically require samples with a minimum surface area of about 20 m^2/g, samples heated above the temperature for pore closure were not expected to return accurate surface areas, but would give an indication of when pore closure occurred. Prior to analysis, samples were outgassed at 150 °C under vacuum for eight hours. For air-dried samples, the outgassing temperature was reduced to 50 °C.

Density measurements

Microsphere density was determined using a pycnometer with deionized water. The pycnometer, deionized water, ceria sample, and pipet were allowed to reach thermal equilibrium with the environment and care was taken to minimize heat transfer to the pycnometer through handling. The water temperature was measured using the average of two thermometers and the associated density recorded (ρ_w). The following steps were performed:

1) Calibration:

The dry, room-temperature pycnometer was massed using an analytical scale with 0.1 mg accuracy three times and averaged. Calibration was performed by filling the pycnometer with water and massing three times in succession and the average mass for the pycnometer full of water was determined. The water mass (m_{w0}) was obtained by subtracting the average empty pycnometer mass (m_{pe}) from the average mass of the water and pycnometer (m_{pw}). After calibration, the pycnometer was rinsed with acetone and allowed to dry completely.

2) Sample mass determination:

The dry, room-temperature pycnometer was massed using an analytical scale with 0.1 mg accuracy three times and averaged. A ceria sample was added to the dry pycnometer, which was massing three times in succession and the average mass for the pycnometer with ceria was determined. The ceria mass (m_c) was obtained by subtracting the new average empty pycnometer mass (m_{pe}) from the average combined mass of the ceria and pycnometer (m_{pc}).

3) Displaced water determination:

Distilled water was slowly added to the pycnometer containing ceria taking care to prevent and eliminate any bubbles. Once full, the pycnometer with ceria and water was massed. Next, about half of the water was slowly pipetted out of the pycnometer and discarded. Fresh water was added to refill the pycnometer, which was massed again. About half of the water was pipetted and removed, followed by re-filling with water and a third massing. The average mass for pycnometer with water and ceria (m_{pwc}) was calculated from the three measurements. The ceria density was then calculated using the equations

$$m_{w1} = m_{pwc} - m_{pc}\,, \tag{3.3}$$

where m_{w1} is the mass of water in the pycnometer with the sample,

$$m_{wd} = m_{w0} - m_{w1}\,, \tag{3.4}$$

where m_{wd} is the mass of water displaced by the ceria,

$$V_{wd} = \frac{m_{wd}}{\rho_w}\,, \tag{3.5}$$

where V_{wd} is the volume of the water displaced by the ceria, and

$$\rho_c = \frac{m_c}{V_{wd}}\,, \tag{3.6}$$

where ρ_c is the ceria density.

Samples heat treated to varying extents were used in sequence for BET surface area, density, and x-ray diffraction experiments. X-ray diffraction experiments were performed last since spheres had to be finely ground into a powder for analysis. Surface area experiments were conducted prior to density measurements to avoid introduction of water into the pore network that might disrupt nitrogen adsorption. Performing experiments in the order (1) BET surface area analysis, (2) density determination by water pycnometry, and (3) x-ray diffraction was not anticipated to cause any interference. To be certain, a separate sample of microspheres was used as a control set. Microspheres from another batch prepared using the same feed parameters, gelation conditions, and washing techniques were first heated to 150 °C for four hours. Half of these spheres were finely ground and used for x-ray diffraction. The other half was subjected to BET analysis followed by density measurements with deionized water and drying in isopropyl alcohol. Once dry, the second half was also used for x-ray diffraction. Comparison of the two x-ray diffraction spectra and crystallite sizes predicted by the Scherrer equation were used to verify that BET and density experiments did not modify subsequent crystallite size determination.

Chapter 4

Results

"PuFF is an example of a DOE Program Office relying upon a subsequent mission or user of a facility to fund the decontamination (or refurbishment) of that facility even though it was contaminated doing work for the previous user. One problem with this approach is that the facility will eventually be unable to attract future users, and the Program Office will be forced to turn to Congress for new money to pay for final decontamination and decommissioning. As in the case of PuFF, this amounts to a deferred and hidden DOE subsidy of the sponsoring agencies' actual program costs. In addition, deferred decontamination is often more expensive and more hazardous than if the facility had been decontaminated at the end of production."

- "Report of an Investigation into Deterioration of the Plutonium Fuel Form Fabrication Facility (PuFF) at the DOE Savannah River Site," U.S. Department of Energy Office of Nuclear Safety

This chapter presents the production of dust-free, spherical cerium dioxide particles by internal gelation methods. Due to minimal prior art on cerium in the internal gelation process and the failure of previous research endeavors to produce monodisperse microspheres in the size range of interest, this chapter will cover a wide range of topics beginning with the selection of a cerium-bearing compound for use in experiments. Having identified optimal feed solution parameters, the second section presents sol-gel processing considerations and the equipment

developed for the fabrication of gelled, monodisperse microspheres with a final diameter near 100 μm. In section three, needle size and stripping oil flow rates were varied to determine the resulting microsphere sizes and their corresponding degree of monodispersity. Pressurized water treatments are assessed in section four for their capacity to remove impurities and prevent microsphere cracking upon drying and heat treating. Section five provides an analysis of microsphere density, crystallite size, and specific surface area as a function of heat treatment. The results presented on cerium oxide process development and material characterization are intended to serve as a basis for evaluating whether more targeted research is merited into producing plutonium oxide microspheres for pressing into pellets.

4.1 Cerium Gelation

4.1.1 Cerous Nitrate Gelation

Prior to automated production of microspheres using a two-fluid nozzle, initial work was performed using mixed feed solutions prepared from cerous nitrate. Concentrated solutions were easily prepared from cerous nitrate hexahydrate by dissolution with deionized water, but attempts to pre-neutralize nitrate in the solution using either ammonium hydroxide or sodium hydroxide were unsuccessful. Upon addition of a concentrated hydroxide solution, a precipitate formed that prevented further use. For this reason, cerous nitrate feed solutions were not made acid deficient prior to sphere-forming experiments or gelation trials.

Cerous nitrate mixed feed solutions could only be used to prepare spheres for a short time before noticeable color changes and solution hardening took place. A change in color was indicative of the onset of a hardening reaction, which generally took several minutes if the mixed feed solution was cooled or at room temperature. Upon heating mixed feed solutions, a light-khaki, wax-like substance formed more quickly that hardened with time.

Gelation trials using 3 M cerous nitrate with various R values resulted in mixed feed solutions that changed color in less than five minutes, despite vigorous mixing and chilling to 0 °C. As indicated in Figure 4.1, mixed feed solutions that were initially transparent first became cloudy then changed to an opaque white color. Variability in the times recorded included 1-2 seconds for visual judgment. Times reported for repeated trials were typically within 5-10% of each other. Despite variability observed in the data, trials with low R values appeared to result in quicker color transitions than high R-value mixtures. However, each trial used 1 mL of cerous nitrate while volumes of HMTA/urea solution ranged from 1.2-3.3 mL depending on the R value.

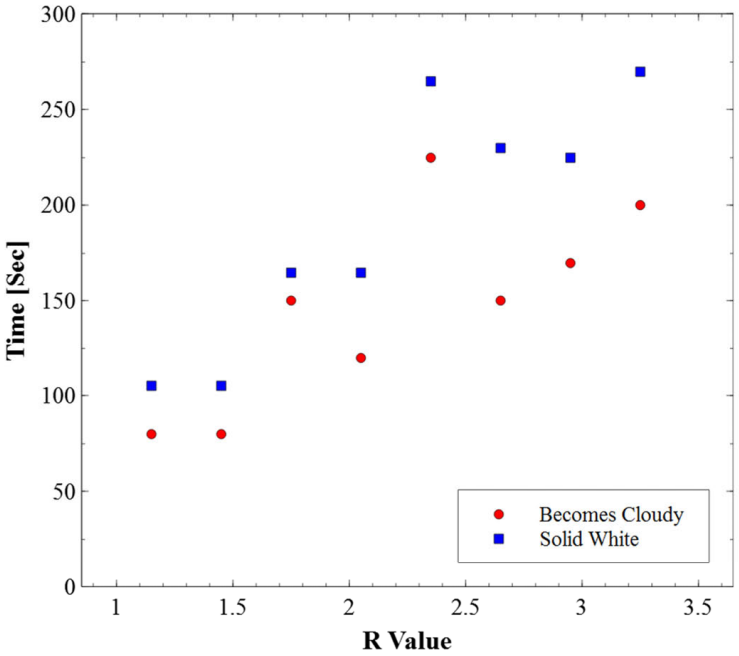

R Value	Cloudy [sec]	White [sec]
1.15	80	105
1.45	80	105
1.75	150	165
2.05	120	165
2.35	225	265
2.65	150	230
2.95	170	225
3.25	200	270

Figure 4.1: Mixed feed solutions prepared from cerous nitrate gelled minutes after mixing despite cooling to 0 °C.

4.1.2 Ceric Ammonium Nitrate Gelation

Feed solutions

Solutions of ceric ammonium nitrate with a concentration of 1.675 M were easily prepared and made acid deficient by dropwise addition of concentrated ammonium hydroxide. Although a precipitate crust formed upon adding the hydroxide, it was easily dispersed and re-dissolved into the solution with rapid stirring. The pH of resulting acid deficient CAN solutions is given in Table 4.1. Although the values are all negative, an increasing pH trend is seen with larger NH_4OH additions. The pH of the HMTA/urea solution was also measured and found to be 9.29.

Table 4.1: Acid deficient ceric ammonium nitrate pH values increased with increasing ammonium hydroxide addition.

OH^-/Ce^{4+} Ratio	[Ce]	pH
0.00	1.675	-0.61
0.25	1.631	-0.54
0.50	1.588	-0.48
0.75	1.548	-0.39
1.00	1.51	-0.27

Gelation trials

All mixed feed solutions prepared from ceric ammonium nitrate were stable while chilled at 0 °C but underwent a noticeable reaction upon heating. After immersing in the 85 °C hot water bath, samples eventually became either viscous or solid, directly preceded by a color change. Since the heating geometry was the same between trials and the heat transfer conditions were expected to be very similar, no compensation was made for the trial sample volume. Higher values for OH^-/Ce^{4+} and R resulted in faster gelation and the production of progressively harder, and sometimes translucent, yellow gels. Trials with low OH^-/Ce^{4+} and R values produced gels that tended to be soft and an opaque, pale yellow color.

Gelled mixed feed solutions were first assessed on the basis of gelation time, aged gel pH, color, and apparent hardness. Gelation times and final pH are shown in Figure 4.2 and Figure 4.3, respectively. Variability in the times recorded included 1-2 seconds for visual judgment. Times reported for repeated trials were typically within 5-10% of each other. Trends observed for the rigidity and color of aged gels corresponded to final pH values. Gels with a pH below 5.35 were an opaque, pale yellow, while gels with a pH above 5.35 were more tan or khaki in color. Similarly, the hardest gels had a final pH above 4.65 while those that did not solidify generally had a pH below 4.0. Pale yellow gels with low final pH tended to be more powdery while tan gels with pH above 5.3 were solid and evolved a clear supernatant upon aging. Repeated measurements of sample pH indicated agreement within 5%.

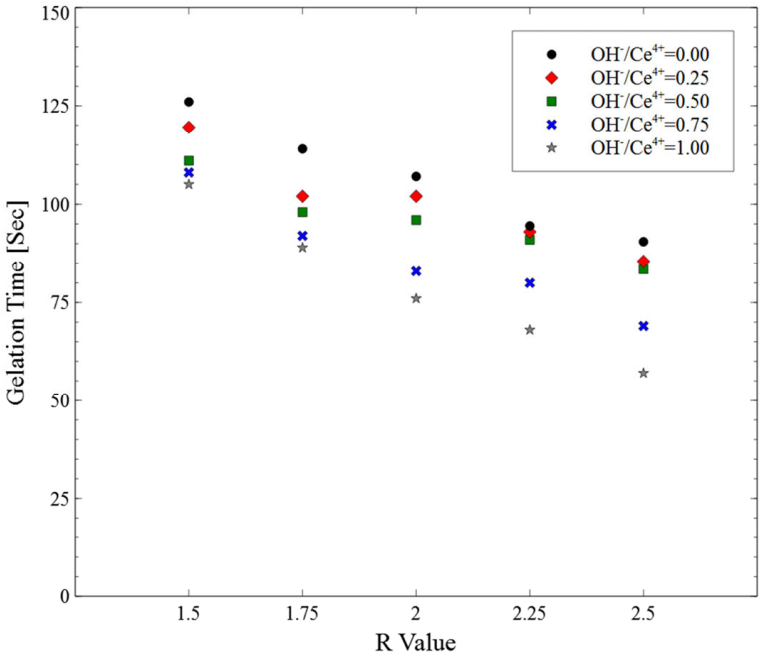

Figure 4.2: Mixed feed solution gelation times decreased with increasing acid deficiency and increasing R values.

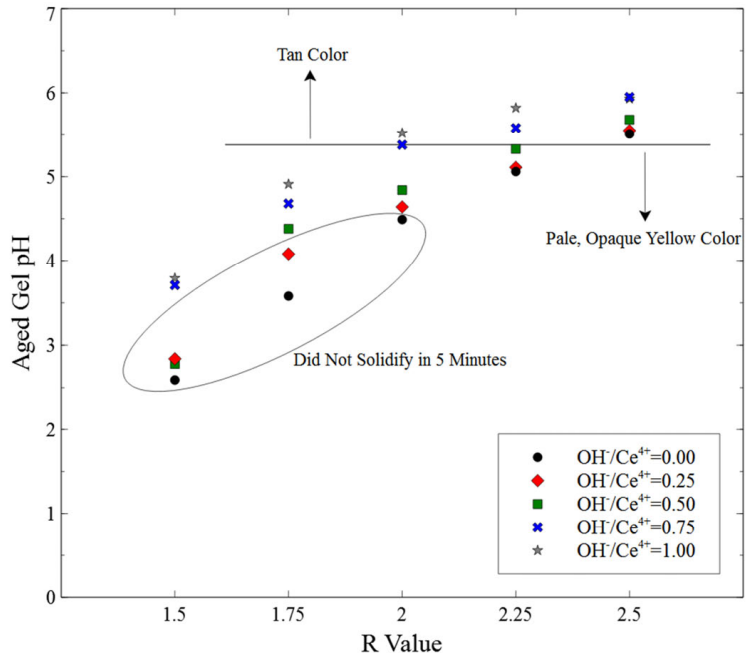

Figure 4.3: Aged gel pH values increased as acid deficiency and R values increased.

The pH of mixed feed solutions was also measured prior to heating to provide a metric for total pH change occurring during gelation. Figure 4.4 presents the pH of chilled, mixed feed solutions prior to heating. Notably, the initial pH of feed solutions changes little except at high values of both acid deficiency and OH^-/Ce^{4+}. Based on this observation, Figure 4.5 was prepared showing the change in pH between chilled, mixed feed solutions and their corresponding aged gels. Observing Figure 4.5, it is apparent that there is a peak in the change in pH at a particular R value for each acid deficiency ratio. Considering the implications of pH change in the internal gelation process, the change in pH plot may provide a unique metric for optimal parameter selection.

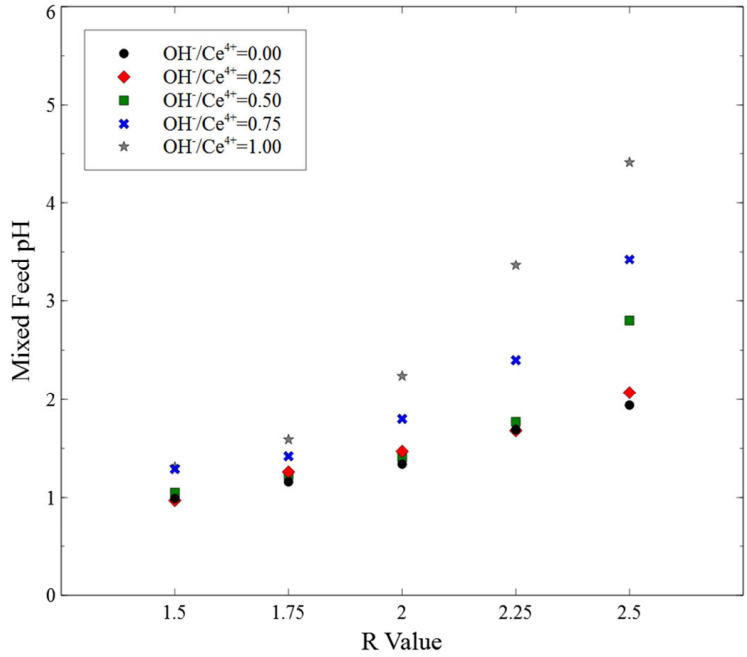

Figure 4.4: The pH of chilled, mixed feed solutions prior to heating increased as acid deficiency and R values increased.

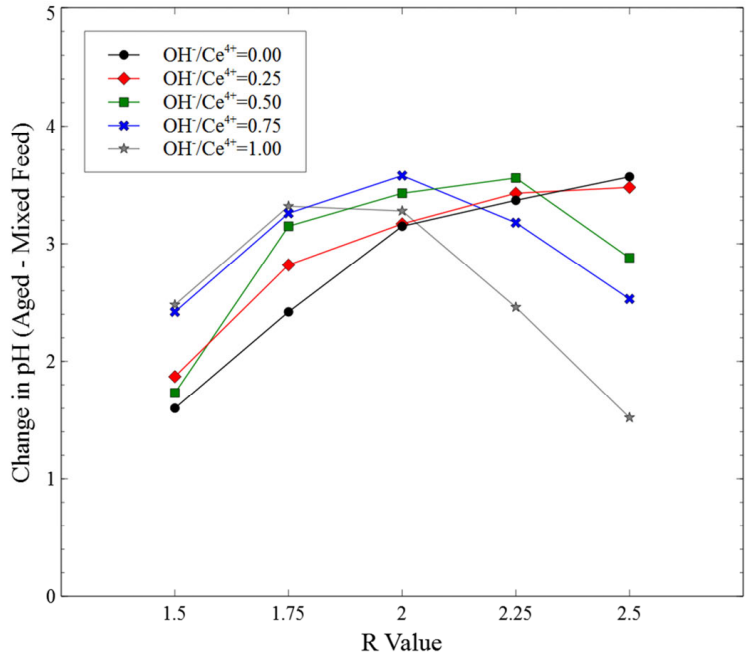

Figure 4.5: Plots of the change in pH appear to provide a tool for optimal parameter selection.

4.2 Construction and Scale-Up of a Sol-Gel Rig

After establishing that solid cerium oxide gels could be produced from ceric ammonium nitrate by the internal gelation method, the next phase of work involved the construction of an apparatus to produce gelled microspheres. While preliminary system development was based on published information on internal gelation equipment, it was soon discovered that production of monodisperse microspheres with final diameters in the range 50-200 μm would require entirely new hardware and procedures. Based on the development work performed, this section has been split into three subsections representing phases of the sol-gel equipment and procedures. Key experiments performed in each phase are presented. In the first subsection, preliminary experiments using cerous nitrate to elucidate tradeoffs in temperatures and needle sizes are described. The second subsection presents hardware developed for automated sphere formation and initial efforts to wash and heat treat gelled microspheres. Final equipment modifications necessary for monodisperse microsphere formation at higher throughputs are described in the third subsection.

4.2.1 Preliminary Setup

To understand the basic operating principles of microsphere fabrication by internal gelation, initial experiments were performed to assess the forming column temperature requirement, propensity for needle clogging, and the effects of washing and heating gelled microspheres. Cerous nitrate used as a feed material in these tests was adequate for simple investigations, but its instability upon mixing with HMTA/urea solutions motivated a search for more stable feed solutions.

Temperature requirement:

The temperature of oil in the forming column had a significant impact in the final integrity of gelled microspheres. At 80 °C, spheres were observed to change from transparent to cloudy in the bottom half of the column, but tended to recombine upon stacking at the bottom of the column. While spheres produced at 90 °C turned opaque higher in the column, they also were very soft and tended to flatten like pancakes or recombine at the bottom of the column. Spheres produced at column temperatures ≥ 100 °C also turned opaque at the top of the column, but maintained their independent identities at the bottom of the column, allowing for extraction and initial washing trials. All gelled spheres produced in these initial trials with cerous nitrate were very soft and crushed easily.

Needle clogging:

Needle size and chilling mixed feed solutions had significant impacts on sphere production. Room-temperature mixed feed solutions resulted in quicker sphere gelation in the heated forming column, but also solidified in the dispensing syringe, clogged needles, and prematurely ended the experiment. Feed solutions chilled to 0 °C prior to mixing and dispensing with a syringe took longer to solidify in the heated forming column, but did not clog the syringe or needle in the ten minutes it took to disperse all the feed. Larger, 20 gauge needles took longer to clog with room-temperature solutions, but produced spheres with diameters of approximately 2 mm that passed through the forming column in approximately 15 seconds. Many of the 2 mm spheres did not solidify sufficiently in the column and recombined at the bottom due to the short transit time and larger thermal mass. Smaller, 30 gauge needles produced spheres with diameters less than 1 mm that had a residence time of about 40 seconds in the forming column. Smaller

spheres tended to gel more quickly than the 2 mm spheres and retained their independent identity at the bottom of the column. However, 30 gauge needles clogged readily. The effects of needle size and mixed feed solution chilling are summarized in Figure 4.6.

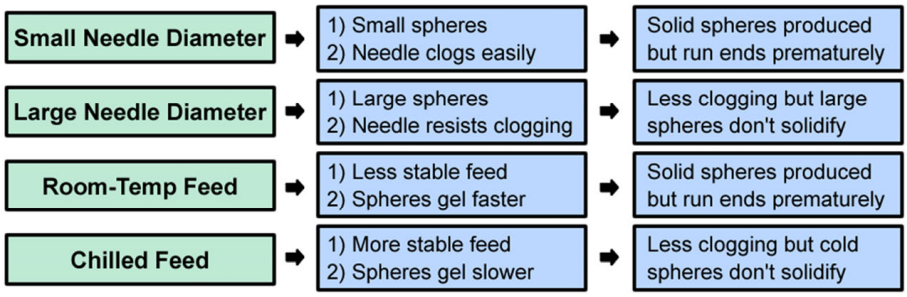

Figure 4.6: Changes in needle size and mixed feed chilling impacted needle clogging and sphere solidification.

Washing and heating:

Spheres surviving the gelation step without recombination or pancaking were washed using acetone and 2 M NH_4OH. Initial washing trials used acetone in place of trichloroethylene due to the carcinogenic properties of TCE. However, acetone was found to erode and rupture some spheres, particularly those that appeared softer. An attempt to use carbon tetrachloride to remove silicone oil did not appear to be more effective than using acetone, and also resulted in catastrophic failure of spheres upon heating. Ammonium hydroxide washes, however, resulted in a color change and apparent hardening of the microspheres, allowing for subsequent heat treatment. Upon heating at 100 °C, microspheres dried and became hollow. Many disintegrated into smaller fragments, and those that were intact had a structure like raspberries, as seen in Figure 4.7. Heating to higher temperatures resulted in distinct color changes. After heating to 250 °C, spheres were black but became pale yellow after heating to 600 °C. As can be seen in Figure 4.7, none of the microspheres produced from cerous nitrate had desirable surface

properties after drying and heating. Additionally, large quantities of fines were produced during the heat treatment process.

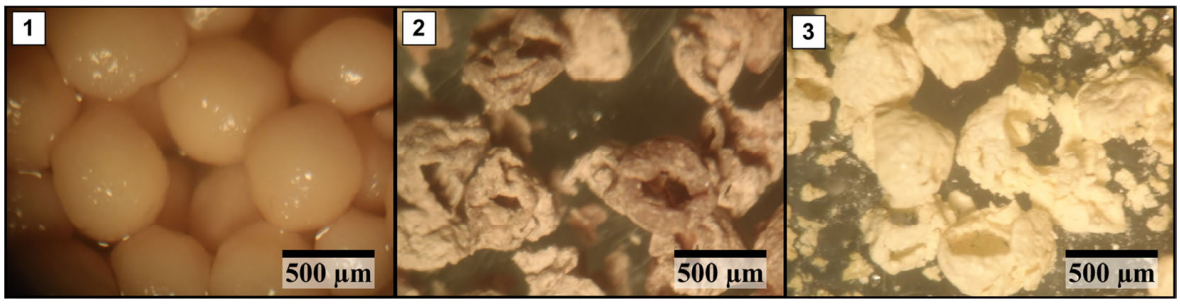

Figure 4.7: Cerium oxide spheres produced from cerous nitrate in the (1) gelled, (2) 100 °C dried, and (3) 600 °C heated state. Note: scale bars are approximate.

4.2.2 Automated Sphere Formation

The two-fluid nozzle pictured in Figure 3.3 was installed on top of the heated gelation column to automate sphere formation. Sphere dispersion was accomplished by pneumatic metering of a chilled mixed feed solution containing ceric ammonium nitrate through a needle and into a continuous flow of silicone oil. Functional feed flow rates, stripping oil speeds, and forming column conditions were found empirically, using the sol-gel rig shown in Figure 3.5, and stronger, more spherical cerium oxide microspheres were produced. During automated sphere production runs, several facts became apparent, including:

1) Microsphere diameter was a strong function of the stripping oil speed.
2) The overpressure applied to the feed solution impacted the frequency of microsphere formation significantly, but had little apparent impact on the microsphere diameter.
3) As the feed overpressure was increased, uniform droplet production eventually transitioned into rapid formation of larger spheres with a wide distribution of diameters.

4) There was no capability for quantitative determination of the stripping oil speed or mixed feed overpressure, thus limiting run-to-run reproducibility.

Flowing silicone oil through the gelation column resulted in favorable changes to microsphere behavior in that region. Without flowing silicone oil through the column, spheres became crowded in the stagnant oil and often coalesced prior to gelation, resulting in larger spheres with volumes corresponding to integer multiples of individual microspheres formed at the needle. However, with oil flowing through the column, microspheres followed a common path through the center of the column in a single-file line resembling a long string of pearls. Figure 4.8 shows three portions of the column as oil flow began and microspheres formed a line. Randomly dispersed microspheres were generated while the oil was stagnant, but tightly-spaced spheres can be seen moving with the oil flow. Spheres following a single-file line exhibited a reduced tendency to agglomerate or coalesce, improving monodispersity. Using this procedure, approximately 0.75 g of cerium dioxide microspheres were produced and recovered for washing with mixtures of isopropyl alcohol, ammonium hydroxide, and deionized water.

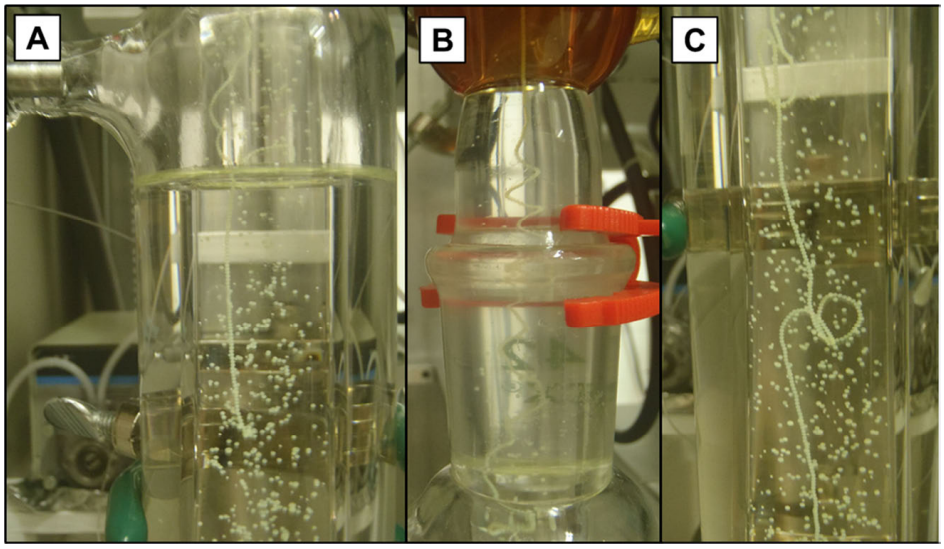

Figure 4.8: As oil in the forming column began to flow, microspheres fell through the column in a single file line. Gelled microspheres falling down the center of the column in a straight line can be seen at the top of image (B). Upon entering a slower region of flow in the collection area, shown in images (A) and (C), spheres began to stack up.

Microspheres produced using ceric ammonium nitrate feeds in the automated sol-gel rig were solid and survived washing steps. To avoid microsphere degradation, an acetone wash was replaced by 50% isopropyl alcohol and 50% 0.5 M ammonium hydroxide. Isopropyl alcohol was intended to disperse spheres and remove silicone oil while ammonium hydroxide acted to further solidify microspheres. Although the spheres were well dispersed in the wash solutions, silicone oil removal was incomplete, and microspheres retained a sheen from the oil after drying with nitrogen gas. Silicone oil evolved during heating operations but many microspheres cracked and had poor surface quality. Figure 4.9 shows the progression of microspheres through the washing, drying, and heating stages.

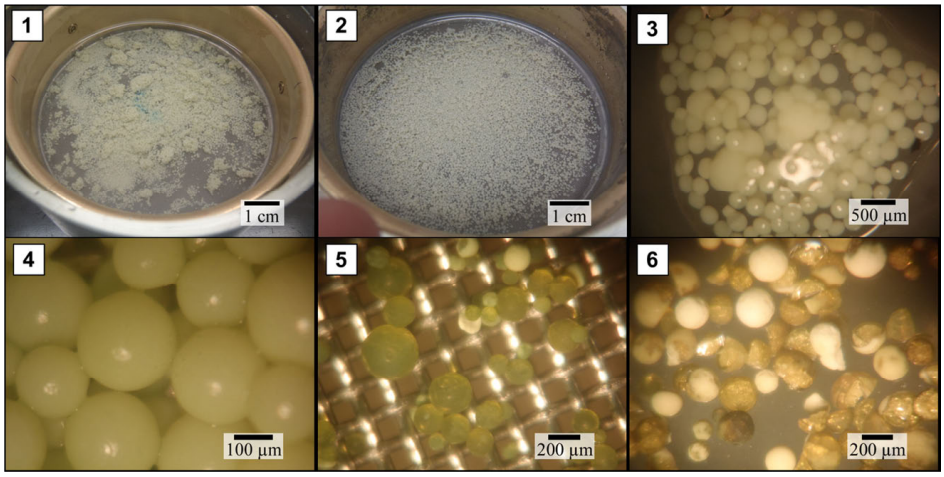

Figure 4.9: Spheres produced from ceric ammonium nitrate using an automated system survived the washing step but cracked during heat treatments. Microspheres are shown (1) during dispersion in a 50% isopropyl alcohol, 50% 0.5 M NH_4OH wash solution, (2) during a 0.5 M NH_4OH wash, (3) wet after washing, (4) dried under flowing N_2, (5) heated to 80 °C, and (6) cracked after heating to 300 °C. Note: scale bars are approximate.

Automated sphere production was complicated by the propensity for needles to clog during operation. In some cases, needles clogged within the first five minutes of a run or even before any microspheres were produced despite efforts to chill the sphere dispersion device with cooling lines. The two-fluid nozzle design shown in Figure 3.3 proved to be problematic as it required complete disassembly for needle replacement, necessitating the end of a run. The glass-Teflon device pictured in Figure 3.7 was designed to facilitate easy needle replacement during a run. While the glass-Teflon sphere forming device functioned as designed, 2-inch-long McMaster Carr needles consistently failed, likely due to a combination of poor quality and insufficient cooling. Fabrication of a sphere forming device that accommodated short, half-inch needles in a chill-able, two-fluid nozzle configuration proved to be an engineering challenge. Once fabricated, however, the aluminum-Teflon sphere forming device shown in Figure 3.8 was effective. The combination of improved cooling, shorter needles, and pre-cleaning high-quality Hamilton Company needles with aqua regia resulted in average lifetimes for 28 gauge needles exceeding four hours, which was similar to the length of typical sphere production runs.

4.2.3 Scaled-Up Production of Monodisperse Microspheres

Addition of a chilled oil vessel, copper chilling block for feed transfer lines, glass mixed feed vessel, an oil pre-heater feeding the gelation column, an ultrasonic bath for oil de-gassing, and a conical mesh for sphere collection resulted in an increased throughput of high-quality, monodisperse microspheres suitable for characterization experiments. The chilled oil vessel with pneumatic transfer to the sphere forming device helped reduce temperatures at the needle and reduce the incidence of clogging. The ability to adequately clean the mixed feed vessel and properly chill feed transfer lines with a copper block also prevented premature gelation of feed solutions and reduced the introduction of small particulates that cause needle blockages. Pre-heating oil before it entered the column helped spheres gel more quickly near the top of the column and overcame lower oil temperatures at the top of the column from chilled stripping oil. A significant improvement to monodispersity was achieved using an ultrasonic bath to de-gas silicone oil during operation.

Bubble generation in the gelation column proved to be a significant problem for producing monodisperse microspheres. After producing spheres for approximately 30 minutes, bubbles began to grow on the inner wall of the gelation column until they became large enough to detach and rise to the top of the column. This phenomenon was not noticed until longer sphere production runs were performed. As bubbles rose in the column, they often collided with microspheres, causing them to deviate from a single-file line and travel random paths. Bubbles were particularly problematic near the top of the column, where they tended to circulate until growing large enough to escape the column through an oil overflow line. Bubbles at the top of the column caused coalescence of un-gelled spheres and resulted in polydispersity. While modifications to the geometry of the top of the column reduced the problem, it was not mitigated

until a system was installed to de-gas silicone oil in the circulation loop using an ultrasonic bath. Periodic de-gassing was sufficient to minimize bubble formation and allow monodisperse microsphere production.

Installation of larger peristaltic pumps for silicone oil flow through the column permitted faster flow rates and fast microsphere production without microspheres stacking up and coalescing. Maximum daily yields were increased from 1-2 g/day to approximately 8-10 g/day of cerium dioxide. Although higher silicone oil flow rates resulted in a reduction of average oil temperature and microsphere residence time in the column, the oil pre-heater installed above the column mitigated the effect on microsphere gelation.

The sol-gel production run described in section 3.2.3 proceeded as intended and yielded microspheres with excellent properties. A flow rate of 4.0 mL/min was established and remained constant, as verified by a digital readout from a flow rate meter. Microspheres were formed at a fixed, desirable frequency with feed overpressures in the range 3.2-3.7 psi. Three hours into the experiment, the first needle clogged and was removed. A new needle was installed that functioned for the remaining 5 hours of the run. Spheres recovered from the mesh cone are shown covered in oil in Figure 4.10. Three successive batches of microspheres made in two days are shown during the washing procedure in Figure 4.11. Washing spheres in mesh sieves and glass dishes allowed for easy effluent draining between washing steps. Air-dried microspheres were a pale, translucent yellow color and had an average diameter of 120 μm, as shown in Figure 4.12.

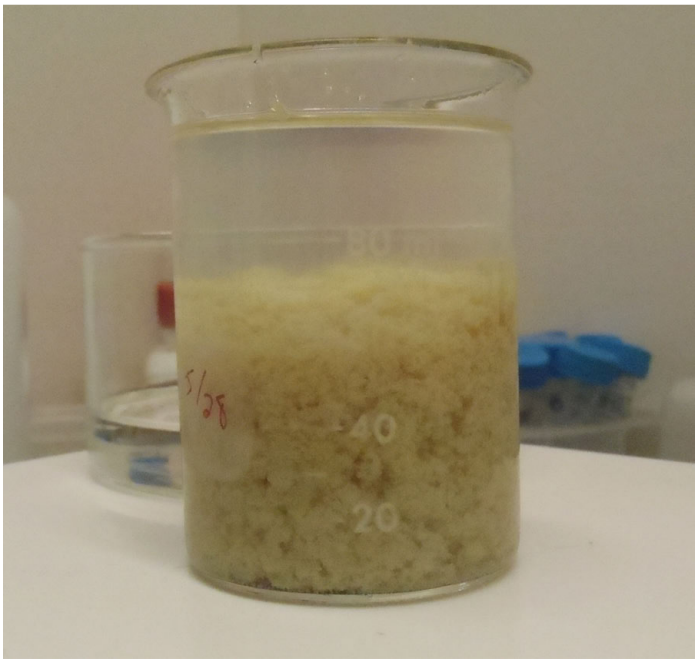

Figure 4.10: Approximately 70mL of gelled microspheres were produced and stored in oil overnight prior to washing.

Figure 4.11: Three batches of microspheres were washed in separate mesh sieves held in glass dishes.

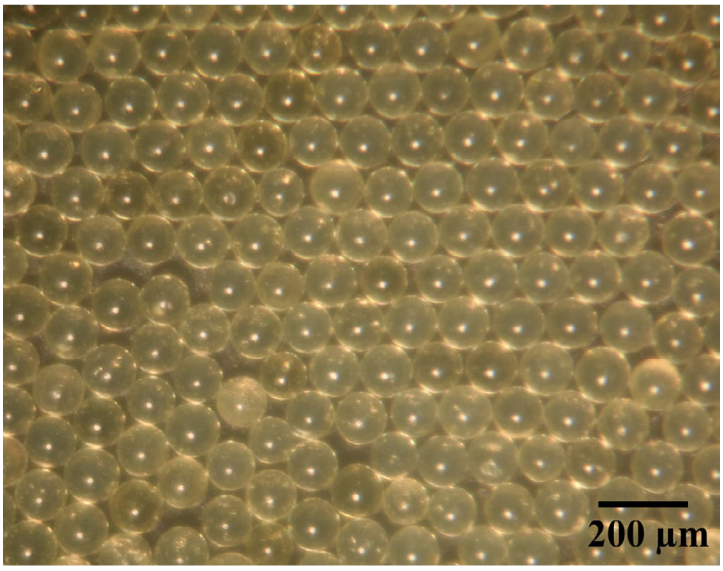

Figure 4.12: Microspheres dried to 150 °C were very uniform with average diameters near 120 µm.

Effect of curing time

An additional experiment produced seven separate samples of microspheres, each with a unique curing time in 85 °C silicone oil. After washing and drying, each sample had a mass of approximately 0.5 g. After washing samples with TCE to remove residual silicone oil, spheres were washed with 25 mL, 0.5 M ammonium hydroxide for 30 minutes. After draining, the effluent conductivity was measured. Washed microspheres were air-dried and massed to provide a mass correction to the effluent conductivity measurements. The resulting specific conductivities as a function of aging time in hot oil are shown in Figure 4.13. Specific conductivities are reported for the first and second ammonium hydroxide washes. In each case, it does not appear that there was any trend indicating a change in microspheres' capability to leach impurities as a result of aging time. However, samples that were not aged in hot silicone oil exhibited a slightly higher initial effluent conductivity.

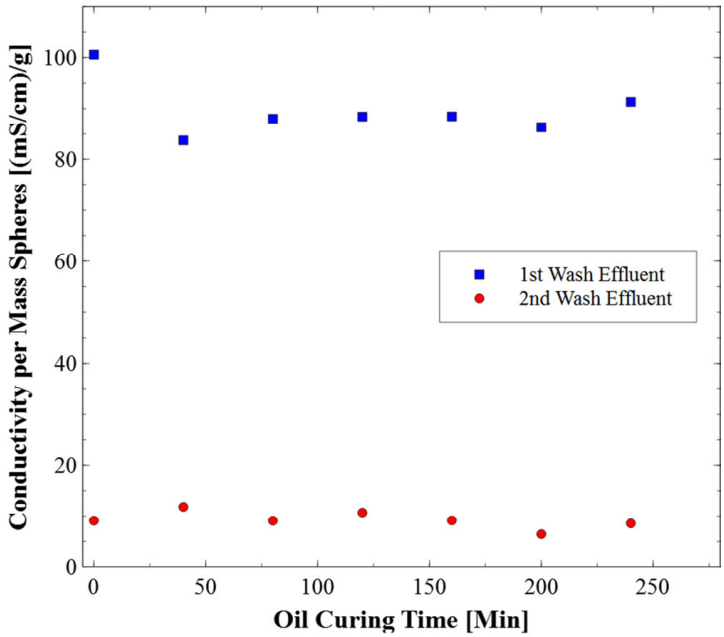

Figure 4.13: Microsphere aging times in 85 °C silicone oil after gelation did not appear to have an impact on the leaching of conductive impurities.

4.3 Determination of Size Uniformity

With sol-gel equipment development complete, an experiment was performed to determine the sizes and monodispersities of microspheres produced using 26, 28, and 32 gauge needles with stripping oil flow rates of 1.5, 4.0, and 6.5 mL/min. Each of the nine samples produced were washed, dried, and sintered to 1500 °C. Sintered microspheres were bonded to glass slides, imaged with an optical microscope, and sized using a contrast-based method. Particle diameters and shape factors were measured and used to obtain the average diameter of microspheres in each sample. The resulting average diameters and standard deviations are summarized in Table 4.2. Constraints imparted on particle size and shape factor for the analysis are also provided in Table 4.2. Microsphere sizes covered a range from 65.5-211 μm with standard deviations in most cases less than 4%. Needle size appeared to have a more significant impact as the stripping oil speed was reduced. The diameter of microspheres produced at the

fastest stripping oil speeds varied by less than 10% across needles compared to 22-25% for intermediate and slower oil speeds. The dynamic range of microsphere sizes also tended to increase with larger needle sizes; microspheres produced by the 26 gauge needle encompassed nearly the entire dynamic range of all three needles tested.

Table 4.2: Average microsphere diameters were measured using three needle sizes and stripping oil flow rates of 1.5, 4.0, and 6.5 mL/min. Average diameters ranged from 65-211 µm with standard deviations as low as 2.23%.

	26 Gauge Needle			28 Gauge Needle			32 Gauge Needle		
Constraints:	**1.5 mL/min**	**4 mL/min**	**6.5 mL/min**	**1.5 mL/min**	**4 mL/min**	**6.5 mL/min**	**1.5 mL/min**	**4 mL/min**	**6.5 mL/min**
Mean Diameter Range: [µm]	194-238	100-160	50-90	150-220	90-110	58-88	144-180	84-120	54-78
Shape Factor Range:	0.82 - 1	0.9 - 1	0.93 - 1	0.82 - 1	0.88 - 1	0.87 - 1	0.8 - 1	0.86 - 1	0.92 - 1
Results:									
Average Diameter: [µm]	211.28	127.9	70.56	176.34	100.28	71.85	159.05	99.21	65.5
Standard Deviation: [µm]	4.71	7.40	5.48	5.39	2.70	3.92	4.92	3.77	2.43
Standard Deviation: [%]	2.23%	5.78%	7.77%	3.06%	2.69%	5.46%	3.09%	3.80%	3.71%
Spheres Counted:	560	446	247	247	492	809	972	1395	2113

While analyzing sphere sizes, it became apparent that the software was unable to accurately determine the diameter of microspheres in contact with one another. Therefore, size thresholds were employed to eliminate groups of two or more microspheres. In each image analyzed, unique thresholds were determined to ensure that larger microspheres were not discounted from analysis. Upon scanning images for particle sizes, it became apparent that there were several size modes, as indicated in Figure 4.14. Individual microspheres comprised the largest size group and are shown in red. Another clear peak was identified corresponding to two adjoined spheres, or doublets. Additionally, larger sizes recorded by the software were easily identified as agglomerations of three or more microspheres. Based on this analysis, generous size windows were defined as constraints for average microsphere diameter analysis while excluding agglomerations of two or more spheres. Lower bounds were also set to eliminate dust and microspheres cut in half by image stitching operations from analysis.

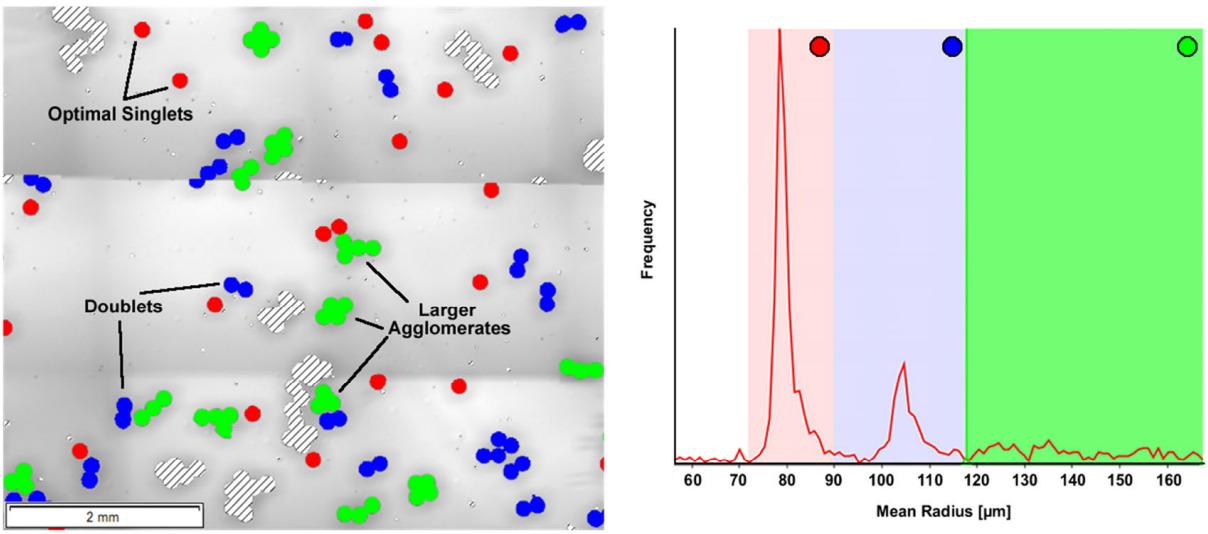

Figure 4.14: Sphere size was easily separated into categories of single spheres, doublets, and larger agglomerations.

Sizing analysis based on particle-background contrast was complicated in a few samples by thicknesses of photoresist that caused a shadow feature around some microspheres. As can be seen in Figure 4.15, ripples in the photoresist and resulting shadows caused the software to misrepresent the actual microsphere size and shape. However, not all single microspheres had shadows and misinterpreted microspheres were removed from analysis by application of a shape factor constraint. Shape factor windows used in the analysis are provided in Table 4.2 and were as wide as 0.8-1.0 and as restrictive as 0.93-1.0. Observed values of shape factors on microspheres without shadows were in the range 0.95-1.0 using the Olympus Stream micro-imaging software. Further, shape factors of 0.97-1.0 were obtained using ImageJ on high-quality scanning electron microscope photographs of microspheres. The exclusion of microspheres based on shape factor was not expected to unreasonably improve the standard deviation of average microsphere diameters. Rather, actual monodispersities are expected to be better than reported for spheres produced using a 26 gauge needle at 4.0-6.5 mL/min stripping oil flow rates due to conservative shape factor and diameter range constraints.

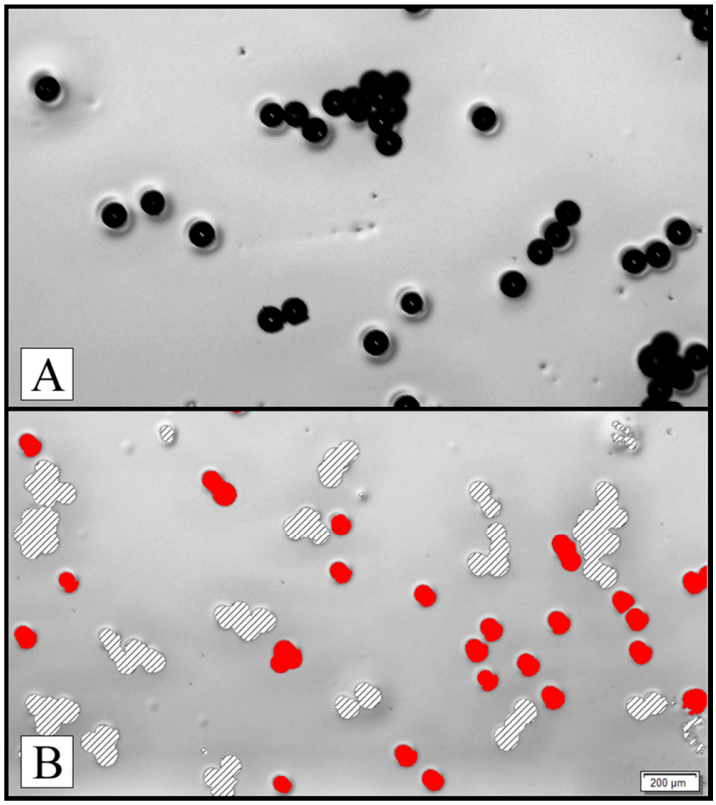

Figure 4.15: Microspheres with shadows yielded an inaccurate representation of diameter and had to be removed from analysis.

While the average microsphere diameter was observed to shrink as needle diameters decreased, the most significant parameter controlling microsphere size was the stripping oil speed, as seen in Figure 4.16. While microspheres produced using the 26 gauge needle at a stripping oil flow rate of 1.5 mL/min were the largest produced in the experiment with an average diameter of 211 µm, increasing the stripping oil flow rate to 6.5 mL/min resulted in microspheres with an average diameter of 70.5 µm, which was within 5 µm of the smallest spheres produced using the smallest needle, as shown in Figure 4.17. Microspheres produced using 26, 28, and 32 gauge needles are shown in Figure 4.18, Figure 4.19, and Figure 4.20, respectively, after drying at 150 °C and sintering to 1500 °C for four hours. Pale yellow, translucent microspheres in the air-dried state became translucent orange after drying at 150 °C and an off-white, pearl color after sintering.

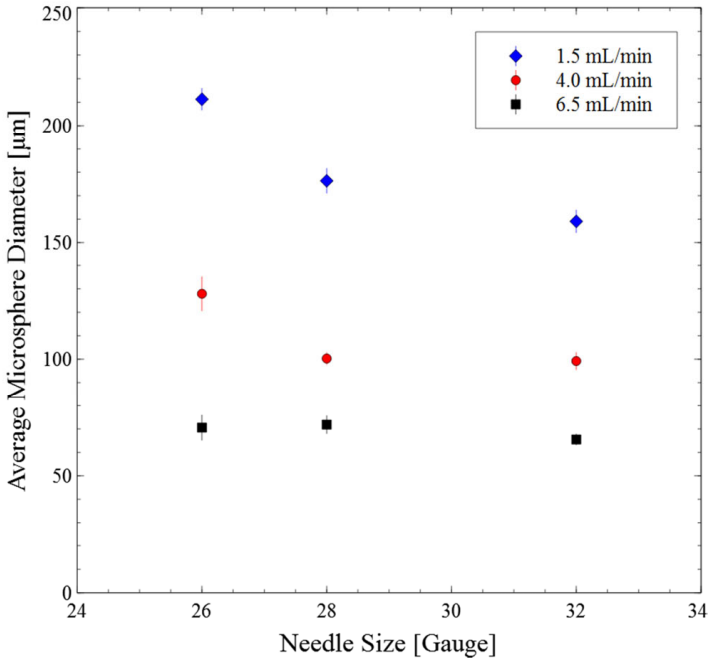

Figure 4.16: Stripping oil flow rates had a larger impact on microsphere diameter than the size of the dispensing needle.

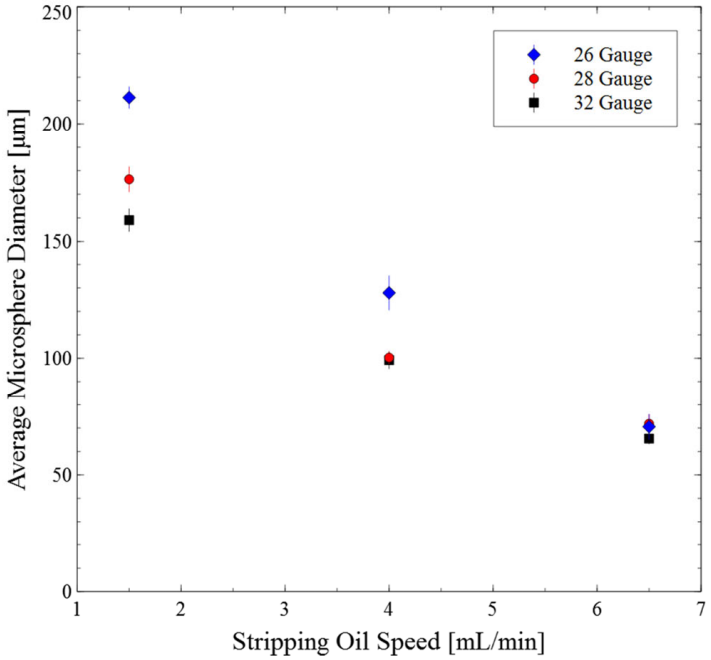

Figure 4.17: Microsphere diameters produced from different needles became more similar at fast stripping oil flow rates.

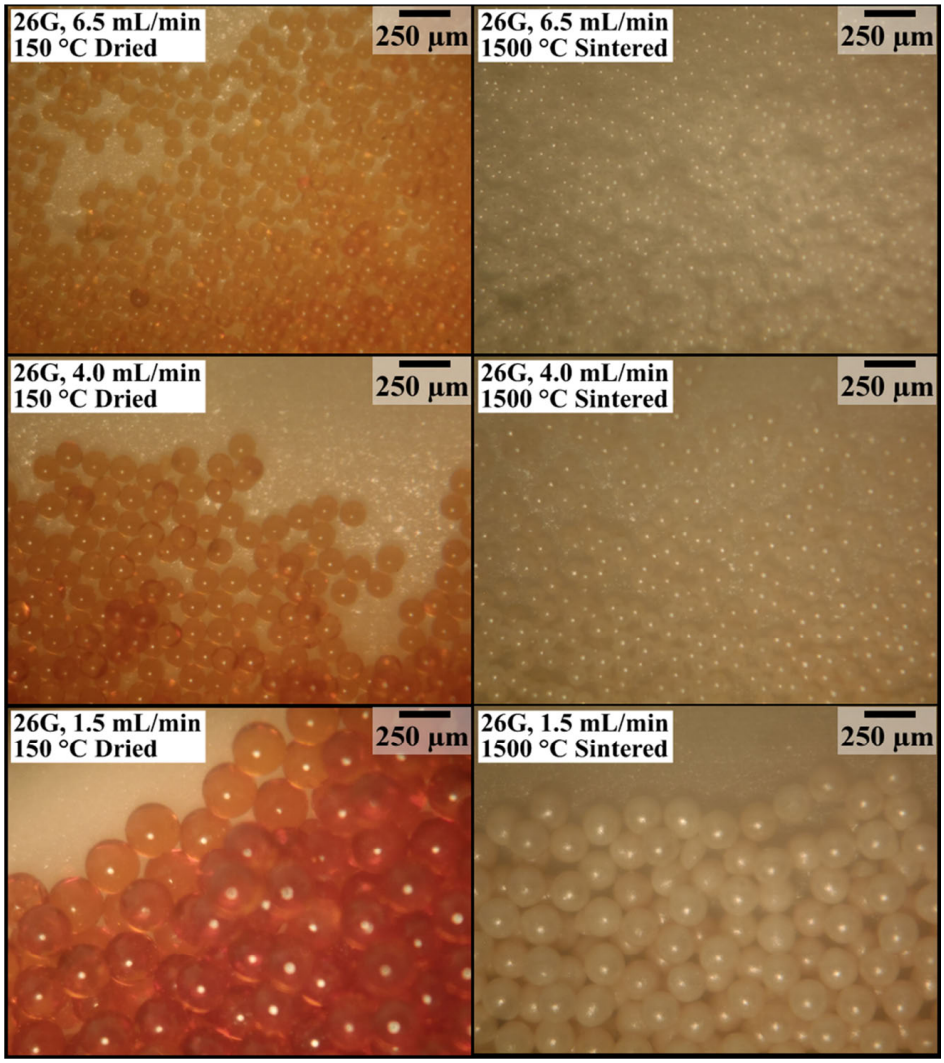

Figure 4.18: A 26 gauge needle produced the largest microspheres in the sizing study but also exhibited the largest dynamic range of diameters by varying stripping oil flow rates.

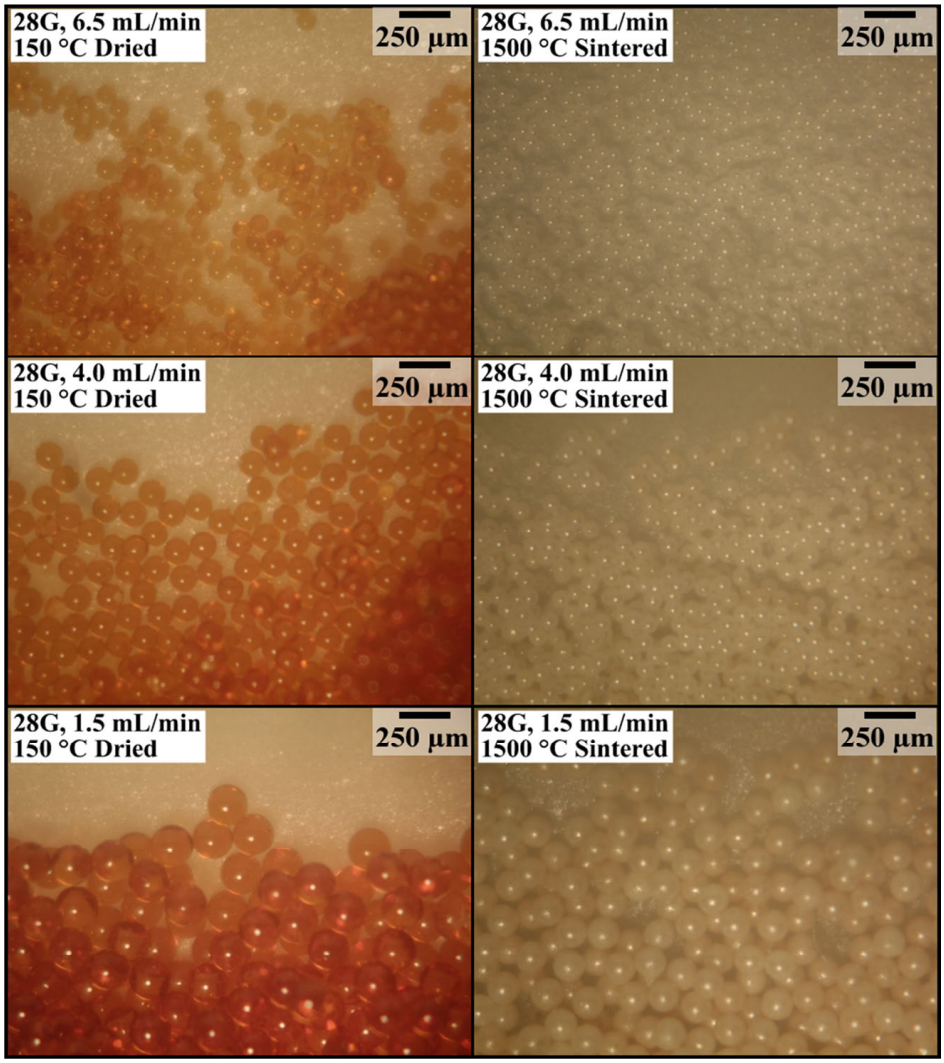

Figure 4.19: A 28 gauge needle produced microspheres with average sintered diameters from 72-176 µm.

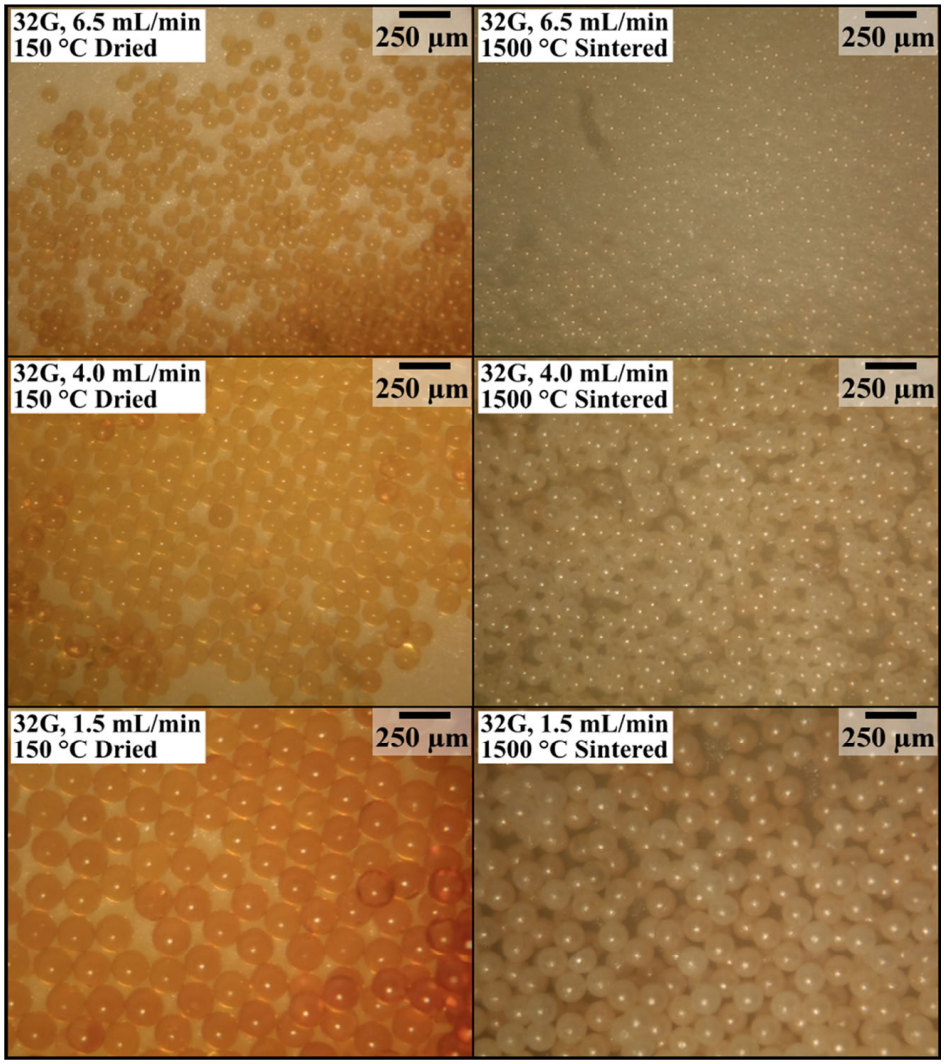

Figure 4.20: A 32 gauge needle produced the smallest microspheres in the sizing study with an average diameter of 65.5 µm after sintering.

4.4 Microsphere Washing Techniques

Two of the key questions regarding the suitability of internal gelation sol-gel methods for Pu-238 pellet fabrication revolve around the generation of fines from microsphere cracking and the final impurity levels. During work with the sol-gel process, it became clear that at the heart of these issues is the washing technique used to remove excess reagents and reaction products from gelled microspheres. While traditional two-step washing techniques often resulted in

microsphere cracking, easy-to-implement modifications to these methods prevented microsphere cracking and demonstrated impurity removal. In the first subsection, the effects of a pressurized water treatment are presented. The second subsection provides the results of several impurity analyses on sintered cerium dioxide microspheres.

4.4.1 Comparison of Baseline and Pressurized Water Treatment Processes

Based on an apparent reduction in microsphere cracking after a two-hour pressurized water treatment at the end of washing operations, several experiments were performed to elucidate the mechanisms responsible and the other effects of a pressurized water treatment. The first subsection compares measurements of microsphere diameters after washing, autoclaving, and drying in air. The same microspheres were used for an experiment in the next subsection comparing the degree of cracking after being heat treated to 600 °C. Transmission electron microscopy was performed in the third subsection on the same microspheres after grinding to a fine powder to compare the crystallite sizes. The fourth subsection describes thermal gravimetric analysis of microspheres and the last subsection presents results from electron-impact mass spectroscopy.

4.4.1.1 Shrinkage Comparison

Gelled microspheres that cooled overnight were washed and sized to determine the extent of shrinkage during pressurized water treatments. The resulting average diameters of wet, gelled microspheres at the end of each stage are listed in Table 4.3. While the 7 μm reduction in average diameter due to rinsing microspheres with deionized water is difficult to distinguish from statistical variation, a diameter reduction of approximately 24% from 384 μm to 292 μm was observed after a pressurized water treatment. A 24% diameter reduction is equivalent to a volume reduction of 56%, indicating that a large volume reduction occurred for wet, gelled

microspheres during the hydrothermal treatment. Reductions in microsphere volume correlated with increases in the pressurized water treatment effluent volume. After air-drying, autoclaved microspheres had an average diameter of 174 μm compared to 205 μm for microspheres dried in ammonium hydroxide without autoclaving. Based on these measurements, pressurized water treatments reduced the air-dried volume of microspheres by 39% compared to spheres processed by baseline washing and drying methods. After heating to 600 °C, microspheres air-dried in ammonium hydroxide had an average diameter of 147.5 μm compared to 157.7 μm for microspheres treated with pressurized water. The smaller diameter of microspheres dried in ammonium hydroxide after heating can be partially attributed to cracking, as discussed in the next section.

Table 4.3: Pressurized water treatments (PWT) caused significant shrinkage of gelled microspheres.

	Average Diameter	Standard Deviation	% Standard Deviation
Post-NH_4OH Wash	384	22.9	6.0%
Post-H_2O Rinse	377	20.5	5.4%
Post-2hr PWT	292	24.3	8.3%
Post-2hr PWT + 4hr PWT	295	22.7	7.7%
PWT + Air-Dried	174	10.4	6.0%
NH_4OH Air-Dried	205	15.7	7.6%
PWT + 600 °C	157.7	7.9	5.0%
NH_4OH + 600 °C	147	6.4	4.3%

4.4.1.2 Cracking Comparison

Air-dried microspheres from the previous section were slowly heated to 600 °C, as indicated in Figure 3.18, and cracking behavior was compared between those simply dried in ammonium hydroxide and those subjected to a two-hour pressurized water treatment.

Comparing the masses of samples before and after heating revealed a volatile mass loss of 6.4% in autoclaved microspheres and a volatile mass loss of 32.6% for microspheres dried in ammonium hydroxide. No measureable fines were detected for the former, although approximately 1.2% by mass of the latter fractured into particles less than 150 μm. The same experiment repeated at a faster ramp rate of 5 °C/min resulted in similar volatile mass losses for each sample but increased cracking fractions. At fast ramp rates, autoclaved microspheres generated 0.08 % fines by mass while ammonium hydroxide dried spheres produced 2.05 % fines less than 150 μm by mass.

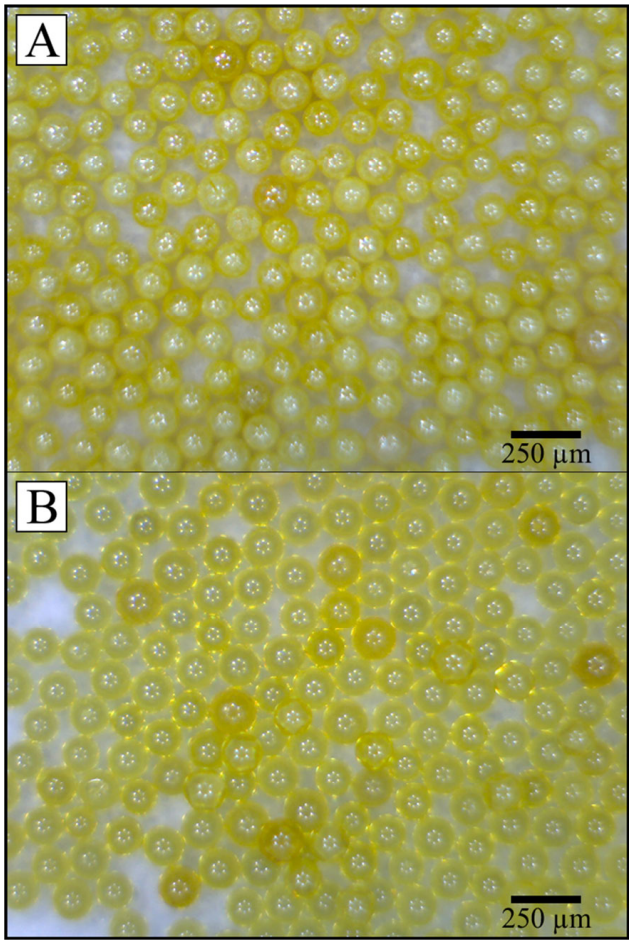

Figure 4.21: After heat treating microspheres to 600 °C, microspheres air-dried in ammonium hydroxide (A) turned opaque and had a rough texture while autoclaved microspheres (B) remained smooth and translucent.

While microspheres air-dried in ammonium hydroxide have slightly smaller diameters after heating to 600 °C, some reduction could be attributed to diameter reductions caused by particles spalling from friable microspheres. Shown in Figure 4.22, microspheres washed and dried without a pressurized water treatment underwent extensive cracking during heat treatments to 600 °C. Visible networks of cracks throughout the microspheres resulted in rough surfaces caused by fragmentation. Although difficult to see at low magnifications, even microspheres that appeared smooth and spherical contained a multitude of fine cracks. It is likely that the rate of surface spalling increased with microsphere handling.

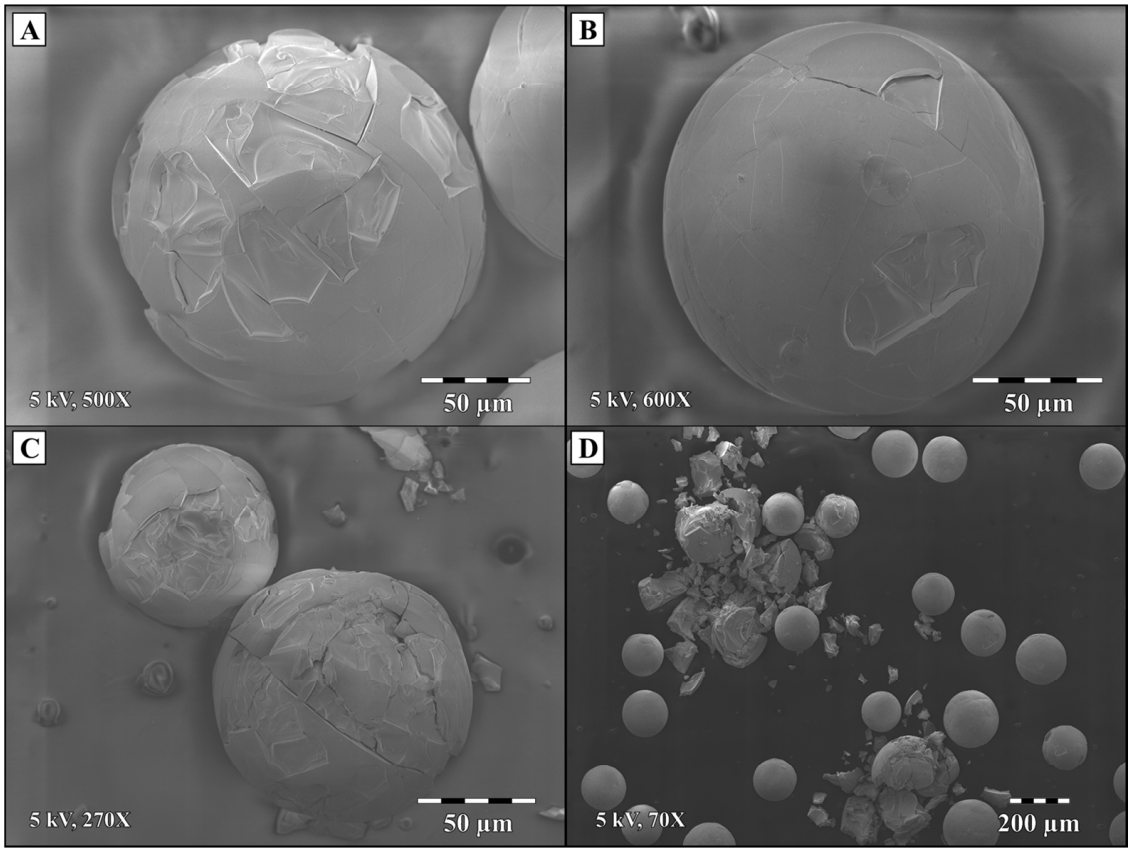

Figure 4.22: Microspheres air-dried in ammonium hydroxide and heated to 600 °C became friable, developing many cracks. Micrographs (A) and (B) show the surface of particles that have lost many fragments. A loose piece of spall is seen near the top of image (B). Deep cracks and catastrophic particle failure resulting in the generation of fines are shown in images (C) and (D).

Microspheres exposed to a two-hour pressurized water treatment exhibited very smooth surfaces free from fine cracks. Cracking in pressurized water treatment samples was rare, but appeared to manifest differently from cracks in the microspheres air-dried in ammonium hydroxide. As shown in image (C) in Figure 4.23, cracks appear more as large splits in particles compared to shattered spheres seen in Figure 4.22.

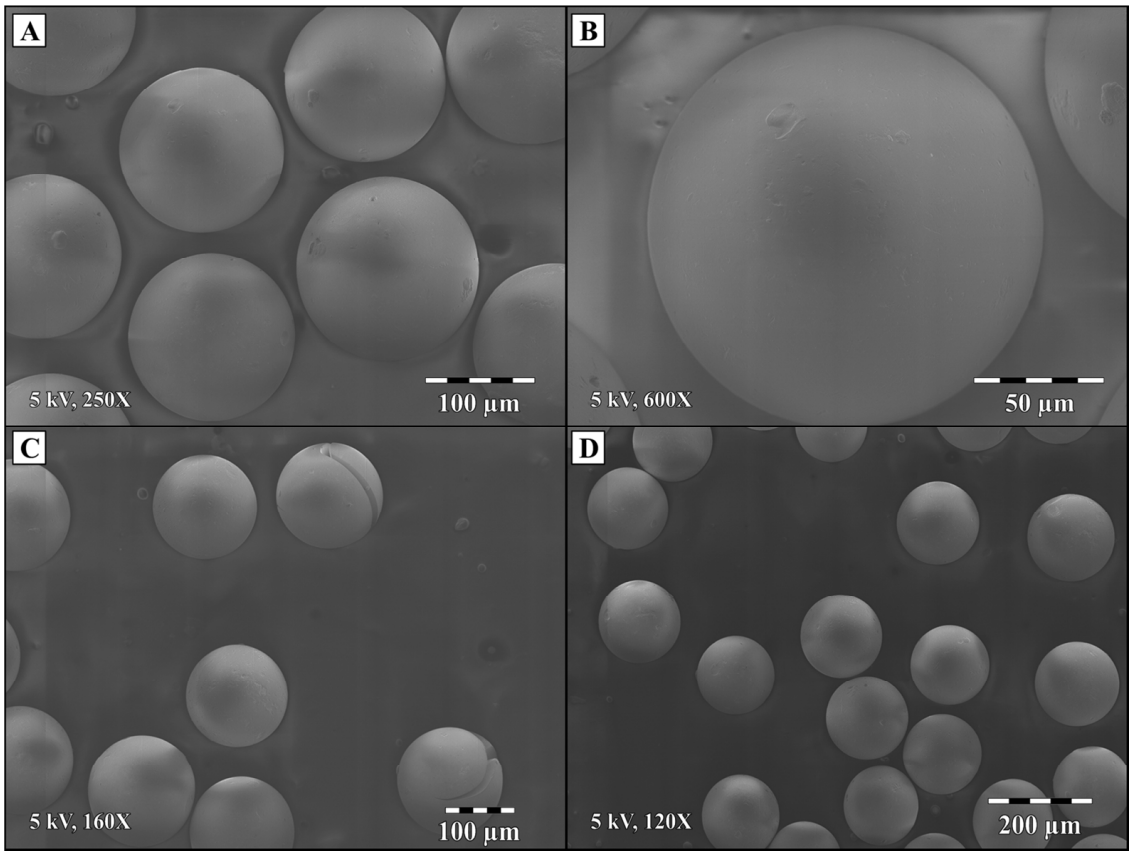

Figure 4.23: Microspheres heated to 600 °C had smooth surfaces and minimal cracking when subjected to a pressurized water treatment after washing steps. Smooth surfaces with no visible cracks are shown in images (A), (B), and (D). The only cracking observed is shown in image (C), where two microspheres appear to have split open.

4.4.1.3 Crystallite Size Comparison

X-ray diffraction spectra and transmission electron microscopy images were obtained to determine crystallite sizes in samples of microspheres processed with and without a pressurized

water treatment. Peak broadening from powder x-ray diffraction spectra was used as a lower bound for average crystallite size after correcting for instrumental broadening. Diffraction patterns for air-dried microspheres after drying in ammonium hydroxide, autoclaving for two hours, and autoclaving for two hours then four hours are shown in Figure 4.24. For comparison, an x-ray diffraction pattern for 99.9% CeO_2 was obtained and is plotted with its Miller indices. All of the peaks obtained for pure CeO_2 were observed in the microsphere samples, although some are difficult to discern without peak deconvolution due to significant peak broadening. Peaks widths were narrower for microspheres heated to 200 °C in pressurized water than those simply dried in ammonium hydroxide, as would be expected due to thermally-induced crystallite growth. However, no additional gains were observed for an additional four-hour pressurized water treatment.

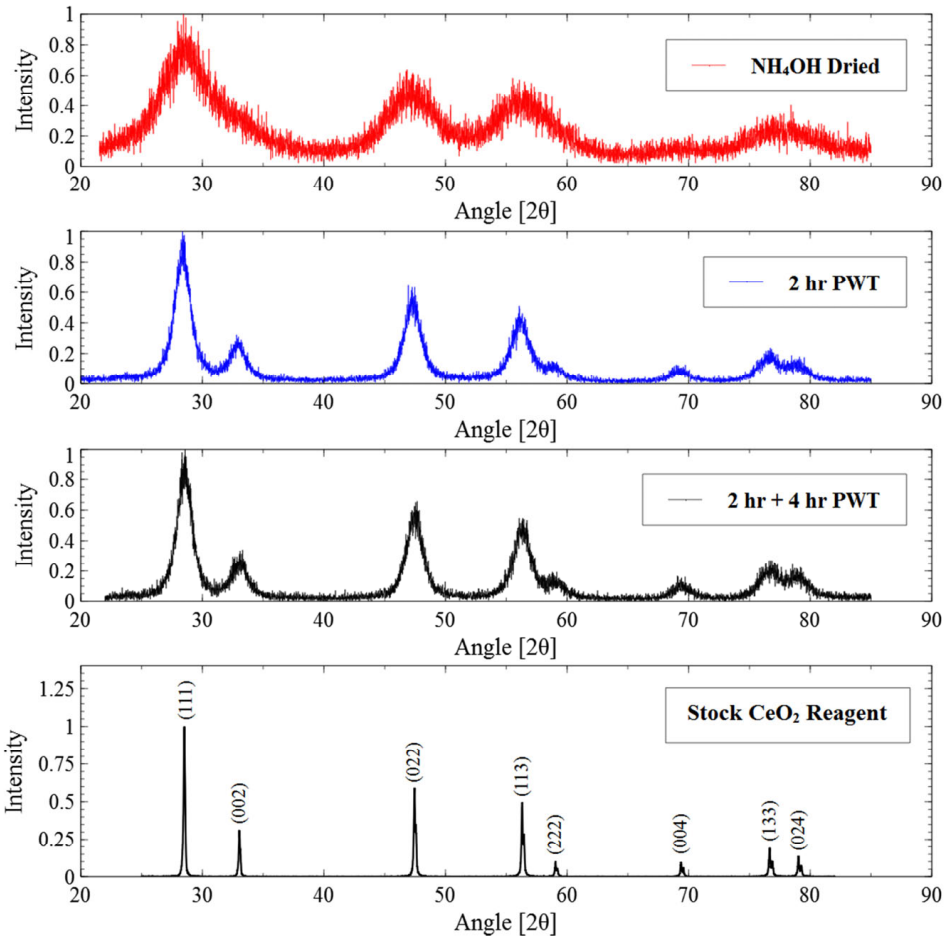

Figure 4.24: Pressurized water treatments resulted in air-dried microspheres with increased crystallinity. A diffraction spectrum for fluorite structure 99.9% cerium dioxide reagent is provided for reference.

Using full width at half maximum values for each peak in the Scherrer formula defined in equation 3.2, estimates of average crystallite size were calculated using each well-defined peak. Figure 4.25 shows the resulting, lower-bound average crystallite sizes. While the largest peaks centered at 2θ angles of 28.5°, 47.5°, and 56.4° provided the lowest standard deviations for all three samples, calculations were also performed at peaks centered at 33.1°, 69.4°, and 76.7° for pressurized water treatment samples. Peak locations determined by peak fitting algorithms all matched theoretical 2θ peak angles generated using the ATOMS atomic structure display code within 0.4 %. Inverse variance weighting techniques were used to minimize the uncertainty in

average crystallite sizes, which were calculated to be 1.71 ± 0.097 nm for microspheres air-dried in ammonium hydroxide, 5.37 ± 0.116 nm for two-hour pressurized water treatment microspheres, and 5.55 ± 0.130 nm for microspheres subjected to two-hour and four-hour long pressurized water treatments.

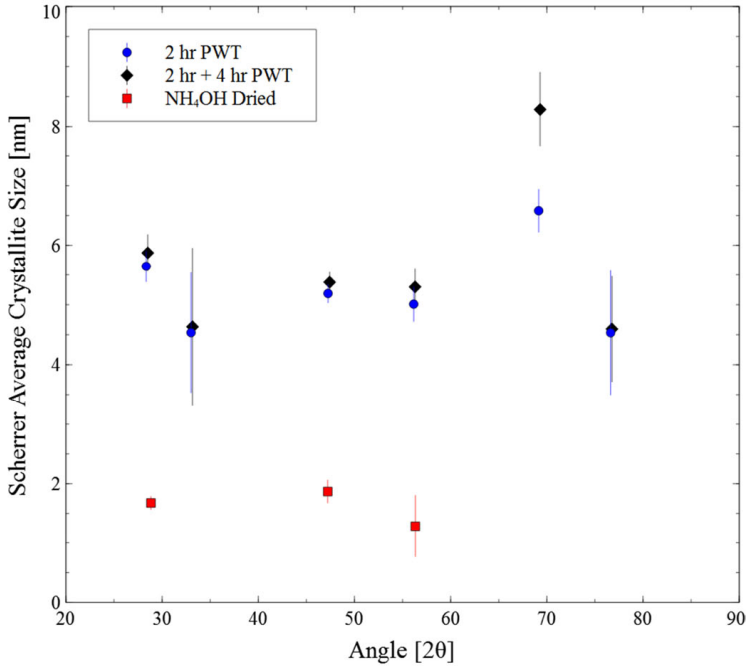

Figure 4.25: Peaks from x-ray diffraction analysis were used to calculate average crystallite size using the Scherrer equation. Larger crystallite sizes resulted from spheres treated with pressurized water at 200 °C.

Transmission electron microscopy of finely ground and dispersed air-dried microspheres prior to heat treatments discussed in the previous section allowed for visualization and direct measurement of crystallite sizes. While most objects viewed under the microscope for the ammonium hydroxide dried sample were too thick or potentially amorphous to distinguish crystallite sizes, a few thin regions were imaged where small crystallites of approximately 1-2 nm could be seen, as shown in Figure 4.26. Crystallites were readily observed and visibly larger

for air-dried samples of microspheres subjected to pressurized water treatments. Shown in Figure 4.27, autoclaved microspheres had crystallites with sizes ranging from 2-4 nm.

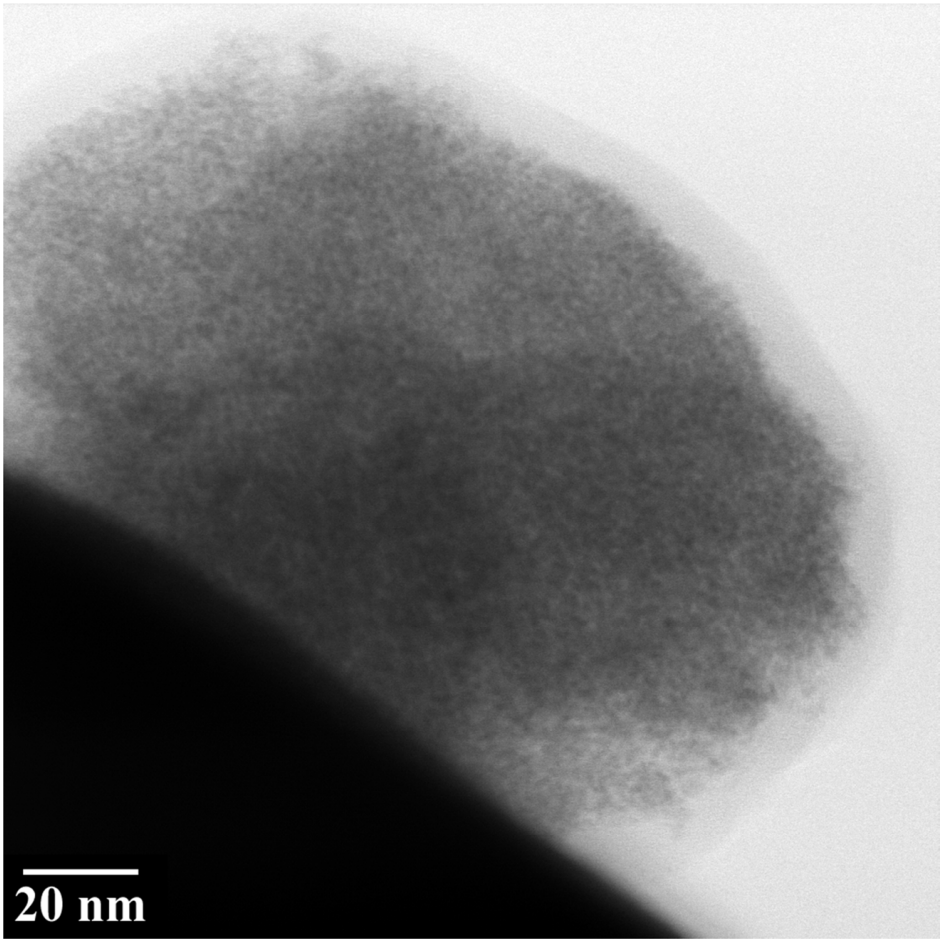

Figure 4.26: Transmission electron microscopy showed crystallite sizes of 1-2 nm for microspheres dried in ammonium hydroxide prior to heat treatments.

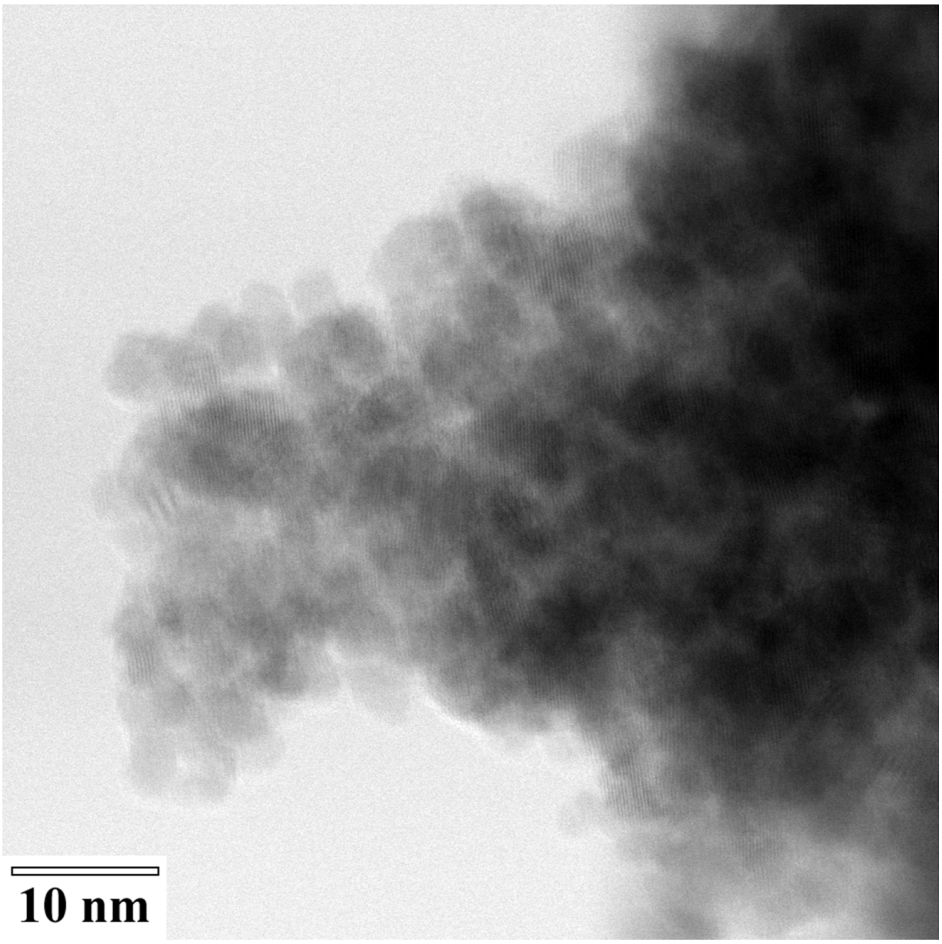

Figure 4.27: Transmission electron microscopy of microspheres air-dried after autoclaving showed crystallites with sizes ranging from 2-4 nm.

4.4.1.4 Thermal Gravimetric Analysis Comparison

Effect of a pressurized water treatment on volatile mass loss

Volatile mass losses upon heating microspheres washed with and without a pressurized water treatment were compared as a function of temperature using thermal gravimetric analysis. Microspheres previously heated to 600 °C in a box furnace were also analyzed using the TGA instrument to ensure instrument stability over the desired temperature range. Less than 0.35% mass reduction was observed in the 600 °C pre-heated sample, indicating instrument stability over the desired temperature range. As indicated in Figure 4.28, microspheres treated with

pressurized water at 200 °C prior to air-drying exhibited a gradual mass loss of 6.4%, mostly at temperatures less than 300 °C. However, microspheres that were air-dried in ammonium hydroxide without autoclaving had a total mass loss of 29.3% with a 12% mass loss occurring between 230-285 °C and an additional 9.6% mass loss above 300 °C.

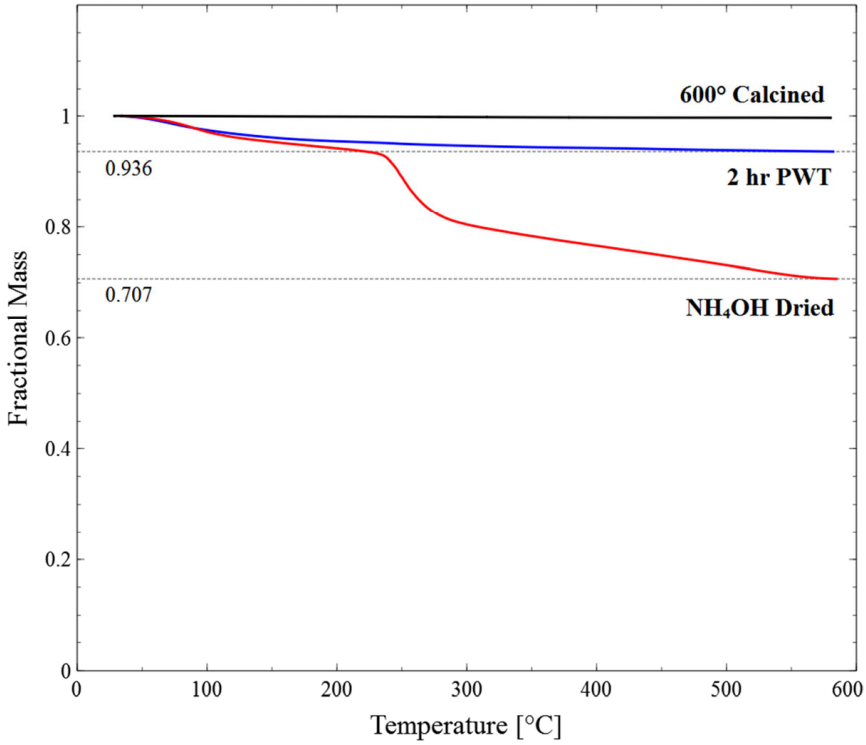

Figure 4.28: Thermal gravimetric analysis of air-dried samples to 600 °C resulted in a 29.3% mass reduction for microspheres air-dried in NH_4OH compared to 6.4% for microspheres air-dried after a pressurized water treatment.

Investigation of volatile impurities

Thermal gravimetric analysis was also performed using urea and HMTA stock reagents as well as residues dried from pressurized water treatment effluents. Pure HMTA evolved by sublimation and mass loss was complete by 222 °C. Mass loss occurred in stages for urea, as shown in Figure 4.29, with complete mass loss by 403 °C. Solids obtained from a dried 3.18 M solution of HMTA and urea also lost mass in multiple stages, but mass loss was not complete

until a temperature of 692 °C, which is 470 °C above pure HMTA reagents and 289 °C higher than pure urea. Residues obtained from pressurized water treatment effluents lost mass in a similar profile to the HMTA/urea residue and also had a very similar end point temperature of 688 °C. Based on the similarity of the mass loss profiles and end point temperatures of the HMTA/urea and pressurized water treatment residues, mass spectroscopy experiments were performed to confirm the presence of HMTA and urea in the pressurized water treatment residues and determine if there were any other constituents.

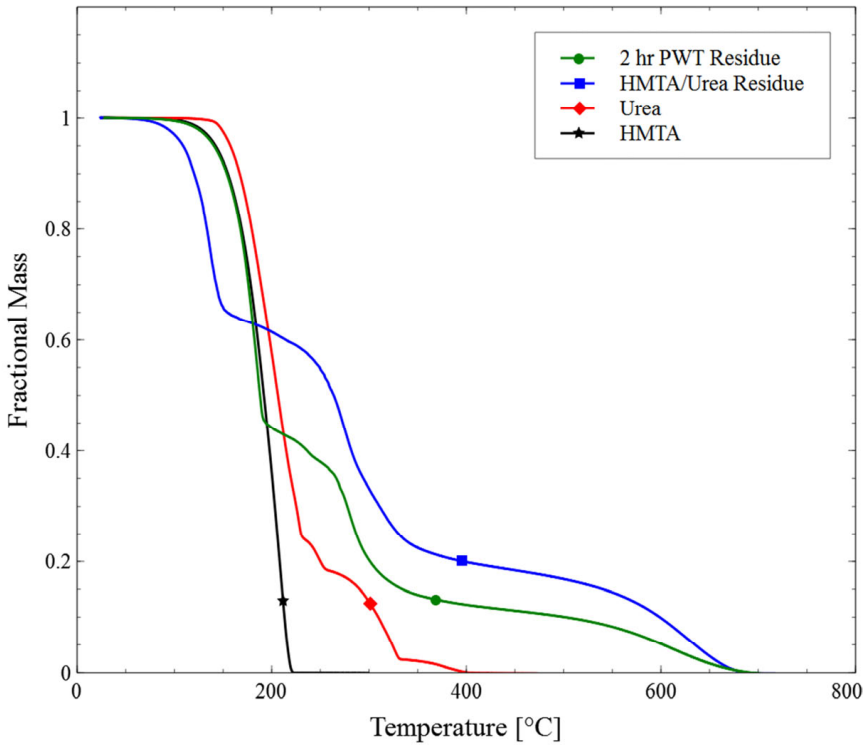

Figure 4.29: Thermal gravimetric analysis indicated similarities between dried residues of HMTA/urea solutions and pressurized water treatment effluents.

4.4.1.5 Electron-Impact Mass Spectroscopy Comparison

Careful preparation of pressurized water treatment effluent residues and microsphere processing allowed for correlation between residue mass and sintered CeO_2 microsphere mass.

The sintered mass of microspheres processed in the pressurized water treatment equated to 9.42 g. Based on the mass of residue obtained from drying a portion of the effluent, the total mass of dissolved solids removed from microspheres was calculated to be 2.012 g. Therefore, for each gram of sintered microspheres produced, 0.218 g of impurities was removed during the autoclaving step. This mass percentage was in close agreement to thermal gravimetric analysis results, which showed microspheres subjected to a pressurized water treatment had a mass loss of 6.4% compared to 29.3% for those without the hydrothermal treatment. This indicates that nearly all of the difference in mass loss during thermal gravimetric analysis was attributable to the extraction of water-soluble impurities.

Considering the large mass transfer of water-soluble impurities from the microspheres to the pressurized water treatment effluent, electron-impact mass spectroscopy (EI-MS) was performed to identify the removed species. Although the effluent drying step was performed at room temperature to prevent the loss of constituent materials prior to EI-MS, a strong odor during dehydration suggested the evolution of volatile species aside from water. Additionally, conductivity measurements of the effluent before and after heating showed a dramatic conductivity increase from 2.89 μs/cm to 7.77 mS/cm, indicating the extraction of ionic impurities. However, no ionic species were identified during mass spectroscopy, indicating their removal during the dehydration step. Upon insertion of effluent residues into the EI-MS at 30 °C, peaks were identified with mass-to-charge ratios (m/z) corresponding to water and HMTA. The HMTA signal was matched to a NIST reference database and their similarity can be seen in Figure 4.30. The water (m/z = 18) and HMTA (m/z = 140, 112, 85, 42) peaks remained the primary signal until temperatures were raised above 100 °C, at which point ammonia (m/z = 17), carbon dioxide (m/z = 44), and urea (m/z = 58, 59, 60) peaks were identified and matched to the

NIST reference, as shown in Figure 4.31. Although urea has a molar mass of 60.055 g/mol, peaks at m/z = 58 and 59 were also considered to be a urea signal since fragments are created by the removal of one or two hydrogen atoms by the electron beam. As the temperature was increased near 200 °C, peaks corresponding to urea decomposition products were identified, including isocyanic acid (m/z = 43) and cyanuric acid (m/z = 129). Due to arcing in the instrument, increasing the sample temperature above 230 °C was not possible. However, an unheated portion of the residue sample was pre-heated to 190 °C in a box furnace for five minutes, cooled to room temperature, and then placed in the EI-MS and heated in intervals up to 580 °C. Above 200 °C, the signal was dominated by peaks corresponding to water, isocyanic acid, urea, carbon dioxide and ammonia. The water signal declined around 100 °C, at which point carbon dioxide and urea signals increased. When the signal from water diminished above 400 °C, the carbon dioxide signal also vanished. Ammonia release was both elevated and distinguishable from OH water fragments (also m/z = 17) above 100 °C and decreased at the same time as the carbon dioxide. Above 400 °C, the primary signal was from isocyanic acid.

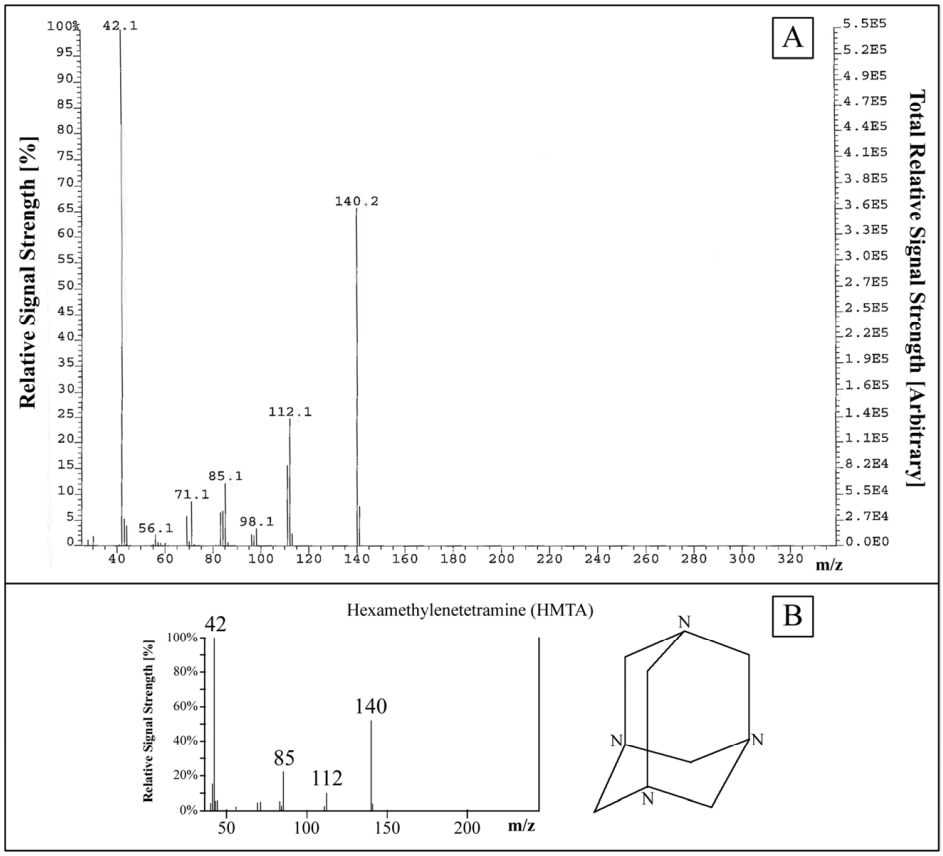

Figure 4.30: Electron-impact mass spectroscopy identified the evolution of HMTA from PWT residues primarily at temperatures below 150 °C. The observed signal shown in part (A) is a close match to the NIST library spectra for HMTA in part (B) [204].

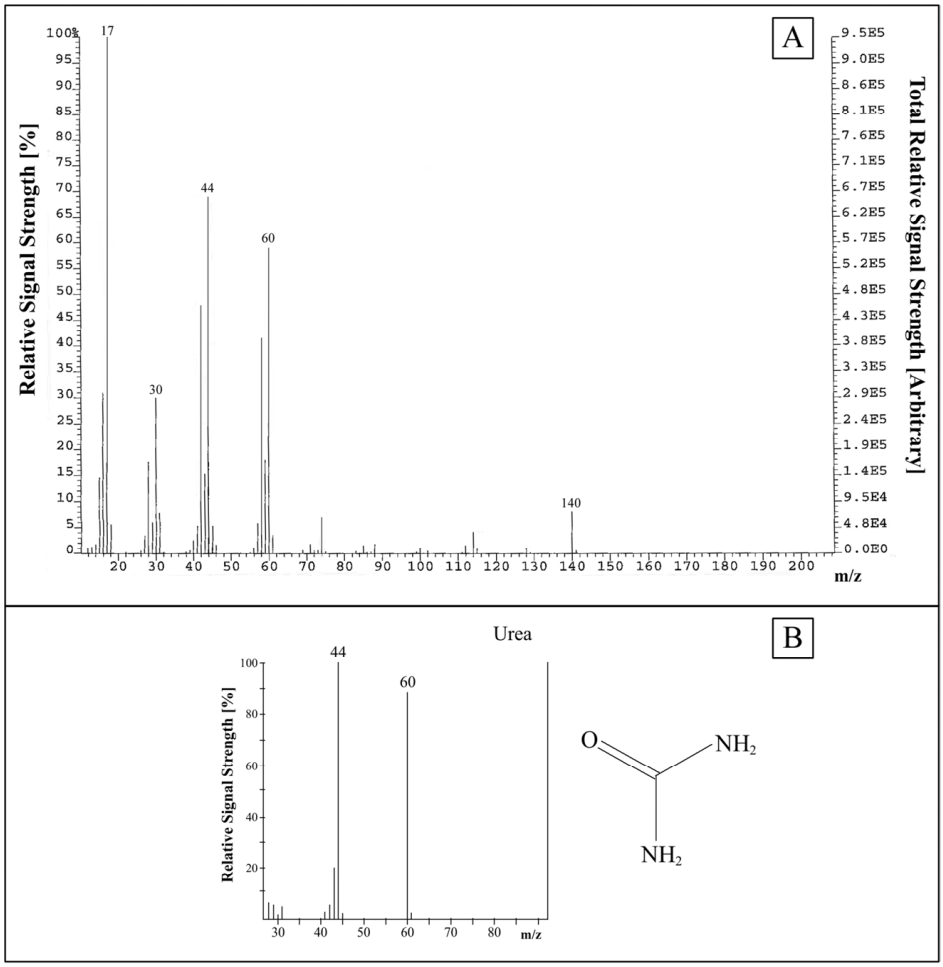

Figure 4.31: Electron-impact mass spectroscopy identified the evolution of urea from PWT residues primarily at temperatures above 100 °C. The observed signal shown in part (A) is a close match to the NIST library spectra for urea in part (B) [204].

The electron-impact mass spectrometer was also used to compare the volatile emissions from microspheres washed by different methods as a function of temperature. Microspheres dried at room temperature after washing by baseline processes with TCE and 0.5 M ammonium hydroxide produced peaks corresponding to water, ammonia, and carbon dioxide. Upon insertion into the instrument at 30 °C, only a signal for water was present until temperatures exceeded 300 °C. Above 300 °C, the water signal dissipated while peaks developed corresponding to ammonia and carbon dioxide that persisted until temperatures exceeded 550 °C,

as shown in Figure 4.32. Microspheres washed by improved methods including isopropyl alcohol and a two-hour pressurized water treatment resulted in mass peaks corresponding to water and carbon dioxide only. Once autoclaved spheres were inserted into the vacuum at 30 °C, water and carbon dioxide signals were immediately strong and slowly reduced in amplitude as the temperature was gradually increased to 580 °C, as shown in Figure 4.33. Although weak peaks for ammonia were observed from approximately 250-350 °C, no other peaks above background levels were identified. Similarly, microspheres that were subjected to two sequential pressurized water treatments had strong water and carbon dioxide signals at low temperatures that dissipated with time and higher temperatures.

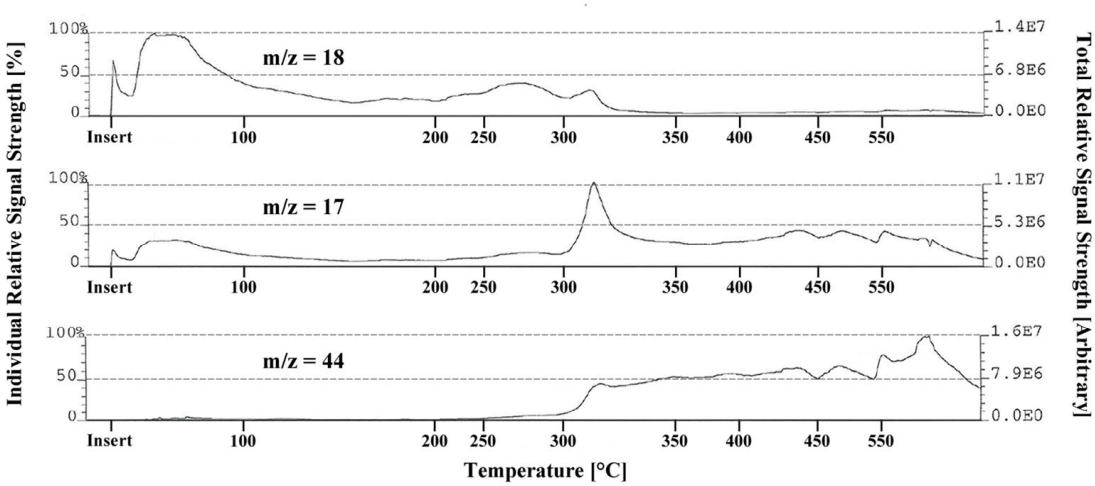

Figure 4.32: Electron-impact mass spectroscopy indicated microspheres air-dried in ammonium hydroxide evolved water (H_2O, m/z = 18) at temperatures below 300 °C and ammonia (NH_3, m/z = 17) and carbon dioxide (CO_2, m/z = 44) above 300 °C. Note that water also produces a hydroxide fragment in EI-MS measurements (OH, m/z = 17).

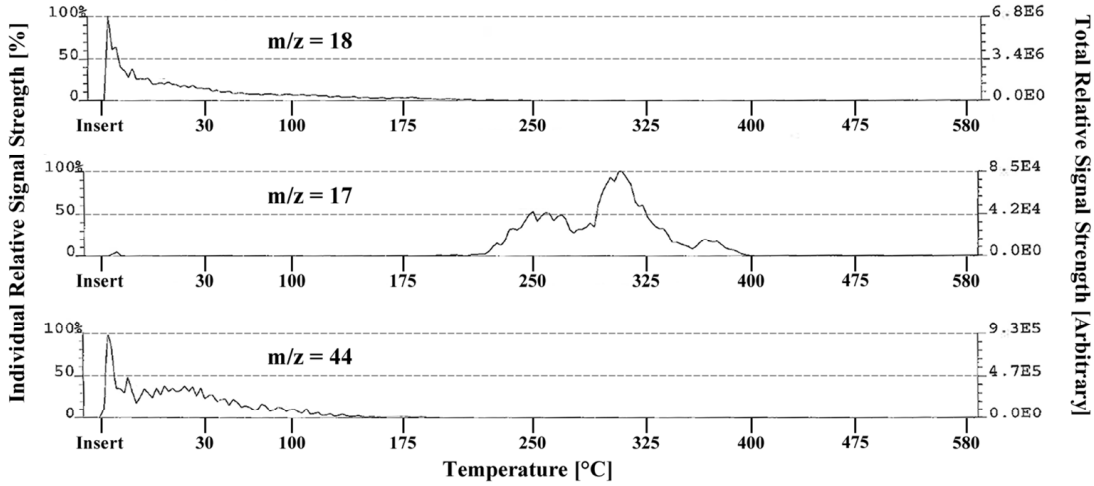

Figure 4.33: Electron-impact mass spectroscopy of air-dried microspheres subjected to a pressurized water treatment indicated the evolution of water (H_2O, m/z = 18) and carbon dioxide (CO_2, m/z = 44) at temperatures below 100 °C and a low-level emission of ammonia (NH_3, m/z = 17) from 250-400 °C.

Based on the different temperature regimes observed for carbon dioxide release from microspheres processed with and without a pressurized water treatment, additional samples were analyzed using new cerium compounds obtained from hydrothermal treatments. To test whether low-temperature CO_2 emissions could be linked to carbonate or hydroxide formation in microspheres, cerium carbonate hydroxide was produced by precipitation during a three-hour, 180 °C hydrothermal precipitation of a solution containing 0.125 M cerous nitrate and 0.5 M urea. Similarly, cerium hydroxide was precipitated during a two-hour, 200 °C hydrothermal treatment of a solution containing 0.125M ceric ammonium nitrate and 0.5 M urea. Resultant precipitates are shown in Figure 4.34. Deionized water effluents after the cerium hydroxide precipitation were extremely effervescent, likely emitting carbon dioxide gas. Mass spectroscopy of the cerium carbonate hydroxide indicated the evolution of water upon insertion into a vacuum at room temperature, but significant carbon dioxide release was not detected until temperatures exceeded 300 °C. Peak CO_2 emissions occurred above 400 °C. Analysis of cerium

hydroxide precipitates, however, resulted in large signals for both water and carbon dioxide immediately upon insertion into a vacuum at room temperature.

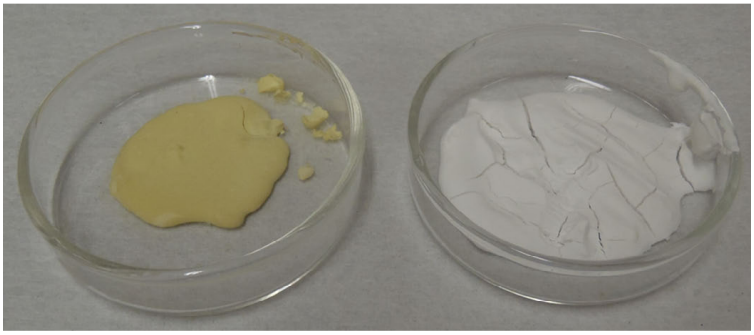

Figure 4.34: Hydrothermal treatment of cerous nitrate and urea yielded cerium carbonate hydroxide (right) while hydrothermal precipitation of ceric ammonium nitrate with urea yielded cerium hydroxide (left).

4.4.2 Determination of Residual Impurities

The effectiveness of three washing methods used to extract impurities from microspheres was compared by analysis of carbon, nitrogen, and hydrogen in sintered spheres. As described previously, the first method was a baseline process using only TCE and 0.5 M ammonium hydroxide. An improved, modified method used isopropyl alcohol as a dispersing agent in intermediate TCE and ammonium hydroxide washes, as indicated in Figure 3.19. The third method used both the improved washing technique and a subsequent two-hour pressurized water treatment at 200 °C.

While washing microspheres, the conductivity of 0.5 M ammonium hydroxide wash effluents was measured to identify a trend for impurity removal as a function of the number of washes. Although HMTA and urea do not contribute significantly to the solution conductivity, ammonium nitrate reaction products exist as conductive ions in solution. Ammonium hydroxide washes took place after washes with TCE and IPA were complete. In each case, washes were performed for 30 minutes with a wash volume of 70 mL. Figure 4.35 shows the exponential

decrease in ammonium hydroxide wash effluent conductivity as subsequent washes are performed. After eight washes, the effluent conductivity was within 10% of the 0.5 M ammonium hydroxide wash solution conductivity. Although 6-8 ammonium hydroxide washes were typically necessary for work in this thesis, the number of washes required varies depending on the mass of spheres being processed.

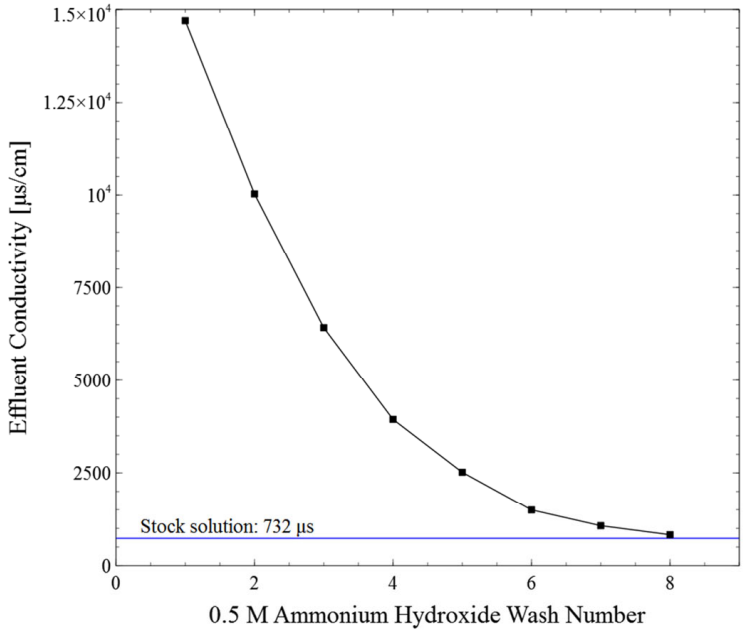

Figure 4.35: The conductivity of wash effluents dropped exponentially and approached the conductivity of the original 0.5 M ammonium hydroxide wash solution.

Traditional washing methods were improved using isopropyl alcohol as a dispersing agent. While most silicone oil was dissolved by 2-3 trichloroethylene washes, as in steps (1) and (2) in Figure 4.36, subsequent washes with 50% TCE, 50% IPA allowed for further removal of silicone oil. Residual water from gelation reactions caused microspheres to form clumps in TCE due to water/TCE immiscibility. Since TCE penetration of the clumps was inhibited, silicone oil removal was incomplete. Isopropyl alcohol, which is soluble in both TCE and water, was used in a TCE/IPA co-solvent to dissolve both water and silicone oil, dispersing microspheres and

allowing for complete silicone oil removal, as shown in steps (3), (4) and (5) of Figure 4.36. Baseline processes using 0.5 M ammonium hydroxide after TCE washes also caused clumping and poor washing due to residual TCE in the microspheres. Providing a drying step for TCE evolution and washing with 50% IPA, 50% ammonium hydroxide allowed for sphere dispersion and residual TCE removal, shown in steps (6) and (7) of Figure 4.36. Several washes with 0.5 M ammonium hydroxide to extract impurities could then be performed with well dispersed microspheres, pictured in step (8). Essentially, TCE/IPA co-solvents dispersed spheres by dissolving water while IPA/0.5 M ammonium hydroxide mixtures dispersed spheres by dissolving TCE.

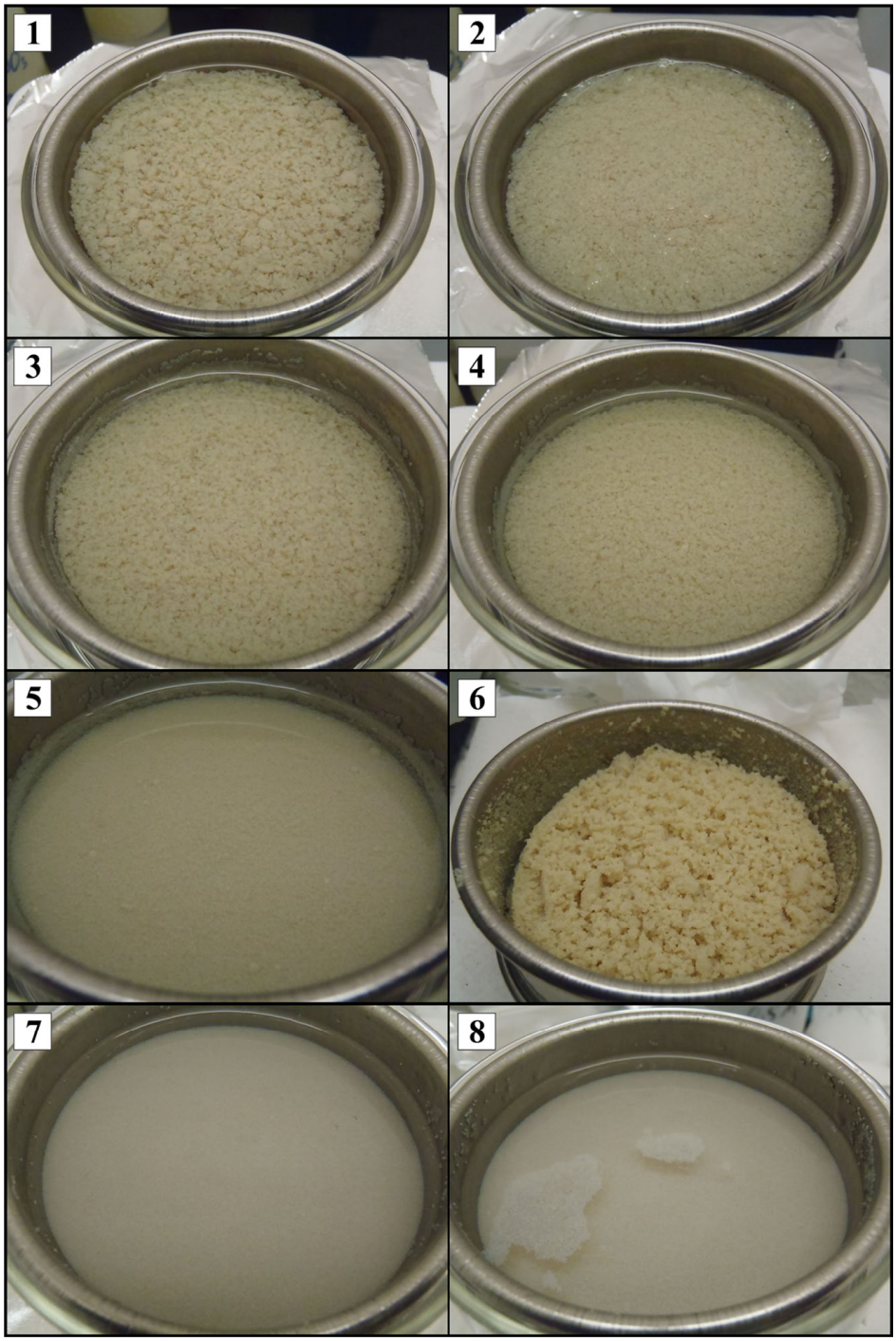

Figure 4.36: Impurity removal was improved using isopropyl alcohol as a dispersing agent and by adding a drying step after TCE washes.

Impurity analyses were performed on internal gelation oxide spheres after sintering to determine whether samples met fuel purity requirements for NASA missions. Carbon, hydrogen,

and nitrogen levels were measured in samples prepared using each of the three washing procedures outlined in Figure 3.19 and are summarized in Table 4.4. Carbon levels were determined by combustion analysis of samples and measurement of gaseous CO and CO_2 using calibrated infrared absorption detectors. Following moisture removal at 100 °C and an inert gas purge, nitrogen and hydrogen levels were determined in separate tests by heating samples to 2500 °C and measuring changes in the conductivity of an inert gas stream. Although a carbon concentration of 26.8 ppm in autoclaved microspheres was slightly higher than other samples, all carbon concentrations were low and indicated excellent carbon removal during washing and heat treatment steps. Nitrogen and hydrogen levels, while low for pressurized water treatment samples, were elevated in samples without a pressurized water treatment step and tended to increase as the extent of washing was reduced. Compared to autoclaved microspheres, nitrogen levels were 64.5% higher for microspheres washed by the improved method without a pressurized water treatment step and 241.8% higher for spheres air-dried in ammonium hydroxide. For microspheres prepared without a hydrothermal treatment, hydrogen levels were approximately ten times higher than nitrogen levels. Although there appears to be a trend in the nitrogen and hydrogen concentrations, outliers evident in Figure 4.37 resulted in high standard deviations for samples prepared without a hydrothermal treatment. Disregarding the outliers in each case, hydrogen concentrations were calculated to be 124.6 ± 38.8 ppm for microspheres washed by the improved method and 594.3 ± 30.9 ppm for those air-dried in ammonium hydroxide.

Table 4.4: Carbon, hydrogen, and nitrogen analysis indicated low levels of residual carbon and nitrogen and hydrogen concentrations corresponding to the extent of washing.

	Carbon [ppm]	Nitrogen [ppm]	Hydrogen [ppm]
NH_4OH Dried	13.5 ± 0.80	48.2 ± 24.1	462.5 ± 205.6
Improved	14.2 ± 3.2	23.2 ± 10.2	231.7 ± 168.7
Improved + PWT	26.8 ± 6.1	14.1 ± 13.3	8.0 ± 2.9

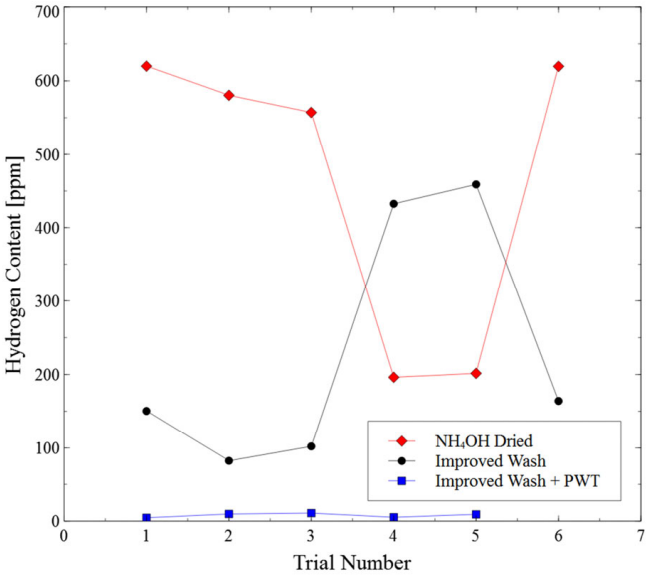

Figure 4.37: Outliers in hydrogen concentration measurements for microspheres without a pressurized water treatment resulted in large standard deviations.

Glow discharge mass spectroscopy was performed using microspheres washed by the improved method and hydrothermal treatment. As seen in Figure 4.38, most elements were detected and confirmed to have concentrations below 1 ppm. Several elements were detected with levels between 1-10 ppm, including lithium, sulfur, potassium, iron, silver, cadmium, cesium, barium, tantalum, praseodymium, gadolinium, and terbium. The highest levels detected corresponded to zirconium (26 ppm), calcium (32 ppm), sodium (46 ppm), aluminum (64 ppm), and silicone (69 ppm). Although a certificate of analysis was included with the 99.99% purity ceric ammonium nitrate reagent used to produce microspheres for impurity analyses, the only

elements included on the certificate that were detected at elevated levels in mass spectroscopy were iron (2.1 ppm), barium (0.6 ppm), and gadolinium (3.5 ppm).

Impurity Levels as Determined by Glow-Discharge Mass Spectroscopy

Blue: x < 1 ppm
Green: 1 ppm < x < 10ppm
Red: x > 10 ppm

H --																	He --
Li 2.2	Be <0.01											B 0.07	C --	N --	O --	F <0.5	Ne --
Na 46	Mg 0.08											Al 64	Si 69	P <0.05	S 9.8	Cl ~0.6	Ar --
K 9.4	Ca 32	Sc 0.04	Ti 0.56	V 0.14	Cr 0.69	Mn 0.11	Fe 5.1	Co <0.05	Ni <0.05	Cu <0.05	Zn 0.28	Ga <0.5	Ge <0.5	As <0.1	Se <0.5	Br ~1	Kr --
Rb <0.05	Sr 0.2	Y 0.9	Zr 26	Nb 0.34	Mo 0.15	Tc --	Ru <0.1	Rh <0.05	Pd <0.5	Ag 5.6	Cd <5	In --	Sn 0.33	Sb <0.1	Te <0.1	I <1	Xe --
Cs <5	Ba 1.5	57-71	Hf 0.63	Ta <5	W <0.1	Re <0.05	Os <0.05	Ir <0.05	Pt <0.1	Au <0.1	Hg <0.5	Tl <0.1	Pb <0.5	Bi <0.1	Po --	At --	Rn --
Fr --	Ra --	89-103	Rf --	Db --	Sg --	Bh --	Hs --	Mt --	Ds --	Rg --	Cn --	Uut --	Fl --	Uup --	Lv --	Uus --	Uuo --

La 0.55	Ce --	Pr 8.1	Nd <0.1	Pm --	Sm <0.1	Eu <0.1	Gd <10	Tb <5	Dy <0.05	Ho <0.01	Er <0.05	Tm <0.01	Yb <0.05	Lu <0.05
Ac --	Th <0.01	Pa --	U 0.17	Np --	Pu --	Am --	Cm --	Bk --	Cf --	Es --	Fm --	Md --	No --	Lr --

Figure 4.38: Glow discharge mass spectroscopy allowed for determination of impurity levels for most elements.

Additional experiments were performed at the University of Michigan using an inductively coupled plasma mass spectrometer (ICP-MS) to determine the levels of sodium, calcium, aluminum, silicon, and cerium in a pressurized water treatment effluent as well as cerium levels in an ammonium hydroxide wash effluent. Based on comparison of sample signals with known concentrations in a NIST standard solution, impurities were estimated to be 6.5 ppm sodium, 8 ppb aluminum, 2 ppm silicon, and 40 ppb cerium in the pressurized water treatment effluent. Calcium content above background levels was not observed. The pressurized water treatment effluent had an initial volume of approximately 130 mL and was used to extract impurities from gelled microspheres with an equivalent sintered mass of 4.5 g. The ammonium

hydroxide wash effluent analyzed for cerium content was the first in a wash series for 3 g of spheres, and was thus expected to have the highest impurity levels. Measurements indicated that the concentration of cerium in ammonium hydroxide wash effluent depended on whether the sample had settled or was shaken prior to analysis. Cerium concentrations were measured to be 2.75 ± 0.14 ppm after settling and 8.48 ± 0.85 ppm after shaking.

4.5 Heat Treatment Effects

A large batch of microspheres washed with a hydrothermal treatment was split into six samples for air-drying and heating to 150 °C, 450 °C, 750 °C, 1050 °C, and 1350 °C to determine the impact of heat treatment temperature on crystallite size, specific surface area, and density. A separate sample of microspheres air-dried in ammonium hydroxide was also used for comparison with pressurized water treatment samples. After heat treatments, small portions of each sample were diverted for TEM imaging while the bulk were used for nitrogen adsorption surface area analysis using the Brunauer, Emmett, and Teller (BET) theory. After BET analysis, samples were used for density determination using a glass pycnometer and deionized water. Once the density measurements were complete, microspheres were air-dried in isopropyl alcohol and then finely ground for powder x-ray diffraction. Since samples were used for different analyses sequentially, a control sample was also used to verify that BET analysis and density measurements had negligible impact on subsequent crystallite size determination experiments based on x-ray diffraction peak widths.

Crystallite size estimation by x-ray diffraction

Experiments were performed to verify that BET and density analysis did not impact subsequent x-ray diffraction experiments or influence the determination of crystallite size using

the Scherrer equation. Crystallite sizes calculated from seven x-ray diffraction peaks for CeO_2 microspheres after heating to 150 °C are shown in Figure 4.39 using red circles. The average crystallite size was calculated to be 8.29 ± .02 nm. Microspheres from the same batch, also heated to 150 °C, were subjected to BET and density experiments and then used for x-ray diffraction and crystallite size calculations. Shown in Figure 4.39 with black diamonds, microspheres used for BET, density measurements, and x-ray diffraction yielded an average crystallite size of 8.22 ± .02 nm. Therefore, samples that underwent additional analysis prior to x-ray diffraction exhibited average crystallite values within 1% of samples without an experimental history.

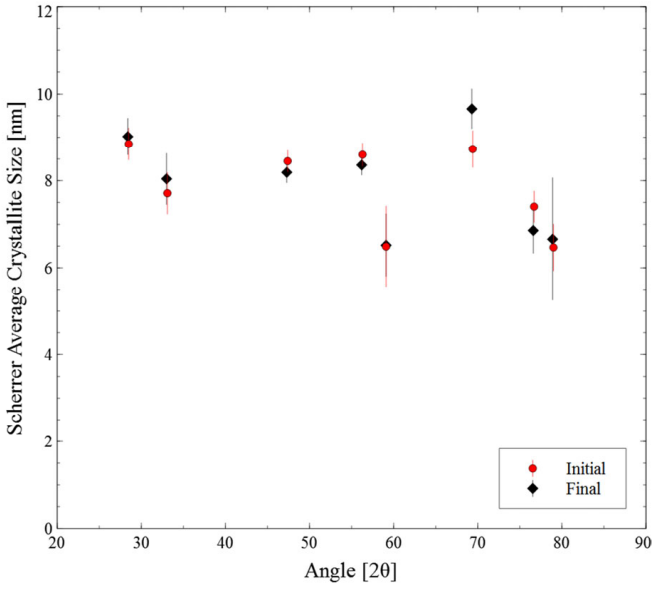

Figure 4.39: Differences observed in calculated crystallite sizes were generally within statistical error, indicating that BET and density measurements had an insignificant impact on subsequent x-ray diffraction analysis.

X-ray diffraction spectra were measured for air-dried microspheres as well as those heated to 150 °C, 450 °C, 750 °C, 1050 °C, and 1350 °C. Application of the Scherrer formula using the full-width at half maximum of diffraction peaks allowed for calculation of average

crystallite sizes, which are reported in Table 4.5. Inverse variance weighting was used to provide a best estimate of average crystallite sizes using calculated values at each diffraction peak. Crystallite sizes calculated for each peak are plotted in Figure 4.40, which indicates that values were relatively constant as a function of diffraction angle. Scherrer analysis matched TEM observations in section 4.4.1.3, indicating microspheres air-dried in ammonium hydroxide had crystallite sizes of approximately 1-2 nm compared to 2-6 nm for those air-dried after a hydrothermal treatment. Little change was observed in average crystallite size with heat treatments up to 450 °C. However, a 538% increase in average crystallite size was observed between microspheres heated to 450 °C and 750 °C, indicating significant crystal growth in that temperature range.

While estimated crystallite sizes matched observations in TEM images for microspheres heated to 750 °C or less, those calculated for samples sintered at 1050 °C and above did not. As can be seen from TEM images in the following section, Scherrer estimates for spheres heated to 1050 °C appeared to be overestimated while crystallite sizes for spheres heated to 1350 °C were underestimated. Crystallite sizes calculated using the Scherrer formula for microspheres heated above 750 °C were determined to be unreliable due to instrumental broadening of the Rigaku x-ray diffractometer. X-ray diffraction of a standard lanthanum hexaborate sample indicated an average instrumental broadening of approximately 0.075 degrees. Establishing an upper limit for crystallite size as that which would produce broadening equal to the instrumental broadening, a diameter of approximately 120 nm was calculated. All samples heated above 750 °C yielded crystallite sizes beyond this limit. Additionally, as shown in Figure 4.41, samples heated to 1050 °C and 1350 °C exhibited increasing values at higher 2θ angles, indicating the introduction of strain in samples, which also distorts crystallite size estimation. Although crystallite sizes

calculated using the Scherrer formula for samples heated to 1050 °C and 1350 °C were considered unreliable, TEM images of these samples provided a determination of expected crystallite size ranges.

Table 4.5: Average crystallite sizes increased with pressurized water treatments and higher temperature treatments.

	Average Crystallite Size, Scherrer [nm]
Baseline:	
Air Dried, NH_4OH	1.71 ± 0.10
PWT:	
Air Dried	5.93 ± 0.02
150 °C	5.78 ± 0.02
450 °C	7.04 ± 0.01
750 °C	37.85 ± 0.74
1050 °C	224.65 ± 70.57[α]
1350 °C	133.73 ± 16.21[α]

[α] Scherrer estimates of crystallite size at 1050 °C and 1350 °C were considered unreliable.

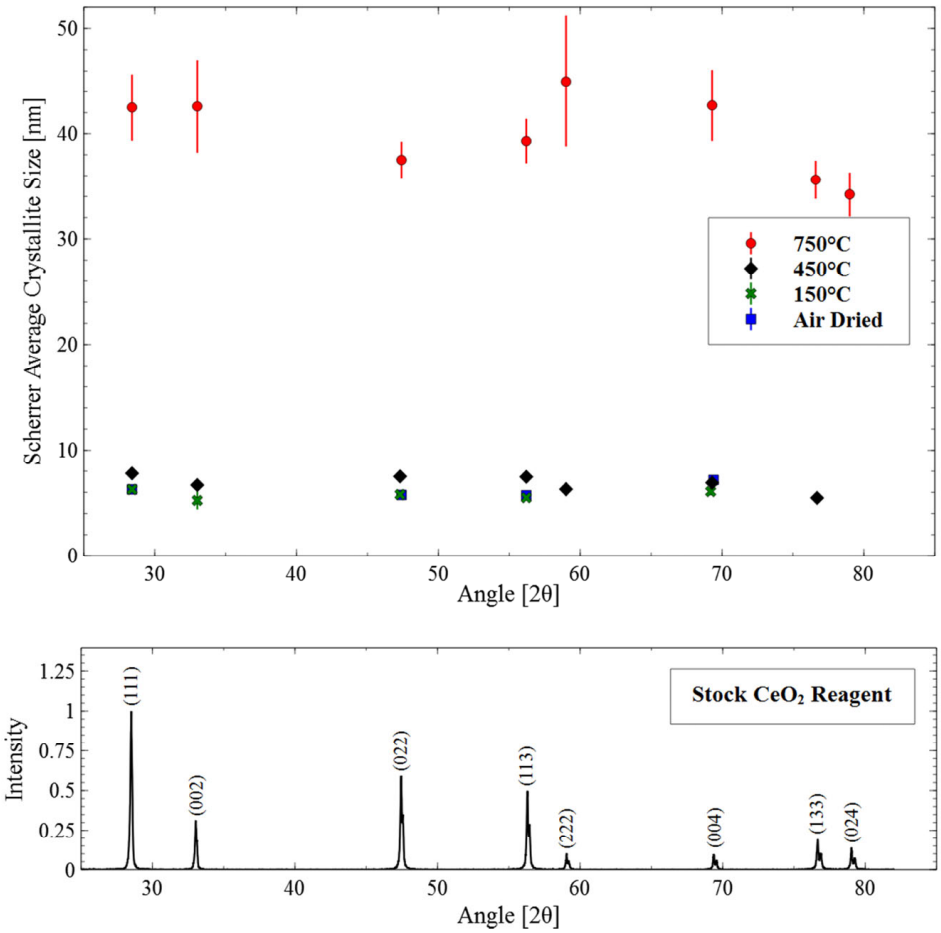

Figure 4.40: Average crystallite sizes estimated using x-ray diffraction and the Scherrer equation also indicate little crystallite growth until heat treatment temperatures exceed 450 °C. An x-ray diffraction pattern for a fluorite structure 99.9% CeO_2 reagent is provided to indicate the reflections used for Scherrer analysis.

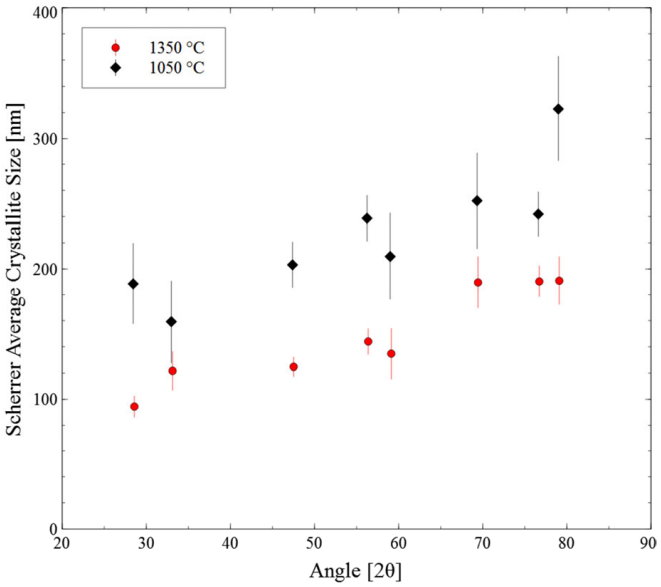

Figure 4.41: Crystallite sizes calculated for samples heated to 1050 °C and 1350 °C exhibited an upward trend with angle and existed in a size range beyond the calculated threshold for Scherrer analysis given measured instrumental broadening.

Transmission electron microscopy

Transmission electron microscopy of dispersed, finely ground microspheres was used to observe the range of crystallite sizes as a function of washing methods and final heat treatment temperature. As discussed in section 4.4.1.3, Figure 4.26 indicates microspheres air-dried in ammonium hydroxide had small crystallites of 1-2 nm compared to autoclaved microspheres, which have crystallites from 2-4 nm as shown in Figure 4.27. Ranges of crystallite sizes observed in samples are summarized in Table 4.6. Microspheres subjected to a pressurized water treatment and heated up to 450 °C were characterized by small crystallites from 3-10 nm, as shown in Figure 4.42 and Figure 4.43. However, significant crystallite growth was observed between 450-750 °C. Figure 4.44 indicates microspheres heated to 750 °C were composed of many crystallites as large as 58 nm. At elevated temperatures from 750-1350 °C, progressively larger crystallites were observed, but smaller crystallites of approximately 3-5 nm remained, as seen in Figure 4.45 and Figure 4.46. Crystals with dimensions as large as 238 nm and 605 nm

were observed in samples heated to 1050 °C and 1350 °C as shown in Figure 4.47 and Figure 4.48, respectively. For samples heated to each temperature, a representative TEM image was chosen and a minimum of 30 crystallite sizes were estimated using Adobe Fireworks. The results provided an indication of the observed spread in crystallite sizes and are shown in Figure 4.49.

Table 4.6: Crystallite sizes, while larger for autoclaved microspheres, did not exhibit significant growth until heated above 450 °C.

	Range of Crystallite Sizes, TEM [nm]
Baseline:	
Air Dried, NH_4OH	1 - 2
PWT:	
Air Dried	2 - 4
150 °C	3 - 10
450 °C	2 - 10
750 °C	4 - 58
1050 °C	4 - 238
1350 °C	4 - 605

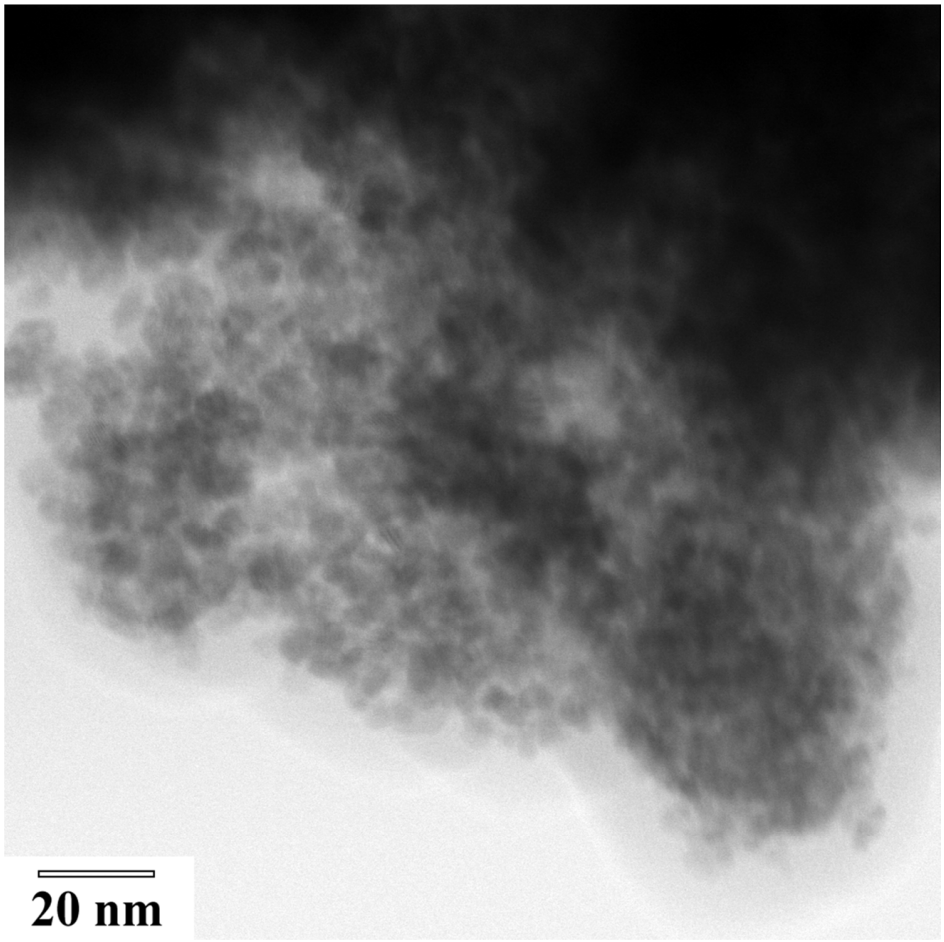

Figure 4.42: Microspheres washed by the improved method, subjected to a pressurized water treatment, and heat treated to 150 °C were composed of crystallites of approximately 3-10 nm.

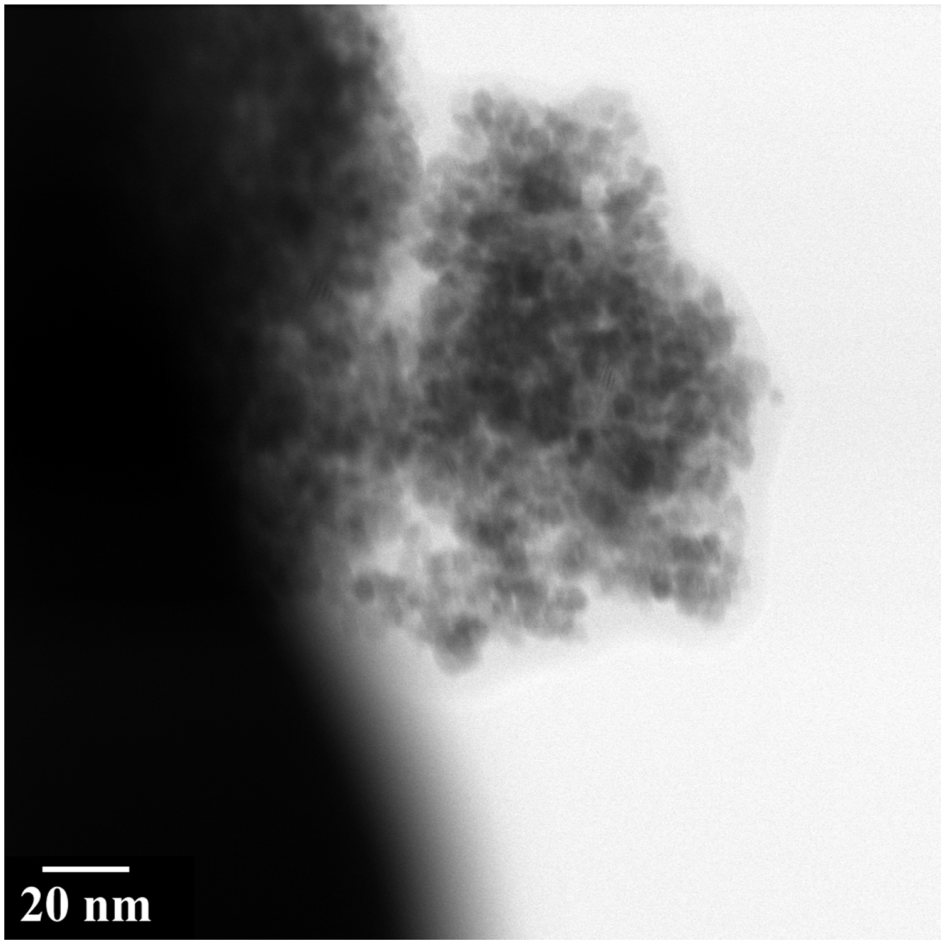

Figure 4.43: Samples heat treated to 450 °C did not exhibit significant crystallite growth relative to microspheres heated to 150 °C.

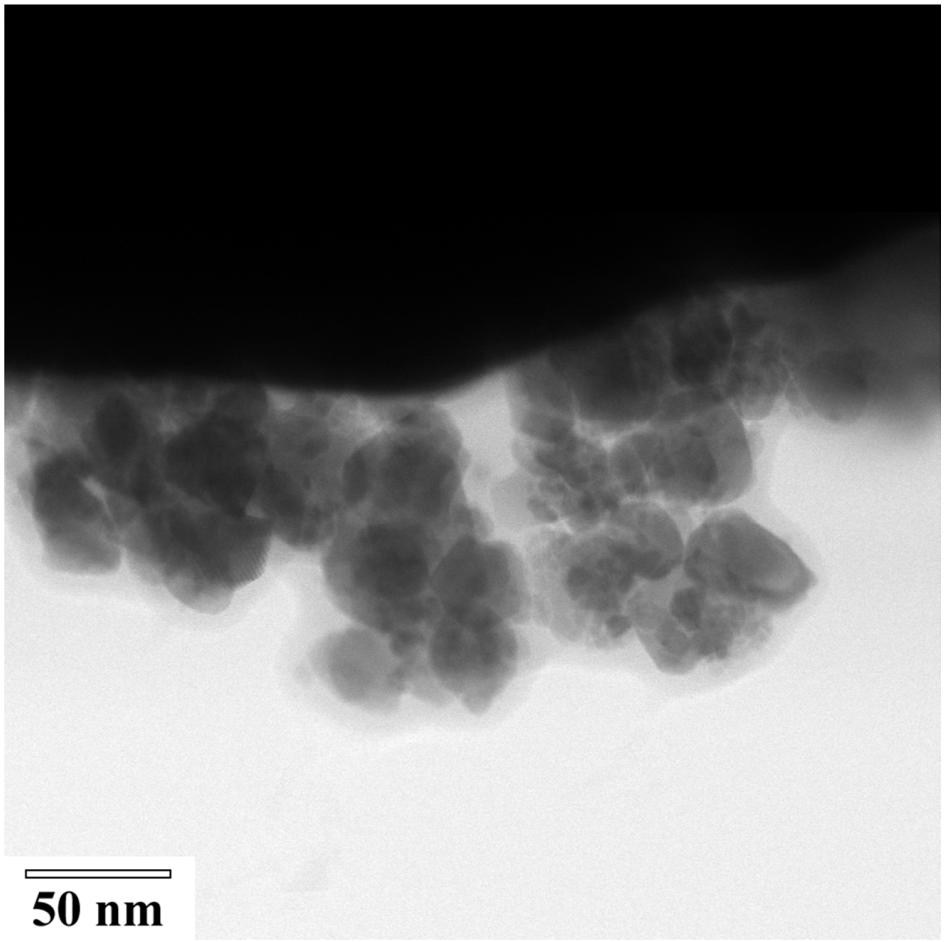

Figure 4.44: Microspheres heated to 750 °C were composed of crystallites from 4-58 nm, indicating significant crystal growth between 450-750 °C.

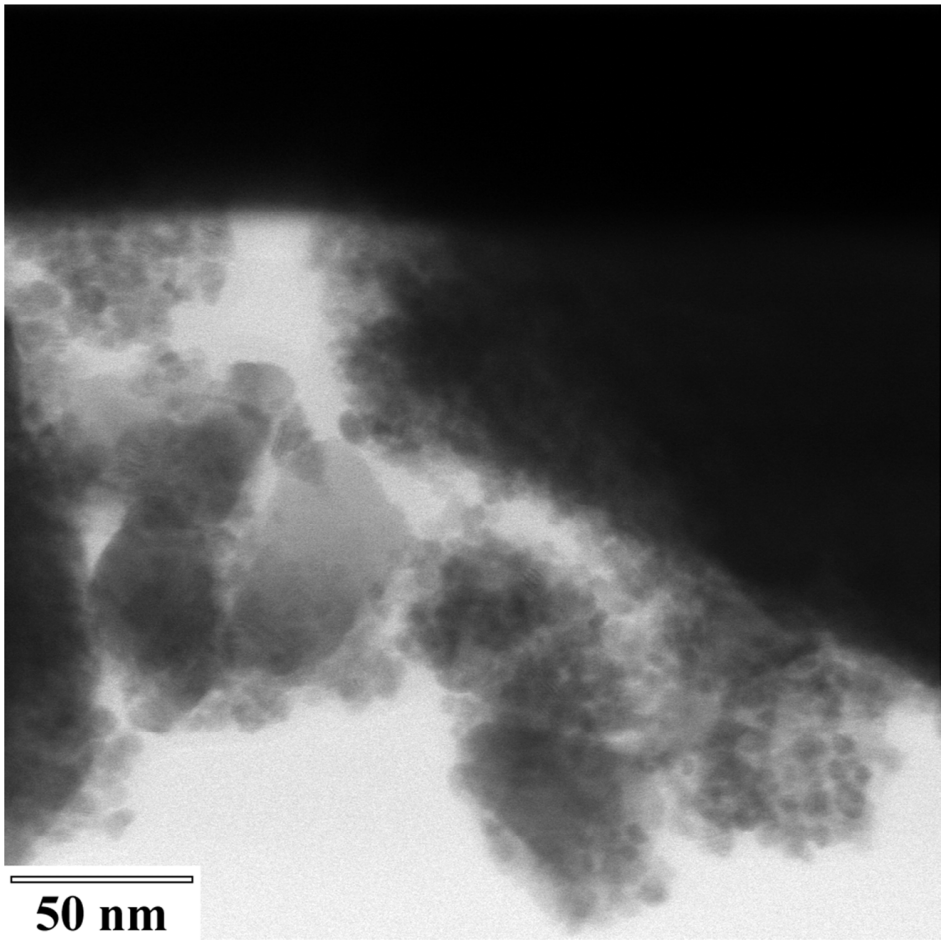

Figure 4.45: Microspheres heated to 1050 °C contained a wide range of crystallite sizes in addition to larger crystals.

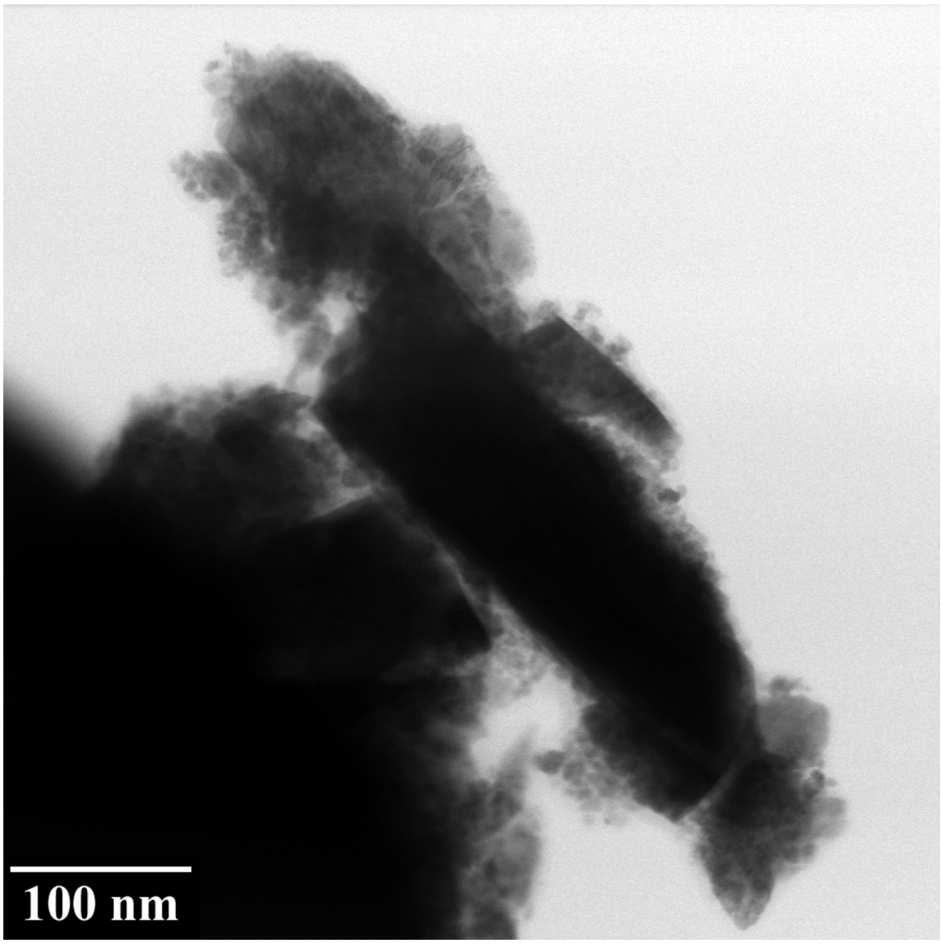

Figure 4.46: Samples sintered to 1350 °C also exhibited a wide range of crystallite sizes.

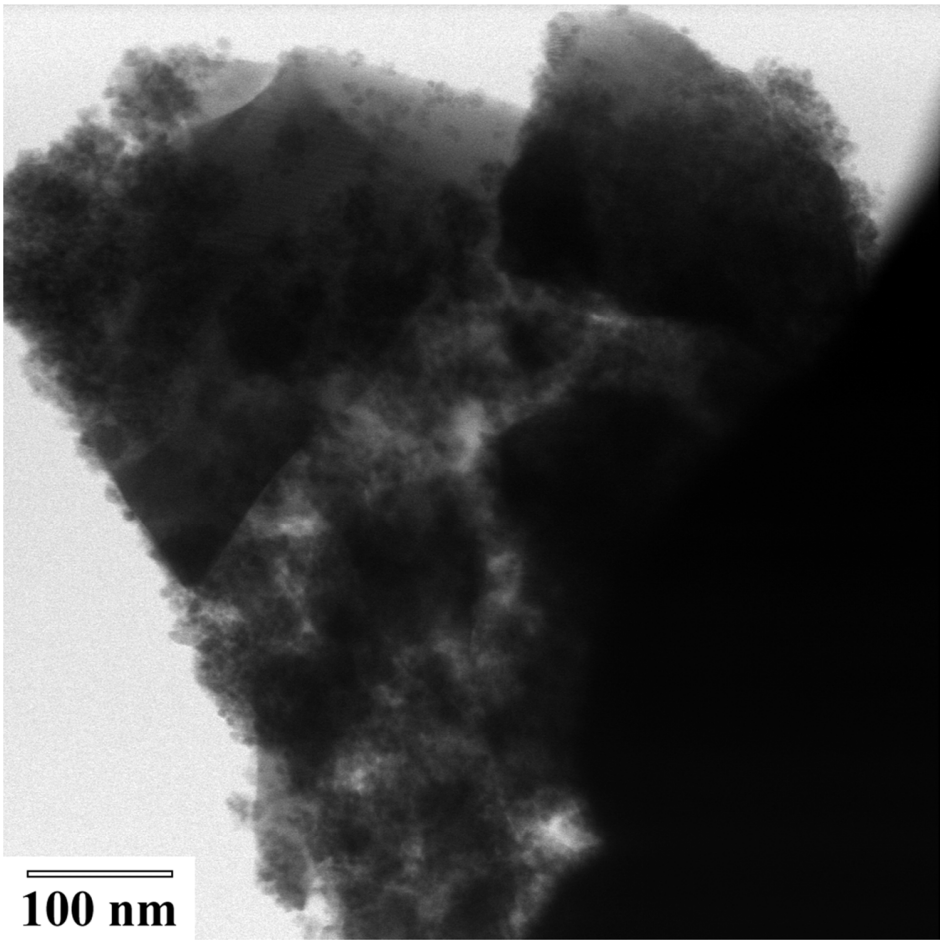

Figure 4.47: Crystallites as large as 238 nm were observed in microspheres heat treated at 1050 °C.

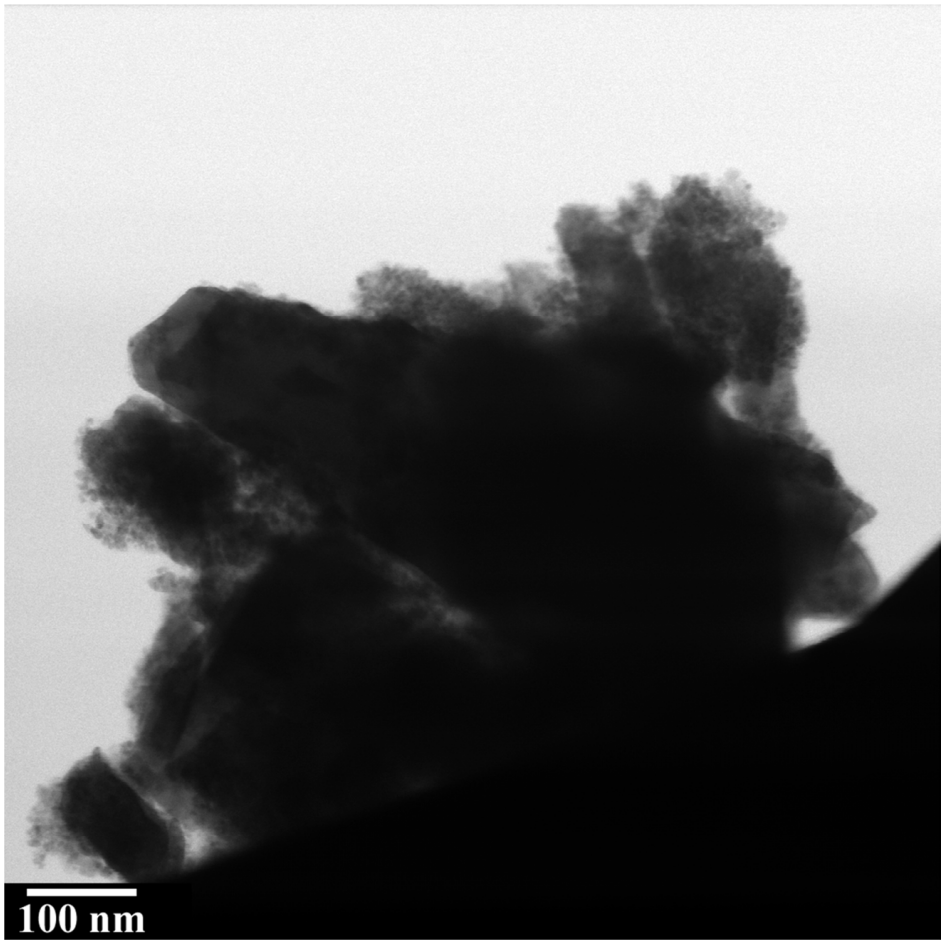

Figure 4.48: Microspheres heated to 1350 °C contained crystallites with dimensions as large as 605 nm.

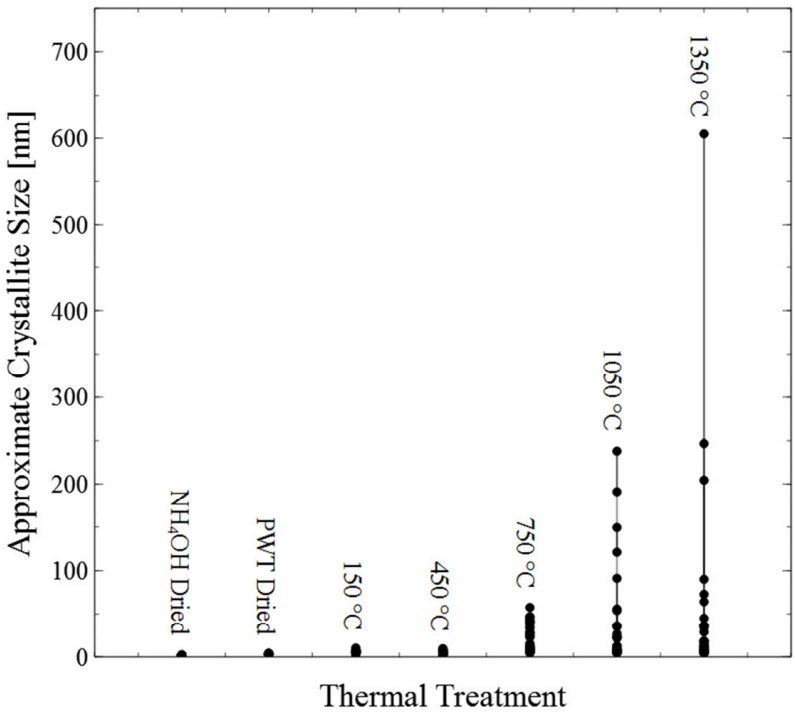

Figure 4.49: Distributions of crystallites sizes indicated that growth occurred during progressively higher heat treatments but that smaller crystallites also remained.

Specific surface area and density measurements

Nitrogen adsorption measurements allowed for determination of BET surface areas and BJH average pore sizes on most samples heated to temperatures below 750 °C. Microspheres air-dried in ammonium hydroxide, while not heated, had insufficient open porosity to allow for accurate measurements. Since accurate determinations can typically be made for samples with a total surface area of 20 m^2/g and samples were approximately 1.5 g each, a specific surface area for ammonium hydroxide dried microspheres can be assumed to be below 13.3 m^2/g before any heating takes place. Air-dried microspheres that were autoclaved had a high specific surface area of 144.9 m^2/g. After heating to 150 °C for four hours, specific surface area increased to 149.8 m^2/g. The surface area of microspheres heated to 450 °C was reduced by approximately

one third to 102.7 m^2/g. Significant surface area reduction and pore closure appears to have occurred between 450-750 °C. Samples heated to 750 °C and above had insufficient mass for surface area determination and can be assumed to have a specific surface area below 13.3 m^2/g. Average pore sizes for air-dried spheres, as well as those heated to 150 °C and 450 °C, were all near 4 nm. In the analyses performed, connected, cylindrical pores were assumed and the average pore size was calculated as four times the ratio of volume to area, with volume and area determined by adsorption. Nitrogen adsorption results are summarized in Table 4.7 along with results for density and crystallite sizes. BJH adsorption pore size distribution measurements also indicated a trend of pore shrinkage as spheres were heated to 150 °C and 450 °C, as shown in Figure 4.50. Pore size distributions also indicated pore sizes are below 20 nm.

Table 4.7: Summary of Microsphere surface area, pore size, density, and crystallite sizes as a function of temperature.

	BET Surface Area [m^2/g]	BJH Average Pore Diameter, Adsorption [nm]	BJH Average Pore Diameter, Desorption [nm]	Density [g/cc]	Average Crystallite Size, Scherrer [nm]	Range of Crystallite Sizes, TEM [nm]
Baseline:						
Air-Dried, NH_4OH	---[α]	---[α]	---[α]	3.06 ± 0.026	1.71 ± 0.10	1 - 2
PWT:						
Air-Dried	144.9	4.15	3.52	5.44 ± 0.026	5.93 ± 0.02	2 - 4
150 °C	149.8	4.08	3.46	5.77 ± 0.026	5.78 ± 0.02	3 - 10
450 °C	102.7	3.92	3.31	5.92 ± 0.047	7.04 ± 0.01	2 - 10
750 °C	---[α]	---[α]	---[α]	6.72 ± 0.061	37.48 ± 0.80	4 - 58
1050 °C	---[α]	---[α]	---[α]	6.95 ± 0.122	---[β]	4 - 238
1350 °C	---[α]	---[α]	---[α]	7.14 ± 0.220	---[β]	4 - 605

[α] Samples of approximately 1.5 grams were insufficient for BET analysis, suggesting specific surface areas below 13.3 m^2/g or closed pores.

[β] Samples heated above 750 °C exhibited significant slope and crystallite sizes beyond the useful range for Scherrer analysis.

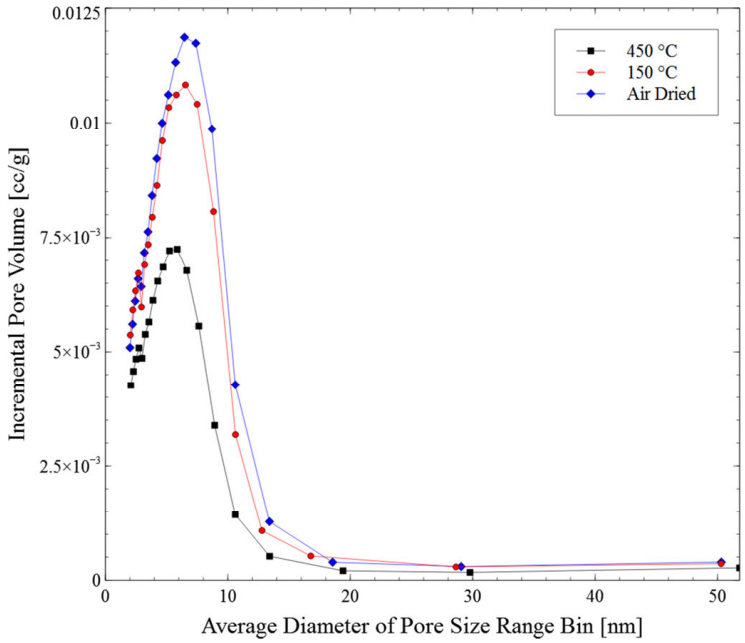

Figure 4.50: BJH adsorption pore size distributions for successful measurements indicated pore sizes were below 20 nm. Pore shrinkage with increased temperature is also observed.

Density measurements were performed using a 10 mL glass pycnometer and deionized water according to the procedure outlined in section 3.5. Microspheres air-dried in ammonium hydroxide had a measured density of 3.06 ± 0.026 g/cc. A 77.8% increase in density was observed for air-dried, autoclaved microspheres, which had a density of 5.44 ± 0.026 g/cc. Samples heated from 150-1350 °C exhibited densities ranging from 5.77 ± 0.026 g/cc to 7.14 ± 0.220 g/cc, corresponding to 79.9-98.8% theoretical density. High densities at sintering temperatures as low as 1050-1350 °C is supported by prior studies indicating that hydrothermally-treated ceria powders exhibited excellent sinterability [116,131]. Density measurements for samples heated from 150-1350 °C are plotted in Figure 4.51 and summarized in Table 4.7. While a difference of only 6.6% theoretical density was observed between air-dried microspheres and those heated to 450 °C, an 11% increase in theoretical density occurred between 450-750 °C. The densification observed from 450-750 °C correlates with surface area and crystallite size measurements indicating crystal growth and pore reduction in that

temperature range. Also of interest is the fact that microspheres processed by baseline methods yielded dried microspheres with low surface area and low density while microspheres dried after a hydrothermal treatment had 75.3% theoretical density together with high specific surface area.

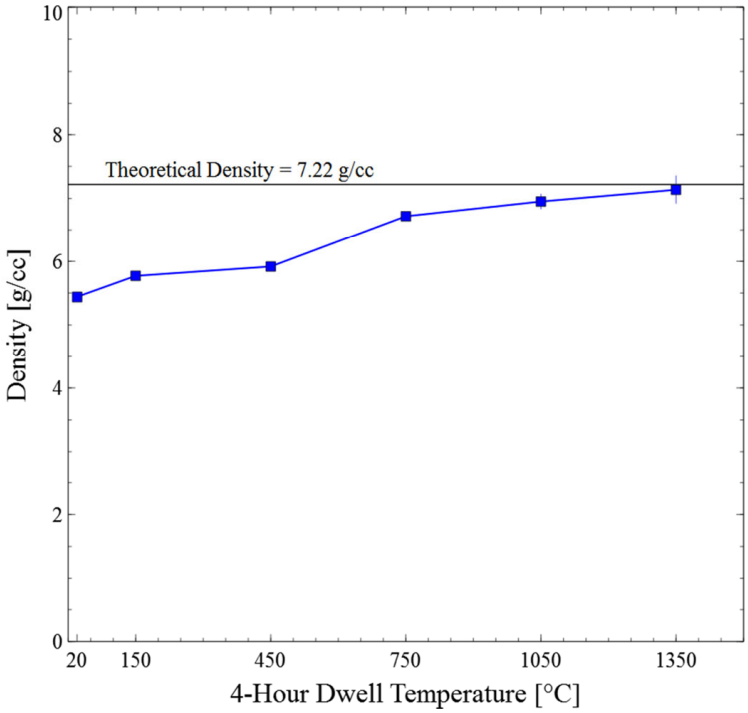

Figure 4.51: Cerium dioxide microspheres heated from 150-1350 °C exhibited 75.3-98.8% theoretical density.

Agglomeration behavior

During the process of heat treating microspheres, differences were observed in their tendency to agglomerate, or sinter together upon heating. Of the spheres that were hydrothermally treated and heated to temperatures from 150-1350 °C, only spheres heated to 1350 °C exhibited any agglomeration; all other spheres were free-flowing and poured easily out of the sintering boat. Those heated to 1350 °C were easily separated using light pressure and then poured easily out of the sintering boat. In other studies, it was observed that spheres heated to 1500 °C also separated easily and became free flowing if they had been subjected to a

pressurized water treatment prior to drying. Microspheres sintered after washing by baseline processes were strongly agglomerated and separation into individual spheres was accomplished with limited success by slugging spheres through a mesh screen. Screening failed to separate some strongly bound agglomerates of samples sintered after air-drying in ammonium hydroxide.

Chapter 5

Discussion

"The current process requires milling Pu-238 material into a fine powder (less than 1 μm). Experience has shown that powder particulates less than 10 μm maximize risk for personnel exposure by inhalation and dispersion to the environment. In addition, this small particle size increases the mobility of the Pu-238 material by airflow and recoil energy produced during alpha decay. These factors increase contamination spread, make decontamination more difficult, and enhance the material's corrosive nature. Pu-238 interacts with process equipment, increasing breakdown and repair times. The fine powder is more difficult to confine, degrades and penetrates gloves and rubber seals, and increases the complexity of transferring material without spreading contamination."

- Expert committee on the evaluation of aqueous and powder processing techniques for production of Pu-238-fueled general purpose heat sources, 2008 [19]

Thesis work resulted in an improved method for internal gelation processes that produced uniform, crack-free microspheres of well controlled sizes in the range 50-200 μm. As will be discussed in the first section of this chapter, adoption of a pressurized water treatment between microsphere washing and drying steps provided for carbon, hydrogen, and nitrogen-bearing impurities extraction, which was shown to nearly eliminate microsphere cracking during drying

and heat treatment steps. Additionally, hydrothermally treated microspheres exhibited temperature-dependent volatile emissions, densification, and porosities that seem attractive for a variety of nuclear fuels. The second section will address evidence suggesting the excellent monodispersities observed can be linked to operation in the simple dripping regime for droplet formation. Desirable tradeoffs between stripping oil flow rates, needle diameters, and microsphere sizes will also be discussed. In the third section, a novel technique for optimal R value and acid deficiency selection is presented which is quantitative in nature. The last section includes a variety of topics and addresses some of the many issues that arose during efforts to effectively and reliably fabricate and wash microspheres. As will be described in the following sections, effective equipment and methodologies were developed to produce high-quality cerium oxide microspheres while minimizing dust generation. While a substantial amount of future work will be needed to demonstrate the production of Pu-238 oxide pellets made from internal gelation microspheres, the work in this thesis provides a basis from which to move forward.

5.1 Effects and Analysis of Pressurized Water Treatments

As will be discussed in the following subsections, the use of a hydrothermal treatment on wet, gelled spheres after washing, but before drying, had a transformational effect on microsphere properties and behavior during subsequent thermal treatments. In addition to lowering impurity levels in the microsphere product and preventing cracking, adopting the use of a pressurized water treatment may allow for use of previously undesirable feed parameters to improve microsphere monodispersity and/or throughput.

5.1.1 Microsphere cracking

Microspheres subjected to a pressurized water treatment did not produce any measureable fines during a heat treatment to 600 °C using the profile in Figure 3.18. In contrast,

microspheres washed and dried in ammonium hydroxide, according to baseline processes, exhibited mass losses over 1% due to cracking and surface spalling, which is apparent in Figure 4.22. The difference in surface properties and fines generation was attributed to impurity extraction, crystal growth, and shrinkage that occurred during a two-hour hydrothermal treatment at 200 °C. Evidence from thermal gravimetric analysis, electron-impact mass spectroscopy, and size measurements during washing and drying steps indicates a substantial extraction of volatile impurities from microspheres during hydrothermal treatments.

Differences in volatile mass losses between samples treated with and without a hydrothermal treatment were linked to the extraction of HMTA and urea during pressurized water treatments. As indicated in Figure 4.28, microspheres subjected to a pressurized water treatment had a volatile mass loss of 6.4% upon heating to 600 °C compared to 29.3% for those simply dried in ammonium hydroxide after washing. The difference of 22.9% mass loss during thermal gravimetric analysis was comparable to the calculated mass fraction removed during a pressurized water treatment. Using the sintered mass of spheres and the equivalent mass of dried residue obtained from the pressurized water treatment effluent, the residue mass constituted 21.8% of the final microsphere mass. Using electron impact mass spectroscopy, it was clear that the bulk of the residue was HMTA and urea, as indicated by Figure 4.30 and Figure 4.31. Additionally, the similarity in mass loss profiles between pressurized water treatment effluent residues and residues obtained from HMTA/urea solutions during thermal gravimetric analysis, shown in Figure 4.29, suggested a similar composition. Therefore, pressurized water treatments extracted a quantity of HMTA and urea from the microspheres approximately equivalent to 20% of their dried mass. Further, despite complete mass losses of pure HMTA and pure urea by 222 °C and 403 °C, respectively, interactions between their decomposition products create species

that are not fully removed until nearly 700 °C, as evidenced by Figure 4.29. Therefore, hydrothermal treatments also reduced the temperature necessary for removal of volatile impurities from 700 °C to less than 450 °C.

Crystallite growth and the development of an open pore network also occurred during pressurized water treatments. As indicated in the TEM images shown in Figure 4.26 and Figure 4.27 as well as by Scherrer analysis of x-ray diffraction peaks summarized in Table 4.6, average crystallites grew from 1-2 nm to 2-4 nm. Crystallization was likely driven by elevated temperatures as well as the removal of HMTA and urea from the microspheres. Neither of these effects was improved appreciably by addition of a second, four-hour pressurized water treatment, indicating that two hours was sufficient for impurity removal. An open pore network was established corresponding with an increase in crystallinity during a two-hour hydrothermal treatment. Nitrogen adsorption measurements summarized in Table 4.7 indicated that after air-drying, hydrothermally treated microspheres had specific surface areas near 145 m^2/g. A similar mass of spheres simply dried in ammonium hydroxide had surface areas insufficient for measurement, indicating they were either below 13.3 m^2/g or had a closed pore structure.

An experiment splitting microspheres gelled and washed in the same batch into one half for air-drying in ammonium hydroxide and one half for autoclaving revealed that microspheres shrink during hydrothermal treatment. Measurement of microsphere diameters during washing and drying indicated volume reductions of more than 50% during pressurized water treatments. Volume reduction of wet, gelled microspheres can be considered “crack-free” shrinkage. Gelled microspheres are permeable to aqueous solutions and extracting water and impurities from gelled spheres does not seem to degrade them in any way, as evidenced by a lack of observed microsphere cracking during washes with ammonium hydroxide or during hydrothermal

treatments. Further, upon air-drying, autoclaved microspheres had average volumes that were 72% of those dried in ammonium hydroxide. Both sets of microspheres reduced to similar sizes upon heating to 600 °C, but ammonium hydroxide dried microspheres had a diameter reduction of 28% while autoclaved microspheres reduced only 9.4% during the heat treatment. It is possible that severe shrinkage caused a radial stress distribution in the microspheres dried in ammonium hydroxide which contributed to their increased rate of fracture.

Microsphere cracking is primarily attributed to an inability to release volatile impurities. Previous studies have suggested that spheres with small crystallites or amorphous structures, caused by rapid gelation with high R values and high temperatures, is tied to cracking as a result of internal pressures generated by volatiles that are unable to escape [43,170,176,180,186,192–194]. Based on analysis of the microspheres tested, those dried in ammonium hydroxide consistently released approximately 30% of their mass as volatile emissions from microspheres without an open pore network to facilitate their escape, which resulted in cracking. However autoclaved microspheres, which consistently released only 6-7% of their mass, were able to evolve water vapor through pores with equivalent diameters less than 20 nm without forming cracks. Thermal gravimetric analysis and electron-impact mass spectroscopy also indicated that autoclaved microspheres evolved gaseous water as their principle emission product at a gradual rate, preventing pressure spikes and allowing slower diffusion out through pores. Microspheres air-dried in ammonium hydroxide still contained carbon and nitrogen-bearing molecules that, at a certain onset temperature, sublimated or decomposed more rapidly by CO_2 and NH_3 emissions, generating a pressure spike represented as a rapid mass decrease near 250 °C in Figure 4.28. Faster emissions of volatiles upon reaching sublimation or decomposition temperatures is

expected to generate higher internal pressures and exacerbate cracking for microspheres dried in ammonium hydroxide.

Pressurized water treatments were also linked to reduced agglomeration of microspheres during heat treatments. While microspheres did not appear to sinter together regardless of washing technique when heated to 600 °C, their agglomeration behavior after sintering was notably different. Upon applying light pressure, hydrothermally treated microspheres separated and became free-flowing. However, sintered microspheres that were air-dried in ammonium hydroxide had to be slugged through a mesh screen and contained some agglomerates that could not be broken apart. Initially, it was assumed that volatile emissions promoted bonding at the microsphere interfaces. Observations that ammonium hydroxide-dried microspheres did not agglomerate by 600 °C after the majority of volatile removal suggests instead that their tendency to sinter together at elevated temperatures was for other reasons. It is possible that cracked, rough surfaces promoted inter-sphere neck formation during sintering that was less pronounced for hydrothermally treated microspheres with smooth surfaces.

Conclusions:

1) **Microsphere cracking during heat treatments was prevented by the application of a pressurized water treatment, which removed HMTA and urea impurities as well as formed an open pore network to accommodate outgassing.**

2) **Problems with microsphere agglomeration during heat treatments were overcome by improved washing techniques, including the addition of a pressurized water treatment. Microspheres processed by new methods were free flowing.**

5.1.2 A New Basis for Acid Deficiency and R Value Selection

Gels formed by internal gelation methods fall into three broad categories for a fixed gelation temperature. At low R values and acid deficiencies, soft gels are produced with long solidification times that tend to erode during washing. High R values and acid deficiencies lead to strong gels that form quickly, but tend to crack upon drying and heating. Thus, intermediate values for R and acid deficiency have been used historically to form crack-free microspheres. However, merely selecting intermediate values is inadequate when the desired materials or necessary processing conditions result in the formation of microspheres that crack upon drying or heating. Impurity removal and crystal growth during hydrothermal treatment of cerium oxide microspheres suggest that historical problems with microsphere cracking can be mitigated by a simple heat treatment in water.

During internal gelation research with cerium oxide, it became clear that the highest material throughputs and best monodispersities are achieved when microspheres gel as quickly as possible in the column. Additionally, reduced plutonium leaching from mixed-oxide microspheres into ammonium hydroxide wash solutions has been observed for higher gelation temperatures [179]. Fast gelation times also prevent coalescence, allow faster droplet formation frequencies, and enable fast, laminar flow through the gelation column. However, fast gelation results in amorphous structures or small crystallites that impede impurity removal during washing and heat treatments, resulting in cracking. Thus, R values and acid deficiencies are typically selected that prevent cracking, at the expense of gelation time, monodispersity, and washing erosion. However, if microspheres are subjected to a pressurized water treatment, the negative consequences of fast gelation are rectified while they are still wet and permeable. The ability of pressurized water treatments to remove impurities and develop open porosity in gelled

microspheres prior to drying rectifies the consequences of fast gelation that cause cracking. Therefore, microspheres that are washed and autoclaved can gel faster with higher R values and acid deficiencies without cracking, allowing increases in throughput and improved monodispersity.

Conclusions:

1) **Microspheres prepared using elevated R values, OH^-/Ce ratios, and formation temperatures gelled faster, which improved monodispersity and production rates.**

2) **Pressurized water treatments prevent microsphere cracking which would otherwise occur at elevated R values, OH^-/Ce ratios, and formation temperatures. Therefore, microspheres can be successfully produced using feed parameters that were previously undesirable.**

5.1.3 Impurity Levels

5.1.3.1 Glow Discharge Mass Spectroscopy

Analysis of previous failures of post-impact containment iridium claddings has motivated low impurity levels in Pu-238 oxide fuels [66,205,206]. For the last several decades, Pu-238 oxide fuels have been sealed in welded, iridium claddings with small, porous clad vent sets to facilitate helium removal [63,207]. DOP-26 iridium alloys are currently used, which incorporate 0.3 weight percent tungsten and 60 ppm thorium [208,209]. Due to very low thorium solubility in iridium, thorium was found to segregate to grain boundaries and prevent intergranular cracking in favor of ductile, transgranular fracture at elevated temperatures [210,211].

Additionally, an Ir_5Th phase formed, which pinned grain boundaries and prevented grain growth [209,212]. Transport of iron, chromium, and nickel from fuel impurities to the iridium cladding is believed to cause thorium diffusion, which has caused grain growth that compromised high temperature impact ductility, increasing the likelihood of plutonium release in the event of re-entry and impact [66,212].

Previous studies of iridium cladding failures after impact testing have linked cladding degradation to the introduction of impurity elements. Iridium claddings were found to fail by intergranular cracking and large grain sizes [206], indicating the depletion of thorium at grain boundaries, which was traced to the introduction of impurities from the Pu-238 oxide fuel [66]. Additionally, the presence of a glassy material composed of a combination of calcium, silicon, oxygen, plutonium, and iron with magnesium or aluminum in porous vents was believed to prevent helium release, motivating the minimization of these impurities in the fuel [66,206]. Analysis of microspheres washed by improved methods with a pressurized water treatment indicated that impurity levels were far below published limits for Pu-238 oxide fuels. For nearly all elements reported by glow-discharge mass spectroscopy, microsphere impurities were also below reported elemental concentrations in Pu-238 oxide products, as summarized in Table 5.1. Aluminum and silicon levels in microspheres were among the highest at 64 and 69 ppm, respectively. While aluminum and silicon were elevated above some reported Pu-238 oxide products, levels were still well below 1996 limits of 500 ppm and 750 ppm [213], respectively, and more conservative 1983 recommended limits of 100 ppm each [66]. Elevated silicon levels are assumed to be introduced by residual silicone oil while the source of aluminum is unknown. However, the initial concentrations of aluminum and silicon in ceric ammonium nitrate are unknown. Calcium, sodium, and zirconium were the only other elements with concentrations

above 10 ppm in sintered cerium oxide microspheres and each had levels below or comparable to typical concentrations in Pu-238 oxide fuels. Phosphorous does not appear to have been introduced at any point in the sol-gel process, which avoids additional compatibility issues with iridium claddings [66]. Despite its other benefits, pressurized water treatments did not appear to extract trace element impurities from microspheres, as indicated by inductively coupled plasma mass spectroscopy.

The very low impurities observed in cerium oxide microspheres cannot be expected to directly carry over for Pu-238 oxide microspheres, but do indicate that the sol-gel process does not introduce problematic quantities of any particular element. The improved purity levels for cerium cannot be expected for Pu-238 simply because of the stock materials used for each. While ceric ammonium nitrate was 99.99% pure, plutonium-238 feeds contain residual impurities from fission products produced during neptunium irradiation as well as potential impurities from precipitation and valence stabilization additives that can include elements such as iron and sodium [213]. While the need for, and selection of, stabilizers for Pu-238 feed solutions in the sol-gel process remain to be determined, current evidence obtained with cerium surrogates indicates that the observed introductions of trace elements during sol-gel processing is not a problem.

Table 5.1: Microsphere impurity levels measured by glow-discharge mass spectroscopy (GDMS) indicated concentrations below published limits for Pu-238 oxide fuels.

Element	CAN COA	CeO_2 GDMS	GDMS Sensitivity	Limits (1972)	Typical Analyses - Product	Limits (1979)	Typical Analyses - Feed	Limits (1996)	Typical Analyses - Feed	Typical Analyses - Product	Typical Analyses - Feed (1996)	Typical Analyses - Product	Analysis of Pellet Interior (1974)
	[ppm]	[ppm]	[ppm]	[ppm]	[ppm]	[ppm]	[ppm]	[µg/g]	[µg/g]	[µg/g]	[µg/g]	[µg/g]	[µg/g]
Al	-	64	0.05	150	< 50	150	83	500	152	121	11.8	84	100
B	0.1	0.07	0.01	-	-	-	< 1	5	5	5	< 5	< 5	-
Ba	0.6	1.5	0.1	-	-	-	< 2	-	-	-	-	-	-
Be	-	<0.01	0.01	-	-	-	< 1	5	1	1	-	-	-
Bi	-	<0.1	0.1	-	-	-	< 1	-	-	-	-	-	-
Ca	-	32	0.1	300	< 250	300	184	300	37	268	1150	160	< 250
Cd	-	<5	0.5	-	-	-	< 10	50	10	10	< 10	< 10	-
Co	-	<0.05	0.05	50	< 50	50	1	-	-	-	-	-	25
Cr	3.4	0.69	0.05	250	70	250	32	500	583	98	49	81	30
Cu	1.4	<0.05	0.05	100	< 50	100	11	200	38	29	12	42	< 10
Fe	2.1	5.1	0.05	800	250	800	176	800	962	126	167	245	500
Hf	-	0.63	0.05	-	-	-	< 25	-	-	-	-	-	-
K	-	9.4	0.1	-	-	-	4	-	-	-	-	-	-
La	-	0.55	0.05	-	-	-	< 25	-	-	-	-	-	-
Li	-	2.2	0.01	-	-	-	< 1	-	-	-	-	-	-
Mg	1.8	0.08	0.05	50	< 20	50	8	100	13	10	72	21	10
Mn	-	0.11	0.05	-	-	-	9	50	14	5	30	68	12
Mo	-	0.15	0.1	-	-	-	4	250	20	20	23	35	-
Na	-	46	0.05	250	< 250	250	4	250	54	50	< 50	< 50	-
Nb	-	0.34	0.01	-	-	-	< 10	-	-	-	-	-	-
Ni	1.2	<0.05	0.05	150	< 50	150	46	500	225	20	71	72	70
P	-	<0.05	0.05	-	-	-	-	25	365	20	-	-	-
Pb	-	<0.5	1	100	25	100	19	100	17	12	30	13	< 10
Rb	-	<0.05	0.05	-	-	-	< 10	-	-	-	-	-	-
Re	-	<0.05	0.05	-	-	-	< 25	-	-	-	-	-	-
Si	-	69	0.05	200	< 50	200	105	750	642	25	294	256	100
Sm	-	<0.1	0.05	-	-	-	-	-	-	-	-	-	-
Sn	-	0.33	0.1	50	< 10	50	7	50	5	5	< 5	< 5	-
Sr	-	0.2	0.05	-	-	-	< 5	-	-	-	-	-	-
Ta	-	<5	5	200	< 100	200	< 100	-	-	-	-	-	-
Ti	0.6	0.56	0.01	-	-	-	13	-	-	-	-	-	-
V	-	0.14	0.05	-	-	-	< 2	-	-	-	-	-	-
W	-	<0.1	0.1	-	-	-	< 10	-	-	-	-	-	-
Y	3.7	0.9	0.1	-	-	-	< 25	-	-	-	-	-	-
Zn	-	0.28	0.1	50	< 50	50	10	50	14	6	7	7	-
Zr	-	26	0.05	-	-	-	< 100	-	-	-	-	-	-
Element	CAN COA	CeO_2 GDMS	GDMS Sensitivity	Limits (1972)	Typical Analyses - Product	Limits (1979)	Typical Analyses - Feed	Limits (1996)	Typical Analyses - Feed	Typical Analyses - Product	Typical Analyses - Feed (1996)	Typical Analyses - Product	Analysis of Pellet Interior (1974)
Source:				[214]	[214]	[18]	[18]	[213]	[213]	[213]	[215]	[215]	[216]

5.1.3.2 Analysis of Carbon, Nitrogen, and Hydrogen Levels in Microspheres

Separate analyses of carbon, nitrogen, and hydrogen levels using instrumental gas analysis were performed on sintered microspheres produced using baseline and improved washing methods as well as improved washing methods with hydrothermal treatment. In all cases, very low carbon concentrations were reported. However, an upward trend in nitrogen and hydrogen levels was observed for microspheres prepared without a pressurized water treatment, as summarized in Table 4.4. Rationale for the elevated levels observed for sintered microspheres processed without autoclaving and those sintered after air-drying in ammonium hydroxide can be understood by examination of electron-impact mass spectroscopy of air-dried microspheres washed with and without a pressurized water treatment.

A key difference observed during electron-impact mass spectroscopy of microspheres air-dried in ammonium hydroxide and those that were air-dried after a hydrothermal treatment was the quantity and temperatures of water, carbon dioxide and ammonia evolution. As indicated in Figure 4.33, ammonia generation was minimal for autoclaved microspheres, and the only signal observed over the entire temperature range was water and carbon dioxide, which evolved primarily upon insertion into vacuum at low temperatures. In contrast, microspheres dried in ammonium hydroxide exhibited carbon dioxide and ammonia evolution at temperatures above 300 °C with the water signal decreasing above 300 °C. The emission of carbon dioxide from autoclaved microspheres at low temperatures upon insertion into the vacuum was puzzling, since carbon dioxide would be expected to evolve from samples at elevated temperatures due to the decomposition of organic molecules or due to residual carbon combustion.

To understand the difference between the emissions of samples prepared with and without a pressurized water treatment, reactions occurring during a hydrothermal treatment must

be considered. To help understand these reactions and why carbon dioxide is released at low temperatures, mass spectroscopy was performed on additional powder samples prepared by hydrothermal synthesis. A solution of cerous nitrate and urea was used to precipitate cerium carbonate hydroxide in the autoclave at 180 °C according to published methods [104]. Analysis of cerium carbonate hydroxide in the electron-impact mass spectrometer indicated that no carbon dioxide emission occurred until above 300 °C. No ammonia release from cerium carbonate hydroxide was observed. Based on these observations, the formation of carbonates was dismissed as a source of low-temperature carbon dioxide emission from autoclaved microspheres. Cerium hydroxide was also precipitated during a hydrothermal treatment of a solution containing ceric ammonium nitrate and urea heated to 200 °C for two hours. The resulting pale yellow powder, shown in Figure 4.34, immediately released carbon dioxide and water in a manner very similar to the autoclaved microspheres. The low-temperature carbon dioxide release can be understood from the observation that synthesis of ceric hydroxide from ceric ammonium nitrate and urea caused water in the hydrothermal treatment to become very effervescent. It is assumed that urea underwent hydrolysis during the autoclaving step according to the reaction [190]:

$$CO(NH_2)_2 + H_2O - 2NH_3 + CO_2 , \quad (5.1)$$

which caused the water to become carbonated in the pressure vessel. Carbon dioxide produced by urea hydrolysis is presumed to have adsorbed onto cerium hydroxide and outgassed upon insertion into the vacuum chamber for electron-impact mass spectroscopy. Similarly, it is believed that carbon dioxide formed from urea hydrolysis during pressurized water treatment of microspheres was adsorbed onto spheres and was not released until introduced into the vacuum for mass spectroscopy. Since microspheres dried in ammonium hydroxide were not exposed to

carbon dioxide from urea hydrolysis, it was logical that those samples had no low-temperature CO_2 emission.

Additional support for the hydrolysis of urea during pressurized water treatments is the increase in conductivity observed in post-hydrothermal treatment effluents. Hydrothermal treatment effluents had conductivities nearly an order of magnitude larger than those measured for 0.5 M ammonium hydroxide wash solutions used on microspheres. The observed increase in conductivity is explained by urea hydrolysis and release of ammonia into solution. Conductivity was not attributed to ammonium nitrate since it was extracted during 0.5 M ammonium hydroxide washes, as shown in Figure 4.35. Also, HMTA and urea do not contribute significantly to solution conductivity.

Based on the preceding analysis, low-temperature carbon dioxide emission was linked to adsorption of CO_2 from urea hydrolysis during the autoclaving step, but the high-temperature, coupled emission of carbon dioxide and ammonia from microspheres dried in ammonium hydroxide required additional consideration. Investigation of the decomposition behavior of urea indicated a mechanism consistent with the profiles for microspheres dried in ammonium hydroxide shown in Figure 4.33. Above its melting point of approximately 133 °C, urea is believed to have converted to cyanuric acid, which began to decompose into isocyanic acid from 320-360 °C [217,218]. A reaction between isocyanic acid and water produces ammonia and carbon dioxide [218]. In summary, the simultaneous decrease in water with an increase in ammonia and carbon dioxide, seen in Figure 4.33 for microspheres dried in ammonium hydroxide, can be explained by residual urea conversion into cyanuric acid that decomposed into isocyanic acid above 300 °C, followed by isocyanic acid reaction with water to produce volatile ammonia and carbon dioxide.

Similar urea reactions were observed during electron-impact mass spectroscopy of pressurized water treatment residues. For residues, it appears that urea volatilized, formed cyanuric acid, and decomposed directly to isocyanic acid with ammonia release. This observation is evidenced by simultaneous signals for urea, ammonia, and carbon dioxide above the urea melting point, corresponding to urea volatilization, urea decomposition to isocyanic acid with ammonia release, and isocyanic acid decomposition to ammonia and carbon dioxide in the presence of water. Additionally, peaks corresponding to isocyanic acid and cyanuric acid were observed above 200 °C. This indicates that isocyanic acid and cyanuric acid, produced by urea decomposition, both volatilized and decomposed. Above 400 °C water, ammonia, and carbon dioxide signals diminished, but isocyanic acid was observed in a strong peak. This indicates that isocyanic acid produced from cyanuric acid decomposition at elevated temperatures was no longer able to decompose without the presence of water, and thus it volatilized instead. Based on the differences observed between volatile emissions from microspheres dried in ammonium hydroxide, residues from hydrothermal treatments, and residues from HMTA/urea solutions, it appears that temperature-dependent decomposition paths and mass losses will depend to some extent upon the quantity of water and HMTA present along with urea impurities. None of the decomposition reactions at elevated temperatures were observed in hydrothermally treated microspheres due to urea removal in the pressurized water treatment step prior to electron-impact mass spectroscopy.

Analysis of pressurized water treatment residues, as well as volatile emissions from microspheres, indicates that HMTA and urea are either leached during hydrothermal treatments or volatilized at elevated temperatures during thermal treatments. As indicated by thermal gravimetric analysis shown in Figure 4.28 and Figure 4.29, reactions involving carbon, nitrogen,

and hydrogen-bearing impurity molecules are not complete until nearly 700 °C. Reactions of microsphere impurities at these elevated temperatures are believed to be the cause of elevated nitrogen and hydrogen levels in microspheres washed without a hydrothermal treatment. One possibility is that localized reducing conditions are generated as a result of interactions with decomposition species such as ammonia. In the presence of these reducing conditions, it is theorized that limited amounts of cerium nitride, hydride, and/or hydroxide are formed, and that some of these products persist through the sintering cycle. A study of the formation of cerium and uranium nitrides has shown that ammonia gas acts both to form nitrides as well as remove carbon due to its high nitriding and hydriding activities [219]. Other studies have shown that zirconium as well as cerium intermetallics undergo nitriding and hydriding in the presence of ammonia gas at temperatures in the approximate range of 200-500 °C [220,221]. While elevated nitrogen impurities are unlikely to cause any reactions below 2000 °C in plutonium fuels [214], hydrogen may contribute to reducing conditions in the fuel. At the levels detected, however, nitrogen and hydrogen impurities are unlikely to pose a problem.

Differences observed between microspheres washed by baseline processes and those washed by improved methods were attributed to the improved removal of carbon, nitrogen, and hydrogen-bearing species during washing steps. It is believed that improved removal of silicone oil through use of TCE/IPA co-solvents, and improving TCE removal prior to ammonium hydroxide washes, using an IPA/NH_4OH mixture, allowed for improved impurity removal by eliminating immiscible barriers surrounding microspheres. According to this line of thought, microspheres dried in ammonium hydroxide have the largest amount of impurities undergoing high-temperature reactions during heat treatments, while those washed by improved methods

have less, and those washed by improved methods and subjected to a pressurized water treatment have the least.

Carbon levels of 13.5-26.8 ppm in the three samples analyzed were low, indicating excellent removal of organics during washing and/or heat treatment processes. Limited carbon content in the fuel is desirable for two main reasons. During development of RTGs, a cyclical reaction was found to take place whereby carbon monoxide (CO) reduced plutonium oxide and became CO_2, transported the oxygen to the graphite matrix where it was reduced to CO, and again reduced the plutonium fuel [222]. This cyclic reaction resulted in the generation of CO and CO_2 gases that degraded thermoelectric converters and necessitated the installation of a gas management system for use during terrestrial storage prior to evacuation in outer space [223]. Pits in graphite components were also observed opposite frit vents [206]. While CO is believed to be outgassed from graphite components, it is also possible for CO to be generated from carbon impurities in fuel at elevated temperatures [222]. Additionally, carbothermic reduction causing substoichiometric fuels below $PuO_{1.9}$ can be problematic for fuel-iridium compatibility [214]. Measured carbon levels in sintered microspheres were similar to concentrations of 22-34 ppm taken from the exterior and interior of Pu-238 oxide pellets prepared from hydroxide precipitated shards in 1974 [216] and were less than typical analyses of 200 ppm for Pu-238 oxide used in multi-hundred watt generators in 1973 [214].

Conclusion:

1) **Pressurized water treatments and sintering in air led to internal gelation cerium oxide microspheres with impurity concentrations well below published limits for plutonium-238 oxide fuels.**

5.1.4 Pellet Production from Internal Gelation Microspheres

Microspheres produced using improved washing methods with a pressurized water treatment are anticipated to be suitable for pressing fuel pellets. A characterization of cerium oxide microspheres performed as a function of heat treatment temperature indicated that microspheres subjected to a hydrothermal treatment are more dense and have higher specific surface areas than those prepared by baseline washing processes. Pathways for microsphere processing after air-drying will depend on the desired fuel properties and application.

For Pu-238 oxide pellet production, a microsphere thermal seasoning process similar to that used in the current process flowsheet will be necessary to adjust microsphere sinterability. Uniform, coarse porosity in Pu-238 oxide pellets with final densities around 85% theoretical is desired to prevent thermal stress fractures and permit helium escape [65,67,70]. Additionally, due to the internal heat generation and high operating temperature for Pu-238 oxide fuel pellets, it is important that sintered pellets are unable to undergo additional sintering and shrinking post-processing [65]. Otherwise, networks of cracks on the pellet surface are created due to non-uniform shrinkage [67]. In baseline processes, variations in powder size and morphology are overcome by ball milling to obtain consistent powders used for granule formation to prevent cracking and ensure consistent pellet density from batch to batch [67]. It is anticipated that monodisperse internal gelation microspheres will provide a uniform “granule” feed to create consistent pellets with uniform, coarse porosity. Microspheres subjected to a pressurized water treatment can be heated to ≤ 450 °C to remove volatile impurities, followed by heating to the desired temperatures for thermal seasoning. Although optimal pre-heating temperatures for desirable pellet consolidation are yet to be determined, it is believed that spheres will be split into two fractions and heated to minimum temperatures of 750 °C and 1050 °C to reduce

sinterability prior to mixing and hot pressing into a pellet. Pre-heating microspheres should allow for what has been referred to as a "blackberry structure" in the pellet [167,171,175], which represents the coarse, uniform porosity desirable for Pu-238 oxide pellets [65,67]. Although cerium oxide microspheres exhibited high densities upon drying and sintering, this is not expected to be problematic for Pu-238 oxide pellet production since high granule density is desirable for achieving coarse microstructures. Even if microspheres heated to 750 °C do not crush easily, microspheres heated to 450 °C are expected to have high enough specific surface areas and low enough densities to provide ample pellet consolidation when mixed with a higher density fraction.

Small crystallites of 1-10 nm observed in air-dried cerium oxide microspheres were formed due to mixed feed parameters and high temperatures that caused fast gelation. Although larger crystallites developed upon heating above 450 °C, which has also been observed in the literature [74,126,130], a portion of small crystallites also remained. Because microspheres reached high densities during sintering treatments, pellet shrinkage post-sintering would be expected. However, the crystallite and grain growth behavior at sustained operating temperatures for Pu-238 oxide fuels is unknown. Since grains of ≥ 10 μm are desirable to prevent fines generation in the event of impact and intergranular fuel fracture [65], future investigations with pellet production and analysis will need to assess grain size as a function of pellet heat treatments. Also, while cerium provides a baseline for comparison, crystallite sizes in plutonium microspheres will depend upon the mixed feed solution parameters that are deemed necessary. It is possible that radiolysis and self-heating effects will require lower plutonium concentrations with corresponding changes to acid deficiency and R value.

In addition to removing impurities and preventing cracking, the ability of pressurized water treatments to create porosity and high specific surface areas may allow for pellet production without using carbon as a pore former or making compromises in the mixed feed solution parameters. Reports of uranium oxide or mixed oxide pellet fabrication from microspheres have indicated that microspheres must be soft, or porous, enough to crush into a homogeneous pellet without forming a "blackberry" structure while also having sufficient density to prevent high compaction ratios, which can cause pellet defects [167,171,175,179]. In the past, carbon pore formers or the use of mixed feed solutions that gel more slowly were used to produce softer microspheres to facilitate crushing [169,171,172]. For pellets containing uranium, specific surface areas of 4-7 m^2/g have been reported as optimal for green pellet pressing following preliminary uranium calcination and reduction, at temperatures of 500-800 °C [171,175,179]. Based on observations that cerium oxide microspheres produced in this study had a specific surface area of 102.7 m^2/g after heating for four hours at 450 °C but less than 13.3 m^2/g after heating at 750 °C for four hours, it seems probable that functional microsphere heat treatments can be developed for hydrothermally treated microspheres to press homogeneous green pellets. However, evidence that a reduction in average pore diameter is occurring by 450 °C, as shown in Figure 4.50, suggests that further studies are needed into temperature/porosity behavior in the 450-750 °C temperature range and the effect on green pellet pressing. Microspheres exhibited excellent sinterability and reached high values of theoretical density, which should allow for dense pellets to be produced if microspheres can be sufficiently crushed during green pellet pressing after pre-heating to the necessary temperatures for volatile impurity removal and oxidation adjustments.

Pressurized water treatments may be particularly well suited for improving the crystallinity of uranium microspheres produced by internal gelation. Evidence that species in the ammonium diuranate (ADU), $UO_3 \cdot NH_3 \cdot H_2O$, system are formed during internal gelation [192], just as in uranium precipitation with ammonium hydroxide [92,93], have been supported by studies suggesting the release of coordinated ammonia from internal gelation gels at 200-300 °C using mass spectroscopy [197]. Additionally, crystallinity has been shown to decrease with increasing ammonia content [93]. Values of x in species of the form $UO_3 \cdot xNH_3 \cdot (2\text{-}x)H_2O$ decrease to 1/3 in the presence of water, effectively exchanging ammonia for water. Amorphous UO_3 in precipitates also tends to convert to crystalline $UO_3 \cdot 2H_2O$ upon exposure to water [92]. Therefore, subjecting uranium oxide microspheres to a pressurized water treatment rather than air-drying in ammonium hydroxide is also expected to remove ammonia, improve crystallinity, and thus reduce cracking.

Some fuels envisioned for future space nuclear power sources involve the encapsulation of Pu-238 oxide fuels in a tungsten matrix for high-temperature applications [224]. While microspheres are expected to provide a more uniform feed material than angular powders and allow for improved filling of metal around the fuel, microsphere coatings may be necessary to prevent tungsten-plutonium interactions since compatibility studies between tungsten and plutonium have shown the reduction of plutonium and formation of WO_2 and/or WO_3 at elevated temperatures [214]. Depending on the coating desired, fluidized beds could be used for their application to spheres. The excellent size uniformity, and thus weight uniformity, of sol-gel microspheres lends well to their use in fluidized beds for the deposit of coatings from heated gases.

Conclusion:

1) **The necessary temperature for volatile impurity removal was reduced by application of pressurized water treatments. Impurity removal at lower temperatures and an open porosity provide greater flexibility in microsphere heat treatments prior to pellet pressing that meet the particular needs of specific applications.**

5.2 Production of Monodisperse Microspheres with Diameters 50-200 μm

The degree of monodispersity observed in microspheres suggests that droplet formation occurred in a simple dripping flow regime where spheres of a uniform size were stripped from the dispensing needle at regular intervals. Microfluidics experiments producing uniform emulsions of water or solvents in oil have documented the production of 2-200 μm particles with minimum polydispersities less than three percent [202]. These experiments made use of similar sphere stripping techniques in the dripping flow regime to achieve highly uniform particles. Therefore, the narrow size distributions of 2.23-3.80% standard deviation reported in Table 4.2 for cerium oxide microspheres produced in this thesis were near to those observed in similar equipment in the literature. Incidences of higher standard deviations in three test cases from 5.46-7.77% are believed to be elevated due to misinterpretation of shadows and particle agglomerations by optical image analysis software.

The dripping regime, also known as periodic dripping, can be easily explained by an analogy to a leaking faucet. At very slow flow rates, liquid accumulates in a droplet until the force due to gravity exceeds the cohesive forces in the liquid, and the droplet breaks off from the faucet at a distance of approximately one droplet diameter. During sol-gel microsphere

formation, the force of gravity can be ignored in the dispersion apparatus, but it is replaced with shear forces from the coaxial flow of silicone oil. At slow feed flow rates, droplets grow on the tip of the needle until shear forces exceed cohesive forces in the feed and the droplet is stripped off into the oil flow [225]. As long as flow rates remain constant, droplet formation occurs at a set frequency. This simple dripping behavior transitions to complex dripping at faster liquid flow rates and is characterized by quasi-periodic or chaotic sphere sizes [226–228]. At still faster feed flow rates, liquid jets are formed.

The jetting regime, characterized by varicose or Rayleigh breakup of liquid jets, can also be explained using the example of a faucet. At faster flow rates, a thin column of fluid falls from the faucet under the influence of gravity. Due to small perturbations in the system, the column becomes deformed. These deformations, caused by varicose perturbations, result in regions of increased and decreased diameter [161,225]. Variations in the jet diameter result in regions of high and low pressure, which cause further pinching of the jet into droplets due to surface tension. Jet breakup into spheres occurs to minimize surface area. In a two fluid nozzle with silicone oil as the continuous phase, gravity is again ignored and the column of feed, or jet, is produced by the inertial energy of the feed and shear forces from the faster-flowing silicone oil.

While many previous sol-gel systems have produced uniform microspheres larger than 200-300 μm using vibration to promote regular jet breakup, the work performed in this thesis is believed to be in the simple dripping regime. The apparently linear change in microsphere size while changing the stripping oil velocity at fixed feed flow rates is indicative of droplet formation in the simple dripping mode [229]. Additionally, increasing the feed flow rate at a fixed stripping oil velocity causes the eventual formation of irregular sized microspheres one would expect from complex dripping or uncontrolled jetting [226–228]. As an additional

measure to evaluate the flow regime during microsphere production, values for Weber and capillary numbers were calculated for typical flow conditions. Although many different methods are used to predict the transition from dripping to jetting, it can be estimated to occur when the sum of the Weber and capillary number is approximately equal to one [225]. Alternatively, uniform droplet formation at a fixed frequency can be assumed if We << 1 [226]. The Weber number for typical conditions used in this thesis was estimated to be 2×10^{-5}, while the capillary number was calculated and varied between 0.2-0.8 for low-to-high stripping oil flow rates. Based on these calculations, it appears that desirable flow rates for microsphere formation in the sol-gel rig result in simple, periodic dripping. However, the sol-gel rig is also capable of developing undesirable complex dripping or jetting regimes at fast stripping oil speeds and high feed solution overpressures.

Use of 26, 28, and 32 gauge needles to produce uniform microspheres with diameters of 65.5-211.3 μm came very close to the original goal of making monodisperse spheres from 50-200 μm. Based on previously published work on Pu-238 oxide pellet fabrication from powder-based granules, microspheres sizes of 100-125 μm are expected to be the best substitution. Since Pu-238 oxide pellets fabricated by pressing plutonium precipitates after oxide conversion or by pressing ball-milled powders caused pellet cracking, hot pressing thermally seasoned granules became necessary [65]. Heat treatment of the granules prior to hot pressing the pellet allowed for a reduction in sinterability and an increase in strength to ensure a coarse porosity with small neck formations between individual granules [65]. Further, use of granules <125 μm rather than <297 μm resulted in a more uniform porosity and better granule-to-granule contact, which was desirable to stabilize the microstructure and prevent additional shrinkage at high operating temperatures [65]. The use of microspheres with diameters near 100 μm is expected to allow

pre-heating treatments and hot pressing such that pellets have a uniform coarse porosity without having to process fines less than 50 μm generated during traditional powder granulation. While powder-based granulates have a porous, friable surface that introduce fines, microspheres are very smooth and have a lower exterior surface area. Also, use of screened, angular granulates with a variety of sizes has resulted in the formation of 1000-2000 μm dense aggregates due to self-heating during storage that adversely affected the homogeneity of pellets [230]. The uniform size and shape of microspheres should prevent high density aggregates.

Demonstrated microsphere size distributions less than 5% at 100 μm are expected to be more than adequate for Pu-238 oxide pellet pressing and should be applicable to other fuel applications. High density microspheres with tightly controlled diameters in two or three size fractions are often desired for vibratory packed fuels. In the past, small microsphere fractions were polydisperse since they were produced by rapid stirring emulsification. Alternatively, small shards were vibro-compacted, including Pu-238 oxide milliwatt power sources [65]. Uniform microspheres below 200 μm would allow for improved packing and less dust generation from powder processing. Additionally, accurate control of particle size would be expected to improve homogeneity and perhaps allow higher sintered densities compared to angular powders used in inert matrix fuels produced by powder metallurgy.

Variation of stripping oil speed appeared to have a much larger impact on microsphere diameter than the pressure exerted on feed solutions in the feed flow regime of interest. Observation of microsphere production at a variety of stripping oil speeds and feed solution overpressures revealed that desirable stripping oil speeds encompassed a wide range of flow rates spanning nearly an order of magnitude from 1-9 mL/min. However, desirable feed solution overpressures were in a much smaller range from 3.0-4.5 psi. Within the range 3.0-4.5 psi, the

change in microsphere size was negligible compared to the change in microsphere size with variation of the stripping oil speed. For this reason, the stripping oil speed was used to vary microsphere size while the feed overpressure was used to adjust microsphere formation frequency. However, if the feed flow rate crossed a threshold value, generally above 4.5 psi, uniform microspheres in a single-file line transitioned into a distributed stream of larger, polydisperse spheres. As discussed previously, these observations led to the belief that optimal flow conditions for monodisperse microsphere formation existed in the dripping regime where droplet formation occurred due to shearing forces from stripping oil rather than in the jetting regime.

Analysis of microsphere sizes produced using different needle gauges and stripping oil flow rate revealed that 26 gauge needles had the greatest utility. While varying the stripping oil flow rate decreased the microsphere diameter by as much as a factor of three, reduction in microsphere diameters with smaller needles was only 7.7-33%. The range of sizes from the 26 gauge needle encompassed 96.5% of the entire range of spheres produced with all three needles. Therefore, while small needles can be used to make uniform microspheres of the desired size, using larger needles and higher stripping oil flow rates is desirable to minimize the likelihood of needle clogging. Extrapolating, it is possible that large needle sizes could be used with low plutonium concentrations in feed solutions with high R values and high gelation temperatures. Large needles and low plutonium concentrations would prevent needle clogging and result in gelled spheres that required a large degree of shrinkage. However, this shrinkage may be accommodated, along with excess impurity removal, by a pressurized water treatment to yield small plutonium oxide spheres from large droplets.

Conclusions:

1) **Excellent monodispersities for microspheres with diameters from 65-211 μm were achieved by operating in the dripping regime. This size and monodispersity is attractive for granules used to press Pu-238 oxide pellets and advantageous for some microsphere-based fuels or targets requiring a small sphere size.**

2) **Use of larger needles with faster stripping oil flow rates resulted in smaller microsphere diameters while minimizing the risk of needle clogging.**

5.3 Selection of Mixed Feed Solution Parameters

During experiments using traditional testing procedures to determine desirable parameters for internal gelation mixed feed solutions, a unique method for R value and acid deficiency selection was discovered. While variation of R values, acid deficiencies, and subjective evaluations of the resulting gels was instructive, comparison of pH values was found to be a more quantitative method for analysis. A new technique for parameter selection is presented with rationale.

Ceric ammonium nitrate proved to be an excellent feed material for production of cerium oxide microspheres by internal gelation. Many feed combinations yielded firm gels quickly enough for solidification of microspheres in a heated forming column. Additionally, mixed feed solutions were stable as long as they were chilled near 0 °C. Compared to cerous nitrate, mixed feed solutions using ceric ammonium nitrate had approximately 25% less cerium per unit volume at the desired R values, but this did not appear to be problematic. Solutions of ceric ammonium

nitrate allowed for acid deficienciency, yielded stable mixed feed solutions, and formed solid gels that did not erode upon washing.

Gelation trials with ceric ammonium nitrate indicated three primary classes of gels formed over the range of feed compositions tested. Low acid deficiencies and R values were not useful for making microspheres, since soft gels were formed that took too long to solidify in the gelation column. At high acid deficiencies and R values, strong gels formed quickly, but tended to be more brittle and shrink as they evolved a clear supernatant from excess HMTA/urea solution. Intermediate acid deficiencies and R values, which are typically used for uranium oxide microsphere preparation [43,170], resulted in solid gels that can produce acceptable microspheres despite longer gelation times. However, the longer microspheres dwell in the formation column prior to gelation, the more opportunities exist for coalescence and polydispersity, which is problematic. Operating experience has shown that the best spheres tend to result from feed parameters on the boundary between intermediate and high acid deficiencies and R values, allowing for fast gelation with limited shrinkage and supernatant generation.

Trends observed in the current study between gelation times, acid deficiency, and R values were in close agreement with the only other known ceric ammonium nitrate gelation study [180]. In that investigation, qualitative evaluations of gel rigidity were used with mixed feed gelation times in thin-walled centrifuge tubes to select desirable parameters. However, no subsequent work on washing, drying, or heat treatment of cerium oxide microspheres was reported. While feed parameters are often chosen based on subjective evaluations of gel rigidity and the time required for gelation, additional consideration of the feed parameters' impact on impurity leaching from microspheres, propensity for cracking, and density must be considered.

Based on work performed in this thesis, it is believed that comparison of pH values provides the best quantitative assessment of pertinent reactions occurring in the gel.

After mixing, heating, aging, and cooling, gels produced from mixed feeds had pH values ranging from 2.59-5.95. While distinct color changes and increases in viscosity were observed in all of the samples tested, not every sample produced an acceptable, solid gel. Therefore, merely raising the mixed feed solution pH above the value of 2.65 for cerium(IV) precipitation in a nitrate solution was insufficient to form satisfactory gels. Experiments indicated that samples with final pH values below 4.0 were not solid, indicating an incomplete reaction. Although HMTA aids in the formation of a stable gel network through hydrogen bonding [189], a lack of HMTA for this purpose does not appear to be the cause of unsolidified gels in the current experiments. Rather, the increase in gel solidification at fixed R values as the acid deficiency is increased indicates that stronger gels are formed as the hydrolysis reaction approaches completion. Making feed solutions acid deficient by pre-neutralization can be thought of as a pre-hydrolysis step, as explained by the following formulas for a uranium nitrate solution with a nitrate/uranium ratio equal to 1.5 [187]:

$$2UO_2(OH)_{0.5}(NO_3)_{1.5} + 3H_2O \overset{\text{heat}}{\Leftrightarrow} 2UO_2(OH)_2 + 3HNO_3, \text{ and} \quad (5.2)$$

$$2UO_2(OH)_2 \Leftrightarrow 2UO_3 \cdot 2H_2O_{(s)} . \quad (5.3)$$

A stoichiometric solution with a nitrate/uranium ratio equal to two would have produced four nitric acid molecules to be neutralized, compared to three in the formula above. Thus, pre-neutralization of ceric ammonium nitrate using ammonium hydroxide converts a fraction of the nitrate in the solution into ammonium nitrate, eliminating the need to neutralize it later during the gelation step and allowing a higher final pH value. Based on observations of gels and measured pH values, it appeared that complete hydrolysis and solid gels occurred with final pH values

above 4.65. Additionally, the fastest forming gels had final pH values above 5.3. However, this analysis was still based on subjective evaluations. By comparison of the change in pH between chilled, mixed feed solutions and heated, aged gels, there appears to be a new and improved metric for parameter selection.

For internal gelation, it is desirable to have sufficient acid deficiency and HMTA content to allow for rapid gelation. Although excess acid deficiency and HMTA accelerate gelation, they also promote the formation of spheres that shrink excessively and have limited crystallite growth, which causes cracking [43,170,176,180,186,192–194]. Additionally, high acid deficiencies and R values tend to reduce mixed feed solution stability and increase the likelihood of needle clogging. Ideally, the acid deficiency would be sufficiently high to promote rapid gelation while the R value would be limited to the amount necessary to complete the gelation reaction.

The change in pH between chilled, mixed feed solutions and heated, aged gels plotted in Figure 4.5, together with the gelation time, should provide a quantitative basis for selecting optimal acid deficiencies and R values. In Figure 4.5, the maximum change in pH occurs when the chilled, mixed feed solution's pH is kept as low as possible while complete gelation still occurs, causing a high final pH indicative of the reaction reaching completion. Values on the curves in Figure 4.5 to the left of the maxima correspond to cases where the initial pH is low, but the final pH is also low due to incomplete gelation. This is an undesirable region since it leads to soft or unsolidified gels. Values on the curves to the right of maxima correspond to cases where initial pH values are high due to increased acid deficiency and R values, and high final pH values correspond to a complete gelation reaction. In this case, the change in pH is smaller due to an unnecessarily high initial pH from excessive acid deficiency and R value. However, the maximum point on each acid deficiency curve appears to represent the R value that was

sufficient for complete gelation without excess reagents. Selecting R values corresponding to these maxima allows for complete gelation without excessive shrinkage or unnecessarily limiting crystallite growth. A degree of acid deficiency can then be selected that provides gelation times sufficiently fast to avoid coalescence and polydispersity, but no faster than necessary so as to allow crystallite growth in the gelation process. Based on these selection criteria, an OH^-/Ce^{4+} ratio of 0.75 and R value of 2.0 was chosen for microsphere production using Figure 4.2 and Figure 4.5. This feed formulation was found to be optimal both by the selection criteria discussed and through empirical trial and error.

It is anticipated that experimental trials similar to those described for ceric ammonium nitrate will be necessary for future process development with neptunium and plutonium. Here, an additional complication will be the variety of oxidation states possible and the need for valence stabilization. Precipitation of plutonium(IV) in gelation reactions may be preferable to Pu(III) due to the exceedingly low solubility of Pu(IV)OH in solution [72,231], but the pH for the onset of Pu(III) and Pu(IV) precipitation in nitrate solutions must also be considered. Additionally, the tendency for tetravalent plutonium to polymerize [231] will have to be accounted for in the preparation of feed solutions. It is also possible that radiolysis reactions and self-heating will limit Pu-238 concentration in feed solutions.

Conclusion:

1) **A new technique was developed for optimizing R values and acid deficiency ratios. Differences in pH between aqueous feed solutions and aged gels provided a quantitative metric for parameter selection compared to qualitative comparisons of aged gel rigidity and color.**

5.4 Other Lessons Learned

Efforts to develop a sol-gel apparatus to produce uniform microspheres with diameters near 100 μm by internal gelation were met with significant difficulty. While well-established methods existed for making small, polydisperse spheres as well as large monodisperse spheres, fabricating small, monodisperse microspheres proved to be a challenge. Small needles have a propensity to clog and slowly moving feed solutions solidify in regions with insufficient cooling. Further, turbulence in the forming column causes microsphere coalescence and polydispersity. In this section, modifications to traditional equipment and processes to overcome such obstacles are discussed. Lessons learned throughout cerium oxide sol-gel development are presented in the following subsections.

5.4.1 Gelation Column Conditions: Flow and Bubbles

Modifications made to the sol-gel apparatus resulted in significant improvements in gelled microsphere yields and monodispersity. Faster oil flow rates through the gelation column allowed for faster microsphere formation frequencies without microsphere stacking and agglomeration. Also, the removal of bubbles from the gelation column by degassing silicone oil was necessary to achieve optimal monodispersity in long-duration production runs.

Faster silicone oil flow rates through the gelation column increased microsphere yields to 8-10 g/day of cerium oxide product, corresponding to an elemental cerium mass of 6.51-8.15 g. Based on the relative molar masses of cerium and Pu-238, this would amount to 11.07-13.85 g/day of elemental Pu-238, or 12.6-15.7 g/day of Pu-238 oxide. While this level of production was sufficient for surrogate process development, demonstration, and preliminary material characterization, actual Pu-238 daily yields would need to be doubled or tripled to meet anticipated national demand. Scale-up to these levels could be accomplished most simply by

using multiple gelation columns. Alternatively, with additional equipment development, single column yields could be increased through the use of higher silicone oil flow rates with a longer gelation column or multiple sphere-forming nozzles. In either case, modifications to current designs must prevent coalescence of microspheres prior to gelation, which appears to have been a significant problem in previous attempts to use multiple dispensing needles [24].

Flow

Flow conditions in the gelation column had a major impact on microsphere coalescence, which effected monodispersity. Without oil flowing down the column, microspheres and cool stripping oil exiting the Teflon nozzles, shown in Figure 3.3, Figure 3.7, and Figure 3.8, into stagnant oil created a transitional region of flow, causing microspheres to be directed in random directions with varying velocities. Random motion of un-gelled microspheres resulted in collisions and coalescence of multiple un-gelled particles into larger spheres. Increasing the temperature of oil in the gelation column was mostly ineffective, since coalescence occurred largely in the shroud of cooler stripping oil entering the column with microspheres. As oil flowed through the column, however, microspheres could be injected from the Teflon nozzle into a region of developed flow. Due to friction at the walls of the column, oil flowed fastest at the centerline, directing microspheres into a single-file line and preventing coalescence of un-gelled microspheres. Although flow conditions can be visually identified as laminar by microsphere behavior, laminar conditions were also verified by calculation of the Reynolds number, defined as [232]:

$$Re = \frac{\rho v D}{\mu}, \tag{5.4}$$

where ρ is the fluid density, v is velocity, D is the hydraulic diameter of the pipe, and μ is the fluid dynamic viscosity. Additionally, the entrance length was calculated, as defined by [232]:

$$l_e = 0.06ReD, \tag{5.5}$$

for laminar flows where Re is the Reynolds number and D is the pipe diameter. Silicone oil viscosity and density were interpolated as 0.41 g/cm-s and 0.919 g/cm^3 at 80 °C from published values at 50 °C and 100 °C [233]. Observed flow velocities in the 1.5 cm diameter column were below 3 cm/s, corresponding to Reynolds numbers less than 10 and entrance lengths less than 1 cm. Laminar flow in pipes can be expected for Reynolds numbers less than 2300 [232]. Visual perturbations observed in the top of the column where oil was entering also agree with an entrance length less than a centimeter.

Bubbles

Bubble generation in hot silicone oil was a major barrier to producing monodisperse microspheres. While the rate of bubble formation was inhibited by lower oil temperatures, the decreased temperatures compromised monodispersity by increasing the time window for sphere coalescence to occur. The cause of bubbles was tracked to three possible sources. First, very small bubbles formed by oil falling through the cone mesh for microsphere collection became entrained in flow and were pumped through the system and into the column where they coalesced into larger bubbles over time. Bubble formation by cavitation was prevented by simple changes in the mesh cone geometry and oil levels. While this reduced the amount of bubbles to some extent, there was clearly an additional source. Since the remaining bubbles were observed to nucleate on hot surfaces in the jacketed gelation column, it was presumed that the oil contained a dissolved species that was able to vaporize in heated regions.

Although water evolved from spheres in the mesh cone during production runs and could have potentially vaporized in the hot column, silicone oil has a low solubility for water. It is also possible that formaldehyde formed as a reaction product in the gelation process may have reacted with hot silicone oil and evolved in the column. Silicone oil is known to undergo oxidizing reactions above 150 °C that also result in the generation of formaldehyde and water [233]. While silicone oil temperatures in the sol-gel apparatus were not expected to exceed 125 °C in any location, it is possible that silicon-formaldehyde reactions occurred at lower temperatures due to the introduction of formaldehyde by microspheres. This theory is further supported by the observation that bubbles are not generated in the column under operating conditions until after microsphere production has taken place for more than 20-30 minutes, allowing time for significant quantities of microspheres to accumulate and release formaldehyde. Additionally, a strong odor reminiscent of formaldehyde was present in the sphere collecting device during runs and had to be vented to a fume hood during operation.

Another possibility is that chilled silicone oil used for stripping microspheres from the needle dissolved a significant quantity of nitrogen gas used to provide an overpressure up to 15-20 psi. Silicone oil also has an increased solubility for air, nitrogen, and carbon dioxide compared to other oils [233], and it is possible that dissolved nitrogen gas escaped upon reaching a lower pressure region. Since efforts to mitigate the source of bubbles were relatively ineffective, periodic degassing using an ultrasonic bath proved to be a simple, non-intrusive solution to the problem.

Conclusion:

1) **Monodispersity was improved by eliminating causes of microsphere coalescence. Laminar flow through the gelation column and bubble removal by periodic oil degassing prevented turbulent conditions that led to coalescence.**

5.4.2 Design of a Droplet Dispersing Device

Based on the results of preliminary experiments with manual drop formation using cerous nitrate feeds, sol-gel equipment was designed and installed to automate microsphere production from ceric ammonium nitrate feeds. Automated sphere forming devices led to significant improvements in microsphere production. Two-fluid nozzles with a variety of needles and configurations were tested to limit needle clogging and allow for longer production runs. Aside from increasing yields from a handful of spheres to 0.5-2 g per batch, improved dispersion devices resulted in microspheres with diameters nearer to desired values. These batches of gelled spheres were used to test washing techniques and their impact on microspheres after drying and heat treatment steps. However, the batch yield, size distribution, and tendency to crack upon heating were unacceptable and required additional modifications to equipment and procedures.

Considering the degree of monodispersity desired in small microspheres, development of sphere forming devices was focused on two-fluid nozzles. In each of the devices tested, a continuous, laminar flow of silicone oil was used to strip microspheres from the tip of a needle in a coaxial configuration, as shown in Figure 3.8. Initial experiments with this arrangement agreed with previous, unrelated research in the field of microfluidics [202] indicating that excellent control over the particle size could be expected by variation of the flow rates of the silicone oil and mixed feed. However, limitations of the two-fluid nozzle device given the constraints of the

internal gelation process became readily apparent. While the apparatus had to seal tightly around the needle to prevent silicone oil leakage, needle replacement had to be accommodated without requiring the end of a production run. Also, long needles were desired to allow laminar flow of silicone oil to develop prior to reaching the needle tip. Long needles also allowed for alignment of the needle into the center of the narrow stripping region away from the sidewalls. However, geometries allowing for these conditions to be met made it difficult to cool the needle adequately. Keeping the long, narrow needle chilled in close proximity to hot oil in the gelation column was particularly challenging. While the Swagelok dispersion device pictured in Figure 3.3 resulted in monodisperse microspheres and was conductive for cooling, it required complete disassembly for needle replacement and was impractical. Next generation designs using Teflon and glass, shown in Figure 3.7, also resulted in monodisperse spheres but could not be adequately chilled. Based on the significant improvement seen in needle lifetime upon use of half-inch needles in the aluminum-Telfon device pictured in Figure 3.8, it is presumed that the narrow needle stem is the most vulnerable to premature gelling and that direct chilling of the needle shaft is necessary at the desired flow rates in this study. Reduction of the needle length from two inches to a half inch and closely surrounding it with a chilled aluminum block greatly reduced needle clogging.

Although advancements in needle lifetimes during the current study were adequate for the present analysis, additional improvements will likely be necessary for future work with radioactive material in a glovebox. Needle clogging has been linked to unwashed needles containing foreign objects, feed gelling in the needle due to overheating, and blockages from chunks of hardened feed released from within the system due to poor cleaning between runs. Aside from improved cleaning of needles and lines, simple modifications could be made to the

sphere forming apparatus design to further reduce the occurrence of clogging and needle replacement. The most significant improvements would be realized by direct integration of the cooling loop with the aluminum sphere forming device and by improved chilling of the stripping oil. To a lesser extent, additional gains may be achieved by minimizing the length of feed transfer lines and use of replaceable tubing to limit the likelihood of particulates in the lines causing a needle blockage. Alternatively, more extensive, automated line washing procedures could be adopted at the end of each run.

Conclusion:

1) **Development of a chill-able two-fluid nozzle provided for fine control of microsphere size while avoiding clogging caused by feed gelling in the needle.**

5.4.3 Optimization of Microsphere Washing Techniques

Early attempts to use acetone or isopropyl alcohol to remove silicone oil from spheres were met with failure, causing microsphere cracking and residual silicone impurities. Acetone appeared to cause microsphere failure, likely since it was used on soft microspheres produced from cerous nitrate. While isopropyl alcohol was able to disperse clusters of microspheres made from ceric ammonium nitrate, its limited solubility for silicone oil prevented complete removal. Severe cracking and even hollow microspheres, due to extensive volatile emissions, resulted when inadequate silicone oil removal prevented impurity extraction during ammonium hydroxide washes. Further, residual silicone oil decomposition during heat treatments above 450 °C leaves behind SiO_2 impurities [233] that are not removed during subsequent heating due to the high SiO_2 melting point above 1600 °C. Studies of Pu-238 fuel compatibility with DOP-26

alloy iridium claddings have indicated that elevated silicon impurities contribute to plutonium vaporization out of the clad vent set and vent plugging [66]. Additionally, silicon released from the fuel has been shown to form Ir-Si-Pu intermetallics near the vent that can contribute to iridium grain growth, crack initiation, and potentially compromise the cladding's impact ductility [66,68]. Eventually, trichloroethylene was used due to its increased solubility with silicone oil and was found to remove silicone oil effectively. TCE was also recovered by distillation and reused without issue. Approximately 5-10mL of silicone oil waste remained after distillation of approximately 0.5 L TCE wash effluent. Although other solvents may also prove effective at removing silicone oil [234], reclamation of TCE by distillation and waste volume reduction could be beneficial for work with plutonium.

Isopropyl alcohol was found to be a useful addition to baseline washing procedures. The best silicone oil removal was achieved by first washing with TCE to remove the bulk of silicone oil followed by washes with a 50% TCE, 50% IPA cosolvent. Since water and TCE are immiscible, gelled microspheres formed clumps in pure TCE due to their wetness, which prevented complete TCE penetration and silicone oil removal. The cosolvent allowed for a small degree of water solubility, which dispersed microspheres and allowed for complete silicone oil removal. Since similar problems with microsphere clumping were encountered during ammonium hydroxide washes due to residual, immiscible TCE, washes with 50% IPA, 50% 0.5 M ammonium hydroxide allowed for complete TCE removal prior to 100% 0.5 M ammonium hydroxide washes. With the immiscible TCE boundary removed from spheres, impurity leaching was expected to improve.

Conclusion:

1) **Effective silicone oil removal and microsphere dispersion were accomplished using trichloroethylene/isopropyl alcohol cosolvents and isopropyl alcohol/ammonium hydroxide solutions to remove immiscible barriers.**

5.4.4 Effect of Microsphere Curing Time in Hot Oil

Baseline processes for uranium oxide microsphere preparation by internal gelation include a 20-30 minute aging step in hot TCE or hot silicone oil to allow for crystallite growth [42,43,188,192]. An experiment was conducted to assess the necessity of an aging step for gelled cerium oxide microspheres and determine if aging times as long as several hours might cause cracking by reducing impurity leaching, as evidenced by removal of conductive impurities. Results comparing the conductivity of wash effluents from gelled cerium samples aged from 0-240 minutes in 85 °C silicone oil indicated that no significant changes in impurity leaching occurred for samples aged 20-240 minutes, as shown in Figure 4.13. Since microspheres sit in heated silicone oil from the time they are gelled until the end of a run, this result suggests that impurity removal from any particular microsphere will not be a function of when that sphere was formed in the run. Therefore, large batches of microspheres produced over a span of several hours are anticipated to have the same impurity leaching behavior during ammonium hydroxide washes so long as the whole batch is aged in hot silicone oil for 20-30 minutes after a run to allow microspheres produced near the end of the run to age. With regard to cerium leaching, inductively coupled mass spectroscopy of ammonium hydroxide wash effluents reported cerium concentrations below 10 ppm, which implies minimal leaching occurred for aged microspheres produced at elevated gelation temperatures. Observations that un-aged microspheres had higher wash effluent conductivities suggest that an aging step allows complete gelation of microspheres

and prevents erosion upon washing. Although un-aged spheres could have leached a larger fraction of impurities, it is believed that they were slightly eroded during the wash. Therefore, an aging step of 20-30 minutes initially developed to cure uranium oxide microspheres formed in hot TCE appears to also be a valuable processing step for cerium oxide microspheres formed in hot silicone oil. Further, since no evidence for decreased conductive impurity leaching was observed for long aging times in either the first or second ammonium hydroxide wash, an increased rate of cracking for long aging times was neither expected nor observed.

Conclusion:

1) **Leaching of conductive impurities from microspheres was unaffected by microsphere aging times in hot silicone oil longer than 30 minutes, allowing microspheres to remain submerged in hot silicone oil during production runs.**

5.4.5 Gelation and Preliminary Sphere Forming Experiments with Cerous Nitrate

Gelation Trials

None of the cerous nitrate gelation trials produced a mixed feed solution that was stable for longer than five minutes. Some early experiments using cerous nitrate mixed feed solutions lasted longer than five minutes, but opaque, reacted material was dispensed from needles into the column. Since a color change in the solution was observed to precede solution hardening, cerous nitrate feed solutions would require very short sphere production runs or else risk gelling and blocking feed transfer lines. Due to the throughput required and instability of cerous nitrate mixed feed solutions, ceric ammonium nitrate solutions were assessed.

During cerous nitrate gelation trials, the time until solutions became cloudy was found to rise as R values increased, as shown in Figure 4.1. This was somewhat unexpected, since higher R values typically result in less stable solutions that gel more quickly upon heating. Mixed feed solutions were not heated, however, and did not react immediately upon addition of the HMTA/urea solution. While the difference in sample volumes could have had an impact on the trend observed, it is also possible that there are other tradeoffs occurring between urea/Ce^{3+} and HMTA/Ce^{3+} ratios. Due to the unsatisfactory nature of all attempts to make microspheres from cerous nitrate, the issue was not investigated further.

Previous attempts to produce cerium oxide microspheres by internal gelation at Texas A&M University used cerous nitrate feed solutions exclusively. Results with cerous nitrate in the current experiments were similar to those observed in the Texas A&M study. In those studies, a variety of R values and gelation conditions were tested. High-quality microspheres were not produced by those efforts, likely due to the choice of cerous nitrate as the feed solution. Soft, gelled microspheres produced from cerous nitrate tended to erode in the washing solutions and form irregular spheres [199], likely due to incomplete gelation at insufficient pH. Cerium in the +3 oxidation state precipitates at a pH of 8.1 in a nitrate solution [200]. It is presumed that hydrolysis reactions in mixed feed droplets were incomplete and additional precipitation and solidification took place during high pH ammonium hydroxide washes. Since soft microspheres resulted despite processing at higher temperatures and longer aging times in hot oil, weak gels were attributed to incomplete hydrolysis rather than insufficient temperatures. Cerium(IV) in ceric ammonium nitrate feed solutions, which precipitates at a pH of 2.65 in nitrate solutions, yielded strong, fully gelled spheres at the same column temperatures. Since hydrated UO_3

precipitates from uranyl nitrate in the pH range 3.3-4.0 [187], it appears that precipitation at lower pH values is preferential for strong gels.

Preliminary Sphere Forming Experiments

Although ceric ammonium nitrate proved to be the superior feed solution for internal gelation processing, initial experiments using cerous nitrate provided insights into key variables in the internal gelation process and helped inform sol-gel rig design. Important lessons included:

1) Using small needles to produce microspheres with desirable diameters increases the risk of needle clogging.
2) Despite the added complexity, chilling feed solutions, transfer lines, and needles is necessary to avoid clogging.
3) High oil temperatures are required in the forming column to promote rapid gelation of chilled mixed feed droplets with short residence times.
4) Complete gelation and solidification of microspheres is necessary to prevent erosion during washing steps that remove silicone oil and impurities.

Experiments using 20 and 30 gauge hypodermic needles illustrated the tradeoffs between needle size, microsphere size, and the potential for needle clogging. As was discussed in previous sections, microsphere diameters from traditional droplet formations techniques based on the breakup of jets are approximately twice that of the inner diameter of the needle. For a 100 μm sintered sphere and assuming 250% diameter reduction from the initial droplet, this would correspond to a needle inner diameter of 125 μm, or approximately a 31 gauge needle. To avoid

clogging in such a narrow orifice, droplet dispersion techniques allowing for larger needles was desirable. Based on this observation, designs using a two-fluid nozzle discussed in section 5.4.2 allowed for larger needles to be used for small microsphere production. Due to relatively slow feed flow rates, however, extensive chilling of mixed feed transfer lines and the sphere dispersion device was necessary.

While determining the impact of oil temperature in the forming column, it was observed that all spheres changed from transparent to opaque in the column, but only spheres formed in oil at a temperature of 100 °C or above were solid upon recovery. This suggests that the thermally-induced gelation reaction required elevated temperatures for a minimum of several seconds to reach completion. Results from cerous nitrate gelation trials supports this observation since samples took 15-80 seconds to become completely white after initially turning cloudy, suggesting that the reaction was ongoing. Also, during ceric ammonium nitrate gelation trials, mixed feed solutions with the lowest acid deficiencies and R values changed color without ever solidifying. Ceric ammonium nitrate mixed feed solutions had progressively shorter periods between color change and solidification as the acid deficiency and R value increased. Based on these results, it is clear that microspheres with different feed parameters require corresponding unique minimum residence times in the heated gelation column to ensure the gelation reaction has an opportunity to proceed to completion.

Conclusions:

1) **Gelation studies were consistent with the two previously published attempts to fabricate cerium oxide spheres by internal gelation. Cerous nitrate produced soft gels that were undesirable, likely due to incomplete hydrolysis reactions. Desirable**

gels from ceric ammonium nitrate feed were attributed to a lower pH value for precipitation of Ce(IV) in nitrate solutions.

2) **The likelihood of needle clogging increases as its diameter decreases and the temperature of mixed feed solutions increase.**

Chapter 6

Conclusions

"Those who do not know history's mistakes are doomed to repeat them."

- George Santayana, American philosopher

1) **Dust generation during microsphere processing was eliminated by pressurized water treatments of gelled microspheres. Hydrothermal treatments prevented microsphere cracking by removing volatile impurities and developing an open pore network.**

2) **Techniques and equipment were developed to produce microspheres with controlled diameters from 65-211 µm. The best known monodispersities for internal gelation microspheres in this size range were achieved.**

3) **A new, quantitative method was developed for optimizing R values and acid deficiencies. Changes in pH provide a quantitative indicator of reaction completion compared to previous, subjective assessments of gel rigidity and color.**

4) **A combination of pressurized water treatments and sintering in air resulted in impurity levels well below published limits for plutonium-238 oxide fuels.**

5) **Improved washing processes with pressurized water treatments were developed that prevented microsphere agglomeration upon sintering. Spheres made using new processes were free-flowing after heat treatments, solving the existing problem of processing strong agglomerates into fuels.**

6) **Using a trichloroethylene/isopropyl alcohol cosolvent for silicone oil removal and an isopropyl alcohol/ammonium hydroxide solution for subsequent trichloroethylene removal improved microsphere dispersion during washing steps.**

7) **Pressurized water treatments allowed air-dried microspheres to be heated to lower temperatures for volatile impurity removal prior to additional processing by removing carbon and nitrogen-bearing impurities from gelled microspheres prior to drying.**

8) **Microsphere coalescence was effectively reduced by introducing laminar flow in the gelation column and by preventing bubble formation by periodic silicone oil degassing. Minimization of un-gelled microsphere coalescence resulted in the best monodispersities while operating in the dripping regime.**

9) **Use of larger gauge needles and faster stripping oil flow rates accomplished the production of microspheres with final diameters near 100 µm with fewer incidences of needle clogging.**

10) **Chilling the stripping oil, two-fluid nozzle, and feed transfer line was necessary to fabricate monodisperse microspheres with diameters less than 200 µm, but has not been reported for other internal gelation systems in the literature.**

Chapter 7

Future Work

"The problem with the future is that it keeps turning into the present."

- Bill Watterson, *Calvin and Hobbes*

At the outset of this thesis, the author's goal was to produce cerium oxide microspheres to help answer three questions regarding the internal gelation process posed by a committee of experts who evaluated dust-free alternative processing options for plutonium-238 pellets. This committee found that while ball-milled Pu-238 oxide powders have caused numerous worker exposures and contaminated facilities, sol-gel routes to pellet production could be an attractive, dust-free alternative. However, questions of sol-gel particle sizes, chemical purity, and excess sinterability were called into question. Current work with cerium oxide has shown that the desired sizes can be produced, purity requirements can be met, and that pressurized water treatments modify microsphere properties such that they do not produce fines or strongly agglomerate during heat treatments. Using microspheres produced by newly developed methods in this study, additional steps remain to be completed to determine optimal microsphere heat treatments to achieve the desired final pellet microstructures. The internal gelation process must

also be demonstrated with plutonium. It is the author's hope that this thesis will both motivate and serve as a baseline for such future work.

Based on findings in the present work that microspheres of the desired size can be fabricated with low impurity levels and minimal dust generation, future work is proposed in two principle areas prior to demonstration efforts with plutonium-238. First, additional work with cerium oxide surrogates to produce microsphere-based pellets and increase daily microsphere yields is necessary. Based on the results of cerium oxide pellet production and scale-up studies, additional work with plutonium-239 surrogates can be considered. For plutonium-239, an approach similar to that taken with cerium in this thesis is recommended.

Additional research into pellet production from microspheres and the development of a sol-gel rig for increased throughput inside of a glovebox would benefit from preliminary investigations using cerium oxide surrogates to minimize costs and simplify modifications to equipment and procedures. A detailed analysis of microsphere-pellet microstructures is recommended as a function of both microsphere thermal seasoning and hot pressing conditions to identify desirable parameters as a baseline for future plutonium work. In this effort, microspheres heated to a single temperature prior to pressing could be tested alongside the traditional process of blending low-fired and high-fired particles. Additionally, pressed pellets could be heated for prolonged periods at elevated temperatures to simulate storage or operation conditions to determine the stability of the pellet microstructure. If the desired pellet microstructures are not produced, modifications to mixed feed solution concentrations and gelation parameters could be revisited in an attempt to modify the starting microstructures of air-dried microspheres. For initial pelletization studies, reduced-scale pellets could be fabricated from 1-10 g of microspheres to limit the quantity of microspheres required. Full scale, crack-

free pellets must also be demonstrated, however, which will likely require scaling up microsphere production rates. Depending on the time, money, and glovebox space available, a decision can be made between using multiple gelation columns with single dispensing needles, or developing a single column with a new two-fluid nozzle system that accommodates multiple needles. Once satisfactory pellets have been produced from cerium oxide microspheres and increased throughputs have been achieved, investigations with plutonium-239 would be merited.

Similar to research efforts to produce cerium oxide microspheres in this thesis, future development of internal gelation plutonium oxide microspheres must demonstrate stable feed solutions, solid gelled microspheres with minimal leaching during washing operations, and dust-free processing prior to pellet pressing studies. If possible, initial experiments with Pu-238 solutions to determine the maximum theoretical feed solution concentration would be useful to inform research efforts with surrogate Pu-239. An initial knowledge of the anticipated plutonium concentration in feed solutions would allow for processes to be developed from the beginning considering that particular constraint. Gelation trials similar to those described for cerous nitrate and ceric ammonium nitrate are recommended to determine the optimal plutonium valence state and the need for stabilizers as well as desirable R values and acid deficiencies. Once solid microspheres are produced that exhibit minimal plutonium leaching during washes, additional trials will be necessary to determine whether hydrothermal treatments adequately prevent dust generation. Similar to the cerium oxide work proposed, reduced-size pellets could be used for pelletization studies prior to full-scale pellet demonstration.

After development of the internal gelation process with plutonium surrogates, additional process development will still be necessary for plutonium-238 due to the effects of radiolysis and self-heating. However, if an initial plutonium-238 concentration and valence stabilization

experiment is performed prior to plutonium-239 work, it is presumed that some of the necessary process and equipment modifications can be accommodated with surrogate work. The goal of full-scale Pu-238 oxide pellet production from sol-gel microspheres should be to produce pellets that are the most similar to those made by baseline processes in an attempt to prevent the need for fuel requalification testing. However, if the latter cannot be avoided, it is recommended to generate new qualification criteria based on pellet properties rather than an accepted process. Additional process development is also encouraged for neptunium-237 for the recycle of target materials that also contain plutonium-238 and fission product impurities that were not extracted. Incorporation of neptunium and plutonium sol-gel processing into shielded glove box equipment is expected to simplify operations and prevent powder contamination of hot cell facilities.

Appendix A

Chemicals used in the production of sol-gel microspheres

Chemical:	Structural Formula:	Molecular Formula:	Molar Mass: [g/mol]
Deionized Water	H_2O	H_2O	18.0153
Cerous Nitrate Hexahydrate	$Ce(NO_3)_3 \cdot 6H_2O$	$H_{12}N_3CeO_{15}$	434.2264
Ceric Ammonium Nitrate (CAN)	$(NH_4)_2Ce(NO_3)_6$	$H_8N_8CeO_{18}$	548.2263
Hexamethylenetetramine (HMTA)	$(CH_2)_6N_4$	$C_6H_{12}N_4$	140.1881
Urea	$CO(NH_2)_2$	CH_4N_2O	60.0556
Ammonium Hydroxide	NH_4OH	H_5NO	35.0458
Nitric Acid*	HNO_3	NHO_3	63.0128
Polydimethylsiloxane (Silicone Oil)	$[(CH_3)_2SiO]_n$	$[C_2H_6OSi]_n$	---
Trichloroethylene (TCE)	C_2HCl_3	C_2HCl_3	131.3880
Carbon tetrachloride**	CCl_4	CCl_4	153.8218
GenTech (90% n-propyl bromide)**	$CH_3(CH_2)_2Br$	C_3H_7Br	122.9926
Hexane**	$CH_3(CH_2)_4CH_3$	C_6H_{14}	86.1772
Isopropyl Alcohol (IPA)	$(CH_3)_2CHOH$	C_3H_8O	60.0959
Acetone	$(CH_3)_2CO$	C_3H_6O	58.0800
Ethylene Glycol	$OH(CH_2)_2OH$	$C_2H_6O_2$	62.0684

*Used 70 wt% (15.7 M) nitric acid

**Evaluated as substitutes to TCE for silicone oil removal

Reagent:	Supplier:	Purity: [%]	Quantity: [g]	Lot #
Cerous Nitrate	Sigma Aldrich	99.0	500	MKBH0612V
Cerous Nitrate	Sigma Aldrich	99.99	100	MKBF8706V
Ceric Ammonium Nitrate	Sigma Aldrich	99.99	50	05118JD
Ceric Ammonium Nitrate	Sigma Aldrich	99.99	50	MKBL5098V
Ceric Ammonium Nitrate	Acros Organics	99.5	1000	A0331425
Cerium Dioxide	Sigma Aldrich	99.9	100	MKBF2924V
HMTA	Alfa Aesar	99+	1000	10149148
HMTA	Sigma Aldrich	>99.5	500	SZBA2210V
HMTA	Sigma Aldrich	>99.5	1000	SZBB2510V
Urea	J.T. Baker	99.7	1000	J41628
Urea	Sigma Aldrich	>99.5	500	BCBD7141V

Appendix B

Calculation of Cerium Dioxide Theoretical Density

CeO_2
Space group: Fm-3m
Atomic positions: Ce at 0, 0, 0
Atomic positions: O at 0.25, 0.25, 0.25
Unit cell dimensions: a = 5.41 Å
Cerium molar mass: 140.116 g/mol
Oxygen molar mass: 15.9994 g/mol

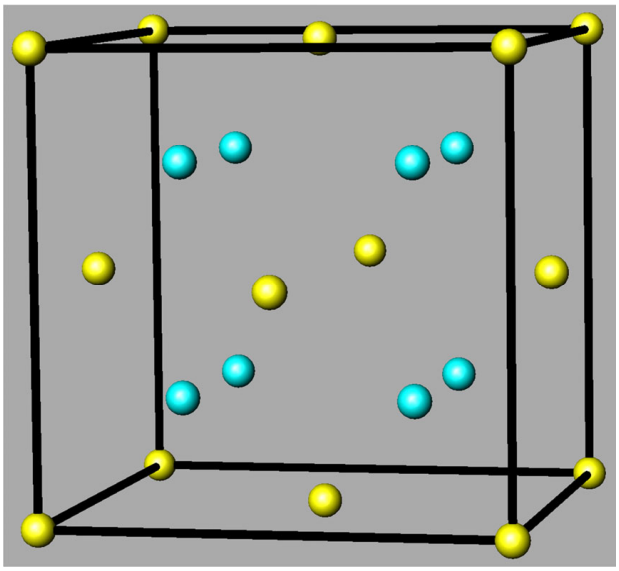

Figure B.1: Model of cerium dioxide structure made with the Atoms program. Cerium is shown in yellow and oxygen in blue.

$$\frac{(4)(140.116)}{(6.022*10^{23})} + \frac{(8)(15.9994)}{(6.022*10^{23})} = 1.1432 * 10^{-21} \text{g/unit cell}$$

$$(5.41 * 10^{-8})^3 = 1.5834 * 10^{-22} \text{ cc/unit cell}$$

$$\frac{1.1432*10^{-21}}{1.5834*10^{-22}} = 7.220 \text{ g/cc}$$

Theoretical density = 7.22 g/cc

Appendix C

Preparation of Uranyl Nitrate from Uranium Oxide

During the course of sol-gel work, laboratory standard operating procedures were developed for preparing concentrated solutions of acid-deficient uranyl nitrate. Depleted uranium oxide powder (0.25-0.3 wt% U-235) with a mixture of U_3O_8 and UO_2 oxidation states was obtained from International Bio-Analytical Industries, Inc. Experiments measuring the change in sample mass due to oxygen pickup upon heating indicated that the stock oxide powder was approximately 50% UO_2, 50% U_3O_8 by mass and that heating at 600 °C for two hours allowed for full conversion to U_3O_8. Conversion to a known oxidation state was necessary to gain an accurate knowledge of the uranium concentration in solutions prepared from powders. Incomplete oxygen pickup occurred in powders heated in a full beaker whereas powders loaded a quarter-inch deep on a tray had complete conversion, shown in Figure C.1, as evidenced by mass measurements and the color of solutions formed upon dissolution in nitric acid. Yellow solutions were indicative of U_3O_8 whereas green solutions indicated the presence of UO_2 as shown in Figure C.2. Dissolution of oxide powder in a substoichiometric quantity of concentrated nitric acid took several days but was accelerated by heating at 60 °C.

Figure C.1: Uranium oxide powder was heated at 600 °C for two hours for conversion to U_3O_8.

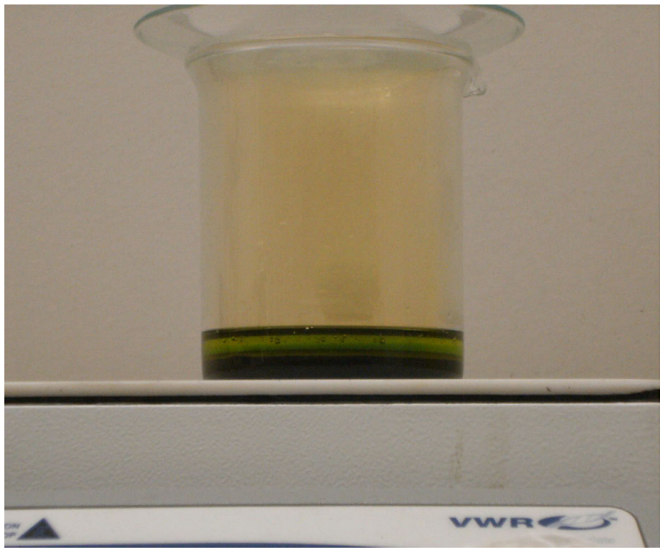

Figure C.2: Incomplete conversion of UO_2 to U_3O_8 due to heating geometry in a box furnace was evidenced by the presence of a green solution upon dissolution in nitric acid.

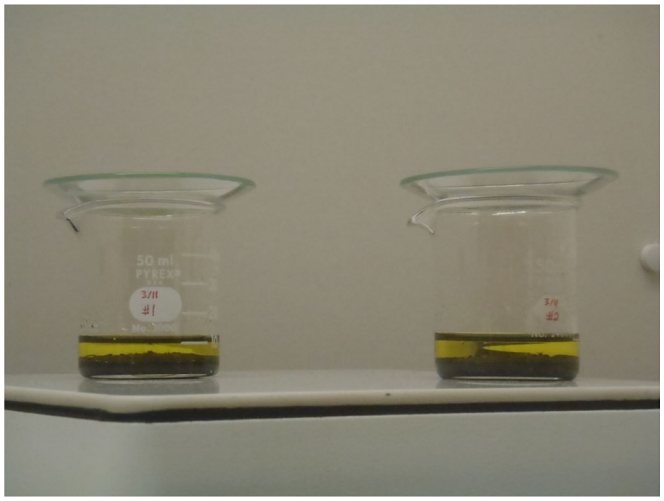

Figure C.3: Uranium oxide dissolved in a substoichiometric amount of 70% nitric acid occurred over the course of several days.

After dissolution, an insoluble fraction remained, visible in Figure C.4, that had to be filtered out using filter paper. As shown in Figure C.5 and Figure C.6, the filter paper removed particulates but also absorbed the uranyl nitrate solution and required extensive rinsing for removal. Rinsing steps diluted the uranyl nitrate solution and required heating at 60 °C to evolve the excess water. For sol-gel procedures, samples would have been reduced to the required volume to achieve the desired uranium concentration in the solution. Experiments were also performed to measure the solution density and pH to verify the degree of acid deficiency.

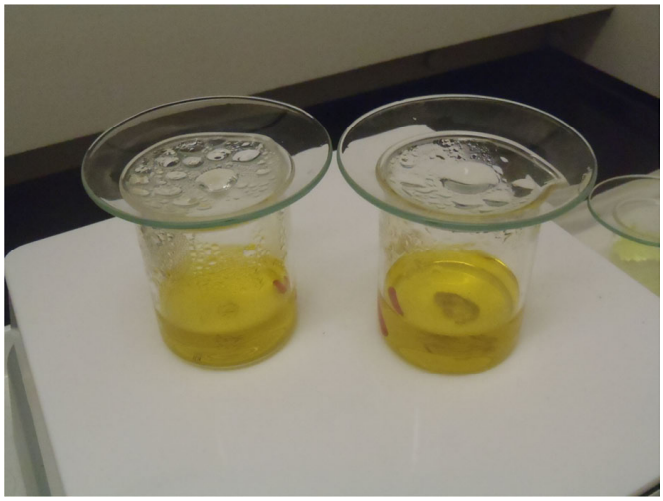

Figure C.4: After dissolution of the bulk of oxide powders, a small insoluble fraction remained that was removed by filtration.

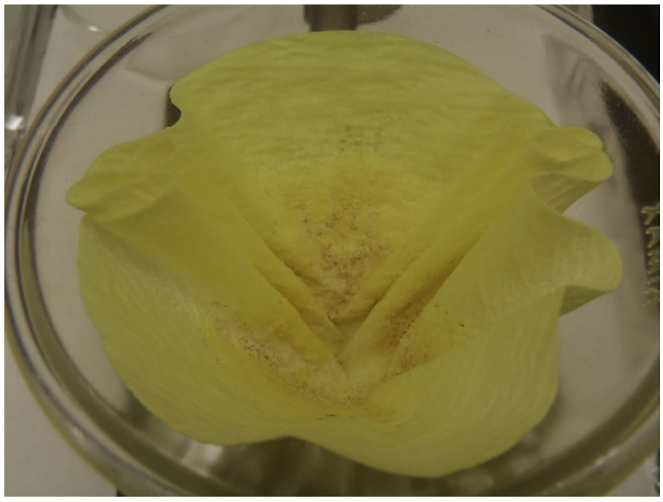

Figure C.5: Filter paper had to be rinsed with large volumes of deionized water to remove all the uranyl nitrate. The resulting excess volume of water in uranyl nitrate was evolved by heating near 60 °C.

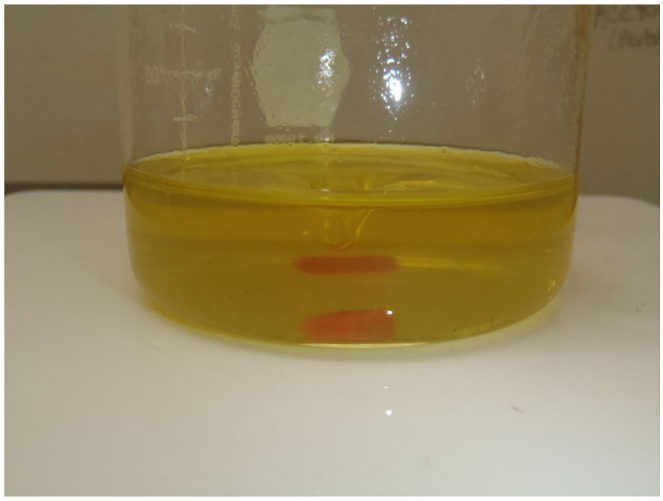

Figure C.6: Acid-deficient uranyl nitrate was golden yellow in color.

With feed solution preparation established, standard operating procedures for the recycle of excess solutions or uranium waste were also considered. Additionally, the preparation of uranyl nitrate hexahydrate as a starting material was assessed. Uranyl nitrate solutions were dried to produce crystals, as shown in Figure C.7 and Figure C.8. However, due to an inability to determine the hydration state of the crystals, and thus the uranium concentration per unit mass, uranyl nitrate was an unacceptable starting material for feed preparation. Dried uranyl nitrate was heated to 300 °C to produce UO_3, shown in Figure C.9, and heated to 600 °C to convert back to U_3O_8 for recycle.

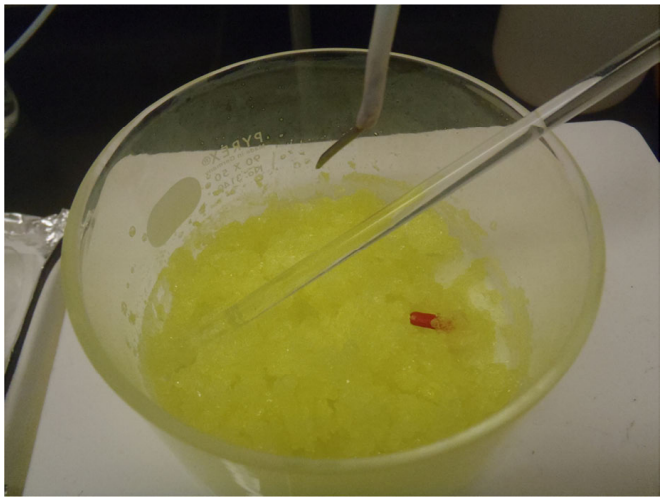

Figure C.7: Dehydration of uranyl nitrate resulted in the formation of yellow crystals presumed to be uranyl nitrate hexahydrate.

Figure C.8: Dehydration of uranyl nitrate crystals above lithium chloride in a desiccator led to a substance with constant mass, but an uncertain hydration state.

Figure C.9: Heating of dried uranyl nitrate to 300 °C for two hours is believed to have resulted in conversion to UO_3, as evidenced by the orange coloration.

Appendix D

Flow Meter Calibration

Stripping oil flow rates were correlated to voltage output signals from a Sensirion SLQ-HC60 flow meter. Volumes of chilled stripping oil were collected in graduated cylinders and timed using a stopwatch. Measurements were performed in duplicate and excellent agreement within 2% was observed with all points except the lowest voltage, which agreed within 6%.

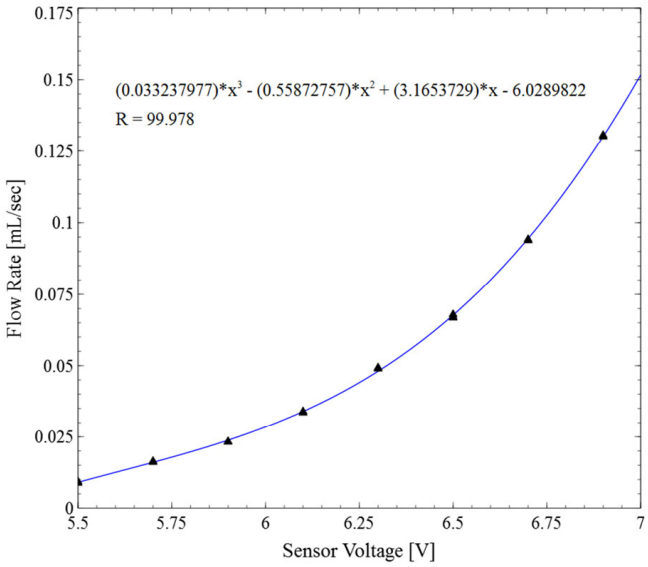

Figure D.1: A calibration curve was generated for flow rates of 0.5 - 9 mL/min.

Table D. 1: A calibration curve was generated from a range of voltages with a step size of 0.2 V. Data points were measured in duplicate to ensure good consistency.

Sensor Voltage [V]	Collected Volume [mL]:	Collection Time [sec]:	Rate [mL/sec]:
5.5	10	1138	0.00879
5.5	10	1076	0.00929
5.7	15	912	0.01645
5.7	16	995	0.01608
5.9	25	1072	0.02332
5.9	21	906	0.02318
6.1	30	896	0.03348
6.1	32	942	0.03397
6.3	50	1023	0.04888
6.3	42	852	0.04930
6.5	70	1043	0.06711
6.5	65	957	0.06792
6.5	60	899	0.06674
6.7	90	955	0.09424
6.7	85	906	0.09382
6.9	120	923	0.13001
6.9	120	919	0.13058

Appendix E

Sphere Sizing Data

Shape factors and mean radii are reported for microspheres measured using contrast-based sizing software with 26, 28, and 32 gauge needles and stripping oil flow rates of 1.5, 4.0, and 6.5 mL/min.

Table F.1: Microspheres were analyzed to determine shape factors and mean radii as a function of needle size and stripping oil flow rate.

Shape Factor	Mean Radius [µm]	Needle Gauge	Oil Flow Rate [mL/min]	Shape Factor	Mean Radius [µm]	Needle Gauge	Oil Flow Rate [mL/min]	Shape Factor	Mean Radius [µm]	Needle Gauge	Oil Flow Rate [mL/min]	Shape Factor	Mean Radius [µm]	Needle Gauge	Oil Flow Rate [mL/min]
0.83	106	26	1.5	0.92	49.1	28	4	0.85	80.1	32	1.5	0.92	33.9	32	6.5
0.88	111	26	1.5	0.94	49.4	28	4	0.87	79.1	32	1.5	0.95	32.4	32	6.5
0.83	108	26	1.5	0.93	48.7	28	4	0.87	78.2	32	1.5	0.93	34.2	32	6.5
0.9	105	26	1.5	0.93	48.8	28	4	0.91	76.3	32	1.5	0.94	32.8	32	6.5
0.9	104	26	1.5	0.94	49.9	28	4	0.86	82.6	32	1.5	0.95	31.4	32	6.5
0.85	106	26	1.5	0.95	49.2	28	4	0.84	78.8	32	1.5	0.94	34.1	32	6.5
0.91	107	26	1.5	0.91	49.1	28	4	0.89	76.5	32	1.5	0.94	33	32	6.5
0.91	104	26	1.5	0.91	48.4	28	4	0.91	78.1	32	1.5	0.94	33.2	32	6.5
0.9	104	26	1.5	0.93	49.8	28	4	0.89	87.3	32	1.5	0.93	34.7	32	6.5
0.84	111	26	1.5	0.93	49.5	28	4	0.92	78.5	32	1.5	0.92	35.9	32	6.5
0.83	101	26	1.5	0.93	49.4	28	4	0.83	79.9	32	1.5	0.95	37.7	32	6.5
0.87	104	26	1.5	0.93	49.4	28	4	0.89	78.7	32	1.5	0.94	33.1	32	6.5
0.9	104	26	1.5	0.93	49.7	28	4	0.92	77.1	32	1.5	0.93	32	32	6.5
0.9	108	26	1.5	0.94	49.5	28	4	0.86	79.9	32	1.5	0.97	33.7	32	6.5
0.88	104	26	1.5	0.93	50.5	28	4	0.84	80	32	1.5	0.94	32.3	32	6.5
0.9	105	26	1.5	0.91	52.5	28	4	0.89	79	32	1.5	0.93	32.8	32	6.5
0.85	106	26	1.5	0.91	49.3	28	4	0.84	78	32	1.5	0.94	34.8	32	6.5
0.89	104	26	1.5	0.93	49.6	28	4	0.91	78.5	32	1.5	0.96	32.3	32	6.5
0.91	105	26	1.5	0.92	49.8	28	4	0.9	78.9	32	1.5	0.94	33.4	32	6.5
0.9	103	26	1.5	0.92	50.4	28	4	0.9	78.3	32	1.5	0.95	34	32	6.5
0.88	107	26	1.5	0.92	49.5	28	4	0.87	79.4	32	1.5	0.95	33.3	32	6.5
0.83	107	26	1.5	0.93	50	28	4	0.92	78.8	32	1.5	0.95	33.9	32	6.5
0.9	104	26	1.5	0.91	49.3	28	4	0.9	79.8	32	1.5	0.94	35.5	32	6.5
0.91	104	26	1.5	0.93	50	28	4	0.87	79.4	32	1.5	0.93	36.4	32	6.5
0.91	103	26	1.5	0.9	49.3	28	4	0.9	77.5	32	1.5	0.93	31.7	32	6.5
0.9	105	26	1.5	0.92	50.1	28	4	0.88	78.8	32	1.5	0.94	35.9	32	6.5
0.91	105	26	1.5	0.91	52	28	4	0.92	79.4	32	1.5	0.94	30.6	32	6.5
0.9	105	26	1.5	0.89	50.4	28	4	0.92	77.6	32	1.5	0.93	32.2	32	6.5
0.91	105	26	1.5	0.92	50.2	28	4	0.84	79.3	32	1.5	0.93	33.6	32	6.5
0.9	104	26	1.5	0.89	50.3	28	4	0.92	77.6	32	1.5	0.95	35.1	32	6.5
0.89	110	26	1.5	0.92	50.5	28	4	0.89	78.1	32	1.5	0.92	36.7	32	6.5
0.9	105	26	1.5	0.88	50.8	28	4	0.9	80.6	32	1.5	0.94	33.2	32	6.5
0.88	108	26	1.5	0.9	50.3	28	4	0.91	77.8	32	1.5	0.95	34	32	6.5
0.83	109	26	1.5	0.93	50.4	28	4	0.89	78.2	32	1.5	0.94	33.2	32	6.5
0.9	104	26	1.5	0.92	50.2	28	4	0.91	77.4	32	1.5	0.96	32.4	32	6.5
0.9	106	26	1.5	0.93	48.4	28	4	0.85	78.8	32	1.5	0.95	32.8	32	6.5
0.89	104	26	1.5	0.92	49.4	28	4	0.91	78.9	32	1.5	0.93	34.3	32	6.5
0.89	104	26	1.5	0.93	50.6	28	4	0.88	79.1	32	1.5	0.96	31.3	32	6.5
0.89	110	26	1.5	0.93	49.9	28	4	0.91	78	32	1.5	0.92	37.4	32	6.5

0.88	103	26	1.5	0.88	47.8	28	4	0.9	78.3	32	1.5	0.94	31.3	32	6.5
0.86	104	26	1.5	0.93	49.2	28	4	0.9	76.5	32	1.5	0.93	36	32	6.5
0.88	110	26	1.5	0.95	48.7	28	4	0.9	79.2	32	1.5	0.95	32.3	32	6.5
0.91	104	26	1.5	0.93	48.6	28	4	0.88	79.4	32	1.5	0.93	32.8	32	6.5
0.91	114	26	1.5	0.91	49.9	28	4	0.88	80.1	32	1.5	0.95	33.4	32	6.5
0.9	106	26	1.5	0.9	50.6	28	4	0.92	77.6	32	1.5	0.94	32.3	32	6.5
0.91	106	26	1.5	0.93	53.4	28	4	0.84	80.2	32	1.5	0.94	33	32	6.5
0.9	106	26	1.5	0.92	50.2	28	4	0.9	79.7	32	1.5	0.95	31.6	32	6.5
0.9	104	26	1.5	0.93	51.4	28	4	0.87	81.6	32	1.5	0.92	34.1	32	6.5
0.9	106	26	1.5	0.93	49.7	28	4	0.91	79.5	32	1.5	0.95	33	32	6.5
0.83	107	26	1.5	0.93	49.1	28	4	0.92	79.6	32	1.5	0.96	34.2	32	6.5
0.9	104	26	1.5	0.93	49.9	28	4	0.87	79.6	32	1.5	0.94	31.9	32	6.5
0.91	104	26	1.5	0.92	48.9	28	4	0.89	78.5	32	1.5	0.94	31.9	32	6.5
0.91	104	26	1.5	0.92	50.1	28	4	0.86	80	32	1.5	0.95	33.2	32	6.5
0.9	105	26	1.5	0.94	49.8	28	4	0.89	79.5	32	1.5	0.95	33	32	6.5
0.91	104	26	1.5	0.94	49.1	28	4	0.81	79	32	1.5	0.92	32.5	32	6.5
0.9	106	26	1.5	0.89	51.1	28	4	0.89	80	32	1.5	0.95	34	32	6.5
0.9	105	26	1.5	0.92	49.2	28	4	0.92	79.6	32	1.5	0.94	33	32	6.5
0.87	113	26	1.5	0.88	50.9	28	4	0.85	85.8	32	1.5	0.96	32.8	32	6.5
0.86	109	26	1.5	0.89	51.7	28	4	0.84	82.8	32	1.5	0.95	30.4	32	6.5
0.91	105	26	1.5	0.91	50.2	28	4	0.91	78.8	32	1.5	0.92	32.7	32	6.5
0.91	106	26	1.5	0.91	50.1	28	4	0.92	76.6	32	1.5	0.93	35	32	6.5
0.89	104	26	1.5	0.89	50.5	28	4	0.9	78.9	32	1.5	0.95	32.4	32	6.5
0.89	102	26	1.5	0.92	49.1	28	4	0.87	89.8	32	1.5	0.93	32.6	32	6.5
0.89	102	26	1.5	0.94	49.7	28	4	0.83	84.1	32	1.5	0.94	34.2	32	6.5
0.87	106	26	1.5	0.9	49.9	28	4	0.86	79.2	32	1.5	0.94	31.4	32	6.5
0.87	108	26	1.5	0.89	49.2	28	4	0.91	78.2	32	1.5	0.94	31.2	32	6.5
0.88	107	26	1.5	0.93	49.8	28	4	0.91	77.8	32	1.5	0.94	32.9	32	6.5
0.86	105	26	1.5	0.93	50.3	28	4	0.9	78.1	32	1.5	0.94	33.2	32	6.5
0.9	107	26	1.5	0.94	50.1	28	4	0.82	83.2	32	1.5	0.93	31.5	32	6.5
0.91	104	26	1.5	0.94	49	28	4	0.82	78.3	32	1.5	0.97	31.8	32	6.5
0.91	103	26	1.5	0.92	50.6	28	4	0.9	78.1	32	1.5	0.96	32.5	32	6.5
0.91	105	26	1.5	0.93	50	28	4	0.86	81.8	32	1.5	0.95	31.3	32	6.5
0.92	106	26	1.5	0.9	51.6	28	4	0.92	78	32	1.5	0.94	33.4	32	6.5
0.84	108	26	1.5	0.89	51.2	28	4	0.92	75.1	32	1.5	0.92	35.6	32	6.5
0.89	104	26	1.5	0.94	51	28	4	0.87	85.8	32	1.5	0.95	33.1	32	6.5
0.89	106	26	1.5	0.93	47.9	28	4	0.86	81.3	32	1.5	0.95	32.8	32	6.5
0.91	104	26	1.5	0.92	48.5	28	4	0.91	77.8	32	1.5	0.94	33.9	32	6.5
0.84	106	26	1.5	0.92	49.4	28	4	0.85	86.8	32	1.5	0.92	33.9	32	6.5
0.91	103	26	1.5	0.94	49.2	28	4	0.85	82.6	32	1.5	0.94	32.2	32	6.5
0.86	109	26	1.5	0.91	51.2	28	4	0.86	82.6	32	1.5	0.95	34	32	6.5
0.88	110	26	1.5	0.91	50.2	28	4	0.92	78.5	32	1.5	0.93	31.9	32	6.5
0.88	106	26	1.5	0.9	49.8	28	4	0.89	78.9	32	1.5	0.95	31.8	32	6.5
0.9	105	26	1.5	0.9	50.5	28	4	0.91	76.2	32	1.5	0.92	32.7	32	6.5
0.83	109	26	1.5	0.92	49.2	28	4	0.89	80	32	1.5	0.94	32.5	32	6.5
0.9	106	26	1.5	0.93	49.1	28	4	0.89	78.9	32	1.5	0.95	32	32	6.5
0.89	105	26	1.5	0.92	51.9	28	4	0.92	78.5	32	1.5	0.92	32.7	32	6.5
0.85	113	26	1.5	0.94	49.2	28	4	0.89	80.4	32	1.5	0.94	32.7	32	6.5
0.89	110	26	1.5	0.92	49.3	28	4	0.9	83	32	1.5	0.95	32.2	32	6.5
0.83	109	26	1.5	0.92	49.8	28	4	0.91	76.9	32	1.5	0.94	32.5	32	6.5
0.87	108	26	1.5	0.91	49.5	28	4	0.92	78.7	32	1.5	0.95	32.7	32	6.5
0.89	104	26	1.5	0.95	49.2	28	4	0.91	78.7	32	1.5	0.93	32.5	32	6.5
0.9	105	26	1.5	0.93	49.2	28	4	0.9	77.4	32	1.5	0.92	33.8	32	6.5
0.9	108	26	1.5	0.92	50.2	28	4	0.92	78.6	32	1.5	0.94	33.5	32	6.5
0.86	104	26	1.5	0.93	49.8	28	4	0.91	79	32	1.5	0.95	32.8	32	6.5
0.91	105	26	1.5	0.89	54.7	28	4	0.9	78.4	32	1.5	0.94	32.1	32	6.5
0.91	103	26	1.5	0.91	53.9	28	4	0.92	78.3	32	1.5	0.95	32.6	32	6.5
0.87	108	26	1.5	0.93	50.2	28	4	0.91	77.7	32	1.5	0.93	32.4	32	6.5
0.88	107	26	1.5	0.93	50.4	28	4	0.86	78.5	32	1.5	0.96	33.1	32	6.5
0.89	104	26	1.5	0.93	51.8	28	4	0.91	77.7	32	1.5	0.93	32	32	6.5
0.9	105	26	1.5	0.95	49.5	28	4	0.86	81.2	32	1.5	0.94	33.2	32	6.5
0.9	107	26	1.5	0.92	48.7	28	4	0.9	79.7	32	1.5	0.92	33.3	32	6.5
0.91	104	26	1.5	0.91	49.3	28	4	0.87	79.6	32	1.5	0.94	33.6	32	6.5
0.89	110	26	1.5	0.9	53.1	28	4	0.92	76.6	32	1.5	0.93	33.4	32	6.5
0.91	105	26	1.5	0.93	50	28	4	0.9	78.3	32	1.5	0.94	34.3	32	6.5
0.92	104	26	1.5	0.92	50.6	28	4	0.87	79	32	1.5	0.95	33.7	32	6.5
0.92	104	26	1.5	0.92	49.8	28	4	0.88	78.6	32	1.5	0.93	33.9	32	6.5
0.91	105	26	1.5	0.92	50.9	28	4	0.91	78.2	32	1.5	0.94	33	32	6.5
0.86	106	26	1.5	0.92	50.3	28	4	0.91	78	32	1.5	0.93	31.9	32	6.5
0.91	105	26	1.5	0.93	49.4	28	4	0.9	77.8	32	1.5	0.92	33.5	32	6.5
0.84	107	26	1.5	0.93	49.7	28	4	0.92	78.7	32	1.5	0.94	32.6	32	6.5
0.88	115	26	1.5	0.92	49.1	28	4	0.91	79.8	32	1.5	0.94	33.7	32	6.5
0.91	107	26	1.5	0.93	50.4	28	4	0.91	77	32	1.5	0.93	32.8	32	6.5
0.91	103	26	1.5	0.92	50.3	28	4	0.82	80.7	32	1.5	0.93	33.5	32	6.5
0.89	106	26	1.5	0.94	51.5	28	4	0.89	79	32	1.5	0.94	33.9	32	6.5

0.9	104	26	1.5	0.89	49.9	28	4	0.87	78.3	32	1.5	0.93	30.7	32	6.5
0.88	106	26	1.5	0.9	54.5	28	4	0.92	79.6	32	1.5	0.94	31.7	32	6.5
0.9	105	26	1.5	0.9	49.7	28	4	0.83	78.8	32	1.5	0.96	32.4	32	6.5
0.89	108	26	1.5	0.94	49.6	28	4	0.86	82.8	32	1.5	0.93	33.1	32	6.5
0.91	104	26	1.5	0.91	51.8	28	4	0.85	84.2	32	1.5	0.95	33.7	32	6.5
0.89	109	26	1.5	0.92	51.2	28	4	0.89	78.9	32	1.5	0.92	32.8	32	6.5
0.91	105	26	1.5	0.92	51.9	28	4	0.9	78.2	32	1.5	0.95	33.1	32	6.5
0.86	103	26	1.5	0.93	51.5	28	4	0.91	78.9	32	1.5	0.96	33.4	32	6.5
0.91	103	26	1.5	0.92	50.5	28	4	0.91	79	32	1.5	0.95	33.1	32	6.5
0.83	109	26	1.5	0.93	51.2	28	4	0.91	78.9	32	1.5	0.93	33.6	32	6.5
0.85	104	26	1.5	0.92	52.1	28	4	0.9	79.3	32	1.5	0.95	31.6	32	6.5
0.86	106	26	1.5	0.92	48.9	28	4	0.91	78.7	32	1.5	0.95	33.1	32	6.5
0.9	106	26	1.5	0.93	48.4	28	4	0.91	78.3	32	1.5	0.93	30.5	32	6.5
0.84	108	26	1.5	0.93	52.3	28	4	0.86	79.9	32	1.5	0.93	31.4	32	6.5
0.9	106	26	1.5	0.93	50.3	28	4	0.91	78.9	32	1.5	0.93	32.8	32	6.5
0.91	108	26	1.5	0.93	49.1	28	4	0.86	82	32	1.5	0.94	31.6	32	6.5
0.91	106	26	1.5	0.94	51.1	28	4	0.82	80.2	32	1.5	0.93	33.2	32	6.5
0.91	106	26	1.5	0.95	49.8	28	4	0.83	79.4	32	1.5	0.96	32.6	32	6.5
0.83	104	26	1.5	0.91	51	28	4	0.89	78.4	32	1.5	0.96	33.3	32	6.5
0.92	106	26	1.5	0.92	49.2	28	4					0.95	33.2	32	6.5
0.88	104	26	1.5	0.91	55	28	4	0.94	49.9	32	4	0.92	31.7	32	6.5
0.9	104	26	1.5	0.93	48.7	28	4	0.91	48.6	32	4	0.95	29.8	32	6.5
0.91	106	26	1.5	0.94	49.2	28	4	0.89	48.5	32	4	0.94	32.8	32	6.5
0.85	104	26	1.5	0.93	49.6	28	4	0.93	47	32	4	0.95	32	32	6.5
0.91	106	26	1.5	0.93	49.4	28	4	0.92	49.9	32	4	0.93	33.4	32	6.5
0.88	110	26	1.5	0.92	49.6	28	4	0.91	50	32	4	0.95	30.6	32	6.5
0.89	107	26	1.5	0.93	49.6	28	4	0.91	49.7	32	4	0.93	32.3	32	6.5
0.9	104	26	1.5	0.92	49.8	28	4	0.93	49.6	32	4	0.94	33.2	32	6.5
0.84	107	26	1.5	0.88	54.4	28	4	0.93	48.3	32	4	0.94	30.9	32	6.5
0.91	106	26	1.5	0.92	50.9	28	4	0.91	50.8	32	4	0.92	34	32	6.5
0.89	110	26	1.5	0.93	49.6	28	4	0.93	56.8	32	4	0.96	31.9	32	6.5
0.89	104	26	1.5	0.92	50.2	28	4	0.88	50	32	4	0.95	32.7	32	6.5
0.91	104	26	1.5	0.93	49.8	28	4	0.87	42.6	32	4	0.97	33.3	32	6.5
0.9	106	26	1.5	0.91	51	28	4	0.89	50.8	32	4	0.94	32.2	32	6.5
0.89	108	26	1.5	0.94	50	28	4	0.91	51.2	32	4	0.94	31.4	32	6.5
0.87	105	26	1.5	0.92	50.6	28	4	0.92	53.9	32	4	0.93	33.6	32	6.5
0.91	102	26	1.5	0.91	49.7	28	4	0.89	50.1	32	4	0.92	32.9	32	6.5
0.88	104	26	1.5	0.93	50.3	28	4	0.91	50.2	32	4	0.94	33.5	32	6.5
0.9	107	26	1.5	0.91	49.4	28	4	0.89	54.1	32	4	0.93	31.9	32	6.5
0.91	105	26	1.5	0.93	51.5	28	4	0.93	50.6	32	4	0.93	31.4	32	6.5
0.91	104	26	1.5	0.93	49.2	28	4	0.92	49.6	32	4	0.95	31.4	32	6.5
0.9	106	26	1.5	0.91	51.8	28	4	0.91	50.2	32	4	0.93	32.8	32	6.5
0.91	105	26	1.5	0.9	50.8	28	4	0.92	49.4	32	4	0.93	33	32	6.5
0.91	105	26	1.5	0.93	49.6	28	4	0.91	49.8	32	4	0.93	33.7	32	6.5
0.9	106	26	1.5	0.9	49.3	28	4	0.92	50	32	4	0.96	32.6	32	6.5
0.91	105	26	1.5	0.93	49.1	28	4	0.94	53.4	32	4	0.93	33.1	32	6.5
0.91	106	26	1.5	0.92	54.2	28	4	0.92	51.1	32	4	0.96	31.2	32	6.5
0.91	105	26	1.5	0.93	49.4	28	4	0.93	47.4	32	4	0.94	33.7	32	6.5
0.91	103	26	1.5	0.94	50	28	4	0.87	44.2	32	4	0.93	32.7	32	6.5
0.9	104	26	1.5	0.88	49.7	28	4	0.92	48.9	32	4	0.94	33.1	32	6.5
0.87	112	26	1.5	0.92	50.7	28	4	0.94	50.9	32	4	0.94	32.2	32	6.5
0.88	107	26	1.5	0.9	54.6	28	4	0.93	49.6	32	4	0.93	31.9	32	6.5
0.89	105	26	1.5	0.92	49.4	28	4	0.91	52.9	32	4	0.93	33.2	32	6.5
0.91	106	26	1.5	0.93	49.4	28	4	0.9	50.4	32	4	0.95	33	32	6.5
0.91	105	26	1.5	0.93	50	28	4	0.91	47.9	32	4	0.94	31.4	32	6.5
0.87	107	26	1.5	0.94	50.4	28	4	0.91	45.5	32	4	0.95	32.8	32	6.5
0.87	110	26	1.5	0.93	51	28	4	0.9	51	32	4	0.95	32.3	32	6.5
0.83	111	26	1.5	0.89	52.7	28	4	0.92	49.7	32	4	0.95	32.5	32	6.5
0.87	104	26	1.5	0.93	50.5	28	4	0.88	59.1	32	4	0.94	30	32	6.5
0.87	108	26	1.5					0.92	50.7	32	4	0.95	32.2	32	6.5
0.91	106	26	1.5	0.9	34.7	28	6.5	0.93	48.8	32	4	0.94	32.7	32	6.5
0.89	109	26	1.5	0.95	35.7	28	6.5	0.92	50.7	32	4	0.93	32.4	32	6.5
0.91	103	26	1.5	0.94	37.3	28	6.5	0.93	47.9	32	4	0.94	31.4	32	6.5
0.91	105	26	1.5	0.94	36.5	28	6.5	0.9	44.4	32	4	0.96	32.2	32	6.5
0.88	105	26	1.5	0.95	36	28	6.5	0.93	48.8	32	4	0.94	33.7	32	6.5
0.86	107	26	1.5	0.94	36	28	6.5	0.94	50.6	32	4	0.92	32.7	32	6.5
0.91	105	26	1.5	0.96	35.7	28	6.5	0.91	50.7	32	4	0.95	33.5	32	6.5
0.91	107	26	1.5	0.94	35.6	28	6.5	0.92	52.1	32	4	0.96	31.5	32	6.5
0.92	103	26	1.5	0.93	36.1	28	6.5	0.93	46.9	32	4	0.93	34.6	32	6.5
0.91	105	26	1.5	0.91	37.2	28	6.5	0.93	50.9	32	4	0.94	31.7	32	6.5
0.85	108	26	1.5	0.95	36.5	28	6.5	0.89	43.5	32	4	0.95	32.7	32	6.5
0.9	105	26	1.5	0.95	37.1	28	6.5	0.94	48.2	32	4	0.96	33.3	32	6.5
0.91	104	26	1.5	0.92	38.7	28	6.5	0.92	53.8	32	4	0.96	33.1	32	6.5
0.87	116	26	1.5	0.93	29.7	28	6.5	0.92	48.4	32	4	0.93	32.2	32	6.5
0.91	104	26	1.5	0.94	36.6	28	6.5	0.93	49.2	32	4	0.94	32.5	32	6.5

0.9	105	26	1.5	0.92	36.9	28	6.5	0.92	49.8	32	4	0.95	32.5	32	6.5
0.89	107	26	1.5	0.94	35.2	28	6.5	0.88	52.7	32	4	0.96	33.7	32	6.5
0.91	107	26	1.5	0.95	34.3	28	6.5	0.93	50.3	32	4	0.94	33.3	32	6.5
0.87	104	26	1.5	0.93	36.9	28	6.5	0.92	52.1	32	4	0.97	33.2	32	6.5
0.88	104	26	1.5	0.95	34.8	28	6.5	0.93	49.8	32	4	0.93	33.7	32	6.5
0.84	105	26	1.5	0.93	36.4	28	6.5	0.87	52.2	32	4	0.92	32.6	32	6.5
0.87	110	26	1.5	0.92	36.2	28	6.5	0.94	51.1	32	4	0.95	32.8	32	6.5
0.91	104	26	1.5	0.92	36.9	28	6.5	0.91	50	32	4	0.93	30.2	32	6.5
0.89	105	26	1.5	0.94	38.6	28	6.5	0.93	50	32	4	0.94	33.1	32	6.5
0.89	114	26	1.5	0.93	39.6	28	6.5	0.91	49.7	32	4	0.95	32.5	32	6.5
0.9	101	26	1.5	0.93	36.7	28	6.5	0.91	55.6	32	4	0.92	31.2	32	6.5
0.9	104	26	1.5	0.95	34.7	28	6.5	0.94	50.2	32	4	0.94	32.8	32	6.5
0.91	105	26	1.5	0.94	36.3	28	6.5	0.92	51	32	4	0.95	31.3	32	6.5
0.91	104	26	1.5	0.95	36.8	28	6.5	0.93	51	32	4	0.93	33.2	32	6.5
0.91	109	26	1.5	0.92	38.9	28	6.5	0.92	51.2	32	4	0.93	29.2	32	6.5
0.91	105	26	1.5	0.94	36.3	28	6.5	0.92	51	32	4	0.94	33.2	32	6.5
0.83	108	26	1.5	0.93	35.4	28	6.5	0.92	50.1	32	4	0.95	33.6	32	6.5
0.9	104	26	1.5	0.93	36.2	28	6.5	0.93	49.2	32	4	0.95	33.7	32	6.5
0.91	104	26	1.5	0.93	30	28	6.5	0.94	46.6	32	4	0.94	31.5	32	6.5
0.88	105	26	1.5	0.96	34.4	28	6.5	0.87	56.1	32	4	0.93	32.3	32	6.5
0.88	104	26	1.5	0.92	39	28	6.5	0.93	49.7	32	4	0.96	33.4	32	6.5
0.91	104	26	1.5	0.96	32.9	28	6.5	0.91	49.5	32	4	0.94	32.8	32	6.5
0.91	106	26	1.5	0.94	36.4	28	6.5	0.94	51.3	32	4	0.96	33	32	6.5
0.88	108	26	1.5	0.94	35.8	28	6.5	0.89	54	32	4	0.95	33.4	32	6.5
0.84	108	26	1.5	0.92	36.7	28	6.5	0.91	49.4	32	4	0.94	32.5	32	6.5
0.91	102	26	1.5	0.92	35.5	28	6.5	0.92	50.3	32	4	0.94	33.6	32	6.5
0.9	106	26	1.5	0.94	37.7	28	6.5	0.91	49.2	32	4	0.94	33.1	32	6.5
0.9	105	26	1.5	0.94	36.2	28	6.5	0.94	47.9	32	4	0.94	30.8	32	6.5
0.88	105	26	1.5	0.9	39.7	28	6.5	0.91	50.9	32	4	0.95	34.4	32	6.5
0.9	103	26	1.5	0.91	35.4	28	6.5	0.88	56.7	32	4	0.92	33.8	32	6.5
0.9	107	26	1.5	0.91	31.3	28	6.5	0.93	50.6	32	4	0.93	32.2	32	6.5
0.9	105	26	1.5	0.91	37.5	28	6.5	0.92	50	32	4	0.95	33.1	32	6.5
0.91	107	26	1.5	0.93	37.9	28	6.5	0.92	47.9	32	4	0.93	32.5	32	6.5
0.89	109	26	1.5	0.89	37.5	28	6.5	0.92	52.4	32	4	0.96	31.2	32	6.5
0.82	107	26	1.5	0.92	38.2	28	6.5	0.92	49.6	32	4	0.92	34.9	32	6.5
0.9	105	26	1.5	0.89	38.7	28	6.5	0.93	49.6	32	4	0.93	34.6	32	6.5
0.82	105	26	1.5	0.89	40.3	28	6.5	0.92	50.1	32	4	0.94	33.4	32	6.5
0.9	105	26	1.5	0.95	35.9	28	6.5	0.92	50.3	32	4	0.94	35.1	32	6.5
0.9	104	26	1.5	0.95	32	28	6.5	0.92	46.9	32	4	0.94	33.8	32	6.5
0.88	109	26	1.5	0.95	36.4	28	6.5	0.91	49.3	32	4	0.93	33.8	32	6.5
0.91	103	26	1.5	0.96	32.9	28	6.5	0.93	46.9	32	4	0.94	30.9	32	6.5
0.89	108	26	1.5	0.92	36.5	28	6.5	0.94	48.5	32	4	0.94	33	32	6.5
0.87	107	26	1.5	0.9	35.7	28	6.5	0.93	51.2	32	4	0.92	31.7	32	6.5
0.88	109	26	1.5	0.94	34.6	28	6.5	0.92	51.1	32	4	0.95	33.2	32	6.5
0.9	104	26	1.5	0.92	36.2	28	6.5	0.92	47.6	32	4	0.94	33.3	32	6.5
0.9	103	26	1.5	0.94	36.7	28	6.5	0.88	52.6	32	4	0.95	33.2	32	6.5
0.9	106	26	1.5	0.91	38.2	28	6.5	0.95	48.7	32	4	0.92	32.6	32	6.5
0.9	105	26	1.5	0.87	38.9	28	6.5	0.91	51	32	4	0.93	34.4	32	6.5
0.91	105	26	1.5	0.95	36.3	28	6.5	0.93	51	32	4	0.95	30.9	32	6.5
0.89	106	26	1.5	0.92	37.9	28	6.5	0.94	48.8	32	4	0.93	33.7	32	6.5
0.91	104	26	1.5	0.91	38.5	28	6.5	0.9	51.2	32	4	0.95	33.4	32	6.5
0.88	104	26	1.5	0.94	38.3	28	6.5	0.92	49.9	32	4	0.93	33.2	32	6.5
0.91	106	26	1.5	0.91	34	28	6.5	0.92	51.4	32	4	0.93	31.9	32	6.5
0.91	103	26	1.5	0.93	36.2	28	6.5	0.92	51.5	32	4	0.93	33.7	32	6.5
0.9	103	26	1.5	0.95	39	28	6.5	0.94	51	32	4	0.94	31.5	32	6.5
0.91	107	26	1.5	0.93	36.4	28	6.5	0.93	49.1	32	4	0.94	34.2	32	6.5
0.9	104	26	1.5	0.91	39.1	28	6.5	0.91	48.8	32	4	0.92	34.4	32	6.5
0.91	101	26	1.5	0.95	35.7	28	6.5	0.92	52.5	32	4	0.94	33	32	6.5
0.85	110	26	1.5	0.96	36.1	28	6.5	0.9	50.2	32	4	0.94	33.6	32	6.5
0.91	104	26	1.5	0.94	36.6	28	6.5	0.92	52.8	32	4	0.94	33.1	32	6.5
0.89	106	26	1.5	0.9	41.5	28	6.5	0.92	50.7	32	4	0.94	32.6	32	6.5
0.9	107	26	1.5	0.93	38.2	28	6.5	0.93	49.5	32	4	0.93	33	32	6.5
0.89	107	26	1.5	0.87	39	28	6.5	0.93	51.9	32	4	0.94	33	32	6.5
0.89	107	26	1.5	0.93	39.3	28	6.5	0.93	49.9	32	4	0.96	31.7	32	6.5
0.88	105	26	1.5	0.95	36.5	28	6.5	0.93	48.9	32	4	0.93	33	32	6.5
0.87	106	26	1.5	0.94	37.7	28	6.5	0.91	51.7	32	4	0.96	33.2	32	6.5
0.91	103	26	1.5	0.94	37.3	28	6.5	0.91	51.3	32	4	0.93	32.2	32	6.5
0.91	104	26	1.5	0.93	37.4	28	6.5	0.89	53.9	32	4	0.92	33.2	32	6.5
0.89	106	26	1.5	0.93	32	28	6.5	0.94	49.5	32	4	0.93	34.1	32	6.5
0.91	106	26	1.5	0.91	29.3	28	6.5	0.92	49.4	32	4	0.95	32.8	32	6.5
0.91	104	26	1.5	0.93	40.3	28	6.5	0.93	50.3	32	4	0.93	32.8	32	6.5
0.91	98.4	26	1.5	0.94	39.8	28	6.5	0.91	48.8	32	4	0.95	31.5	32	6.5
0.91	104	26	1.5	0.93	38.3	28	6.5	0.92	50.5	32	4	0.94	34.1	32	6.5
0.91	104	26	1.5	0.93	34.6	28	6.5	0.94	51	32	4	0.97	33	32	6.5
0.91	104	26	1.5	0.92	35.9	28	6.5	0.93	50.5	32	4	0.93	31.1	32	6.5

0.91	106	26	1.5	0.94	35.9	28	6.5	0.93	50.8	32	4	0.95	34	32	6.5
0.9	107	26	1.5	0.9	34.8	28	6.5	0.92	49.8	32	4	0.95	34.1	32	6.5
0.91	106	26	1.5	0.9	33.6	28	6.5	0.92	50.8	32	4	0.95	32.8	32	6.5
0.82	108	26	1.5	0.89	37	28	6.5	0.9	50.3	32	4	0.94	33.1	32	6.5
0.9	104	26	1.5	0.92	35.8	28	6.5	0.92	49.3	32	4	0.93	29.7	32	6.5
0.9	106	26	1.5	0.9	39.5	28	6.5	0.94	52	32	4	0.93	32.8	32	6.5
0.88	112	26	1.5	0.94	35.2	28	6.5	0.86	47.7	32	4	0.96	33.8	32	6.5
0.91	103	26	1.5	0.94	36.7	28	6.5	0.93	51.1	32	4	0.93	32.5	32	6.5
0.91	105	26	1.5	0.93	35.4	28	6.5	0.94	49.9	32	4	0.93	33.7	32	6.5
0.86	104	26	1.5	0.92	39.6	28	6.5	0.92	50.4	32	4	0.92	32.7	32	6.5
0.92	104	26	1.5	0.9	37	28	6.5	0.89	54.4	32	4	0.95	32.4	32	6.5
0.91	106	26	1.5	0.93	35.8	28	6.5	0.93	52	32	4	0.96	33.1	32	6.5
0.88	104	26	1.5	0.95	36.1	28	6.5	0.93	49.2	32	4	0.95	32.2	32	6.5
0.83	104	26	1.5	0.9	39	28	6.5	0.93	55	32	4	0.95	33	32	6.5
0.9	108	26	1.5	0.94	35.7	28	6.5	0.93	49.1	32	4	0.93	32.1	32	6.5
0.91	104	26	1.5	0.93	36.7	28	6.5	0.92	50.8	32	4	0.95	32.2	32	6.5
0.9	104	26	1.5	0.94	36.5	28	6.5	0.93	50.5	32	4	0.96	31.8	32	6.5
0.9	105	26	1.5	0.91	34.5	28	6.5	0.93	48.8	32	4	0.93	33.5	32	6.5
0.91	108	26	1.5	0.9	35.7	28	6.5	0.91	48.8	32	4	0.93	33.8	32	6.5
0.9	105	26	1.5	0.92	34.7	28	6.5	0.91	51.2	32	4	0.94	31.8	32	6.5
0.9	107	26	1.5	0.94	38.1	28	6.5	0.92	51.3	32	4	0.93	33.6	32	6.5
0.9	106	26	1.5	0.96	35.8	28	6.5	0.87	51.8	32	4	0.94	32.1	32	6.5
0.87	108	26	1.5	0.93	37.3	28	6.5	0.91	51.1	32	4	0.95	33	32	6.5
0.88	105	26	1.5	0.93	35.8	28	6.5	0.9	51	32	4	0.95	32.9	32	6.5
0.89	106	26	1.5	0.93	35.1	28	6.5	0.94	51.6	32	4	0.93	32.4	32	6.5
0.9	106	26	1.5	0.9	37.2	28	6.5	0.91	50.1	32	4	0.95	32.6	32	6.5
0.88	108	26	1.5	0.93	35.4	28	6.5	0.92	49.9	32	4	0.95	32.1	32	6.5
0.9	106	26	1.5	0.95	34.9	28	6.5	0.92	52.4	32	4	0.94	33.4	32	6.5
0.86	108	26	1.5	0.93	35.4	28	6.5	0.93	51.5	32	4	0.94	35.1	32	6.5
0.88	102	26	1.5	0.95	36.5	28	6.5	0.89	50.7	32	4	0.94	33.8	32	6.5
0.83	105	26	1.5	0.93	37.2	28	6.5	0.92	51.6	32	4	0.95	35.7	32	6.5
0.9	104	26	1.5	0.92	36.2	28	6.5	0.91	46.8	32	4	0.95	33.2	32	6.5
0.9	108	26	1.5	0.91	40.5	28	6.5	0.91	51.8	32	4	0.94	31.8	32	6.5
0.88	108	26	1.5	0.92	39.2	28	6.5	0.89	50.7	32	4	0.93	32.9	32	6.5
0.83	106	26	1.5	0.94	34.8	28	6.5	0.92	50.3	32	4	0.93	33.4	32	6.5
0.88	106	26	1.5	0.94	34.4	28	6.5	0.93	50	32	4	0.95	34	32	6.5
0.91	107	26	1.5	0.93	38.9	28	6.5	0.92	49.1	32	4	0.94	33.2	32	6.5
0.86	109	26	1.5	0.94	39.4	28	6.5	0.89	51	32	4	0.93	33.7	32	6.5
0.91	103	26	1.5	0.95	35.8	28	6.5	0.93	49.9	32	4	0.92	33.3	32	6.5
0.89	110	26	1.5	0.93	38.5	28	6.5	0.93	50.1	32	4	0.94	32.3	32	6.5
0.91	105	26	1.5	0.92	37	28	6.5	0.94	49.9	32	4	0.96	33.5	32	6.5
0.91	106	26	1.5	0.94	41.1	28	6.5	0.9	51	32	4	0.96	33.3	32	6.5
0.9	107	26	1.5	0.95	34.5	28	6.5	0.87	54.7	32	4	0.94	32.1	32	6.5
0.88	105	26	1.5	0.91	34.9	28	6.5	0.9	52.5	32	4	0.93	33.2	32	6.5
0.91	107	26	1.5	0.96	32.7	28	6.5	0.91	51.6	32	4	0.95	33.4	32	6.5
0.92	103	26	1.5	0.93	37.6	28	6.5	0.91	50	32	4	0.95	34.2	32	6.5
0.9	103	26	1.5	0.92	38.4	28	6.5	0.92	51.3	32	4	0.95	32.7	32	6.5
0.88	105	26	1.5	0.93	36.7	28	6.5	0.93	49.9	32	4	0.93	32.9	32	6.5
0.91	104	26	1.5	0.93	38.5	28	6.5	0.94	51	32	4	0.95	32.7	32	6.5
0.87	104	26	1.5	0.92	34.9	28	6.5	0.92	50.7	32	4	0.93	32.7	32	6.5
0.91	103	26	1.5	0.93	36.8	28	6.5	0.93	50	32	4	0.94	32.6	32	6.5
0.91	102	26	1.5	0.92	37.1	28	6.5	0.93	52	32	4	0.92	33.3	32	6.5
0.9	105	26	1.5	0.91	38.9	28	6.5	0.92	51	32	4	0.95	33.9	32	6.5
0.91	105	26	1.5	0.93	39.4	28	6.5	0.93	50.3	32	4	0.93	32.8	32	6.5
0.92	105	26	1.5	0.93	36.7	28	6.5	0.93	50.5	32	4	0.92	34	32	6.5
0.9	105	26	1.5	0.94	35.9	28	6.5	0.9	49.1	32	4	0.92	34.2	32	6.5
0.91	105	26	1.5	0.95	39.3	28	6.5	0.91	47.9	32	4	0.94	32.5	32	6.5
0.86	106	26	1.5	0.96	36.6	28	6.5	0.92	50.4	32	4	0.93	34.1	32	6.5
0.91	106	26	1.5	0.94	36.8	28	6.5	0.9	52.1	32	4	0.93	34.4	32	6.5
0.91	104	26	1.5	0.94	34.8	28	6.5	0.94	47.8	32	4	0.93	33.8	32	6.5
0.84	107	26	1.5	0.94	36.9	28	6.5	0.91	50.3	32	4	0.92	33.5	32	6.5
0.9	107	26	1.5	0.95	36.2	28	6.5	0.92	48.2	32	4	0.93	33.4	32	6.5
0.87	106	26	1.5	0.94	35.5	28	6.5	0.91	48.4	32	4	0.95	33.3	32	6.5
0.91	104	26	1.5	0.94	36.3	28	6.5	0.9	49.3	32	4	0.95	34.1	32	6.5
0.91	104	26	1.5	0.93	33.2	28	6.5	0.93	49.3	32	4	0.94	33.5	32	6.5
0.88	105	26	1.5	0.94	36	28	6.5	0.9	51	32	4	0.93	33.7	32	6.5
0.85	106	26	1.5	0.9	32.6	28	6.5	0.91	50.2	32	4	0.93	33.1	32	6.5
0.9	107	26	1.5	0.94	36.2	28	6.5	0.94	47.7	32	4	0.94	33.5	32	6.5
0.9	104	26	1.5	0.94	35.8	28	6.5	0.92	48.8	32	4	0.94	34.1	32	6.5
0.91	106	26	1.5	0.91	36.6	28	6.5	0.92	48.3	32	4	0.96	33.5	32	6.5
0.92	105	26	1.5	0.92	39.5	28	6.5	0.91	49	32	4	0.93	34.9	32	6.5
0.91	107	26	1.5	0.94	34.7	28	6.5	0.93	51.1	32	4	0.95	33.6	32	6.5
0.91	105	26	1.5	0.95	35.6	28	6.5	0.94	49.6	32	4	0.94	28.4	32	6.5
0.82	104	26	1.5	0.92	36.7	28	6.5	0.92	50.7	32	4	0.96	33.1	32	6.5
0.85	110	26	1.5	0.93	37.5	28	6.5	0.92	50	32	4	0.92	33	32	6.5

0.89	105	26	1.5	0.93	36.3	28	6.5	0.93	52	32	4	0.94	33.5	32	6.5
0.86	108	26	1.5	0.95	35.5	28	6.5	0.93	48.5	32	4	0.94	33.4	32	6.5
0.9	107	26	1.5	0.94	35.1	28	6.5	0.92	49.6	32	4	0.95	32.9	32	6.5
0.91	103	26	1.5	0.95	37.2	28	6.5	0.93	49.9	32	4	0.93	33.9	32	6.5
0.89	104	26	1.5	0.95	35.2	28	6.5	0.92	50.3	32	4	0.92	34.4	32	6.5
0.9	109	26	1.5	0.94	36.9	28	6.5	0.92	51.8	32	4	0.94	32.1	32	6.5
0.91	105	26	1.5	0.94	37.6	28	6.5	0.93	48.5	32	4	0.93	32	32	6.5
0.88	104	26	1.5	0.89	38.2	28	6.5	0.95	47.9	32	4	0.94	33.3	32	6.5
0.88	103	26	1.5	0.91	36.8	28	6.5	0.92	50.2	32	4	0.94	33.4	32	6.5
0.91	107	26	1.5	0.94	34.1	28	6.5	0.92	49.1	32	4	0.93	36	32	6.5
0.88	112	26	1.5	0.92	38.2	28	6.5	0.94	48.9	32	4	0.95	34.5	32	6.5
0.9	107	26	1.5	0.91	31.5	28	6.5	0.93	50.8	32	4	0.95	33.1	32	6.5
0.88	103	26	1.5	0.94	35	28	6.5	0.92	51.3	32	4	0.97	32.6	32	6.5
0.89	104	26	1.5	0.87	38.9	28	6.5	0.93	47.9	32	4	0.94	33.1	32	6.5
0.91	103	26	1.5	0.94	34	28	6.5	0.92	48	32	4	0.92	33.8	32	6.5
0.91	104	26	1.5	0.93	39.7	28	6.5	0.93	49.1	32	4	0.93	33.2	32	6.5
0.9	108	26	1.5	0.92	36.2	28	6.5	0.89	57.3	32	4	0.93	33.7	32	6.5
0.91	104	26	1.5	0.95	36.7	28	6.5	0.92	49.7	32	4	0.94	33.3	32	6.5
0.91	101	26	1.5	0.95	35.8	28	6.5	0.93	49.9	32	4	0.93	33.6	32	6.5
0.87	107	26	1.5	0.88	39.8	28	6.5	0.92	49.3	32	4	0.93	33.8	32	6.5
0.85	106	26	1.5	0.93	39.6	28	6.5	0.93	49.6	32	4	0.93	33.2	32	6.5
0.9	106	26	1.5	0.92	35.6	28	6.5	0.92	49.8	32	4	0.96	32.3	32	6.5
0.9	106	26	1.5	0.94	36.6	28	6.5	0.92	48	32	4	0.94	34.3	32	6.5
0.88	105	26	1.5	0.94	35.4	28	6.5	0.89	50.8	32	4	0.92	34.3	32	6.5
0.89	107	26	1.5	0.95	36.9	28	6.5	0.91	46.6	32	4	0.96	32.5	32	6.5
0.91	104	26	1.5	0.94	37.8	28	6.5	0.88	50.5	32	4	0.95	31.2	32	6.5
0.91	104	26	1.5	0.94	35.4	28	6.5	0.94	48	32	4	0.94	34.6	32	6.5
0.91	104	26	1.5	0.92	38.5	28	6.5	0.91	50.3	32	4	0.94	32.7	32	6.5
0.91	106	26	1.5	0.92	37.9	28	6.5	0.92	49	32	4	0.93	32.9	32	6.5
0.9	109	26	1.5	0.88	34.8	28	6.5	0.92	50.5	32	4	0.95	35.5	32	6.5
0.9	106	26	1.5	0.93	36.2	28	6.5	0.92	47.1	32	4	0.94	32.7	32	6.5
0.87	105	26	1.5	0.93	36.7	28	6.5	0.87	56.5	32	4	0.93	34.1	32	6.5
0.87	107	26	1.5	0.95	35.4	28	6.5	0.93	49.8	32	4	0.92	34.6	32	6.5
0.89	108	26	1.5	0.95	35.2	28	6.5	0.88	47.8	32	4	0.95	33.1	32	6.5
0.91	102	26	1.5	0.91	34.9	28	6.5	0.92	50.1	32	4	0.94	33.7	32	6.5
0.91	104	26	1.5	0.94	35.3	28	6.5	0.92	49.9	32	4	0.93	31.1	32	6.5
0.86	108	26	1.5	0.91	37	28	6.5	0.93	48.6	32	4	0.93	31.3	32	6.5
0.88	103	26	1.5	0.94	37.6	28	6.5	0.93	48.2	32	4	0.95	34.3	32	6.5
0.9	105	26	1.5	0.93	32.8	28	6.5	0.93	47.9	32	4	0.94	33	32	6.5
0.91	102	26	1.5	0.94	36.2	28	6.5	0.93	47.5	32	4	0.93	34.3	32	6.5
0.88	106	26	1.5	0.93	35.5	28	6.5	0.93	48.5	32	4	0.96	33.1	32	6.5
0.91	103	26	1.5	0.93	35.8	28	6.5	0.86	57.5	32	4	0.93	36.2	32	6.5
0.89	104	26	1.5	0.93	35.5	28	6.5	0.94	48.3	32	4	0.93	32.9	32	6.5
0.9	103	26	1.5	0.94	35.3	28	6.5	0.91	49.9	32	4	0.95	33.4	32	6.5
0.91	106	26	1.5	0.91	30	28	6.5	0.92	49.5	32	4	0.94	33.5	32	6.5
0.91	104	26	1.5	0.93	37.3	28	6.5	0.92	51.7	32	4	0.96	33.3	32	6.5
0.86	108	26	1.5	0.94	37.3	28	6.5	0.93	47.6	32	4	0.95	32.8	32	6.5
0.92	105	26	1.5	0.96	30.9	28	6.5	0.9	52	32	4	0.94	35.8	32	6.5
0.9	105	26	1.5	0.9	35.9	28	6.5	0.91	50.2	32	4	0.95	33.5	32	6.5
0.9	106	26	1.5	0.94	37.2	28	6.5	0.93	48.6	32	4	0.95	33.6	32	6.5
0.86	105	26	1.5	0.89	36.3	28	6.5	0.93	50.1	32	4	0.92	34.8	32	6.5
0.91	104	26	1.5	0.95	35.3	28	6.5	0.9	49.9	32	4	0.93	33.8	32	6.5
0.9	104	26	1.5	0.96	36.7	28	6.5	0.91	50.2	32	4	0.92	34.1	32	6.5
0.88	106	26	1.5	0.94	36.8	28	6.5	0.88	50.6	32	4	0.94	33.7	32	6.5
0.89	105	26	1.5	0.92	36.5	28	6.5	0.91	49.7	32	4	0.93	34.3	32	6.5
0.9	112	26	1.5	0.94	39.1	28	6.5	0.88	51	32	4	0.92	33.8	32	6.5
0.91	103	26	1.5	0.93	35.7	28	6.5	0.86	54.2	32	4	0.93	33.3	32	6.5
0.89	106	26	1.5	0.92	37.8	28	6.5	0.93	48.4	32	4	0.93	33.3	32	6.5
0.85	107	26	1.5	0.92	35.9	28	6.5	0.93	54.5	32	4	0.94	33.7	32	6.5
0.91	105	26	1.5	0.92	35.2	28	6.5	0.92	48.8	32	4	0.92	33.3	32	6.5
0.87	111	26	1.5	0.91	35.4	28	6.5	0.92	50.5	32	4	0.94	34.1	32	6.5
0.9	105	26	1.5	0.93	37	28	6.5	0.93	49.5	32	4	0.95	33.9	32	6.5
0.87	104	26	1.5	0.94	36	28	6.5	0.92	49.9	32	4	0.93	33.3	32	6.5
0.9	105	26	1.5	0.92	34.8	28	6.5	0.93	51.6	32	4	0.94	32.2	32	6.5
0.84	110	26	1.5	0.92	35.1	28	6.5	0.91	49.8	32	4	0.93	31.6	32	6.5
0.9	107	26	1.5	0.92	35.2	28	6.5	0.92	48.4	32	4	0.93	31.9	32	6.5
0.85	106	26	1.5	0.92	35.9	28	6.5	0.92	48.7	32	4	0.94	34.2	32	6.5
0.84	101	26	1.5	0.94	36.5	28	6.5	0.93	49.5	32	4	0.95	34	32	6.5
0.9	103	26	1.5	0.93	36.3	28	6.5	0.92	48.2	32	4	0.94	33.1	32	6.5
0.87	105	26	1.5	0.92	35.7	28	6.5	0.9	52	32	4	0.97	31.8	32	6.5
0.9	104	26	1.5	0.93	37.2	28	6.5	0.93	48.9	32	4	0.93	33	32	6.5
0.9	105	26	1.5	0.93	38.2	28	6.5	0.93	50.6	32	4	0.94	32.3	32	6.5
0.89	104	26	1.5	0.93	37.4	28	6.5	0.92	49.9	32	4	0.95	33.4	32	6.5
0.84	114	26	1.5	0.91	36.3	28	6.5	0.93	50.3	32	4	0.96	35.3	32	6.5
0.88	105	26	1.5	0.92	34.7	28	6.5	0.93	50.2	32	4	0.95	31.8	32	6.5

0.91	103	26	1.5	0.93	35.9	28	6.5	0.92	47.8	32	4	0.93	32.7	32	6.5
0.89	104	26	1.5	0.93	34.9	28	6.5	0.93	50.1	32	4	0.95	33.7	32	6.5
0.9	105	26	1.5	0.95	35.9	28	6.5	0.95	50	32	4	0.95	33.2	32	6.5
0.88	104	26	1.5	0.92	36	28	6.5	0.92	48.5	32	4	0.95	34.6	32	6.5
0.88	108	26	1.5	0.92	37.5	28	6.5	0.94	51.7	32	4	0.94	33.2	32	6.5
0.9	104	26	1.5	0.87	30.8	28	6.5	0.92	49.3	32	4	0.97	33.6	32	6.5
0.9	106	26	1.5	0.88	39	28	6.5	0.91	50.1	32	4	0.95	32.6	32	6.5
0.92	106	26	1.5	0.96	35.5	28	6.5	0.91	50.9	32	4	0.96	33.2	32	6.5
0.88	104	26	1.5	0.89	42.9	28	6.5	0.93	49.2	32	4	0.94	33.4	32	6.5
0.9	106	26	1.5	0.93	33.9	28	6.5	0.91	46	32	4	0.94	31.8	32	6.5
0.85	106	26	1.5	0.92	36.1	28	6.5	0.92	51.7	32	4	0.94	33.5	32	6.5
0.91	103	26	1.5	0.93	35.6	28	6.5	0.92	49.5	32	4	0.93	31.5	32	6.5
0.89	104	26	1.5	0.9	34.5	28	6.5	0.93	48.8	32	4	0.93	34	32	6.5
0.91	104	26	1.5	0.93	34.9	28	6.5	0.94	49.6	32	4	0.93	34	32	6.5
0.91	107	26	1.5	0.93	35.7	28	6.5	0.92	51.1	32	4	0.95	34	32	6.5
0.92	103	26	1.5	0.94	36.9	28	6.5	0.91	49.9	32	4	0.95	29.9	32	6.5
0.91	104	26	1.5	0.89	35.9	28	6.5	0.93	52.4	32	4	0.96	32.5	32	6.5
0.9	105	26	1.5	0.9	37.1	28	6.5	0.93	50.1	32	4	0.93	33	32	6.5
0.9	106	26	1.5	0.94	35.2	28	6.5	0.88	52.4	32	4	0.94	33.3	32	6.5
0.85	108	26	1.5	0.94	37	28	6.5	0.91	49.9	32	4	0.94	34.1	32	6.5
0.91	105	26	1.5	0.92	36.9	28	6.5	0.89	56	32	4	0.95	33.6	32	6.5
0.83	108	26	1.5	0.94	37.9	28	6.5	0.93	48.9	32	4	0.94	33	32	6.5
0.9	105	26	1.5	0.91	32.6	28	6.5	0.92	48.5	32	4	0.93	33.6	32	6.5
0.89	108	26	1.5	0.93	35.7	28	6.5	0.9	49.6	32	4	0.93	33.3	32	6.5
0.91	105	26	1.5	0.88	42.7	28	6.5	0.88	49.4	32	4	0.94	36.3	32	6.5
0.91	106	26	1.5	0.91	38.4	28	6.5	0.92	47.5	32	4	0.96	32.5	32	6.5
0.9	108	26	1.5	0.93	34.8	28	6.5	0.94	49.8	32	4	0.93	33.3	32	6.5
0.84	111	26	1.5	0.91	36	28	6.5	0.93	50.7	32	4	0.93	34.5	32	6.5
0.88	107	26	1.5	0.93	35.6	28	6.5	0.92	50.6	32	4	0.95	33	32	6.5
0.91	103	26	1.5	0.93	35.9	28	6.5	0.91	50.8	32	4	0.92	34.9	32	6.5
0.91	104	26	1.5	0.92	36.1	28	6.5	0.93	50.9	32	4	0.93	34	32	6.5
0.89	109	26	1.5	0.94	36	28	6.5	0.91	46.9	32	4	0.92	31.5	32	6.5
0.9	104	26	1.5	0.92	37.3	28	6.5	0.93	46.9	32	4	0.95	32	32	6.5
0.9	104	26	1.5	0.92	36.1	28	6.5	0.92	49.3	32	4	0.96	33.7	32	6.5
0.91	99.8	26	1.5	0.96	34.9	28	6.5	0.89	45.8	32	4	0.95	32.6	32	6.5
0.85	104	26	1.5	0.94	35.7	28	6.5	0.94	48.4	32	4	0.94	34	32	6.5
0.86	107	26	1.5	0.95	34.2	28	6.5	0.92	48.5	32	4	0.95	32.6	32	6.5
0.9	101	26	1.5	0.93	35.8	28	6.5	0.93	49.8	32	4	0.94	31.9	32	6.5
0.91	103	26	1.5	0.95	33.6	28	6.5	0.93	49.9	32	4	0.93	33	32	6.5
0.89	107	26	1.5	0.92	36.8	28	6.5	0.94	50	32	4	0.93	33.3	32	6.5
0.89	105	26	1.5	0.95	38	28	6.5	0.92	48.1	32	4	0.93	31.5	32	6.5
0.87	104	26	1.5	0.96	34.5	28	6.5	0.92	52.6	32	4	0.93	32.9	32	6.5
0.85	110	26	1.5	0.9	36.8	28	6.5	0.89	50.8	32	4	0.93	31.1	32	6.5
0.89	107	26	1.5	0.96	34.8	28	6.5	0.92	48.7	32	4	0.94	33.5	32	6.5
0.9	104	26	1.5	0.9	37.6	28	6.5	0.93	50.7	32	4	0.93	32.4	32	6.5
0.84	108	26	1.5	0.94	35.9	28	6.5	0.93	49.7	32	4	0.95	33.1	32	6.5
0.9	102	26	1.5	0.92	34.3	28	6.5	0.9	51.6	32	4	0.93	32.2	32	6.5
0.87	109	26	1.5	0.95	36	28	6.5	0.89	51.5	32	4	0.94	32.9	32	6.5
0.88	104	26	1.5	0.94	38.4	28	6.5	0.92	49.6	32	4	0.93	31.8	32	6.5
0.83	106	26	1.5	0.96	34.5	28	6.5	0.93	51.2	32	4	0.97	32.8	32	6.5
0.89	104	26	1.5	0.94	37	28	6.5	0.93	49.7	32	4	0.94	32.5	32	6.5
0.87	107	26	1.5	0.93	35	28	6.5	0.92	49.5	32	4	0.94	33.1	32	6.5
0.84	107	26	1.5	0.94	35.5	28	6.5	0.92	51.1	32	4	0.94	31.6	32	6.5
0.88	107	26	1.5	0.94	33.8	28	6.5	0.92	51.1	32	4	0.94	32.2	32	6.5
0.88	104	26	1.5	0.95	34.1	28	6.5	0.91	51.4	32	4	0.94	33.7	32	6.5
0.9	103	26	1.5	0.93	37.8	28	6.5	0.91	48.9	32	4	0.93	33.2	32	6.5
0.89	103	26	1.5	0.94	34.7	28	6.5	0.93	50.3	32	4	0.95	27.3	32	6.5
0.91	105	26	1.5	0.92	34.9	28	6.5	0.93	49.4	32	4	0.95	32.2	32	6.5
0.9	107	26	1.5	0.95	35.3	28	6.5	0.91	46.8	32	4	0.94	32.9	32	6.5
0.89	111	26	1.5	0.91	37.3	28	6.5	0.93	49.2	32	4	0.93	33.1	32	6.5
0.91	105	26	1.5	0.94	36.3	28	6.5	0.93	50.5	32	4	0.94	32.6	32	6.5
0.91	105	26	1.5	0.92	34.7	28	6.5	0.92	49.4	32	4	0.92	33.6	32	6.5
0.9	105	26	1.5	0.94	29.2	28	6.5	0.91	48.6	32	4	0.94	33.6	32	6.5
0.88	106	26	1.5	0.91	36.1	28	6.5	0.92	49.4	32	4	0.95	32.4	32	6.5
0.91	103	26	1.5	0.94	34.9	28	6.5	0.89	50.6	32	4	0.94	32.7	32	6.5
0.91	103	26	1.5	0.95	36.2	28	6.5	0.88	49	32	4	0.93	33.1	32	6.5
0.87	110	26	1.5	0.89	37.6	28	6.5	0.92	47.7	32	4	0.96	32.3	32	6.5
0.9	104	26	1.5	0.95	35.2	28	6.5	0.92	50.6	32	4	0.94	32.2	32	6.5
0.9	105	26	1.5	0.95	36.2	28	6.5	0.91	50.5	32	4	0.95	33	32	6.5
0.91	106	26	1.5	0.93	34.5	28	6.5	0.91	53	32	4	0.94	31.6	32	6.5
0.9	103	26	1.5	0.92	36.3	28	6.5	0.89	53.5	32	4	0.95	32.7	32	6.5
0.89	106	26	1.5	0.91	35.6	28	6.5	0.92	49.7	32	4	0.94	33.3	32	6.5
0.89	103	26	1.5	0.94	35.3	28	6.5	0.9	50.4	32	4	0.93	33.5	32	6.5
0.84	108	26	1.5	0.94	34.4	28	6.5	0.92	50.1	32	4	0.94	33.1	32	6.5
0.91	104	26	1.5	0.94	35.2	28	6.5	0.93	51	32	4	0.93	34.5	32	6.5

0.9	105	26	1.5
0.89	118	26	1.5
0.89	106	26	1.5
0.85	108	26	1.5
0.82	106	26	1.5
0.9	106	26	1.5
0.83	109	26	1.5
0.93	101	26	1.5
0.87	108	26	1.5
0.9	107	26	1.5
0.9	107	26	1.5
0.9	107	26	1.5
0.89	105	26	1.5
0.9	107	26	1.5
0.89	104	26	1.5
0.91	106	26	1.5
0.84	107	26	1.5
0.87	109	26	1.5
0.88	109	26	1.5
0.9	104	26	1.5
0.91	104	26	1.5
0.91	104	26	1.5
0.87	110	26	1.5
0.9	105	26	1.5
0.9	105	26	1.5
0.9	106	26	1.5
0.91	103	26	1.5
0.91	102	26	1.5
0.91	105	26	1.5
0.91	105	26	1.5
0.9	106	26	1.5
0.91	104	26	1.5
0.91	105	26	1.5
0.91	104	26	1.5
0.91	104	26	1.5
0.92	103	26	1.5
0.86	108	26	1.5
0.91	103	26	1.5
0.91	103	26	1.5
0.89	113	26	1.5
0.9	104	26	1.5
0.87	107	26	1.5
0.82	107	26	1.5
0.91	106	26	1.5
0.91	106	26	1.5
0.89	104	26	1.5
0.87	112	26	1.5
0.87	105	26	1.5
0.89	105	26	1.5
0.89	106	26	1.5
0.9	108	26	1.5
0.89	104	26	1.5
0.86	109	26	1.5
0.9	105	26	1.5
0.9	104	26	1.5
0.89	104	26	1.5
0.91	105	26	1.5
0.91	103	26	1.5
0.89	103	26	1.5
0.88	104	26	1.5
0.9	105	26	1.5
0.92	105	26	1.5
0.9	104	26	1.5
0.91	103	26	1.5
0.92	104	26	1.5
0.91	103	26	1.5
0.91	106	26	1.5
0.9	106	26	1.5
0.88	104	26	1.5
0.84	104	26	1.5
0.91	103	26	1.5
0.93	61.3	26	4
0.91	66.2	26	4
0.91	65.6	26	4
0.93	38	28	6.5
0.93	34.9	28	6.5
0.87	36.7	28	6.5
0.94	34.6	28	6.5
0.92	37.1	28	6.5
0.92	37.9	28	6.5
0.94	36.7	28	6.5
0.94	34.2	28	6.5
0.97	30.3	28	6.5
0.94	36.3	28	6.5
0.94	36.9	28	6.5
0.95	35.1	28	6.5
0.95	38.3	28	6.5
0.9	36	28	6.5
0.9	38.4	28	6.5
0.94	38.8	28	6.5
0.94	35.9	28	6.5
0.93	35.7	28	6.5
0.93	40.4	28	6.5
0.95	34.1	28	6.5
0.93	36.2	28	6.5
0.94	34.2	28	6.5
0.94	33.3	28	6.5
0.92	38.1	28	6.5
0.93	35.4	28	6.5
0.93	36.4	28	6.5
0.95	36.1	28	6.5
0.89	38.4	28	6.5
0.94	37.1	28	6.5
0.91	36	28	6.5
0.91	37.8	28	6.5
0.95	36.3	28	6.5
0.96	34	28	6.5
0.94	34.1	28	6.5
0.94	35.7	28	6.5
0.9	29.9	28	6.5
0.94	36.9	28	6.5
0.93	37.6	28	6.5
0.95	35.9	28	6.5
0.94	36.7	28	6.5
0.95	35.1	28	6.5
0.93	36.9	28	6.5
0.93	35.3	28	6.5
0.95	33.7	28	6.5
0.89	38.8	28	6.5
0.95	36.4	28	6.5
0.92	36.5	28	6.5
0.89	36.8	28	6.5
0.93	35.6	28	6.5
0.94	35.1	28	6.5
0.94	35.1	28	6.5
0.89	39.4	28	6.5
0.95	35.9	28	6.5
0.92	34.9	28	6.5
0.92	37.1	28	6.5
0.94	34.3	28	6.5
0.95	35.6	28	6.5
0.95	35.4	28	6.5
0.93	32	28	6.5
0.94	30.6	28	6.5
0.94	37.8	28	6.5
0.93	35.7	28	6.5
0.94	35.9	28	6.5
0.94	35.9	28	6.5
0.94	34.6	28	6.5
0.91	37.4	28	6.5
0.94	35.6	28	6.5
0.94	36.3	28	6.5
0.92	38.3	28	6.5
0.94	35.7	28	6.5
0.96	32.4	28	6.5
0.96	35.6	28	6.5
0.94	35.9	28	6.5
0.93	34	28	6.5
0.94	35	28	6.5
0.93	46.1	32	4
0.92	50.6	32	4
0.91	51.9	32	4
0.92	48.7	32	4
0.93	53	32	4
0.91	47.3	32	4
0.91	50.8	32	4
0.93	51	32	4
0.92	51.6	32	4
0.94	46.1	32	4
0.93	50.3	32	4
0.93	50	32	4
0.92	50.8	32	4
0.92	51.4	32	4
0.93	50.5	32	4
0.92	50.2	32	4
0.92	49.5	32	4
0.91	50.6	32	4
0.92	50.8	32	4
0.93	52.3	32	4
0.9	51.9	32	4
0.91	47.3	32	4
0.92	50	32	4
0.92	49.6	32	4
0.93	49.2	32	4
0.91	51.9	32	4
0.91	52.5	32	4
0.94	50.3	32	4
0.92	50.6	32	4
0.93	51.4	32	4
0.91	48.3	32	4
0.93	54.1	32	4
0.91	49.6	32	4
0.93	50.4	32	4
0.91	50.9	32	4
0.94	46.2	32	4
0.93	49	32	4
0.92	51.4	32	4
0.94	47.6	32	4
0.92	49.8	32	4
0.93	48.8	32	4
0.92	50.1	32	4
0.93	46.1	32	4
0.93	50.6	32	4
0.93	50.8	32	4
0.9	50.5	32	4
0.9	49.3	32	4
0.93	53	32	4
0.89	48	32	4
0.91	49	32	4
0.9	49.3	32	4
0.92	50.9	32	4
0.92	50.2	32	4
0.92	48	32	4
0.93	50.1	32	4
0.93	51.8	32	4
0.9	48.9	32	4
0.93	49.4	32	4
0.93	49.4	32	4
0.92	48.8	32	4
0.92	49.5	32	4
0.91	53.4	32	4
0.91	47.9	32	4
0.91	48.5	32	4
0.93	50.2	32	4
0.89	50.4	32	4
0.9	51.3	32	4
0.92	48.4	32	4
0.92	49.1	32	4
0.92	51.2	32	4
0.91	49.9	32	4
0.93	50.2	32	4
0.92	49.9	32	4
0.93	51	32	4
0.91	49.6	32	4
0.96	32.5	32	6.5
0.95	32.2	32	6.5
0.93	32.6	32	6.5
0.96	31.2	32	6.5
0.95	32.2	32	6.5
0.96	33.1	32	6.5
0.93	33.4	32	6.5
0.95	32.9	32	6.5
0.94	31.9	32	6.5
0.96	32	32	6.5
0.93	32.3	32	6.5
0.97	32.2	32	6.5
0.94	33.9	32	6.5
0.92	34.1	32	6.5
0.92	34.1	32	6.5
0.95	33.4	32	6.5
0.94	32.6	32	6.5
0.97	31.7	32	6.5
0.94	33.3	32	6.5
0.94	32.3	32	6.5
0.93	33.4	32	6.5
0.96	31.8	32	6.5
0.93	31.5	32	6.5
0.94	33.4	32	6.5
0.94	31.4	32	6.5
0.96	32.1	32	6.5
0.95	32.5	32	6.5
0.93	33	32	6.5
0.93	32.3	32	6.5
0.93	33.3	32	6.5
0.95	30.5	32	6.5
0.96	31.8	32	6.5
0.95	33.7	32	6.5
0.94	31.7	32	6.5
0.95	33.2	32	6.5
0.95	31.4	32	6.5
0.94	33.4	32	6.5
0.94	32.9	32	6.5
0.93	33.4	32	6.5
0.94	33.5	32	6.5
0.94	32.1	32	6.5
0.93	34	32	6.5
0.93	31.6	32	6.5
0.96	31.7	32	6.5
0.96	32.9	32	6.5
0.95	31.6	32	6.5
0.96	33.6	32	6.5
0.95	32.4	32	6.5
0.94	31	32	6.5
0.96	32.2	32	6.5
0.95	32.3	32	6.5
0.95	32.8	32	6.5
0.95	32.5	32	6.5
0.94	32.6	32	6.5
0.95	31.9	32	6.5
0.97	31.1	32	6.5
0.93	33.4	32	6.5
0.93	32.5	32	6.5
0.94	33.2	32	6.5
0.92	33.2	32	6.5
0.94	33.3	32	6.5
0.95	31.5	32	6.5
0.94	30.9	32	6.5
0.95	32.8	32	6.5
0.95	33.2	32	6.5
0.93	31.8	32	6.5
0.95	32.7	32	6.5
0.94	33.6	32	6.5
0.95	31.1	32	6.5
0.95	32.9	32	6.5
0.93	32.9	32	6.5
0.96	32.7	32	6.5
0.94	33.5	32	6.5
0.93	31.2	32	6.5
0.93	32.5	32	6.5

0.9	65.1	26	4	0.94	36.3	28	6.5	0.92	45.8	32	4	0.93	33.8	32	6.5
0.9	64.2	26	4	0.95	35.2	28	6.5	0.89	50.8	32	4	0.94	32.9	32	6.5
0.91	66.7	26	4	0.93	35.3	28	6.5	0.93	48.1	32	4	0.94	29.7	32	6.5
0.91	65	26	4	0.91	37	28	6.5	0.88	51.1	32	4	0.94	33.5	32	6.5
0.9	64.8	26	4	0.93	35.9	28	6.5	0.92	50.6	32	4	0.92	33.5	32	6.5
0.9	65.6	26	4	0.94	34.1	28	6.5	0.91	47.1	32	4	0.94	33.2	32	6.5
0.91	62.8	26	4	0.95	35	28	6.5	0.92	50.4	32	4	0.92	33.9	32	6.5
0.93	61.2	26	4	0.88	39.4	28	6.5	0.91	50.8	32	4	0.93	32.1	32	6.5
0.91	69.4	26	4	0.94	32.1	28	6.5	0.9	48	32	4	0.95	32.5	32	6.5
0.91	67.7	26	4	0.94	34.7	28	6.5	0.92	47.4	32	4	0.94	32.8	32	6.5
0.9	67.2	26	4	0.91	34.4	28	6.5	0.94	48	32	4	0.94	33.9	32	6.5
0.92	65.3	26	4	0.94	36	28	6.5	0.9	49.5	32	4	0.96	33.5	32	6.5
0.91	56.3	26	4	0.93	35.4	28	6.5	0.93	49.2	32	4	0.93	31.5	32	6.5
0.92	64.4	26	4	0.94	36.4	28	6.5	0.94	47.8	32	4	0.94	32.5	32	6.5
0.91	67.9	26	4	0.94	35.4	28	6.5	0.94	48.2	32	4	0.93	30.5	32	6.5
0.9	69.8	26	4	0.95	33.7	28	6.5	0.92	47.2	32	4	0.93	32.5	32	6.5
0.91	63	26	4	0.94	35.4	28	6.5	0.92	48.3	32	4	0.92	32.9	32	6.5
0.92	61.4	26	4	0.95	34.7	28	6.5	0.92	49.7	32	4	0.95	32.7	32	6.5
0.92	61.2	26	4	0.95	34.1	28	6.5	0.91	51.3	32	4	0.94	32.9	32	6.5
0.91	65.8	26	4	0.94	35.7	28	6.5	0.9	49.3	32	4	0.94	30.9	32	6.5
0.9	67.6	26	4	0.94	36.5	28	6.5	0.92	50.5	32	4	0.94	32.3	32	6.5
0.91	65.9	26	4	0.94	37.7	28	6.5	0.9	46.7	32	4	0.95	32.4	32	6.5
0.9	65.5	26	4	0.93	35	28	6.5	0.93	50.1	32	4	0.94	31.9	32	6.5
0.9	69.5	26	4	0.93	38.2	28	6.5	0.88	53.7	32	4	0.94	33.2	32	6.5
0.9	68.1	26	4	0.93	33.4	28	6.5	0.91	46.3	32	4	0.95	32.6	32	6.5
0.91	61	26	4	0.96	29.8	28	6.5	0.93	51	32	4	0.93	32.5	32	6.5
0.91	65.9	26	4	0.96	34	28	6.5	0.91	50.4	32	4	0.93	33.1	32	6.5
0.9	63.3	26	4	0.95	34.4	28	6.5	0.92	51.2	32	4	0.95	32.2	32	6.5
0.91	62.8	26	4	0.93	39.6	28	6.5	0.91	50.5	32	4	0.94	33.6	32	6.5
0.91	65.1	26	4	0.93	35.8	28	6.5	0.92	48.1	32	4	0.96	31	32	6.5
0.91	63	26	4	0.92	35.8	28	6.5	0.9	47.6	32	4	0.96	32.8	32	6.5
0.91	63.9	26	4	0.95	36.9	28	6.5	0.93	49.4	32	4	0.93	33.6	32	6.5
0.91	68.9	26	4	0.95	35.6	28	6.5	0.91	49.4	32	4	0.93	31.9	32	6.5
0.9	65.5	26	4	0.93	34.8	28	6.5	0.89	48.5	32	4	0.96	31.9	32	6.5
0.91	65.1	26	4	0.94	35.9	28	6.5	0.93	47.7	32	4	0.95	33	32	6.5
0.91	62.3	26	4	0.91	36	28	6.5	0.88	48.6	32	4	0.93	33.6	32	6.5
0.92	62.3	26	4	0.94	33.2	28	6.5	0.94	48.7	32	4	0.97	32.4	32	6.5
0.9	64.4	26	4	0.94	35.8	28	6.5	0.92	48.4	32	4	0.92	33.9	32	6.5
0.91	65.9	26	4	0.93	33.6	28	6.5	0.92	50.4	32	4	0.92	34	32	6.5
0.91	60.6	26	4	0.94	34.2	28	6.5	0.92	49.1	32	4	0.92	31.4	32	6.5
0.91	63.9	26	4	0.95	33.7	28	6.5	0.91	49.2	32	4	0.94	32.1	32	6.5
0.9	63.8	26	4	0.93	35.8	28	6.5	0.92	51.4	32	4	0.95	33.2	32	6.5
0.92	64.5	26	4	0.95	35.3	28	6.5	0.92	51	32	4	0.95	34.3	32	6.5
0.91	63.3	26	4	0.94	37.2	28	6.5	0.9	53.8	32	4	0.95	32.3	32	6.5
0.91	65.3	26	4	0.94	34.5	28	6.5	0.88	50.6	32	4	0.96	30.2	32	6.5
0.9	69.7	26	4	0.93	35.3	28	6.5	0.91	50.1	32	4	0.94	32.1	32	6.5
0.9	65.6	26	4	0.93	36.5	28	6.5	0.93	50.4	32	4	0.96	32.2	32	6.5
0.91	66	26	4	0.93	29.4	28	6.5	0.91	49.1	32	4	0.96	30.3	32	6.5
0.91	63.2	26	4	0.94	35.4	28	6.5	0.91	48.7	32	4	0.95	33.4	32	6.5
0.91	65	26	4	0.93	34.1	28	6.5	0.9	50.5	32	4	0.94	32.5	32	6.5
0.91	62.9	26	4	0.95	34.8	28	6.5	0.9	51.5	32	4	0.95	32.3	32	6.5
0.91	67.1	26	4	0.88	29.2	28	6.5	0.92	46.3	32	4	0.94	32.6	32	6.5
0.91	68.5	26	4	0.94	34.2	28	6.5	0.9	50.6	32	4	0.95	32.5	32	6.5
0.92	64.1	26	4	0.93	35.1	28	6.5	0.92	50.7	32	4	0.95	32.7	32	6.5
0.9	65.2	26	4	0.94	35.5	28	6.5	0.92	48.5	32	4	0.94	31.4	32	6.5
0.92	60.1	26	4	0.92	33.7	28	6.5	0.93	47.8	32	4	0.95	32.3	32	6.5
0.91	62.5	26	4	0.92	36	28	6.5	0.92	49.6	32	4	0.92	33.4	32	6.5
0.9	68.9	26	4	0.9	39.1	28	6.5	0.93	50.6	32	4	0.95	32.8	32	6.5
0.9	69.5	26	4	0.95	35.3	28	6.5	0.93	47.8	32	4	0.92	33.4	32	6.5
0.9	67	26	4	0.92	35.3	28	6.5	0.9	52.4	32	4	0.94	32.6	32	6.5
0.9	67.1	26	4	0.93	35.4	28	6.5	0.91	48.7	32	4	0.95	33.4	32	6.5
0.91	65.5	26	4	0.93	35.2	28	6.5	0.92	50.6	32	4	0.95	34.1	32	6.5
0.91	61.8	26	4	0.9	33.8	28	6.5	0.88	54.8	32	4	0.96	31.1	32	6.5
0.9	70.2	26	4	0.94	35.1	28	6.5	0.93	48.3	32	4	0.93	32.9	32	6.5
0.91	67.2	26	4	0.94	34.8	28	6.5	0.93	48.1	32	4	0.96	32.3	32	6.5
0.9	67.5	26	4	0.95	36.7	28	6.5	0.92	49.5	32	4	0.92	33.5	32	6.5
0.91	65.1	26	4	0.96	33.3	28	6.5	0.89	49.7	32	4	0.96	33.3	32	6.5
0.9	68	26	4	0.94	34.8	28	6.5	0.91	49.7	32	4	0.95	33.7	32	6.5
0.91	64	26	4	0.93	35.7	28	6.5	0.88	46.8	32	4	0.94	32.3	32	6.5
0.92	65.6	26	4	0.93	35.8	28	6.5	0.93	46.5	32	4	0.92	33.8	32	6.5
0.9	63.8	26	4	0.94	34.3	28	6.5	0.89	55.4	32	4	0.94	32.7	32	6.5
0.91	63.4	26	4	0.93	35.1	28	6.5	0.92	50.1	32	4	0.95	33.5	32	6.5
0.91	67.3	26	4	0.93	33.1	28	6.5	0.88	47.9	32	4	0.94	33.3	32	6.5
0.92	64.6	26	4	0.94	37	28	6.5	0.92	47.4	32	4	0.92	31.7	32	6.5
0.9	65.7	26	4	0.95	34.2	28	6.5	0.93	47.5	32	4	0.93	33.9	32	6.5

0.91	66.8	26	4	0.93	35.6	28	6.5	0.93	49.3	32	4	0.92	32.9	32	6.5
0.91	65.8	26	4	0.94	35.7	28	6.5	0.9	53.7	32	4	0.94	32.5	32	6.5
0.91	67.5	26	4	0.95	35.3	28	6.5	0.91	55	32	4	0.93	31.7	32	6.5
0.92	66.2	26	4	0.95	35.9	28	6.5	0.92	50.5	32	4	0.95	32.5	32	6.5
0.91	68.1	26	4	0.95	37.7	28	6.5	0.9	48.1	32	4	0.92	33.8	32	6.5
0.91	62	26	4	0.94	35.8	28	6.5	0.93	50	32	4	0.97	33.3	32	6.5
0.9	69.3	26	4	0.94	35.8	28	6.5	0.93	49.8	32	4	0.92	32.8	32	6.5
0.9	66.5	26	4	0.91	36.4	28	6.5	0.91	49.1	32	4	0.96	33.2	32	6.5
0.91	66.4	26	4	0.94	37.4	28	6.5	0.89	54.7	32	4	0.94	32.8	32	6.5
0.92	65.4	26	4	0.95	35.2	28	6.5	0.94	48.5	32	4	0.95	32.9	32	6.5
0.91	66.8	26	4	0.95	35.7	28	6.5	0.92	51.1	32	4	0.95	32.8	32	6.5
0.91	65.1	26	4	0.94	35.8	28	6.5	0.93	50.9	32	4	0.93	35.6	32	6.5
0.91	64.7	26	4	0.95	34.6	28	6.5	0.92	48.6	32	4	0.96	30.9	32	6.5
0.91	64.3	26	4	0.93	34.6	28	6.5	0.91	57.2	32	4	0.95	33.6	32	6.5
0.9	67	26	4	0.94	36.6	28	6.5	0.9	50.8	32	4	0.95	31.7	32	6.5
0.9	65.7	26	4	0.95	34.5	28	6.5	0.93	49.2	32	4	0.93	32.8	32	6.5
0.9	67.7	26	4	0.95	33.1	28	6.5	0.9	51.8	32	4	0.94	32.8	32	6.5
0.9	67.6	26	4	0.96	35.6	28	6.5	0.92	49	32	4	0.92	33.5	32	6.5
0.91	66.7	26	4	0.93	35.8	28	6.5	0.91	49.7	32	4	0.93	33	32	6.5
0.9	68.2	26	4	0.96	34.2	28	6.5	0.93	56.8	32	4	0.94	32.9	32	6.5
0.9	67.2	26	4	0.94	37.5	28	6.5	0.91	51	32	4	0.92	34.8	32	6.5
0.9	69.9	26	4	0.95	35.1	28	6.5	0.92	49.2	32	4	0.92	33.4	32	6.5
0.91	68.9	26	4	0.93	35.7	28	6.5	0.92	49.3	32	4	0.94	33.4	32	6.5
0.91	64.8	26	4	0.95	36.1	28	6.5	0.91	48	32	4	0.93	32.8	32	6.5
0.9	69.4	26	4	0.88	40.9	28	6.5	0.87	51.1	32	4	0.93	32.9	32	6.5
0.9	65.9	26	4	0.95	35.3	28	6.5	0.91	49.2	32	4	0.96	32.8	32	6.5
0.92	60.1	26	4	0.92	36.3	28	6.5	0.93	50.2	32	4	0.95	31.7	32	6.5
0.9	68.5	26	4	0.95	36.4	28	6.5	0.92	49.2	32	4	0.93	31.8	32	6.5
0.91	67.5	26	4	0.93	33.7	28	6.5	0.92	49	32	4	0.94	33.9	32	6.5
0.9	66	26	4	0.89	35.5	28	6.5	0.89	53.7	32	4	0.96	31.1	32	6.5
0.91	58.1	26	4	0.95	34.9	28	6.5	0.91	48.9	32	4	0.95	32.9	32	6.5
0.9	68.8	26	4	0.92	32.2	28	6.5	0.92	48	32	4	0.94	34	32	6.5
0.92	58.4	26	4	0.94	32.8	28	6.5	0.92	49.5	32	4	0.92	32.3	32	6.5
0.91	60.8	26	4	0.92	35.5	28	6.5	0.9	49.6	32	4	0.93	33.9	32	6.5
0.92	63.5	26	4	0.94	36.1	28	6.5	0.93	49.7	32	4	0.94	33.5	32	6.5
0.91	63.7	26	4	0.93	35.8	28	6.5	0.94	49.1	32	4	0.92	33.2	32	6.5
0.91	63.2	26	4	0.94	35.6	28	6.5	0.92	50.9	32	4	0.95	33.7	32	6.5
0.9	65.1	26	4	0.95	35	28	6.5	0.92	49.9	32	4	0.93	32.7	32	6.5
0.9	65.9	26	4	0.94	35.6	28	6.5	0.93	48.4	32	4	0.95	33.7	32	6.5
0.9	66.7	26	4	0.96	35.4	28	6.5	0.92	50.5	32	4	0.94	31.2	32	6.5
0.92	65.6	26	4	0.94	36.4	28	6.5	0.91	48.8	32	4	0.94	33.9	32	6.5
0.91	65.2	26	4	0.94	34.6	28	6.5	0.94	50.3	32	4	0.94	31.7	32	6.5
0.91	62.4	26	4	0.92	36.2	28	6.5	0.92	50.8	32	4	0.96	32.9	32	6.5
0.91	64.3	26	4	0.95	36.2	28	6.5	0.92	50	32	4	0.95	32.4	32	6.5
0.93	64.4	26	4	0.94	35.6	28	6.5	0.93	46.4	32	4	0.95	31.7	32	6.5
0.91	64.7	26	4	0.94	35.9	28	6.5	0.91	51.3	32	4	0.94	31.4	32	6.5
0.9	65.2	26	4	0.95	35.9	28	6.5	0.92	50.7	32	4	0.94	33.4	32	6.5
0.91	63	26	4	0.93	36.2	28	6.5	0.94	47.5	32	4	0.93	33	32	6.5
0.91	66	26	4	0.95	36.9	28	6.5	0.92	48.2	32	4	0.95	33.8	32	6.5
0.91	63.8	26	4	0.92	36.9	28	6.5	0.92	46.3	32	4	0.93	33.8	32	6.5
0.91	63.2	26	4	0.94	39.1	28	6.5	0.91	50.3	32	4	0.94	30.6	32	6.5
0.91	66	26	4	0.94	35.5	28	6.5	0.93	48.9	32	4	0.95	31.1	32	6.5
0.9	65.2	26	4	0.96	34.7	28	6.5	0.92	50.6	32	4	0.94	33.4	32	6.5
0.91	66.3	26	4	0.94	35.6	28	6.5	0.93	46.9	32	4	0.95	33.9	32	6.5
0.91	62.8	26	4	0.94	34.8	28	6.5	0.93	49.3	32	4	0.96	32.4	32	6.5
0.92	62.1	26	4	0.9	38.2	28	6.5	0.92	49.6	32	4	0.93	33.1	32	6.5
0.9	67.8	26	4	0.94	36.5	28	6.5	0.93	50.3	32	4	0.96	36	32	6.5
0.91	68.2	26	4	0.91	36.1	28	6.5	0.93	49.1	32	4	0.94	35.1	32	6.5
0.91	64.9	26	4	0.95	35.8	28	6.5	0.92	49	32	4	0.93	32	32	6.5
0.91	66.4	26	4	0.95	36.2	28	6.5	0.92	48.5	32	4	0.93	32.9	32	6.5
0.91	65.2	26	4	0.93	37.1	28	6.5	0.94	49.3	32	4	0.93	33.7	32	6.5
0.9	67.5	26	4	0.95	35.4	28	6.5	0.91	53.5	32	4	0.94	33.2	32	6.5
0.9	64.7	26	4	0.94	35.1	28	6.5	0.93	50.3	32	4	0.94	30.3	32	6.5
0.91	58.8	26	4	0.94	35	28	6.5	0.91	50	32	4	0.96	32.7	32	6.5
0.91	61	26	4	0.94	36.7	28	6.5	0.92	50	32	4	0.94	33.8	32	6.5
0.9	66.6	26	4	0.91	36.3	28	6.5	0.89	51	32	4	0.93	32	32	6.5
0.91	65.7	26	4	0.93	36.3	28	6.5	0.94	47.7	32	4	0.93	32.8	32	6.5
0.9	66.1	26	4	0.93	39.1	28	6.5	0.91	49.1	32	4	0.94	32.6	32	6.5
0.92	65.9	26	4	0.94	38	28	6.5	0.92	50.7	32	4	0.96	32.8	32	6.5
0.91	64.9	26	4	0.96	34.6	28	6.5	0.91	49	32	4	0.92	33.7	32	6.5
0.92	61.3	26	4	0.93	34.4	28	6.5	0.91	53.8	32	4	0.95	33.2	32	6.5
0.91	65.9	26	4	0.94	35.4	28	6.5	0.93	46.6	32	4	0.95	32.3	32	6.5
0.9	65	26	4	0.93	35.7	28	6.5	0.92	48.5	32	4	0.92	31.8	32	6.5
0.91	63.1	26	4	0.92	33.3	28	6.5	0.93	49.6	32	4	0.93	33.5	32	6.5
0.91	60.6	26	4	0.91	34.7	28	6.5	0.93	49.9	32	4	0.92	33.2	32	6.5

0.92	60.7	26	4	0.94	35.2	28	6.5	0.93	48.1	32	4	0.95	33.2	32	6.5
0.9	65.6	26	4	0.94	34.8	28	6.5	0.92	49.2	32	4	0.95	33.1	32	6.5
0.9	69	26	4	0.95	35.5	28	6.5	0.88	59.6	32	4	0.97	33.6	32	6.5
0.92	59.2	26	4	0.94	36.5	28	6.5	0.92	50.6	32	4	0.94	30.5	32	6.5
0.9	64.8	26	4	0.95	34.5	28	6.5	0.92	50	32	4	0.94	32.9	32	6.5
0.91	66.4	26	4	0.95	35.9	28	6.5	0.92	49.3	32	4	0.95	32.8	32	6.5
0.92	62.3	26	4	0.9	36.7	28	6.5	0.91	48.1	32	4	0.96	33.6	32	6.5
0.92	62.9	26	4	0.93	37.3	28	6.5	0.89	53.4	32	4	0.94	33.5	32	6.5
0.91	63.6	26	4	0.91	37.4	28	6.5	0.92	54.7	32	4	0.94	31.9	32	6.5
0.9	66.3	26	4	0.93	36.1	28	6.5	0.92	49.8	32	4	0.93	32.3	32	6.5
0.91	67.7	26	4	0.95	36.1	28	6.5	0.93	50.7	32	4	0.93	32.3	32	6.5
0.91	68.7	26	4	0.95	36.8	28	6.5	0.91	49.3	32	4	0.93	34.1	32	6.5
0.93	62.4	26	4	0.91	37.2	28	6.5	0.92	51.5	32	4	0.93	33.7	32	6.5
0.91	65.9	26	4	0.94	35.7	28	6.5	0.93	50	32	4	0.95	33	32	6.5
0.9	65.8	26	4	0.95	34	28	6.5	0.92	50.4	32	4	0.94	31.3	32	6.5
0.91	63.2	26	4	0.94	34.8	28	6.5	0.93	48.7	32	4	0.94	32.2	32	6.5
0.91	57	26	4	0.93	36.4	28	6.5	0.93	49.4	32	4	0.94	33.5	32	6.5
0.9	68.1	26	4	0.96	34.4	28	6.5	0.89	49.5	32	4	0.94	33	32	6.5
0.9	64	26	4	0.92	38	28	6.5	0.88	48.7	32	4	0.92	31.9	32	6.5
0.9	67.2	26	4	0.93	35.1	28	6.5	0.9	51.4	32	4	0.94	32.6	32	6.5
0.9	68.8	26	4	0.94	34.4	28	6.5	0.89	49.5	32	4	0.95	32.9	32	6.5
0.91	64	26	4	0.9	32.6	28	6.5	0.94	49.7	32	4	0.93	32.7	32	6.5
0.91	63.6	26	4	0.9	36.9	28	6.5	0.92	47.1	32	4	0.95	33.6	32	6.5
0.9	66.6	26	4	0.93	37.4	28	6.5	0.92	49.9	32	4	0.96	32.6	32	6.5
0.91	68.3	26	4	0.95	31.6	28	6.5	0.93	49.2	32	4	0.92	31.5	32	6.5
0.91	63.2	26	4	0.94	36.4	28	6.5	0.92	46.9	32	4	0.94	33.6	32	6.5
0.91	67.2	26	4	0.96	34.7	28	6.5	0.93	48.7	32	4	0.95	32.6	32	6.5
0.91	64.9	26	4	0.95	35.1	28	6.5	0.94	50.9	32	4	0.92	32.7	32	6.5
0.92	64.4	26	4	0.92	38.6	28	6.5	0.92	50.4	32	4	0.95	33.7	32	6.5
0.92	63	26	4	0.92	35.5	28	6.5	0.92	49.9	32	4	0.93	32	32	6.5
0.9	67.5	26	4	0.93	34.5	28	6.5	0.92	48.2	32	4	0.94	33.5	32	6.5
0.91	66.2	26	4	0.91	37.9	28	6.5	0.92	49.8	32	4	0.94	32.6	32	6.5
0.9	65	26	4	0.94	36.7	28	6.5	0.94	49	32	4	0.95	33	32	6.5
0.9	66.8	26	4	0.94	38.5	28	6.5	0.92	49.8	32	4	0.93	34.8	32	6.5
0.9	64.2	26	4	0.92	35.6	28	6.5	0.94	47	32	4	0.93	32.1	32	6.5
0.9	68	26	4	0.93	35.7	28	6.5	0.93	47.5	32	4	0.92	34	32	6.5
0.91	69.9	26	4	0.92	38.6	28	6.5	0.92	49.7	32	4	0.92	33.9	32	6.5
0.92	65.4	26	4	0.93	31.7	28	6.5	0.93	48.4	32	4	0.94	33.4	32	6.5
0.92	66.6	26	4	0.94	35.1	28	6.5	0.89	43.6	32	4	0.95	32.5	32	6.5
0.91	68.8	26	4	0.93	34.2	28	6.5	0.95	48.3	32	4	0.94	34.2	32	6.5
0.91	68.7	26	4	0.94	36.2	28	6.5	0.93	48.3	32	4	0.96	32.1	32	6.5
0.92	60.5	26	4	0.93	34.4	28	6.5	0.91	49	32	4	0.93	32.7	32	6.5
0.91	68.2	26	4	0.93	34.7	28	6.5	0.93	50.9	32	4	0.93	31.5	32	6.5
0.92	63.1	26	4	0.94	34.5	28	6.5	0.92	50.2	32	4	0.93	32.8	32	6.5
0.9	68	26	4	0.93	37.8	28	6.5	0.93	48.7	32	4	0.95	32.1	32	6.5
0.91	62.9	26	4	0.93	35.9	28	6.5	0.94	49.6	32	4	0.94	33.3	32	6.5
0.9	70.5	26	4	0.92	35.1	28	6.5	0.91	49.4	32	4	0.95	33.7	32	6.5
0.9	71.4	26	4	0.95	36.1	28	6.5	0.91	49.4	32	4	0.95	33	32	6.5
0.9	69.5	26	4	0.94	34.7	28	6.5	0.92	46	32	4	0.92	33.2	32	6.5
0.91	68.4	26	4	0.94	33.9	28	6.5	0.92	46.1	32	4	0.93	32.4	32	6.5
0.93	59.5	26	4	0.94	34.2	28	6.5	0.93	50.1	32	4	0.94	33.9	32	6.5
0.91	66.5	26	4	0.95	36.2	28	6.5	0.92	50.4	32	4	0.94	33.6	32	6.5
0.91	62.7	26	4	0.9	38.8	28	6.5	0.94	50	32	4	0.93	33.6	32	6.5
0.93	62.8	26	4	0.95	33.4	28	6.5	0.92	47.5	32	4	0.95	33.1	32	6.5
0.92	62.2	26	4	0.95	34.3	28	6.5	0.92	50.1	32	4	0.92	33.2	32	6.5
0.91	63.2	26	4	0.94	36.2	28	6.5	0.94	49	32	4	0.93	33.3	32	6.5
0.9	59.3	26	4	0.92	33.7	28	6.5	0.93	48.5	32	4	0.95	33	32	6.5
0.9	62.5	26	4	0.93	34.3	28	6.5	0.88	46.2	32	4	0.94	32.2	32	6.5
0.91	65.9	26	4	0.93	35	28	6.5	0.92	50	32	4	0.97	32	32	6.5
0.91	61.8	26	4	0.95	34.8	28	6.5	0.9	49.3	32	4	0.92	35	32	6.5
0.9	63.3	26	4	0.93	37.7	28	6.5	0.92	48.6	32	4	0.94	33.9	32	6.5
0.91	63.6	26	4	0.92	34.5	28	6.5	0.91	49.3	32	4	0.93	33.2	32	6.5
0.91	61.4	26	4	0.94	34.1	28	6.5	0.93	50.4	32	4	0.95	33	32	6.5
0.91	68.1	26	4	0.94	42.5	28	6.5	0.93	49.7	32	4	0.95	32.8	32	6.5
0.9	66.9	26	4	0.96	33.7	28	6.5	0.91	49.6	32	4	0.92	34.6	32	6.5
0.9	68.5	26	4	0.93	35.3	28	6.5	0.92	50.2	32	4	0.93	32.3	32	6.5
0.92	61.6	26	4	0.92	36.3	28	6.5	0.93	48.8	32	4	0.96	31.1	32	6.5
0.91	66.8	26	4	0.93	33.7	28	6.5	0.9	48.7	32	4	0.92	32.2	32	6.5
0.9	63.1	26	4	0.94	34.2	28	6.5	0.9	49.7	32	4	0.92	33.8	32	6.5
0.91	63.2	26	4	0.95	37.4	28	6.5	0.92	50.5	32	4	0.93	32.7	32	6.5
0.92	60.9	26	4	0.92	35.6	28	6.5	0.9	49.8	32	4	0.95	33.5	32	6.5
0.91	61.8	26	4	0.92	34.7	28	6.5	0.91	48	32	4	0.95	33.5	32	6.5
0.91	63.6	26	4	0.95	35.7	28	6.5	0.86	50.4	32	4	0.93	32.3	32	6.5
0.91	63.6	26	4	0.94	35.3	28	6.5	0.87	57.8	32	4	0.93	34	32	6.5
0.91	62.4	26	4	0.93	35.1	28	6.5	0.92	48.5	32	4	0.93	32.7	32	6.5

0.91	66.9	26	4	0.93	35.6	28	6.5	0.92	49	32	4	0.92	32.1	32	6.5
0.9	60	26	4	0.92	33.6	28	6.5	0.94	49.7	32	4	0.94	33.7	32	6.5
0.92	63.5	26	4	0.93	35.3	28	6.5	0.92	49.9	32	4	0.95	33.2	32	6.5
0.91	61.8	26	4	0.92	35.8	28	6.5	0.91	48.6	32	4	0.94	33.6	32	6.5
0.91	68.2	26	4	0.93	35	28	6.5	0.93	49.4	32	4	0.93	34.3	32	6.5
0.92	64.1	26	4	0.93	34.3	28	6.5	0.92	48.8	32	4	0.94	33.5	32	6.5
0.92	62.2	26	4	0.92	36.6	28	6.5	0.93	53.3	32	4	0.94	32.8	32	6.5
0.91	62.5	26	4	0.89	35	28	6.5	0.91	49	32	4	0.93	33.3	32	6.5
0.92	61.6	26	4	0.89	35.3	28	6.5	0.91	48.6	32	4	0.92	34.2	32	6.5
0.93	61.4	26	4	0.94	34.8	28	6.5	0.89	54.6	32	4	0.94	33	32	6.5
0.9	64.5	26	4	0.97	33.5	28	6.5	0.93	52.7	32	4	0.93	34.3	32	6.5
0.91	67.2	26	4	0.94	36.8	28	6.5	0.9	50.3	32	4	0.93	31.9	32	6.5
0.9	64.1	26	4	0.93	37.8	28	6.5	0.94	47.6	32	4	0.95	32.3	32	6.5
0.91	63.1	26	4	0.95	32.9	28	6.5	0.92	49.9	32	4	0.94	32.8	32	6.5
0.91	66.2	26	4	0.94	34.4	28	6.5	0.91	52.5	32	4	0.93	32.8	32	6.5
0.91	69.2	26	4	0.95	35.2	28	6.5	0.89	44.8	32	4	0.94	34.3	32	6.5
0.93	64.7	26	4	0.95	33.9	28	6.5	0.93	49.4	32	4	0.95	32.3	32	6.5
0.91	64.4	26	4	0.95	35.5	28	6.5	0.92	51.9	32	4	0.92	35.6	32	6.5
0.92	62.8	26	4	0.92	32.4	28	6.5	0.88	50.5	32	4	0.95	33.2	32	6.5
0.91	64.9	26	4	0.95	35.4	28	6.5	0.91	50.9	32	4	0.95	32.8	32	6.5
0.91	63.7	26	4	0.94	36.6	28	6.5	0.93	48.3	32	4	0.94	31.7	32	6.5
0.92	59.1	26	4	0.91	36.1	28	6.5	0.9	49.7	32	4	0.94	32.3	32	6.5
0.91	62.8	26	4	0.94	35.2	28	6.5	0.91	49.8	32	4	0.96	31.5	32	6.5
0.91	66.3	26	4	0.94	37	28	6.5	0.92	49.4	32	4	0.94	32.8	32	6.5
0.9	64.3	26	4	0.95	34.6	28	6.5	0.91	49.6	32	4	0.92	34.2	32	6.5
0.92	63.9	26	4	0.96	33.7	28	6.5	0.91	50.4	32	4	0.93	34.1	32	6.5
0.9	59.5	26	4	0.95	32.4	28	6.5	0.92	51.2	32	4	0.94	30.7	32	6.5
0.92	60.3	26	4	0.94	34.2	28	6.5	0.92	48.9	32	4	0.95	32.6	32	6.5
0.93	60.3	26	4	0.96	34.8	28	6.5	0.92	47.7	32	4	0.94	31.2	32	6.5
0.92	60.8	26	4	0.95	34.5	28	6.5	0.91	48.8	32	4	0.94	31.6	32	6.5
0.91	64.7	26	4	0.94	38.4	28	6.5	0.89	50.3	32	4	0.93	32.7	32	6.5
0.91	63.6	26	4	0.93	35.9	28	6.5	0.93	47.7	32	4	0.95	32.6	32	6.5
0.91	67.3	26	4	0.95	35.9	28	6.5	0.92	50.8	32	4	0.95	33.1	32	6.5
0.91	60.6	26	4	0.95	35.3	28	6.5	0.87	52.4	32	4	0.96	32.1	32	6.5
0.92	66.5	26	4	0.95	35.1	28	6.5	0.93	45.9	32	4	0.95	30.7	32	6.5
0.92	66.6	26	4	0.95	35	28	6.5	0.92	50.6	32	4	0.95	29.8	32	6.5
0.92	64.1	26	4	0.93	37	28	6.5	0.92	50.2	32	4	0.93	32.8	32	6.5
0.92	64.5	26	4	0.93	34.4	28	6.5	0.91	51	32	4	0.95	32	32	6.5
0.91	66.7	26	4	0.93	32.8	28	6.5	0.87	47.3	32	4	0.94	34.5	32	6.5
0.91	67.6	26	4	0.95	35.7	28	6.5	0.93	50.9	32	4	0.94	33	32	6.5
0.91	67.4	26	4	0.94	34.7	28	6.5	0.9	48.7	32	4	0.95	32.6	32	6.5
0.91	65.4	26	4	0.93	35.5	28	6.5	0.9	47.4	32	4	0.94	31.1	32	6.5
0.9	65.4	26	4	0.93	37.8	28	6.5	0.9	50.9	32	4	0.94	32.5	32	6.5
0.9	68.1	26	4	0.95	37.3	28	6.5	0.93	49.7	32	4	0.95	32.9	32	6.5
0.91	65.2	26	4	0.92	36.4	28	6.5	0.92	50.4	32	4	0.93	32.5	32	6.5
0.92	65.7	26	4	0.95	35.6	28	6.5	0.92	45.9	32	4	0.94	33.2	32	6.5
0.91	65.1	26	4	0.94	34.2	28	6.5	0.92	49.7	32	4	0.94	32.1	32	6.5
0.9	69.1	26	4	0.92	35.2	28	6.5	0.93	49.3	32	4	0.96	30.5	32	6.5
0.91	66.9	26	4	0.95	36.7	28	6.5	0.91	51.4	32	4	0.96	30.9	32	6.5
0.92	61.6	26	4	0.94	37	28	6.5	0.88	49.7	32	4	0.97	28.1	32	6.5
0.91	61.5	26	4	0.95	35.2	28	6.5	0.91	52	32	4	0.93	30.9	32	6.5
0.9	68.1	26	4	0.9	34.5	28	6.5	0.92	45.8	32	4	0.94	33.3	32	6.5
0.91	67	26	4	0.95	32.7	28	6.5	0.91	48.1	32	4	0.94	32.9	32	6.5
0.92	57.8	26	4	0.93	35.7	28	6.5	0.93	50.4	32	4	0.93	32.1	32	6.5
0.92	60.1	26	4	0.93	36.9	28	6.5	0.89	49.5	32	4	0.95	32.6	32	6.5
0.91	69.5	26	4	0.94	37.4	28	6.5	0.9	51.1	32	4	0.93	33.4	32	6.5
0.9	68.6	26	4	0.94	36.9	28	6.5	0.91	49.5	32	4	0.96	31	32	6.5
0.91	57.2	26	4	0.95	35.5	28	6.5	0.89	51.2	32	4	0.96	31.7	32	6.5
0.92	57.4	26	4	0.94	36.6	28	6.5	0.92	49	32	4	0.95	31.8	32	6.5
0.91	67.8	26	4	0.92	34.8	28	6.5	0.92	52.2	32	4	0.93	32.3	32	6.5
0.9	58.5	26	4	0.94	36.6	28	6.5	0.93	50	32	4	0.93	31.7	32	6.5
0.92	59.2	26	4	0.91	42.4	28	6.5	0.9	50.8	32	4	0.95	32.9	32	6.5
0.92	59	26	4	0.95	35.3	28	6.5	0.94	49.8	32	4	0.94	31.5	32	6.5
0.91	62.8	26	4	0.95	34.7	28	6.5	0.86	48.7	32	4	0.93	32.8	32	6.5
0.91	56.6	26	4	0.94	35	28	6.5	0.93	48.7	32	4	0.95	32.7	32	6.5
0.92	57.1	26	4	0.93	35.8	28	6.5	0.9	50.7	32	4	0.94	31.3	32	6.5
0.9	59.1	26	4	0.95	34.5	28	6.5	0.92	49.3	32	4	0.93	34.7	32	6.5
0.91	63.2	26	4	0.94	34.8	28	6.5	0.91	47.8	32	4	0.95	31.9	32	6.5
0.9	63.5	26	4	0.95	36.6	28	6.5	0.91	49.6	32	4	0.97	31.4	32	6.5
0.91	61.4	26	4	0.95	35.7	28	6.5	0.93	47.3	32	4	0.95	32.2	32	6.5
0.92	63.1	26	4	0.91	35	28	6.5	0.93	48.8	32	4	0.94	33.5	32	6.5
0.91	63.9	26	4	0.93	37.7	28	6.5	0.88	47.9	32	4	0.92	30.5	32	6.5
0.9	66.1	26	4	0.94	35.8	28	6.5	0.9	51.6	32	4	0.94	32.1	32	6.5
0.9	59.9	26	4	0.94	34.1	28	6.5	0.9	46.7	32	4	0.95	30.5	32	6.5
0.91	58.6	26	4	0.94	36.4	28	6.5	0.92	51.8	32	4	0.95	30.6	32	6.5

0.92	58.1	26	4	0.94	35.9	28	6.5	0.93	48.9	32	4	0.95	32.6	32	6.5
0.91	59.5	26	4	0.93	35.6	28	6.5	0.89	51.2	32	4	0.95	32.1	32	6.5
0.9	59.7	26	4	0.88	43.6	28	6.5	0.93	46	32	4	0.94	34	32	6.5
0.91	65.7	26	4	0.94	34.6	28	6.5	0.91	53.2	32	4	0.96	31.3	32	6.5
0.92	62.4	26	4	0.94	34.3	28	6.5	0.92	50.6	32	4	0.96	32.3	32	6.5
0.91	60.3	26	4	0.93	34.6	28	6.5	0.91	49.6	32	4	0.95	33.3	32	6.5
0.91	64.4	26	4	0.91	36.4	28	6.5	0.92	49.6	32	4	0.94	33.2	32	6.5
0.92	65.2	26	4	0.95	33.2	28	6.5	0.9	48.9	32	4	0.93	31.5	32	6.5
0.92	58.9	26	4	0.95	35.1	28	6.5	0.92	47.4	32	4	0.96	32.4	32	6.5
0.9	68.3	26	4	0.93	34.9	28	6.5	0.9	49.9	32	4	0.95	33	32	6.5
0.9	62.9	26	4	0.95	38.2	28	6.5	0.94	48.5	32	4	0.93	32.3	32	6.5
0.91	64	26	4	0.96	35.5	28	6.5	0.93	50.4	32	4	0.94	33.5	32	6.5
0.91	66	26	4	0.91	36.5	28	6.5	0.91	48.2	32	4	0.93	33.7	32	6.5
0.91	65.7	26	4	0.94	35.1	28	6.5	0.94	49.5	32	4	0.95	32.2	32	6.5
0.91	66.8	26	4	0.93	34.7	28	6.5	0.88	51.8	32	4	0.95	32.4	32	6.5
0.91	67.6	26	4	0.93	34.8	28	6.5	0.92	47	32	4	0.94	32.1	32	6.5
0.91	63.3	26	4	0.95	36.5	28	6.5	0.91	48.3	32	4	0.97	32.2	32	6.5
0.9	70.1	26	4	0.95	34.8	28	6.5	0.91	49.3	32	4	0.97	30.5	32	6.5
0.92	56.3	26	4	0.96	35.5	28	6.5	0.92	50.3	32	4	0.94	30.3	32	6.5
0.91	61.9	26	4	0.93	34.9	28	6.5	0.91	50.2	32	4	0.96	32.4	32	6.5
0.9	67.6	26	4	0.95	35.9	28	6.5	0.87	58.6	32	4	0.93	30.4	32	6.5
0.91	56	26	4	0.94	35.4	28	6.5	0.94	46.7	32	4	0.95	31.5	32	6.5
0.92	60.2	26	4	0.95	36.5	28	6.5	0.93	50.3	32	4	0.92	35.4	32	6.5
0.92	61.2	26	4	0.96	36.5	28	6.5	0.9	48.8	32	4	0.95	31.5	32	6.5
0.91	66.8	26	4	0.94	37.3	28	6.5	0.93	45.9	32	4	0.94	31.8	32	6.5
0.9	68.5	26	4	0.92	36.3	28	6.5	0.93	49.7	32	4	0.95	30	32	6.5
0.92	57.6	26	4	0.95	36.1	28	6.5	0.93	47	32	4	0.94	32.8	32	6.5
0.91	59.3	26	4	0.93	35.1	28	6.5	0.9	48.6	32	4	0.94	32.3	32	6.5
0.91	62.5	26	4	0.88	40.3	28	6.5	0.93	49.1	32	4	0.96	32.3	32	6.5
0.91	69.7	26	4	0.96	34.4	28	6.5	0.93	49.8	32	4	0.94	31.6	32	6.5
0.91	55.8	26	4	0.93	36.8	28	6.5	0.93	49.5	32	4	0.94	33.4	32	6.5
0.9	71.8	26	4	0.91	40.3	28	6.5	0.92	50.5	32	4	0.95	31.9	32	6.5
0.92	59.9	26	4	0.9	31.6	28	6.5	0.91	48.3	32	4	0.93	32.9	32	6.5
0.9	59.5	26	4	0.95	34	28	6.5	0.94	47.6	32	4	0.96	31.2	32	6.5
0.91	62.5	26	4	0.93	34.8	28	6.5	0.92	50.4	32	4	0.93	30.2	32	6.5
0.9	68.5	26	4	0.93	32.3	28	6.5	0.91	50.1	32	4	0.95	30.7	32	6.5
0.91	69.8	26	4	0.95	37.4	28	6.5	0.92	48.7	32	4	0.95	32.6	32	6.5
0.9	66.4	26	4	0.95	33.8	28	6.5	0.93	48.9	32	4	0.94	31.6	32	6.5
0.92	56.7	26	4	0.96	34.9	28	6.5	0.91	50.8	32	4	0.96	31.1	32	6.5
0.9	61.6	26	4	0.95	34.1	28	6.5	0.87	48.7	32	4	0.97	30.5	32	6.5
0.91	62.8	26	4	0.92	36.8	28	6.5	0.93	46.8	32	4	0.95	32.3	32	6.5
0.9	61.5	26	4	0.92	36.8	28	6.5	0.91	47.5	32	4	0.93	35.2	32	6.5
0.91	63.1	26	4	0.93	33.4	28	6.5	0.91	54.5	32	4	0.95	32.7	32	6.5
0.91	59	26	4	0.93	33.7	28	6.5	0.93	48.5	32	4	0.95	28.8	32	6.5
0.9	67.9	26	4	0.95	34.4	28	6.5	0.93	45.7	32	4	0.93	35.6	32	6.5
0.9	71.9	26	4	0.93	37.3	28	6.5	0.91	50.8	32	4	0.95	30.9	32	6.5
0.91	59.6	26	4	0.92	31.4	28	6.5	0.91	50	32	4	0.95	33	32	6.5
0.9	62.3	26	4	0.93	39.1	28	6.5	0.91	48.5	32	4	0.94	32.1	32	6.5
0.9	66.5	26	4	0.95	33.7	28	6.5	0.88	50.9	32	4	0.94	32.3	32	6.5
0.92	62.7	26	4	0.95	32.9	28	6.5	0.92	47.6	32	4	0.95	36.6	32	6.5
0.9	67.1	26	4	0.92	31.2	28	6.5	0.92	47.6	32	4	0.93	32.5	32	6.5
0.9	58.1	26	4	0.94	35	28	6.5	0.91	47.6	32	4	0.94	32.6	32	6.5
0.9	69	26	4	0.94	33.1	28	6.5	0.92	50.3	32	4	0.96	32.4	32	6.5
0.9	63.5	26	4	0.93	36.4	28	6.5	0.88	51	32	4	0.94	34.2	32	6.5
0.91	59.3	26	4	0.94	34.2	28	6.5	0.92	48.3	32	4	0.93	32.2	32	6.5
0.92	67.1	26	4	0.9	35.9	28	6.5	0.92	50.1	32	4	0.95	32.3	32	6.5
0.9	62	26	4	0.93	34.2	28	6.5	0.92	49.6	32	4	0.96	32.1	32	6.5
0.9	68.3	26	4	0.92	33.8	28	6.5	0.9	49.9	32	4	0.93	33.5	32	6.5
0.92	63.3	26	4	0.93	34.5	28	6.5	0.93	50.3	32	4	0.95	32.3	32	6.5
0.91	63.3	26	4	0.96	35.7	28	6.5	0.93	48.7	32	4	0.94	33.3	32	6.5
0.91	55.9	26	4	0.94	34.9	28	6.5	0.92	47.8	32	4	0.94	32.1	32	6.5
0.9	64.9	26	4	0.95	33.4	28	6.5	0.93	49.2	32	4	0.94	32.9	32	6.5
0.9	70.4	26	4	0.94	38.2	28	6.5	0.9	50.1	32	4	0.92	32.9	32	6.5
0.91	68.5	26	4	0.93	38.4	28	6.5	0.92	49.9	32	4	0.94	33.4	32	6.5
0.9	67	26	4	0.95	33.8	28	6.5	0.92	48.9	32	4	0.93	32.2	32	6.5
0.91	58.6	26	4	0.93	38.7	28	6.5	0.92	49.5	32	4	0.93	35.2	32	6.5
0.91	58.7	26	4	0.93	32.9	28	6.5	0.91	48.5	32	4	0.95	32.1	32	6.5
0.91	63.4	26	4	0.95	34.7	28	6.5	0.91	48.8	32	4	0.95	32.5	32	6.5
0.91	70.5	26	4	0.95	35.7	28	6.5	0.9	48.1	32	4	0.95	34.5	32	6.5
0.91	61.2	26	4	0.9	38.2	28	6.5	0.94	48.9	32	4	0.95	32.9	32	6.5
0.91	56.9	26	4	0.95	34.4	28	6.5	0.92	49.7	32	4	0.96	32.4	32	6.5
0.9	56.2	26	4	0.94	34.1	28	6.5	0.92	48.7	32	4	0.93	33.4	32	6.5
0.93	58.8	26	4	0.94	34.6	28	6.5	0.93	47.5	32	4	0.96	33	32	6.5
0.91	58.3	26	4	0.95	38	28	6.5	0.94	49.3	32	4	0.94	33	32	6.5
0.92	56.7	26	4	0.9	42.8	28	6.5	0.93	46.9	32	4	0.93	32.7	32	6.5

0.9	61.1	26	4
0.91	63.8	26	4
0.91	58.8	26	4
0.92	57.3	26	4
0.9	62.9	26	4
0.91	57.6	26	4
0.91	65.1	26	4
0.9	69.5	26	4
0.9	63.6	26	4
0.91	63.5	26	4
0.9	59.2	26	4
0.9	57	26	4
0.92	57.2	26	4
0.9	63.4	26	4
0.91	64.8	26	4
0.9	64.2	26	4
0.9	67.8	26	4
0.9	59.1	26	4
0.91	61.6	26	4
0.91	63.2	26	4
0.9	65.6	26	4
0.9	68.8	26	4
0.91	63.8	26	4
0.92	50.1	26	4
0.92	57.9	26	4
0.9	67.6	26	4
0.9	61	26	4
0.91	64.1	26	4
0.92	60.6	26	4
0.9	69.7	26	4
0.91	66.6	26	4
0.9	65.1	26	4
0.93	58.1	26	4
0.91	64.8	26	4
0.91	65.6	26	4
0.92	61	26	4
0.9	60.2	26	4
0.9	60.9	26	4
0.9	60.1	26	4
0.9	68.9	26	4
0.91	60.7	26	4
0.9	68.8	26	4
0.92	57.1	26	4
0.92	56.9	26	4
0.91	57.5	26	4
0.92	57.9	26	4
0.91	50.4	26	4
0.92	58.7	26	4
0.92	58.6	26	4
0.92	55.8	26	4
0.93	57.9	26	4
0.93	56.4	26	4
0.93	56.5	26	4
0.93	57.7	26	4
0.92	56.6	26	4
0.91	66.8	26	4
0.92	56.1	26	4
0.91	68.5	26	4
0.91	56.9	26	4
0.92	60.8	26	4
0.91	65.1	26	4
0.93	61.2	26	4
0.9	62.8	26	4
0.92	58.8	26	4
0.91	70.5	26	4
0.9	63.8	26	4
0.91	68.7	26	4
0.91	63	26	4
0.44	34.9	26	6.5
0.23	36.3	26	6.5
0.23	35.8	26	6.5
0.62	36.4	26	6.5
0.58	30	26	6.5
0.63	35.7	26	6.5

0.94	35.9	28	6.5
0.92	36.9	28	6.5
0.94	39	28	6.5
0.93	36.6	28	6.5
0.92	38.4	28	6.5
0.87	35.4	28	6.5
0.95	33.3	28	6.5
0.91	40.1	28	6.5
0.92	36.3	28	6.5
0.94	37.5	28	6.5
0.93	40.4	28	6.5
0.94	39.2	28	6.5
0.92	39.4	28	6.5
0.94	34.2	28	6.5
0.92	41	28	6.5
0.91	40.6	28	6.5
0.95	34.2	28	6.5
0.93	35.5	28	6.5
0.93	39.3	28	6.5
0.91	35	28	6.5
0.93	37.5	28	6.5
0.94	36.6	28	6.5
0.95	35.1	28	6.5
0.93	40.2	28	6.5
0.92	36.8	28	6.5
0.88	36	28	6.5
0.94	38.3	28	6.5
0.96	35.5	28	6.5
0.92	42	28	6.5
0.93	35.2	28	6.5
0.94	38.9	28	6.5
0.91	36.4	28	6.5
0.93	41.5	28	6.5
0.91	39.9	28	6.5
0.93	35.5	28	6.5
0.92	39.5	28	6.5
0.94	35	28	6.5
0.96	35.5	28	6.5
0.96	35.7	28	6.5
0.91	41.6	28	6.5
0.93	35.9	28	6.5
0.9	33.8	28	6.5
0.92	40.1	28	6.5
0.94	35.3	28	6.5
0.91	79	32	1.5
0.85	75.1	32	1.5
0.92	78.7	32	1.5
0.9	78.5	32	1.5
0.9	79.4	32	1.5
0.9	77.1	32	1.5
0.84	82.4	32	1.5
0.91	78.2	32	1.5
0.91	78.3	32	1.5
0.91	78	32	1.5
0.89	77.4	32	1.5
0.86	85.9	32	1.5
0.8	74	32	1.5
0.91	77	32	1.5
0.89	83.3	32	1.5
0.91	79.1	32	1.5
0.86	79.8	32	1.5
0.91	76.9	32	1.5
0.85	82.3	32	1.5
0.89	83.8	32	1.5
0.92	79	32	1.5
0.92	77.8	32	1.5
0.91	78.2	32	1.5
0.9	82.5	32	1.5
0.91	79.6	32	1.5
0.89	79.5	32	1.5
0.9	78.8	32	1.5
0.91	79.1	32	1.5
0.91	78.9	32	1.5
0.89	77.8	32	1.5

0.93	51	32	4
0.92	49.3	32	4
0.92	49.6	32	4
0.92	50	32	4
0.94	49.7	32	4
0.93	49.9	32	4
0.93	48.6	32	4
0.94	48.8	32	4
0.93	49.6	32	4
0.89	50.1	32	4
0.92	45.3	32	4
0.93	49.6	32	4
0.94	47.4	32	4
0.93	47.9	32	4
0.91	49.8	32	4
0.91	53.1	32	4
0.86	48.2	32	4
0.94	47.8	32	4
0.92	50.3	32	4
0.92	50.4	32	4
0.94	48.8	32	4
0.94	48.7	32	4
0.92	46.8	32	4
0.91	50.1	32	4
0.93	48.8	32	4
0.93	48.3	32	4
0.91	50.8	32	4
0.93	50.2	32	4
0.94	48.9	32	4
0.92	50.6	32	4
0.9	49.4	32	4
0.91	49.1	32	4
0.93	49.7	32	4
0.9	50.3	32	4
0.92	48.9	32	4
0.92	49.3	32	4
0.91	51.8	32	4
0.92	49.8	32	4
0.93	49.7	32	4
0.92	51	32	4
0.91	48.6	32	4
0.93	50.1	32	4
0.89	49.1	32	4
0.92	46.3	32	4
0.93	47	32	4
0.91	48.9	32	4
0.9	53	32	4
0.93	49.5	32	4
0.93	48.8	32	4
0.93	49.7	32	4
0.91	46.3	32	4
0.91	49.2	32	4
0.93	50.1	32	4
0.93	49.4	32	4
0.88	50.9	32	4
0.9	51.7	32	4
0.9	50.2	32	4
0.92	48.5	32	4
0.92	48.7	32	4
0.93	48	32	4
0.93	47.7	32	4
0.92	49.8	32	4
0.88	50.5	32	4
0.92	48.3	32	4
0.89	56.1	32	4
0.87	47.3	32	4
0.91	47.9	32	4
0.93	48.7	32	4
0.87	49.4	32	4
0.9	51.3	32	4
0.92	48.7	32	4
0.91	54	32	4
0.87	44.9	32	4
0.9	48.9	32	4
0.91	50.4	32	4

0.97	33	32	6.5
0.92	31.8	32	6.5
0.93	32.8	32	6.5
0.94	33.5	32	6.5
0.95	31	32	6.5
0.94	33.2	32	6.5
0.92	33.5	32	6.5
0.96	31.6	32	6.5
0.93	32.5	32	6.5
0.94	32.8	32	6.5
0.96	34.6	32	6.5
0.95	31.5	32	6.5
0.96	30.4	32	6.5
0.96	32.3	32	6.5
0.93	33.2	32	6.5
0.95	32.6	32	6.5
0.94	31.9	32	6.5
0.94	35.6	32	6.5
0.93	31	32	6.5
0.96	32.5	32	6.5
0.93	33	32	6.5
0.95	32.4	32	6.5
0.95	31.7	32	6.5
0.93	32.7	32	6.5
0.94	32.4	32	6.5
0.93	32.5	32	6.5
0.93	32.1	32	6.5
0.96	32.5	32	6.5
0.94	32	32	6.5
0.93	32.9	32	6.5
0.95	32	32	6.5
0.95	32.5	32	6.5
0.93	32.7	32	6.5
0.95	32.5	32	6.5
0.96	33	32	6.5
0.94	32.5	32	6.5
0.93	34.3	32	6.5
0.93	32	32	6.5
0.93	33	32	6.5
0.94	32.3	32	6.5
0.96	30.3	32	6.5
0.94	31.6	32	6.5
0.95	32.1	32	6.5
0.94	33.6	32	6.5
0.95	32.8	32	6.5
0.95	31.5	32	6.5
0.95	28.2	32	6.5
0.93	32.8	32	6.5
0.94	33	32	6.5
0.95	32	32	6.5
0.95	35.5	32	6.5
0.94	32.6	32	6.5
0.93	33.3	32	6.5
0.96	32.1	32	6.5
0.94	33.4	32	6.5
0.94	37.7	32	6.5
0.96	30.7	32	6.5
0.93	31.6	32	6.5
0.95	32.3	32	6.5
0.96	32.2	32	6.5
0.95	34.7	32	6.5
0.95	30.9	32	6.5
0.95	30.1	32	6.5
0.95	30.9	32	6.5
0.93	31.6	32	6.5
0.95	33.9	32	6.5
0.94	32.9	32	6.5
0.96	31.7	32	6.5
0.93	30.8	32	6.5
0.94	31.6	32	6.5
0.95	32.5	32	6.5
0.95	32.6	32	6.5
0.93	36.1	32	6.5
0.97	33.3	32	6.5
0.94	32.6	32	6.5

0.52	35.7	26	6.5
0.99	30.2	26	6.5
1.02	35.7	26	6.5
0.95	35.3	26	6.5
0.91	35.9	26	6.5
1.1	36.6	26	6.5
0.94	30.7	26	6.5
0.55	34.9	26	6.5
0.44	31.9	26	6.5
1.18	29.2	26	6.5
0.76	35.3	26	6.5
0.38	37.9	26	6.5
0.62	31.5	26	6.5
0.79	30.9	26	6.5
0.43	36.3	26	6.5
0.41	36.2	26	6.5
0.42	36.3	26	6.5
1.14	37	26	6.5
0.35	36.4	26	6.5
1.35	31.8	26	6.5
0.31	36.2	26	6.5
1.42	35.4	26	6.5
0.8	30.5	26	6.5
0.72	35.5	26	6.5
0.67	35.6	26	6.5
1.08	32.5	26	6.5
0.88	35.2	26	6.5
0.5	34.5	26	6.5
1.09	29.8	26	6.5
0.85	29.6	26	6.5
0.92	35.8	26	6.5
0.9	37	26	6.5
0.8	40.1	26	6.5
0.81	35.8	26	6.5
0.64	36.4	26	6.5
0.19	35	26	6.5
0.44	32.7	26	6.5
0.5	31.1	26	6.5
1.16	34	26	6.5
1.29	33.8	26	6.5
0.54	35.8	26	6.5
0.88	35.2	26	6.5
1.07	36.3	26	6.5
0.73	34.6	26	6.5
0.47	31.6	26	6.5
0.48	32.4	26	6.5
0.64	35.6	26	6.5
0.25	36.1	26	6.5
0.8	37	26	6.5
0.42	34.7	26	6.5
0.64	35.3	26	6.5
0.72	34.6	26	6.5
0.74	37.2	26	6.5
0.32	39.4	26	6.5
0.91	39.1	26	6.5
0.94	39.1	26	6.5
0.22	35.1	26	6.5
0.8	36	26	6.5
1.16	32.8	26	6.5
1	35.1	26	6.5
0.46	35.8	26	6.5
0.31	30.4	26	6.5
1.06	35.9	26	6.5
1.03	35.7	26	6.5
0.04	35.4	26	6.5
0.25	36.2	26	6.5
0.69	35.9	26	6.5
0.94	36.4	26	6.5
0.55	36.8	26	6.5
0.8	38.2	26	6.5
0.2	35.1	26	6.5
0.57	36.1	26	6.5
0.64	36.3	26	6.5
0.91	35.8	26	6.5
0.94	37.3	26	6.5

0.88	79.1	32	1.5
0.92	78.7	32	1.5
0.91	79.2	32	1.5
0.92	79.4	32	1.5
0.92	78.6	32	1.5
0.92	78.6	32	1.5
0.89	80.1	32	1.5
0.91	79.7	32	1.5
0.87	81.2	32	1.5
0.87	78.9	32	1.5
0.92	79.4	32	1.5
0.89	78.6	32	1.5
0.9	78	32	1.5
0.91	78.5	32	1.5
0.82	79.4	32	1.5
0.86	80.1	32	1.5
0.89	79	32	1.5
0.86	74.4	32	1.5
0.92	78.9	32	1.5
0.87	80.1	32	1.5
0.86	79.1	32	1.5
0.86	78	32	1.5
0.91	79	32	1.5
0.85	80.5	32	1.5
0.82	79.6	32	1.5
0.9	78.9	32	1.5
0.83	79.4	32	1.5
0.84	79.2	32	1.5
0.88	78	32	1.5
0.88	80.3	32	1.5
0.9	79.5	32	1.5
0.87	89.3	32	1.5
0.91	78.9	32	1.5
0.81	80.5	32	1.5
0.91	78.8	32	1.5
0.9	78.8	32	1.5
0.86	79.2	32	1.5
0.89	79.8	32	1.5
0.87	78.7	32	1.5
0.91	79.7	32	1.5
0.89	86.4	32	1.5
0.91	79	32	1.5
0.88	78.6	32	1.5
0.88	79.4	32	1.5
0.91	79.3	32	1.5
0.9	79	32	1.5
0.87	80.8	32	1.5
0.84	77.8	32	1.5
0.87	80.4	32	1.5
0.81	82.3	32	1.5
0.89	78.7	32	1.5
0.89	80.1	32	1.5
0.86	79.5	32	1.5
0.91	79.1	32	1.5
0.92	76.6	32	1.5
0.9	78.5	32	1.5
0.84	79.5	32	1.5
0.89	79.3	32	1.5
0.86	75.3	32	1.5
0.91	88.2	32	1.5
0.9	83	32	1.5
0.89	78.9	32	1.5
0.89	81.4	32	1.5
0.86	78.7	32	1.5
0.92	77.1	32	1.5
0.85	88.8	32	1.5
0.91	78.8	32	1.5
0.87	80.2	32	1.5
0.91	77.7	32	1.5
0.9	79.9	32	1.5
0.92	77.7	32	1.5
0.89	79.8	32	1.5
0.92	79.1	32	1.5
0.9	78.9	32	1.5
0.9	77.5	32	1.5

0.92	50.7	32	4
0.93	48.6	32	4
0.92	51.6	32	4
0.94	48.4	32	4
0.91	49.4	32	4
0.92	48.8	32	4
0.91	50	32	4
0.91	50.8	32	4
0.89	49.2	32	4
0.92	49	32	4
0.92	49.7	32	4
0.91	50.3	32	4
0.88	48	32	4
0.89	49.6	32	4
0.93	50.1	32	4
0.92	49.6	32	4
0.92	48.3	32	4
0.9	50.6	32	4
0.89	47.4	32	4
0.9	50.3	32	4
0.92	49.7	32	4
0.91	48.9	32	4
0.91	51.1	32	4
0.92	52.3	32	4
0.92	48.8	32	4
0.92	50	32	4
0.91	50.6	32	4
0.88	49.6	32	4
0.93	50.4	32	4
0.87	51.9	32	4
0.93	49.9	32	4
0.87	52.2	32	4
0.91	49.4	32	4
0.9	47.9	32	4
0.91	52.6	32	4
0.92	47.8	32	4
0.92	49.1	32	4
0.93	51	32	4
0.91	45.7	32	4
0.92	49.9	32	4
0.92	47.1	32	4
0.92	48	32	4
0.92	47.3	32	4
0.94	46.8	32	4
0.91	49.4	32	4
0.92	52.3	32	4
0.88	51.1	32	4
0.88	50	32	4
0.91	50.3	32	4
0.92	50.6	32	4
0.93	50	32	4
0.92	48.8	32	4
0.89	48	32	4
0.92	48.7	32	4
0.88	50.1	32	4
0.91	48.1	32	4
0.95	49.2	32	4
0.93	49.2	32	4
0.88	50	32	4
0.93	49.2	32	4
0.92	49.4	32	4
0.9	47.6	32	4
0.92	49.8	32	4
0.92	49.1	32	4
0.88	50.3	32	4
0.93	50.1	32	4
0.87	51.3	32	4
0.93	48.5	32	4
0.9	51.4	32	4
0.92	49.2	32	4
0.87	49.4	32	4
0.92	49.6	32	4
0.92	49.7	32	4
0.93	48.8	32	4
0.93	48.9	32	4

0.94	31.7	32	6.5
0.94	28.9	32	6.5
0.93	33.6	32	6.5
0.95	31.9	32	6.5
0.93	33.1	32	6.5
0.93	32.4	32	6.5
0.94	32.1	32	6.5
0.93	32.4	32	6.5
0.95	31.9	32	6.5
0.95	29.7	32	6.5
0.93	34.7	32	6.5
0.94	33.5	32	6.5
0.95	31.7	32	6.5
0.94	33.1	32	6.5
0.93	32.5	32	6.5
0.98	30.8	32	6.5
0.94	32.3	32	6.5
0.96	32.8	32	6.5
0.93	32.5	32	6.5
0.93	33.4	32	6.5
0.95	32.2	32	6.5
0.94	32.9	32	6.5
0.94	31.6	32	6.5
0.92	32.2	32	6.5
0.97	30.2	32	6.5
0.94	33.3	32	6.5
0.97	31.4	32	6.5
0.94	32.7	32	6.5
0.93	33	32	6.5
0.94	32.7	32	6.5
0.96	32	32	6.5
0.94	32.7	32	6.5
0.93	32.3	32	6.5
0.95	35.4	32	6.5
0.95	32.7	32	6.5
0.95	31.8	32	6.5
0.94	33.5	32	6.5
0.94	32.5	32	6.5
0.96	33.3	32	6.5
0.95	33.4	32	6.5
0.93	33.2	32	6.5
0.94	33.1	32	6.5
0.93	31.1	32	6.5
0.94	33.7	32	6.5
0.94	34.6	32	6.5
0.96	32.4	32	6.5
0.96	31.3	32	6.5
0.96	31.3	32	6.5
0.93	32.8	32	6.5
0.95	31.4	32	6.5
0.95	30.6	32	6.5
0.95	32.7	32	6.5
0.97	32.4	32	6.5
0.92	33.3	32	6.5
0.92	33.7	32	6.5
0.94	32.4	32	6.5
0.94	32.1	32	6.5
0.94	32	32	6.5
0.93	31.1	32	6.5
0.93	33.8	32	6.5
0.94	33.4	32	6.5
0.96	32.7	32	6.5
0.94	32.9	32	6.5
0.94	32.8	32	6.5
0.96	32.5	32	6.5
0.93	34.9	32	6.5
0.94	32.2	32	6.5
0.94	30.8	32	6.5
0.93	31.6	32	6.5
0.93	31.7	32	6.5
0.93	32.2	32	6.5
0.96	32.2	32	6.5
0.94	31.6	32	6.5
0.93	31.1	32	6.5
0.95	33.7	32	6.5

0.99	32	26	6.5	0.88	88.5	32	1.5	0.94	49.9	32	4	0.95	31.8	32	6.5
0.57	36.4	26	6.5	0.92	77.4	32	1.5	0.91	46.7	32	4	0.95	33.7	32	6.5
0.75	35.9	26	6.5	0.91	77	32	1.5	0.93	50.5	32	4	0.94	32.6	32	6.5
0.58	31.5	26	6.5	0.91	82.8	32	1.5	0.9	49.3	32	4	0.93	32.9	32	6.5
0.8	35.8	26	6.5	0.83	78.7	32	1.5	0.93	46.9	32	4	0.94	33	32	6.5
1	36.4	26	6.5	0.87	79.5	32	1.5	0.91	48.8	32	4	0.92	35.4	32	6.5
1.05	39.9	26	6.5	0.87	80.6	32	1.5	0.93	49.5	32	4	0.96	33.2	32	6.5
0.73	34.9	26	6.5	0.88	81.4	32	1.5	0.92	47.9	32	4	0.94	32.8	32	6.5
0.95	31.7	26	6.5	0.9	77.9	32	1.5	0.92	49.7	32	4	0.96	33.1	32	6.5
1.04	33.2	26	6.5	0.88	81.4	32	1.5	0.94	50.2	32	4	0.94	31.8	32	6.5
0.52	35.7	26	6.5	0.9	78.3	32	1.5	0.93	49.8	32	4	0.94	33.5	32	6.5
0.54	35.9	26	6.5	0.92	78.9	32	1.5	0.94	48.6	32	4	0.94	32.3	32	6.5
1.18	35.7	26	6.5	0.85	79	32	1.5	0.92	49.5	32	4	0.95	31.2	32	6.5
0.47	36.5	26	6.5	0.85	79.4	32	1.5	0.93	49.3	32	4	0.93	32.5	32	6.5
0.17	35.6	26	6.5	0.82	80	32	1.5	0.93	49.4	32	4	0.95	32.2	32	6.5
0.77	36.1	26	6.5	0.91	82.6	32	1.5	0.92	50	32	4	0.95	33.5	32	6.5
1.02	36.4	26	6.5	0.92	78	32	1.5	0.9	46.7	32	4	0.94	33.1	32	6.5
0.7	34.8	26	6.5	0.9	78.1	32	1.5	0.93	48.7	32	4	0.92	32.6	32	6.5
0.94	35.4	26	6.5	0.86	79.8	32	1.5	0.91	47.8	32	4	0.93	33.2	32	6.5
0.73	35.7	26	6.5	0.91	80.5	32	1.5	0.91	49.3	32	4	0.94	33.6	32	6.5
0.89	35.1	26	6.5	0.89	83.3	32	1.5	0.93	50.3	32	4	0.95	33.6	32	6.5
1.16	32.2	26	6.5	0.87	79.1	32	1.5	0.92	49.7	32	4	0.96	33.6	32	6.5
0.56	29.7	26	6.5	0.9	77.5	32	1.5	0.93	48.6	32	4	0.94	33.6	32	6.5
0.43	32.2	26	6.5	0.91	77.5	32	1.5	0.87	48.9	32	4	0.92	35	32	6.5
0.53	35.5	26	6.5	0.89	84.1	32	1.5	0.92	49	32	4	0.94	31.6	32	6.5
1.15	36.4	26	6.5	0.86	85.3	32	1.5	0.94	49.9	32	4	0.93	32.8	32	6.5
0.63	35.8	26	6.5	0.91	77.3	32	1.5	0.91	47.5	32	4	0.92	31.7	32	6.5
0.99	31.2	26	6.5	0.92	75.9	32	1.5	0.92	46.2	32	4	0.94	33.7	32	6.5
1.2	35.8	26	6.5	0.84	72.8	32	1.5	0.94	49.7	32	4	0.94	34.9	32	6.5
0.88	34.5	26	6.5	0.9	78.3	32	1.5	0.92	49.1	32	4	0.96	33.6	32	6.5
1.2	36.5	26	6.5	0.84	80.5	32	1.5	0.92	49.4	32	4	0.94	32.4	32	6.5
0.95	34.6	26	6.5	0.89	85.5	32	1.5	0.94	47.3	32	4	0.93	33.6	32	6.5
0.88	35	26	6.5	0.92	80.3	32	1.5	0.92	49.7	32	4	0.95	33.6	32	6.5
1.33	32.9	26	6.5	0.91	79.2	32	1.5	0.91	47.4	32	4	0.93	33.8	32	6.5
0.14	34.3	26	6.5	0.9	78.6	32	1.5	0.89	48.3	32	4	0.95	29.9	32	6.5
0.28	34.6	26	6.5	0.91	78.9	32	1.5	0.92	47.5	32	4	0.95	31.9	32	6.5
0.6	37.4	26	6.5	0.92	78.4	32	1.5	0.9	49.6	32	4	0.93	31.3	32	6.5
0.34	34.3	26	6.5	0.92	76.1	32	1.5	0.88	49.8	32	4	0.94	33.3	32	6.5
0.83	36	26	6.5	0.9	78.5	32	1.5	0.91	49.2	32	4	0.92	33.4	32	6.5
1.21	34.9	26	6.5	0.91	79.3	32	1.5	0.94	50.2	32	4	0.95	32.5	32	6.5
0.84	36.3	26	6.5	0.91	77.7	32	1.5	0.92	49.9	32	4	0.95	31.5	32	6.5
0.21	31.6	26	6.5	0.9	79.5	32	1.5	0.92	47.5	32	4	0.93	31.6	32	6.5
0.5	31.3	26	6.5	0.91	77.3	32	1.5	0.91	48.7	32	4	0.94	31.7	32	6.5
1	26.5	26	6.5	0.92	77.8	32	1.5	0.88	47.1	32	4	0.96	33.2	32	6.5
0.42	35.1	26	6.5	0.91	79.3	32	1.5	0.92	48.9	32	4	0.94	32.3	32	6.5
0.48	37	26	6.5	0.92	77.7	32	1.5	0.93	47.7	32	4	0.94	33.6	32	6.5
0.1	36.2	26	6.5	0.88	78.5	32	1.5	0.93	49.8	32	4	0.96	33.1	32	6.5
1.2	36.6	26	6.5	0.89	79.4	32	1.5	0.92	52.6	32	4	0.95	32.8	32	6.5
0.54	35.1	26	6.5	0.91	77.9	32	1.5	0.93	49.4	32	4	0.94	33	32	6.5
0.91	35.1	26	6.5	0.91	78	32	1.5	0.92	47.3	32	4	0.96	33.3	32	6.5
0.94	35.3	26	6.5	0.86	78.6	32	1.5	0.9	50	32	4	0.92	32.2	32	6.5
0.9	34.8	26	6.5	0.9	77.5	32	1.5	0.92	49.1	32	4	0.94	33.8	32	6.5
0.72	33	26	6.5	0.91	78.5	32	1.5	0.89	51.5	32	4	0.95	33.8	32	6.5
0.65	33.5	26	6.5	0.9	78.4	32	1.5	0.94	49.8	32	4	0.92	33	32	6.5
0.91	35.8	26	6.5	0.89	80.2	32	1.5	0.93	47.4	32	4	0.95	32.3	32	6.5
0.87	36.9	26	6.5	0.9	78.5	32	1.5	0.94	49.8	32	4	0.95	34	32	6.5
0.88	30.7	26	6.5	0.88	84.4	32	1.5	0.9	50.4	32	4	0.96	31.9	32	6.5
0.25	36	26	6.5	0.92	78.3	32	1.5	0.93	48.6	32	4	0.95	33.3	32	6.5
1.13	36.8	26	6.5	0.9	78.6	32	1.5	0.91	48.9	32	4	0.95	33.4	32	6.5
1.11	35.7	26	6.5	0.89	78.2	32	1.5	0.91	50.4	32	4	0.94	31.8	32	6.5
1.02	36	26	6.5	0.81	83.3	32	1.5	0.91	47.5	32	4	0.92	33.3	32	6.5
1.12	35.9	26	6.5	0.92	78.9	32	1.5	0.92	48.9	32	4	0.93	32.6	32	6.5
0.58	36.8	26	6.5	0.88	83.9	32	1.5	0.93	48.8	32	4	0.95	32.3	32	6.5
0.23	34.8	26	6.5	0.91	79.7	32	1.5	0.93	49.8	32	4	0.96	32.4	32	6.5
0.35	36.5	26	6.5	0.92	78.3	32	1.5	0.93	48.6	32	4	0.94	33.1	32	6.5
0.47	35.8	26	6.5	0.91	77.3	32	1.5	0.92	47.9	32	4	0.93	34	32	6.5
1.61	36.1	26	6.5	0.81	82.2	32	1.5	0.92	48.8	32	4	0.94	33.6	32	6.5
0.72	33.2	26	6.5	0.9	79.5	32	1.5	0.9	49	32	4	0.93	33.5	32	6.5
0.89	30.6	26	6.5	0.91	79.2	32	1.5	0.92	50.8	32	4	0.94	33	32	6.5
0.55	37.4	26	6.5	0.87	78	32	1.5	0.91	47.8	32	4	0.95	31.7	32	6.5
0.42	32	26	6.5	0.9	78.3	32	1.5	0.89	55	32	4	0.94	29.7	32	6.5
0.22	32.2	26	6.5	0.9	78.7	32	1.5	0.92	48.3	32	4	0.93	33.6	32	6.5
0.92	38.1	26	6.5	0.89	80.1	32	1.5	0.9	45.6	32	4	0.95	33	32	6.5
0.84	36.8	26	6.5	0.92	78.1	32	1.5	0.93	49	32	4	0.93	32.8	32	6.5
0.66	41.6	26	6.5	0.9	78.3	32	1.5	0.93	48	32	4	0.96	32.9	32	6.5

0.87	34.7	26	6.5
0.71	36.7	26	6.5
0.84	40.4	26	6.5
0.92	35.6	26	6.5
0.65	35.6	26	6.5
0.53	33.2	26	6.5
0.88	32.2	26	6.5
0.89	42.5	26	6.5
0.3	29.1	26	6.5
0.36	33.5	26	6.5
0.82	26.8	26	6.5
0.91	33.8	26	6.5
0.41	36.4	26	6.5
0.61	30.7	26	6.5
0.61	40.9	26	6.5
0.83	35.6	26	6.5
0.99	37.3	26	6.5
0.56	35.5	26	6.5
0.92	35.7	26	6.5
0.88	29.8	26	6.5
0.63	38	26	6.5
1.18	38.3	26	6.5
1.2	37.1	26	6.5
0.72	34.8	26	6.5
0.28	36.5	26	6.5
0.38	36	26	6.5
0.45	27.7	26	6.5
0.6	34.7	26	6.5
0.58	36.5	26	6.5
0.73	40	26	6.5
0.34	37.3	26	6.5
0.88	33.8	26	6.5
0.88	42.6	26	6.5
0.76	38.5	26	6.5
1.29	36.6	26	6.5
0.37	30.5	26	6.5
0.93	35.1	26	6.5
0.86	39.8	26	6.5
1.35	38.5	26	6.5
0.41	29.2	26	6.5
0.27	38.9	26	6.5
0.61	36	26	6.5
0.87	35.4	26	6.5
0.44	34.1	26	6.5
1.35	40.9	26	6.5
0.49	35.9	26	6.5
0.86	42.6	26	6.5
1.44	36.1	26	6.5
0.47	38.7	26	6.5
1.2	36.2	26	6.5
0.88	35.3	26	6.5
0.92	36.4	26	6.5
0.64	35.6	26	6.5
0.93	37.6	26	6.5
0.43	42.3	26	6.5
0.26	37.6	26	6.5
1.32	29.8	26	6.5
0.58	35.4	26	6.5
0.33	34.7	26	6.5
0.48	37.5	26	6.5
1.61	35.4	26	6.5
1.32	35.7	26	6.5
0.76	40.6	26	6.5
1.14	34	26	6.5
1.01	34.4	26	6.5
0.56	39.3	26	6.5
0.95	30.5	26	6.5
0.39	37.2	26	6.5
0.77	27.2	26	6.5
1.21	34.2	26	6.5
0.95	34.6	26	6.5
0.57	35.9	26	6.5
0.66	38	26	6.5
0.4	38.9	26	6.5
0.79	36.2	26	6.5
0.88	78.7	32	1.5
0.83	79	32	1.5
0.91	79.8	32	1.5
0.9	79.5	32	1.5
0.92	77.2	32	1.5
0.91	76.8	32	1.5
0.91	78.9	32	1.5
0.91	77.9	32	1.5
0.89	79.7	32	1.5
0.92	77.8	32	1.5
0.89	79.1	32	1.5
0.9	87.7	32	1.5
0.91	78.3	32	1.5
0.89	79	32	1.5
0.87	79	32	1.5
0.91	78.8	32	1.5
0.86	85.4	32	1.5
0.92	78.1	32	1.5
0.87	79	32	1.5
0.91	79.2	32	1.5
0.92	79.7	32	1.5
0.85	83.1	32	1.5
0.86	79.2	32	1.5
0.88	85.6	32	1.5
0.9	88.2	32	1.5
0.86	79.2	32	1.5
0.88	78.1	32	1.5
0.87	83.1	32	1.5
0.84	80.2	32	1.5
0.9	86.9	32	1.5
0.91	77.3	32	1.5
0.87	80.6	32	1.5
0.85	81	32	1.5
0.9	79.6	32	1.5
0.8	82.2	32	1.5
0.89	79.6	32	1.5
0.89	77.9	32	1.5
0.88	80.2	32	1.5
0.85	82.4	32	1.5
0.82	80.7	32	1.5
0.9	78.1	32	1.5
0.85	86.1	32	1.5
0.81	82.5	32	1.5
0.88	79.6	32	1.5
0.88	89.5	32	1.5
0.91	78.6	32	1.5
0.91	79.1	32	1.5
0.9	77.8	32	1.5
0.88	79.5	32	1.5
0.88	79.7	32	1.5
0.91	76.1	32	1.5
0.84	80.2	32	1.5
0.91	78	32	1.5
0.91	79	32	1.5
0.89	87.1	32	1.5
0.9	85.1	32	1.5
0.88	79.4	32	1.5
0.85	84.2	32	1.5
0.87	81.9	32	1.5
0.88	79.1	32	1.5
0.91	76.9	32	1.5
0.89	80.5	32	1.5
0.87	82.9	32	1.5
0.91	78.4	32	1.5
0.82	82.6	32	1.5
0.91	86.7	32	1.5
0.85	80	32	1.5
0.91	77.3	32	1.5
0.85	83.2	32	1.5
0.9	80.2	32	1.5
0.87	78.8	32	1.5
0.9	76.9	32	1.5
0.86	79.1	32	1.5
0.89	79.7	32	1.5
0.81	79	32	1.5
0.91	47	32	4
0.91	49.7	32	4
0.92	50.1	32	4
0.88	50.3	32	4
0.93	48.4	32	4
0.89	47.1	32	4
0.9	47.9	32	4
0.94	49.1	32	4
0.92	48	32	4
0.92	48	32	4
0.91	48.8	32	4
0.89	49.6	32	4
0.94	47.7	32	4
0.91	48.2	32	4
0.91	49.1	32	4
0.93	47.2	32	4
0.94	47.2	32	4
0.88	51.7	32	4
0.94	48.6	32	4
0.91	48.2	32	4
0.95	50.5	32	4
0.92	50.5	32	4
0.91	48.7	32	4
0.92	50.2	32	4
0.91	49.1	32	4
0.92	48.6	32	4
0.93	48.9	32	4
0.93	48.5	32	4
0.91	49.7	32	4
0.93	47.3	32	4
0.92	49.3	32	4
0.93	50	32	4
0.91	50.1	32	4
0.92	48.8	32	4
0.92	49	32	4
0.92	50.7	32	4
0.91	49.9	32	4
0.93	48.6	32	4
0.92	49.5	32	4
0.91	50.9	32	4
0.92	48.5	32	4
0.92	49.1	32	4
0.91	46.2	32	4
0.93	48.6	32	4
0.91	46.4	32	4
0.9	50.3	32	4
0.94	49.5	32	4
0.95	49.9	32	4
0.9	49.7	32	4
0.91	50.6	32	4
0.94	49	32	4
0.92	48	32	4
0.92	49.5	32	4
0.91	48.5	32	4
0.89	50.6	32	4
0.9	50.8	32	4
0.92	50.4	32	4
0.93	47.4	32	4
0.92	47.9	32	4
0.91	50.3	32	4
0.94	49.8	32	4
0.93	47.9	32	4
0.92	49.2	32	4
0.88	49.1	32	4
0.91	50.4	32	4
0.89	47.8	32	4
0.93	49.9	32	4
0.92	50.1	32	4
0.89	52.1	32	4
0.94	49.6	32	4
0.92	48.1	32	4
0.92	51.3	32	4
0.91	50.3	32	4
0.92	49.4	32	4
0.92	47.4	32	4
0.93	32.5	32	6.5
0.93	37	32	6.5
0.94	33.3	32	6.5
0.93	31.8	32	6.5
0.94	33.3	32	6.5
0.94	33.2	32	6.5
0.94	33.4	32	6.5
0.94	32.9	32	6.5
0.95	32.4	32	6.5
0.95	32.4	32	6.5
0.96	32.3	32	6.5
0.93	33.7	32	6.5
0.94	31	32	6.5
0.96	34.1	32	6.5
0.94	33.1	32	6.5
0.93	36.3	32	6.5
0.93	31.1	32	6.5
0.95	32.3	32	6.5
0.95	32.8	32	6.5
0.94	32.1	32	6.5
0.93	33.3	32	6.5
0.93	34.3	32	6.5
0.93	32.9	32	6.5
0.93	32.7	32	6.5
0.94	32.1	32	6.5
0.94	32.2	32	6.5
0.93	33	32	6.5
0.94	32.2	32	6.5
0.94	32.8	32	6.5
0.96	33.8	32	6.5
0.95	32.6	32	6.5
0.94	33.2	32	6.5
0.95	33.2	32	6.5
0.93	32.1	32	6.5
0.94	33.4	32	6.5
0.94	32.2	32	6.5
0.92	34.1	32	6.5
0.94	32.8	32	6.5
0.96	32.9	32	6.5
0.96	32.8	32	6.5
0.93	36.7	32	6.5
0.93	32.6	32	6.5
0.93	32.7	32	6.5
0.94	32.2	32	6.5
0.93	38	32	6.5
0.96	31.1	32	6.5
0.92	31.2	32	6.5
0.95	33.8	32	6.5
0.95	33.8	32	6.5
0.93	34.4	32	6.5
0.93	32.3	32	6.5
0.97	32.3	32	6.5
0.93	32	32	6.5
0.96	32.3	32	6.5
0.94	32.6	32	6.5
0.93	33.3	32	6.5
0.94	32.5	32	6.5
0.93	34	32	6.5
0.95	32.1	32	6.5
0.96	31.1	32	6.5
0.93	38.8	32	6.5
0.93	33.4	32	6.5
0.93	33.5	32	6.5
0.95	32.6	32	6.5
0.94	34.3	32	6.5
0.96	32.4	32	6.5
0.97	33.7	32	6.5
0.94	32.5	32	6.5
0.95	36.9	32	6.5
0.95	32.9	32	6.5
0.94	30.2	32	6.5
0.95	31.4	32	6.5
0.94	33	32	6.5
0.94	30.2	32	6.5
0.92	33.3	32	6.5

1.39	35.7	26	6.5
0.4	37	26	6.5
0.67	38.1	26	6.5
0.27	35.4	26	6.5
0.88	37.9	26	6.5
1.26	34.8	26	6.5
0.35	35.1	26	6.5
1.07	37.6	26	6.5
0.71	35.2	26	6.5
0.71	34.7	26	6.5
1.08	36.7	26	6.5
0.56	35.9	26	6.5
0.26	36.6	26	6.5
0.29	36.6	26	6.5
0.7	35.9	26	6.5
0.89	36.9	26	6.5
0.88	88.7	28	1.5
0.83	86.4	28	1.5
0.91	85.5	28	1.5
0.88	86.8	28	1.5
0.91	90.1	28	1.5
0.87	88	28	1.5
0.88	88.5	28	1.5
0.91	89.8	28	1.5
0.9	87.6	28	1.5
0.85	87.1	28	1.5
0.9	90.2	28	1.5
0.91	88.9	28	1.5
0.91	87.3	28	1.5
0.9	90.1	28	1.5
0.9	88.7	28	1.5
0.9	93.5	28	1.5
0.9	90.1	28	1.5
0.92	89.9	28	1.5
0.89	90	28	1.5
0.88	87.8	28	1.5
0.87	87.9	28	1.5
0.9	85.9	28	1.5
0.87	88.1	28	1.5
0.92	84.5	28	1.5
0.9	87.8	28	1.5
0.89	87.2	28	1.5
0.9	86.1	28	1.5
0.9	86.1	28	1.5
0.91	86.4	28	1.5
0.91	90.5	28	1.5
0.88	88	28	1.5
0.87	87.8	28	1.5
0.88	83.1	28	1.5
0.91	89	28	1.5
0.83	88	28	1.5
0.9	87.4	28	1.5
0.92	90.7	28	1.5
0.91	89	28	1.5
0.91	89.8	28	1.5
0.91	91.5	28	1.5
0.84	92.6	28	1.5
0.92	91.8	28	1.5
0.9	91.1	28	1.5
0.86	86.3	28	1.5
0.88	86.9	28	1.5
0.9	87.8	28	1.5
0.9	88.2	28	1.5
0.91	87.2	28	1.5
0.87	86	28	1.5
0.87	86.4	28	1.5
0.87	87.7	28	1.5
0.85	97.3	28	1.5
0.89	88.2	28	1.5
0.89	79.1	28	1.5
0.9	87.1	28	1.5
0.9	93.9	28	1.5
0.9	84.7	28	1.5
0.91	87.8	28	1.5

0.87	79.7	32	1.5
0.86	80.8	32	1.5
0.88	79.6	32	1.5
0.82	82.1	32	1.5
0.91	77.6	32	1.5
0.86	87.3	32	1.5
0.84	80	32	1.5
0.9	78	32	1.5
0.91	78.3	32	1.5
0.88	80.4	32	1.5
0.87	80	32	1.5
0.85	79.7	32	1.5
0.86	79.9	32	1.5
0.91	77.7	32	1.5
0.84	79.4	32	1.5
0.92	75.3	32	1.5
0.91	77.8	32	1.5
0.92	77.2	32	1.5
0.91	77.8	32	1.5
0.91	78.7	32	1.5
0.91	78.2	32	1.5
0.87	79	32	1.5
0.91	78.6	32	1.5
0.92	78.4	32	1.5
0.9	79.6	32	1.5
0.91	78.2	32	1.5
0.91	78	32	1.5
0.91	76.6	32	1.5
0.83	79.4	32	1.5
0.92	78.2	32	1.5
0.91	78.6	32	1.5
0.92	78.6	32	1.5
0.92	76.8	32	1.5
0.91	78.8	32	1.5
0.91	79	32	1.5
0.89	78	32	1.5
0.92	78.3	32	1.5
0.91	81	32	1.5
0.91	78.4	32	1.5
0.91	78.3	32	1.5
0.86	84.4	32	1.5
0.91	78.4	32	1.5
0.89	77.4	32	1.5
0.89	78.7	32	1.5
0.91	78.9	32	1.5
0.9	78.9	32	1.5
0.91	77	32	1.5
0.92	78.4	32	1.5
0.92	77.8	32	1.5
0.91	78.8	32	1.5
0.89	80.2	32	1.5
0.9	77.8	32	1.5
0.91	77.3	32	1.5
0.9	79.4	32	1.5
0.9	79.2	32	1.5
0.81	78.9	32	1.5
0.86	79.1	32	1.5
0.89	79.2	32	1.5
0.92	79.2	32	1.5
0.91	79.3	32	1.5
0.91	77.8	32	1.5
0.88	79.7	32	1.5
0.92	78.5	32	1.5
0.91	77.9	32	1.5
0.91	79.1	32	1.5
0.9	78.2	32	1.5
0.93	78.2	32	1.5
0.88	79.8	32	1.5
0.9	79.3	32	1.5
0.91	78.4	32	1.5
0.92	78.5	32	1.5
0.89	74.3	32	1.5
0.91	79.6	32	1.5
0.9	78.8	32	1.5
0.91	78.9	32	1.5

0.92	49.1	32	4
0.88	51.3	32	4
0.91	50.3	32	4
0.9	48.9	32	4
0.93	48.9	32	4
0.92	49.3	32	4
0.9	49.7	32	4
0.91	49.5	32	4
0.89	52.2	32	4
0.92	46.1	32	4
0.91	48.4	32	4
0.9	48.6	32	4
0.91	47.6	32	4
0.93	47.9	32	4
0.92	48.8	32	4
0.9	49.4	32	4
0.92	49.5	32	4
0.89	50.8	32	4
0.9	47.8	32	4
0.93	52.6	32	4
0.89	50	32	4
0.9	48.6	32	4
0.91	49.6	32	4
0.95	47	32	4
0.89	48.1	32	4
0.88	49.7	32	4
0.92	49.9	32	4
0.91	49.4	32	4
0.94	49.1	32	4
0.91	50.2	32	4
0.92	49.7	32	4
0.88	50.1	32	4
0.88	49	32	4
0.93	49.5	32	4
0.93	49.9	32	4
0.92	49.5	32	4
0.93	48.6	32	4
0.9	51	32	4
0.93	48.8	32	4
0.94	48.4	32	4
0.87	48.6	32	4
0.88	48	32	4
0.91	48.5	32	4
0.93	48.7	32	4
0.93	47.7	32	4
0.93	48	32	4
0.93	49.9	32	4
0.95	49.8	32	4
0.9	51.6	32	4
0.93	48.1	32	4
0.92	46.7	32	4
0.91	50.2	32	4
0.93	47.2	32	4
0.93	46.5	32	4
0.93	48.6	32	4
0.91	46.9	32	4
0.92	49.3	32	4
0.92	47.6	32	4
0.93	49.2	32	4
0.92	50	32	4
0.9	49.6	32	4
0.94	49.8	32	4
0.92	48.2	32	4
0.92	49.1	32	4
0.91	48.4	32	4
0.94	49.4	32	4
0.93	50.2	32	4
0.92	49.2	32	4
0.91	49.5	32	4
0.88	50.5	32	4
0.91	46	32	4
0.93	48.7	32	4
0.93	48.4	32	4
0.93	48.4	32	4
0.94	47.9	32	4

0.92	33.3	32	6.5
0.94	32.6	32	6.5
0.93	31.5	32	6.5
0.95	32.6	32	6.5
0.95	31.7	32	6.5
0.94	30.2	32	6.5
0.94	31.7	32	6.5
0.94	33.1	32	6.5
0.94	30.7	32	6.5
0.94	32.3	32	6.5
0.95	32.5	32	6.5
0.93	33	32	6.5
0.95	32.4	32	6.5
0.95	32.2	32	6.5
0.95	33.2	32	6.5
0.93	31.5	32	6.5
0.95	31.3	32	6.5
0.94	31.9	32	6.5
0.94	32.6	32	6.5
0.94	33	32	6.5
0.95	32.1	32	6.5
0.92	31.3	32	6.5
0.95	31.7	32	6.5
0.96	32.4	32	6.5
0.94	33	32	6.5
0.96	33.4	32	6.5
0.96	32	32	6.5
0.93	32.5	32	6.5
0.96	32	32	6.5
0.93	32.3	32	6.5
0.94	33.6	32	6.5
0.93	33.8	32	6.5
0.93	31.7	32	6.5
0.94	33	32	6.5
0.93	32	32	6.5
0.93	32.3	32	6.5
0.93	33.1	32	6.5
0.94	32.5	32	6.5
0.94	33.3	32	6.5
0.94	32.2	32	6.5
0.93	33.3	32	6.5
0.95	32.4	32	6.5
0.94	32.8	32	6.5
0.96	32.6	32	6.5
0.97	32.2	32	6.5
0.96	32.1	32	6.5
0.95	32.1	32	6.5
0.93	32.8	32	6.5
0.95	32.1	32	6.5
0.97	32.2	32	6.5
0.93	32.4	32	6.5
0.96	30.8	32	6.5
0.93	33.4	32	6.5
0.93	32.1	32	6.5
0.96	32.2	32	6.5
0.93	32.2	32	6.5
0.95	31.7	32	6.5
0.94	31.3	32	6.5
0.96	33.3	32	6.5
0.94	31.5	32	6.5
0.97	30.8	32	6.5
0.95	31.8	32	6.5
0.95	31.6	32	6.5
0.96	32.6	32	6.5
0.95	32.1	32	6.5
0.95	32.1	32	6.5
0.95	30.6	32	6.5
0.93	32.6	32	6.5
0.93	31.9	32	6.5
0.95	31.7	32	6.5
0.96	31.5	32	6.5
0.93	32.5	32	6.5
0.96	31.1	32	6.5
0.94	30.6	32	6.5
0.95	32.5	32	6.5

0.88	85.5	28	1.5
0.87	89.4	28	1.5
0.88	89	28	1.5
0.87	85.9	28	1.5
0.9	89.2	28	1.5
0.91	89.2	28	1.5
0.89	88	28	1.5
0.89	88.1	28	1.5
0.9	90.8	28	1.5
0.92	86.2	28	1.5
0.9	89.1	28	1.5
0.92	88.6	28	1.5
0.91	88.4	28	1.5
0.91	88.3	28	1.5
0.91	90.4	28	1.5
0.91	89.1	28	1.5
0.91	86.2	28	1.5
0.83	84.7	28	1.5
0.92	84.7	28	1.5
0.86	90.5	28	1.5
0.91	86.7	28	1.5
0.86	87.8	28	1.5
0.89	86	28	1.5
0.91	86.3	28	1.5
0.84	76.1	28	1.5
0.92	85.4	28	1.5
0.89	87.9	28	1.5
0.91	87.8	28	1.5
0.9	88.3	28	1.5
0.87	86.5	28	1.5
0.91	85.6	28	1.5
0.9	85.8	28	1.5
0.9	88.3	28	1.5
0.89	89.3	28	1.5
0.9	90.8	28	1.5
0.91	88.1	28	1.5
0.89	87.8	28	1.5
0.9	90.7	28	1.5
0.88	76.5	28	1.5
0.91	90.7	28	1.5
0.92	90	28	1.5
0.9	92.3	28	1.5
0.91	92.1	28	1.5
0.9	91.5	28	1.5
0.9	83.9	28	1.5
0.91	88.6	28	1.5
0.91	90.7	28	1.5
0.89	85.4	28	1.5
0.89	85.1	28	1.5
0.9	87.5	28	1.5
0.87	88.6	28	1.5
0.89	84.5	28	1.5
0.9	86.9	28	1.5
0.89	85.7	28	1.5
0.9	87.7	28	1.5
0.91	87.3	28	1.5
0.91	86.3	28	1.5
0.9	88.8	28	1.5
0.9	87.1	28	1.5
0.91	89.3	28	1.5
0.88	87.7	28	1.5
0.91	87.6	28	1.5
0.89	88.7	28	1.5
0.91	86.6	28	1.5
0.92	86.7	28	1.5
0.88	87.3	28	1.5
0.91	92.4	28	1.5
0.87	90.8	28	1.5
0.92	90.5	28	1.5
0.9	90.3	28	1.5
0.9	87.8	28	1.5
0.9	91.7	28	1.5
0.87	94.8	28	1.5
0.92	92.5	28	1.5
0.85	94.8	28	1.5
0.89	78.2	32	1.5
0.92	78	32	1.5
0.92	77.9	32	1.5
0.81	79.8	32	1.5
0.89	78.2	32	1.5
0.9	79.4	32	1.5
0.9	78.9	32	1.5
0.8	78.8	32	1.5
0.89	80.8	32	1.5
0.9	78.8	32	1.5
0.89	79.8	32	1.5
0.9	78.4	32	1.5
0.9	79.4	32	1.5
0.81	83.1	32	1.5
0.85	79	32	1.5
0.89	84.7	32	1.5
0.87	84.1	32	1.5
0.91	77	32	1.5
0.91	78.1	32	1.5
0.91	79	32	1.5
0.91	78.4	32	1.5
0.82	81.1	32	1.5
0.91	77.4	32	1.5
0.85	80.7	32	1.5
0.91	77.4	32	1.5
0.92	77.9	32	1.5
0.91	78.9	32	1.5
0.81	79.7	32	1.5
0.9	80.9	32	1.5
0.9	78.7	32	1.5
0.9	78.2	32	1.5
0.91	78.7	32	1.5
0.87	78.8	32	1.5
0.9	79.7	32	1.5
0.91	76.2	32	1.5
0.89	79.8	32	1.5
0.87	77.6	32	1.5
0.85	83.4	32	1.5
0.82	80.1	32	1.5
0.89	78.6	32	1.5
0.89	79.4	32	1.5
0.84	77.7	32	1.5
0.86	79.3	32	1.5
0.9	79.1	32	1.5
0.9	78.8	32	1.5
0.89	79	32	1.5
0.9	84.5	32	1.5
0.9	83.7	32	1.5
0.87	79.1	32	1.5
0.9	76.8	32	1.5
0.82	80.5	32	1.5
0.9	78.5	32	1.5
0.91	79.3	32	1.5
0.88	80.7	32	1.5
0.92	78	32	1.5
0.87	80.8	32	1.5
0.86	78.3	32	1.5
0.91	77.5	32	1.5
0.9	78.5	32	1.5
0.9	85	32	1.5
0.88	84.3	32	1.5
0.92	80	32	1.5
0.9	78.1	32	1.5
0.9	78.8	32	1.5
0.89	79.7	32	1.5
0.91	77.1	32	1.5
0.9	79	32	1.5
0.86	80	32	1.5
0.83	78.6	32	1.5
0.91	77.4	32	1.5
0.92	76.6	32	1.5
0.89	80.7	32	1.5
0.91	78.5	32	1.5
0.89	79	32	1.5
0.86	79.4	32	1.5
0.93	49.2	32	4
0.94	48.1	32	4
0.92	50.4	32	4
0.91	49.3	32	4
0.93	48.4	32	4
0.92	48.9	32	4
0.93	47.1	32	4
0.92	49.1	32	4
0.9	49.4	32	4
0.92	42.7	32	4
0.9	50.7	32	4
0.93	48	32	4
0.92	48.8	32	4
0.91	47.3	32	4
0.93	49.7	32	4
0.93	47.6	32	4
0.9	49.1	32	4
0.92	52.7	32	4
0.93	48	32	4
0.91	48.3	32	4
0.93	50.3	32	4
0.93	48.6	32	4
0.9	56.2	32	4
0.91	50	32	4
0.91	47.6	32	4
0.92	50.8	32	4
0.9	52	32	4
0.91	49.8	32	4
0.92	48.8	32	4
0.92	49.3	32	4
0.92	47.9	32	4
0.94	45.6	32	4
0.92	54.7	32	4
0.92	45.8	32	4
0.93	48.9	32	4
0.94	48.5	32	4
0.9	50.5	32	4
0.91	46.5	32	4
0.89	51.8	32	4
0.91	46.9	32	4
0.92	47.3	32	4
0.91	47.2	32	4
0.92	49.7	32	4
0.93	50.1	32	4
0.92	48.1	32	4
0.9	50.2	32	4
0.91	47.3	32	4
0.92	49.9	32	4
0.9	48.3	32	4
0.9	49	32	4
0.89	42	32	4
0.93	49.8	32	4
0.91	49	32	4
0.87	51.8	32	4
0.95	49.3	32	4
0.92	49.4	32	4
0.93	49.9	32	4
0.92	49	32	4
0.93	49.4	32	4
0.93	49.3	32	4
0.93	47.4	32	4
0.91	47.6	32	4
0.92	47.4	32	4
0.93	50.6	32	4
0.92	50	32	4
0.93	48.5	32	4
0.92	47.6	32	4
0.89	51	32	4
0.93	47.5	32	4
0.9	52.2	32	4
0.92	48.2	32	4
0.91	49.1	32	4
0.89	50.7	32	4
0.93	50.7	32	4
0.92	49.3	32	4
0.93	30.3	32	6.5
0.95	32.5	32	6.5
0.95	30.9	32	6.5
0.95	33.2	32	6.5
0.93	33.3	32	6.5
0.93	32.7	32	6.5
0.93	31.9	32	6.5
0.93	32.5	32	6.5
0.95	31.8	32	6.5
0.95	32.5	32	6.5
0.95	32	32	6.5
0.96	32.5	32	6.5
0.94	31.6	32	6.5
0.95	30.9	32	6.5
0.94	32.6	32	6.5
0.94	33.5	32	6.5
0.97	30.2	32	6.5
0.94	33.2	32	6.5
0.95	32.4	32	6.5
0.93	32.7	32	6.5
0.95	31.7	32	6.5
0.94	33.8	32	6.5
0.94	32.7	32	6.5
0.95	32.5	32	6.5
0.93	32.2	32	6.5
0.94	32.5	32	6.5
0.94	33.1	32	6.5
0.95	32.6	32	6.5
0.96	31.6	32	6.5
0.94	31	32	6.5
0.94	32.5	32	6.5
0.93	32.2	32	6.5
0.94	32.1	32	6.5
0.96	33.5	32	6.5
0.95	32.2	32	6.5
0.95	32.2	32	6.5
0.93	33	32	6.5
0.94	33.5	32	6.5
0.94	32.9	32	6.5
0.96	32.3	32	6.5
0.94	31.7	32	6.5
0.94	32.1	32	6.5
0.93	31.2	32	6.5
0.93	32.9	32	6.5
0.93	31.4	32	6.5
0.94	31.6	32	6.5
0.94	32.8	32	6.5
0.95	32.3	32	6.5
0.94	30.4	32	6.5
0.95	32.4	32	6.5
0.96	32.4	32	6.5
0.95	31.4	32	6.5
0.95	33.6	32	6.5
0.95	30.7	32	6.5
0.94	32.6	32	6.5
0.94	31	32	6.5
0.94	32.3	32	6.5
0.97	31.2	32	6.5
0.96	32.9	32	6.5
0.96	32.5	32	6.5
0.94	33.9	32	6.5
0.95	32.6	32	6.5
0.96	32.8	32	6.5
0.93	33.4	32	6.5
0.93	33.7	32	6.5
0.94	33.4	32	6.5
0.94	33.1	32	6.5
0.95	32.9	32	6.5
0.95	31.7	32	6.5
0.95	32.1	32	6.5
0.95	32.5	32	6.5
0.95	33.4	32	6.5
0.95	32.7	32	6.5
0.92	32.1	32	6.5
0.94	32.8	32	6.5

0.9	83.7	28	1.5
0.91	91	28	1.5
0.9	89.3	28	1.5
0.87	85.9	28	1.5
0.9	87.4	28	1.5
0.89	86.5	28	1.5
0.91	93	28	1.5
0.9	88.4	28	1.5
0.87	87.2	28	1.5
0.91	88.6	28	1.5
0.88	91.5	28	1.5
0.88	86.7	28	1.5
0.84	87.5	28	1.5
0.89	87.4	28	1.5
0.89	89.3	28	1.5
0.92	86.9	28	1.5
0.9	88.9	28	1.5
0.89	89.8	28	1.5
0.91	89.6	28	1.5
0.89	93	28	1.5
0.9	87.9	28	1.5
0.88	85.7	28	1.5
0.91	90.3	28	1.5
0.89	94.7	28	1.5
0.87	87.5	28	1.5
0.9	93.5	28	1.5
0.9	92.3	28	1.5
0.89	93.6	28	1.5
0.85	86.4	28	1.5
0.87	86.2	28	1.5
0.88	90.2	28	1.5
0.88	91.3	28	1.5
0.87	85.7	28	1.5
0.89	90.1	28	1.5
0.9	91.1	28	1.5
0.89	88.3	28	1.5
0.9	86.8	28	1.5
0.9	88.6	28	1.5
0.88	87.6	28	1.5
0.9	90.2	28	1.5
0.9	94.6	28	1.5
0.89	87.4	28	1.5
0.9	91.2	28	1.5
0.89	88.2	28	1.5
0.91	89.9	28	1.5
0.88	88.7	28	1.5
0.92	88.4	28	1.5
0.9	86.2	28	1.5
0.89	86	28	1.5
0.9	84.5	28	1.5
0.88	86.8	28	1.5
0.89	91.5	28	1.5
0.91	84.9	28	1.5
0.89	89.9	28	1.5
0.9	87.7	28	1.5
0.9	86.5	28	1.5
0.87	88.7	28	1.5
0.9	84.8	28	1.5
0.92	88.8	28	1.5
0.9	89.2	28	1.5
0.9	85.1	28	1.5
0.89	84.3	28	1.5
0.92	89.7	28	1.5
0.9	88.8	28	1.5
0.9	86.2	28	1.5
0.91	87.3	28	1.5
0.9	91.7	28	1.5
0.89	95	28	1.5
0.86	89.1	28	1.5
0.87	87.5	28	1.5
0.87	85.2	28	1.5
0.86	86.9	28	1.5
0.9	87.1	28	1.5
0.88	85.7	28	1.5
0.9	85.8	28	1.5
0.89	79.6	32	1.5
0.91	77.6	32	1.5
0.91	78.3	32	1.5
0.91	78.7	32	1.5
0.92	77.9	32	1.5
0.91	79.1	32	1.5
0.92	78.2	32	1.5
0.92	77.9	32	1.5
0.89	78.9	32	1.5
0.9	75.9	32	1.5
0.92	78.8	32	1.5
0.9	78.9	32	1.5
0.91	79.6	32	1.5
0.9	76.8	32	1.5
0.92	76.6	32	1.5
0.87	79.7	32	1.5
0.9	78.7	32	1.5
0.89	78.4	32	1.5
0.91	77.7	32	1.5
0.92	78.6	32	1.5
0.92	77.9	32	1.5
0.83	81.4	32	1.5
0.91	78	32	1.5
0.89	78.5	32	1.5
0.89	74.9	32	1.5
0.91	78.8	32	1.5
0.9	79.6	32	1.5
0.89	78.4	32	1.5
0.92	74.6	32	1.5
0.91	77	32	1.5
0.88	79.5	32	1.5
0.88	77.9	32	1.5
0.88	79.8	32	1.5
0.91	78.5	32	1.5
0.89	78.5	32	1.5
0.91	78.9	32	1.5
0.88	79.2	32	1.5
0.88	80.4	32	1.5
0.91	79.4	32	1.5
0.9	78.7	32	1.5
0.84	79.6	32	1.5
0.91	77.9	32	1.5
0.85	82.9	32	1.5
0.91	78.6	32	1.5
0.91	88	32	1.5
0.93	78	32	1.5
0.91	79.5	32	1.5
0.86	79.2	32	1.5
0.92	77.8	32	1.5
0.86	82.1	32	1.5
0.81	79.8	32	1.5
0.9	75.1	32	1.5
0.91	79.4	32	1.5
0.88	81.7	32	1.5
0.9	77.7	32	1.5
0.84	84.9	32	1.5
0.92	77.8	32	1.5
0.92	78.9	32	1.5
0.91	77.8	32	1.5
0.88	88.9	32	1.5
0.92	77.4	32	1.5
0.9	77.9	32	1.5
0.9	78.7	32	1.5
0.9	79.2	32	1.5
0.87	82.8	32	1.5
0.86	83.2	32	1.5
0.92	78.7	32	1.5
0.91	78.2	32	1.5
0.91	78.7	32	1.5
0.89	88	32	1.5
0.91	87.6	32	1.5
0.91	78.3	32	1.5
0.91	78.2	32	1.5
0.89	78.5	32	1.5
0.89	79.6	32	1.5
0.92	49.4	32	4
0.91	48	32	4
0.87	50.9	32	4
0.86	48.8	32	4
0.93	49.9	32	4
0.89	50.2	32	4
0.91	51.3	32	4
0.9	51.5	32	4
0.92	52.2	32	4
0.91	49.3	32	4
0.87	50.9	32	4
0.88	55	32	4
0.91	47.7	32	4
0.91	55.4	32	4
0.92	53.3	32	4
0.88	50.4	32	4
0.93	47.8	32	4
0.92	50.1	32	4
0.89	50.7	32	4
0.92	48.9	32	4
0.9	50.9	32	4
0.91	49.4	32	4
0.91	48.4	32	4
0.88	49.9	32	4
0.92	48.1	32	4
0.92	50	32	4
0.92	47.5	32	4
0.92	51.1	32	4
0.92	54.8	32	4
0.88	50.1	32	4
0.92	48	32	4
0.93	48.1	32	4
0.91	48.8	32	4
0.94	46.6	32	4
0.93	51.2	32	4
0.91	50.3	32	4
0.86	50.9	32	4
0.94	49.9	32	4
0.93	50	32	4
0.93	48.4	32	4
0.92	49.8	32	4
0.89	49	32	4
0.88	50.6	32	4
0.93	50.2	32	4
0.93	51.1	32	4
0.86	56.9	32	4
0.89	51.2	32	4
0.91	50.2	32	4
0.9	49.4	32	4
0.91	49.4	32	4
0.93	49.9	32	4
0.93	49.7	32	4
0.92	50.5	32	4
0.94	46.9	32	4
0.93	49.6	32	4
0.93	49.9	32	4
0.94	46.5	32	4
0.92	48.4	32	4
0.91	50.1	32	4
0.92	47.6	32	4
0.91	50.2	32	4
0.93	49.4	32	4
0.94	46.8	32	4
0.91	49.3	32	4
0.89	51.2	32	4
0.92	48.8	32	4
0.92	48.7	32	4
0.91	48.9	32	4
0.94	50.6	32	4
0.91	49.2	32	4
0.9	51.2	32	4
0.92	51.3	32	4
0.93	47	32	4
0.89	59.2	32	4
0.94	47.5	32	4
0.96	32.5	32	6.5
0.92	33	32	6.5
0.96	32.7	32	6.5
0.96	32.4	32	6.5
0.94	32.1	32	6.5
0.92	32.3	32	6.5
0.93	30	32	6.5
0.94	31.2	32	6.5
0.96	32.1	32	6.5
0.95	33	32	6.5
0.94	32.7	32	6.5
0.96	32	32	6.5
0.95	32	32	6.5
0.94	31.5	32	6.5
0.93	33.3	32	6.5
0.96	31.3	32	6.5
0.95	33.2	32	6.5
0.94	33.3	32	6.5
0.92	32.9	32	6.5
0.95	32	32	6.5
0.93	33.2	32	6.5
0.94	33.5	32	6.5
0.94	32.9	32	6.5
0.92	32.8	32	6.5
0.94	33.2	32	6.5
0.95	33.4	32	6.5
0.96	32.6	32	6.5
0.93	34.1	32	6.5
0.93	31.5	32	6.5
0.95	31	32	6.5
0.95	33	32	6.5
0.94	31.6	32	6.5
0.94	30.8	32	6.5
0.95	31.6	32	6.5
0.95	31.4	32	6.5
0.96	30	32	6.5
0.96	33.1	32	6.5
0.92	31.1	32	6.5
0.96	32.4	32	6.5
0.95	32.4	32	6.5
0.95	33	32	6.5
0.94	32.8	32	6.5
0.94	31	32	6.5
0.98	33.1	32	6.5
0.94	30	32	6.5
0.94	33.1	32	6.5
0.95	33	32	6.5
0.97	33.3	32	6.5
0.95	33.7	32	6.5
0.93	31.7	32	6.5
0.94	34.7	32	6.5
0.93	34.1	32	6.5
0.96	33.8	32	6.5
0.95	33.1	32	6.5
0.95	32.4	32	6.5
0.97	32.5	32	6.5
0.94	33.8	32	6.5
0.94	33.9	32	6.5
0.94	32.8	32	6.5
0.93	33.4	32	6.5
0.94	33.4	32	6.5
0.93	32.7	32	6.5
0.95	33.6	32	6.5
0.94	32.1	32	6.5
0.94	32.2	32	6.5
0.94	32.5	32	6.5
0.94	33	32	6.5
0.94	33.5	32	6.5
0.97	31.7	32	6.5
0.94	33.5	32	6.5
0.97	32.8	32	6.5
0.93	31.8	32	6.5
0.93	32.2	32	6.5
0.94	32.9	32	6.5
0.93	33.2	32	6.5

0.82	88.7	28	1.5
0.91	84.9	28	1.5
0.87	86.8	28	1.5
0.9	87.9	28	1.5
0.9	87.9	28	1.5
0.91	88.5	28	1.5
0.9	87	28	1.5
0.9	88	28	1.5
0.82	86.9	28	1.5
0.89	88.7	28	1.5
0.9	91	28	1.5
0.88	87.7	28	1.5
0.91	89.1	28	1.5
0.88	87.3	28	1.5
0.9	87.3	28	1.5
0.89	86.1	28	1.5
0.91	88.6	28	1.5
0.9	89.2	28	1.5
0.89	93.3	28	1.5
0.89	84.7	28	1.5
0.9	85.2	28	1.5
0.88	85.6	28	1.5
0.84	84.9	28	1.5
0.89	88.5	28	1.5
0.86	86.1	28	1.5
0.9	84.8	28	1.5
0.9	85.2	28	1.5
0.91	87.4	28	1.5
0.9	86.2	28	1.5
0.87	88.4	28	1.5
0.86	86.4	28	1.5
0.91	93.6	28	1.5
0.89	88.4	28	1.5
0.89	87.7	28	1.5
0.9	87	28	1.5
0.89	86.4	28	1.5
0.89	86.3	28	1.5
0.91	88.2	28	1.5
0.86	90.4	28	1.5
0.92	50.3	28	4
0.91	49.4	28	4
0.92	49.6	28	4
0.91	49.6	28	4
0.9	51.2	28	4
0.92	49.9	28	4
0.91	50.6	28	4
0.92	48.5	28	4
0.93	48	28	4
0.92	50.7	28	4
0.93	50.8	28	4
0.94	48.8	28	4
0.93	49.1	28	4
0.93	51.2	28	4
0.92	50.9	28	4
0.94	50.1	28	4
0.89	52.4	28	4
0.92	52.8	28	4
0.92	49.2	28	4
0.92	49.4	28	4
0.92	48.5	28	4
0.92	49	28	4
0.89	53.3	28	4
0.94	49.7	28	4
0.9	49.7	28	4
0.93	50.8	28	4
0.94	50.2	28	4
0.93	49.6	28	4
0.91	49.7	28	4
0.92	49.7	28	4
0.92	49.5	28	4
0.93	48.8	28	4
0.92	51	28	4
0.9	52.6	28	4
0.92	49.4	28	4

0.87	83.6	32	1.5
0.85	79.2	32	1.5
0.87	80.2	32	1.5
0.91	79.3	32	1.5
0.9	87	32	1.5
0.89	79.1	32	1.5
0.82	79.8	32	1.5
0.85	80.2	32	1.5
0.86	81.2	32	1.5
0.9	78.6	32	1.5
0.92	77.9	32	1.5
0.91	78.5	32	1.5
0.87	80.7	32	1.5
0.91	78.3	32	1.5
0.87	80.5	32	1.5
0.82	78.8	32	1.5
0.88	77.3	32	1.5
0.89	81.8	32	1.5
0.85	79.4	32	1.5
0.87	79.7	32	1.5
0.87	79.7	32	1.5
0.84	79.4	32	1.5
0.9	79.8	32	1.5
0.89	78.1	32	1.5
0.82	79.4	32	1.5
0.88	88.7	32	1.5
0.84	79.8	32	1.5
0.91	77.9	32	1.5
0.88	78.9	32	1.5
0.9	78.7	32	1.5
0.89	79.5	32	1.5
0.85	80	32	1.5
0.88	79.4	32	1.5
0.87	85.5	32	1.5
0.84	80.4	32	1.5
0.81	78.5	32	1.5
0.91	75.9	32	1.5
0.9	79.9	32	1.5
0.9	78.3	32	1.5
0.92	77.1	32	1.5
0.84	84.8	32	1.5
0.89	79	32	1.5
0.86	79.4	32	1.5
0.92	77.8	32	1.5
0.93	76.7	32	1.5
0.91	79.6	32	1.5
0.9	77.9	32	1.5
0.91	76.6	32	1.5
0.91	77.9	32	1.5
0.89	77.5	32	1.5
0.92	78	32	1.5
0.84	78.9	32	1.5
0.9	78.9	32	1.5
0.91	78.7	32	1.5
0.9	77	32	1.5
0.92	78	32	1.5
0.84	80.9	32	1.5
0.88	78.8	32	1.5
0.81	85.7	32	1.5
0.9	80.1	32	1.5
0.91	78.6	32	1.5
0.89	78.1	32	1.5
0.89	78.2	32	1.5
0.87	83.5	32	1.5
0.86	79.9	32	1.5
0.91	77.6	32	1.5
0.91	77.7	32	1.5
0.86	80.4	32	1.5
0.84	89.2	32	1.5
0.91	77.3	32	1.5
0.92	78.7	32	1.5
0.92	78.6	32	1.5
0.88	78.8	32	1.5
0.86	81.2	32	1.5
0.9	78.2	32	1.5

0.92	49.2	32	4
0.92	51.1	32	4
0.93	48	32	4
0.92	49.8	32	4
0.93	48	32	4
0.93	49.6	32	4
0.93	49.6	32	4
0.94	47.8	32	4
0.93	46	32	4
0.94	49	32	4
0.93	48.1	32	4
0.9	49.9	32	4
0.93	48.5	32	4
0.92	47.9	32	4
0.9	49.5	32	4
0.94	46.2	32	4
0.92	50.4	32	4
0.92	46.6	32	4
0.89	56.9	32	4
0.92	48.1	32	4
0.92	50.6	32	4
0.94	47.5	32	4
0.91	53.4	32	4
0.93	47.1	32	4
0.9	48.2	32	4
0.93	49.7	32	4
0.93	50.4	32	4
0.89	49.7	32	4
0.87	51.4	32	4
0.93	48	32	4
0.9	48	32	4
0.92	49.5	32	4
0.93	49.9	32	4
0.94	48.1	32	4
0.92	48.3	32	4
0.91	49	32	4
0.92	47.7	32	4
0.93	49.4	32	4
0.92	50.2	32	4
0.93	50.1	32	4
0.88	53.7	32	4
0.92	49.2	32	4
0.94	49.7	32	4
0.91	49.8	32	4
0.92	49.2	32	4
0.91	48.2	32	4
0.93	48.2	32	4
0.92	50.3	32	4
0.91	47.1	32	4
0.89	46.6	32	4
0.92	48	32	4
0.9	49.5	32	4
0.93	48	32	4
0.91	48.6	32	4
0.92	49.3	32	4
0.91	49	32	4
0.93	49.4	32	4
0.92	48.4	32	4
0.92	47.5	32	4
0.9	47	32	4
0.86	49.9	32	4
0.9	48.1	32	4
0.87	49.2	32	4
0.91	50.7	32	4
0.93	49.4	32	4
0.94	34	32	6.5
0.94	32.2	32	6.5
0.92	33.6	32	6.5
0.94	33.9	32	6.5
0.94	33.6	32	6.5
0.93	33	32	6.5
0.96	29.7	32	6.5
0.96	34.2	32	6.5
0.94	33	32	6.5

0.95	31.4	32	6.5
0.93	33	32	6.5
0.96	30.8	32	6.5
0.95	32.2	32	6.5
0.95	32.6	32	6.5
0.92	32.5	32	6.5
0.95	33	32	6.5
0.94	31.4	32	6.5
0.95	33.2	32	6.5
0.95	32.7	32	6.5
0.95	32.8	32	6.5
0.96	33	32	6.5
0.96	33.7	32	6.5
0.97	32.8	32	6.5
0.94	32.3	32	6.5
0.93	32.1	32	6.5
0.94	33.3	32	6.5
0.95	33.1	32	6.5
0.95	32.6	32	6.5
0.92	32.9	32	6.5
0.96	32.9	32	6.5
0.93	32.9	32	6.5
0.95	31.5	32	6.5
0.93	33.3	32	6.5
0.94	32.6	32	6.5
0.93	32.8	32	6.5
0.96	33.4	32	6.5
0.93	31.1	32	6.5
0.95	30.9	32	6.5
0.95	33.7	32	6.5
0.97	31.9	32	6.5
0.95	34	32	6.5
0.94	33	32	6.5
0.94	33.9	32	6.5
0.93	31.1	32	6.5
0.94	32.9	32	6.5
0.96	32.8	32	6.5
0.92	33.3	32	6.5
0.95	31.6	32	6.5
0.95	32.2	32	6.5
0.96	31.6	32	6.5
0.95	31.4	32	6.5
0.94	29.4	32	6.5
0.93	31	32	6.5
0.95	32.8	32	6.5
0.97	29.6	32	6.5
0.96	33.1	32	6.5
0.96	33.1	32	6.5
0.92	36	32	6.5
0.94	28.6	32	6.5
0.96	32.9	32	6.5
0.92	34.6	32	6.5
0.94	32.8	32	6.5
0.92	34.1	32	6.5
0.95	30	32	6.5
0.93	33.8	32	6.5
0.95	29.9	32	6.5
0.93	33.8	32	6.5
0.97	27.6	32	6.5
0.94	28.8	32	6.5
0.95	28	32	6.5
0.96	31.1	32	6.5
0.93	35.2	32	6.5
0.94	34.3	32	6.5
0.96	33.1	32	6.5
0.94	32.7	32	6.5
0.94	33	32	6.5
0.94	35	32	6.5
0.93	32.7	32	6.5
0.95	32.1	32	6.5
0.92	32.5	32	6.5
0.93	32.9	32	6.5
0.95	33	32	6.5
0.94	32.1	32	6.5
0.95	32.3	32	6.5

0.92	51.5	28	4
0.94	50.5	28	4
0.94	49.1	28	4
0.88	54.3	28	4
0.93	52.7	28	4
0.93	48.8	28	4
0.91	53	28	4
0.9	52.3	28	4
0.94	48.6	28	4
0.88	53.6	28	4
0.93	49.4	28	4
0.92	52.7	28	4
0.93	49.3	28	4
0.92	49.9	28	4
0.91	49.9	28	4
0.93	50.2	28	4
0.93	52.6	28	4
0.91	50.2	28	4
0.91	48.8	28	4
0.94	50.5	28	4
0.92	49.2	28	4
0.93	50.6	28	4
0.89	49.6	28	4
0.93	49.9	28	4
0.93	51.1	28	4
0.89	50.7	28	4
0.92	52.1	28	4
0.93	50.2	28	4
0.91	50.3	28	4
0.93	50.7	28	4
0.89	51.1	28	4
0.93	47.7	28	4
0.94	51.2	28	4
0.94	48.2	28	4
0.93	49.1	28	4
0.91	49.4	28	4
0.93	49	28	4
0.93	48.1	28	4
0.89	52	28	4
0.93	50.6	28	4
0.93	51.6	28	4
0.92	52.1	28	4
0.92	47.8	28	4
0.92	49.7	28	4
0.91	48	28	4
0.92	49.1	28	4
0.93	47.7	28	4
0.91	49.3	28	4
0.93	49.7	28	4
0.93	48.1	28	4
0.93	48.5	28	4
0.91	48.6	28	4
0.94	49.3	28	4
0.93	48.6	28	4
0.93	49	28	4
0.92	48.6	28	4
0.92	48.9	28	4
0.93	49	28	4
0.92	49.8	28	4
0.93	50.7	28	4
0.92	50.2	28	4
0.93	50.4	28	4
0.93	49.6	28	4
0.94	48.9	28	4
0.92	49.4	28	4
0.93	49.2	28	4
0.92	49.9	28	4
0.93	49.1	28	4
0.92	49.2	28	4
0.92	50.6	28	4
0.91	49.2	28	4
0.93	48.2	28	4
0.92	50.5	28	4
0.92	50.6	28	4
0.91	49.5	28	4
0.92	78.8	32	1.5
0.91	79	32	1.5
0.87	84	32	1.5
0.9	78.5	32	1.5
0.92	78.1	32	1.5
0.91	77.3	32	1.5
0.91	75.5	32	1.5
0.88	79.1	32	1.5
0.92	77.2	32	1.5
0.91	78.2	32	1.5
0.88	78.9	32	1.5
0.89	79.5	32	1.5
0.92	76.8	32	1.5
0.85	84.6	32	1.5
0.88	78.6	32	1.5
0.89	79.6	32	1.5
0.85	80.8	32	1.5
0.89	79.1	32	1.5
0.91	77.5	32	1.5
0.88	81.4	32	1.5
0.91	80.2	32	1.5
0.91	79	32	1.5
0.91	79.7	32	1.5
0.89	78.2	32	1.5
0.89	78	32	1.5
0.89	78.7	32	1.5
0.91	78.4	32	1.5
0.88	79.4	32	1.5
0.9	78.1	32	1.5
0.85	86.5	32	1.5
0.92	78.7	32	1.5
0.92	78	32	1.5
0.89	79.3	32	1.5
0.9	79.9	32	1.5
0.91	78.1	32	1.5
0.91	78.8	32	1.5
0.89	79.2	32	1.5
0.87	79.2	32	1.5
0.9	79.2	32	1.5
0.9	79	32	1.5
0.9	78.5	32	1.5
0.91	79.5	32	1.5
0.86	83.2	32	1.5
0.88	77	32	1.5
0.89	78.4	32	1.5
0.84	79.3	32	1.5
0.8	84.4	32	1.5
0.9	78.2	32	1.5
0.87	87.4	32	1.5
0.9	77.3	32	1.5
0.8	81.2	32	1.5
0.86	80.4	32	1.5
0.89	78.3	32	1.5
0.84	80.4	32	1.5
0.87	80.9	32	1.5
0.88	80	32	1.5
0.87	76.6	32	1.5
0.91	77.8	32	1.5
0.91	78.4	32	1.5
0.84	80.4	32	1.5
0.87	79.8	32	1.5
0.86	79.2	32	1.5
0.81	82.4	32	1.5
0.81	81.8	32	1.5
0.87	80.3	32	1.5
0.89	80.7	32	1.5
0.87	85.7	32	1.5
0.89	81.4	32	1.5
0.85	87.3	32	1.5
0.81	78	32	1.5
0.88	78.6	32	1.5
0.86	85.7	32	1.5
0.88	80.5	32	1.5
0.88	80.7	32	1.5
0.87	80.9	32	1.5
0.96	32.6	32	6.5
0.93	32.6	32	6.5
0.94	31.9	32	6.5
0.95	31.1	32	6.5
0.95	33	32	6.5
0.95	32.8	32	6.5
0.95	33	32	6.5
0.93	32.5	32	6.5
0.95	33.1	32	6.5
0.94	31.6	32	6.5
0.95	31.3	32	6.5
0.96	33.5	32	6.5
0.94	32.1	32	6.5
0.92	35.4	32	6.5
0.93	37.1	32	6.5
0.94	31.6	32	6.5
0.93	32	32	6.5
0.94	32.9	32	6.5
0.93	32.3	32	6.5
0.94	32.6	32	6.5
0.94	31.5	32	6.5
0.95	32.8	32	6.5
0.94	31.6	32	6.5
0.93	33.1	32	6.5
0.94	34.8	32	6.5
0.95	32.9	32	6.5
0.95	34.3	32	6.5
0.94	33.2	32	6.5
0.94	34	32	6.5
0.96	33.1	32	6.5
0.96	33.6	32	6.5
0.94	33.2	32	6.5
0.95	32.6	32	6.5
0.94	32.5	32	6.5
0.95	33.4	32	6.5
0.94	33.3	32	6.5
0.94	33	32	6.5
0.94	32.3	32	6.5
0.95	30.9	32	6.5
0.97	30.8	32	6.5
0.95	32	32	6.5
0.93	33.7	32	6.5
0.95	33.2	32	6.5
0.93	33.5	32	6.5
0.93	37	32	6.5
0.92	32	32	6.5
0.96	32.1	32	6.5
0.94	34	32	6.5
0.93	32	32	6.5
0.93	33.1	32	6.5
0.95	33.6	32	6.5
0.95	32.3	32	6.5
0.96	32.9	32	6.5
0.94	33.4	32	6.5
0.95	32.3	32	6.5
0.94	33.7	32	6.5
0.95	32.4	32	6.5
0.94	32	32	6.5
0.95	33.6	32	6.5
0.93	30.5	32	6.5
0.94	33	32	6.5
0.94	32.9	32	6.5
0.94	32.3	32	6.5
0.93	33.4	32	6.5
0.96	35	32	6.5
0.93	32.7	32	6.5
0.94	32.5	32	6.5
0.94	32.6	32	6.5
0.96	33.6	32	6.5
0.94	37.5	32	6.5
0.95	33.2	32	6.5
0.95	32.5	32	6.5
0.94	35.2	32	6.5
0.95	32.1	32	6.5
0.94	33.3	32	6.5
0.96	31	32	6.5
0.94	34.5	32	6.5
0.93	31.1	32	6.5
0.93	38.1	32	6.5
0.94	32.9	32	6.5
0.93	32.9	32	6.5
0.93	32	32	6.5
0.93	33.5	32	6.5
0.95	33	32	6.5
0.95	32.6	32	6.5
0.94	29.9	32	6.5
0.95	33.1	32	6.5
0.95	32.1	32	6.5
0.96	32.7	32	6.5
0.96	32.4	32	6.5
0.94	33	32	6.5
0.94	33.5	32	6.5
0.96	32	32	6.5
0.94	33.1	32	6.5
0.95	31.5	32	6.5
0.95	32.3	32	6.5
0.96	33.3	32	6.5
0.94	32.4	32	6.5
0.94	32	32	6.5
0.95	33.1	32	6.5
0.93	33	32	6.5
0.95	33.2	32	6.5
0.94	31	32	6.5
0.95	32	32	6.5
0.93	33	32	6.5
0.96	32	32	6.5
0.92	34.1	32	6.5
0.95	31.5	32	6.5
0.94	32.2	32	6.5
0.95	32.3	32	6.5
0.94	31.2	32	6.5
0.95	30.7	32	6.5
0.95	33.2	32	6.5
0.96	32.8	32	6.5
0.94	32.7	32	6.5
0.94	33	32	6.5
0.95	33.4	32	6.5
0.95	32	32	6.5
0.95	31.7	32	6.5
0.95	31.4	32	6.5
0.95	31.8	32	6.5
0.93	27.7	32	6.5
0.93	32.2	32	6.5
0.94	33.4	32	6.5
0.96	31.5	32	6.5
0.95	31.7	32	6.5
0.95	32.1	32	6.5
0.96	32.4	32	6.5
0.93	34.5	32	6.5
0.95	30.9	32	6.5
0.95	34.2	32	6.5
0.94	32.5	32	6.5
0.94	31.8	32	6.5
0.95	29.4	32	6.5
0.92	31.7	32	6.5
0.93	31	32	6.5
0.95	32.4	32	6.5
0.96	31.7	32	6.5
0.96	32.2	32	6.5
0.96	31.3	32	6.5
0.95	32.4	32	6.5
0.94	33.2	32	6.5
0.95	30.6	32	6.5
0.95	33.1	32	6.5
0.93	33.8	32	6.5
0.95	31.9	32	6.5
0.94	33.2	32	6.5
0.94	33.5	32	6.5
0.96	31.1	32	6.5
0.92	28.2	32	6.5

0.93	49.1	28	4
0.89	54	28	4
0.93	48.4	28	4
0.92	47.7	28	4
0.92	45.7	28	4
0.9	48.5	28	4
0.9	54.8	28	4
0.93	48.5	28	4
0.93	49.7	28	4
0.94	47.8	28	4
0.94	49.9	28	4
0.9	48.5	28	4
0.93	48.6	28	4
0.91	45.8	28	4
0.93	49.6	28	4
0.91	48.2	28	4
0.93	50.2	28	4
0.9	53.8	28	4
0.92	50.4	28	4
0.91	51.4	28	4
0.89	54.4	28	4
0.94	47.7	28	4
0.93	51.1	28	4
0.92	49.7	28	4
0.92	48.6	28	4
0.92	54.8	28	4
0.9	50.4	28	4
0.9	51	28	4
0.92	49.4	28	4
0.9	50.9	28	4
0.94	49.6	28	4
0.91	51	28	4
0.93	52	28	4
0.94	51.3	28	4
0.9	50.5	28	4
0.93	50.6	28	4
0.9	50.2	28	4
0.93	50	28	4
0.94	49.9	28	4
0.91	54	28	4
0.93	51.1	28	4
0.92	51.3	28	4
0.93	51.7	28	4
0.92	51.6	28	4
0.93	54.6	28	4
0.94	48.7	28	4
0.91	52.2	28	4
0.9	51.4	28	4
0.93	48.9	28	4
0.92	53.1	28	4
0.91	48.8	28	4
0.92	50.8	28	4
0.93	49.4	28	4
0.92	49.2	28	4
0.93	52.8	28	4
0.91	49.5	28	4
0.93	49.5	28	4
0.93	49.8	28	4
0.93	49.6	28	4
0.94	49.7	28	4
0.93	51.1	28	4
0.92	49.9	28	4
0.89	49.5	28	4
0.93	49.2	28	4
0.92	51.1	28	4
0.9	50.9	28	4
0.92	49.8	28	4
0.93	49.3	28	4
0.92	49.4	28	4
0.93	49.3	28	4
0.91	49.5	28	4
0.91	49.5	28	4
0.93	49.5	28	4
0.92	50.6	28	4
0.92	49.3	28	4

0.85	79	32	1.5
0.92	76.6	32	1.5
0.89	78.7	32	1.5
0.93	77.5	32	1.5
0.91	79.9	32	1.5
0.92	77.1	32	1.5
0.82	81.5	32	1.5
0.9	78.4	32	1.5
0.88	80.3	32	1.5
0.81	77	32	1.5
0.81	80.2	32	1.5
0.89	78.5	32	1.5
0.88	83	32	1.5
0.86	83.1	32	1.5
0.85	79	32	1.5
0.91	77.4	32	1.5
0.8	83.7	32	1.5
0.88	81.7	32	1.5
0.91	77.6	32	1.5
0.88	78.8	32	1.5
0.88	78.2	32	1.5
0.89	83.7	32	1.5
0.86	85.4	32	1.5
0.92	79.2	32	1.5
0.91	83.3	32	1.5
0.88	77.6	32	1.5
0.9	84.1	32	1.5
0.81	81.4	32	1.5
0.91	76.9	32	1.5
0.87	87.3	32	1.5
0.86	79.8	32	1.5
0.9	78.9	32	1.5
0.89	85.4	32	1.5
0.89	78.4	32	1.5
0.92	78.4	32	1.5
0.88	83.8	32	1.5
0.9	77.2	32	1.5
0.92	77.9	32	1.5
0.92	76.8	32	1.5
0.91	77	32	1.5
0.91	79.2	32	1.5
0.92	78.8	32	1.5
0.89	85.5	32	1.5
0.9	78.8	32	1.5
0.88	82.5	32	1.5
0.86	80.7	32	1.5
0.87	83.7	32	1.5
0.9	77.5	32	1.5
0.93	77.4	32	1.5
0.91	77.5	32	1.5
0.8	80.8	32	1.5
0.83	76.2	32	1.5
0.85	85.4	32	1.5
0.88	85.7	32	1.5
0.87	79.3	32	1.5
0.91	78.1	32	1.5
0.92	79.6	32	1.5
0.86	84.2	32	1.5
0.85	78.6	32	1.5
0.9	79.5	32	1.5
0.92	78.2	32	1.5
0.92	78.8	32	1.5
0.88	85.7	32	1.5
0.92	84.5	32	1.5
0.92	79.2	32	1.5
0.89	78.5	32	1.5
0.89	78.7	32	1.5
0.86	78.7	32	1.5
0.89	80.3	32	1.5
0.91	78.2	32	1.5
0.92	78	32	1.5
0.91	79	32	1.5
0.89	80.2	32	1.5
0.85	84.9	32	1.5
0.89	79.8	32	1.5

0.94	32.4	32	6.5
0.93	34	32	6.5
0.93	34.9	32	6.5
0.92	33.3	32	6.5
0.95	33.8	32	6.5
0.94	33.9	32	6.5
0.95	32.1	32	6.5
0.95	31.5	32	6.5
0.94	32.8	32	6.5
0.95	33.1	32	6.5
0.95	33.1	32	6.5
0.96	32.5	32	6.5
0.95	30.9	32	6.5
0.95	32.9	32	6.5
0.95	32.5	32	6.5
0.93	33.3	32	6.5
0.96	33.3	32	6.5
0.94	33.7	32	6.5
0.92	34	32	6.5
0.94	32.5	32	6.5
0.95	33.9	32	6.5
0.94	32.7	32	6.5
0.94	33.4	32	6.5
0.93	32.6	32	6.5
0.96	32.3	32	6.5
0.92	36.8	32	6.5
0.95	32.2	32	6.5
0.95	33.7	32	6.5
0.94	33.2	32	6.5
0.94	31.9	32	6.5
0.93	33.1	32	6.5
0.93	29.8	32	6.5
0.95	32.5	32	6.5
0.93	33.7	32	6.5
0.96	33.5	32	6.5
0.94	33.6	32	6.5
0.96	33.4	32	6.5
0.93	33.3	32	6.5
0.95	32.6	32	6.5
0.96	34.7	32	6.5
0.95	32.7	32	6.5
0.94	37.8	32	6.5
0.95	32.8	32	6.5
0.94	33.6	32	6.5
0.94	38.4	32	6.5
0.94	30.7	32	6.5
0.93	33.5	32	6.5
0.93	32.2	32	6.5
0.94	33.7	32	6.5
0.92	32.9	32	6.5
0.95	32.5	32	6.5
0.95	33.1	32	6.5
0.93	32.8	32	6.5
0.95	34.1	32	6.5
0.96	33.6	32	6.5
0.95	33	32	6.5
0.97	33.7	32	6.5
0.96	33.3	32	6.5
0.95	33.6	32	6.5
0.93	33.7	32	6.5
0.96	33.6	32	6.5
0.95	33.5	32	6.5
0.93	34.5	32	6.5
0.95	34.1	32	6.5
0.96	32.5	32	6.5
0.93	34.1	32	6.5
0.96	31	32	6.5
0.94	33.9	32	6.5
0.95	32.3	32	6.5
0.93	33.3	32	6.5
0.94	33.9	32	6.5
0.93	35.2	32	6.5
0.94	34.3	32	6.5
0.95	32.3	32	6.5
0.93	34.1	32	6.5

0.94	31.5	32	6.5
0.95	30.9	32	6.5
0.95	32.9	32	6.5
0.95	32.4	32	6.5
0.96	32.4	32	6.5
0.92	32.3	32	6.5
0.95	31	32	6.5
0.93	32.3	32	6.5
0.94	31.2	32	6.5
0.92	32.7	32	6.5
0.95	31.5	32	6.5
0.94	31.8	32	6.5
0.95	33.8	32	6.5
0.94	31.6	32	6.5
0.96	31.5	32	6.5
0.94	34.1	32	6.5
0.96	28.1	32	6.5
0.95	31.6	32	6.5
0.95	31.8	32	6.5
0.93	32	32	6.5
0.96	31.3	32	6.5
0.92	31	32	6.5
0.95	33	32	6.5
0.94	31.7	32	6.5
0.96	33.6	32	6.5
0.95	30.6	32	6.5
0.94	33.3	32	6.5
0.95	30.4	32	6.5
0.96	32.8	32	6.5
0.96	32.5	32	6.5
0.94	31.7	32	6.5
0.94	32.6	32	6.5
0.96	32.8	32	6.5
0.94	34.7	32	6.5
0.94	32.6	32	6.5
0.95	32.9	32	6.5
0.95	32.5	32	6.5
0.94	32.4	32	6.5
0.92	32.2	32	6.5
0.93	32	32	6.5
0.93	33.7	32	6.5
0.93	32.8	32	6.5
0.94	33.4	32	6.5
0.95	32.3	32	6.5
0.95	32.5	32	6.5
0.94	32.7	32	6.5
0.95	32.5	32	6.5
0.93	32.5	32	6.5
0.95	32.9	32	6.5
0.95	32.8	32	6.5
0.95	30.9	32	6.5
0.96	33.3	32	6.5
0.94	31.9	32	6.5
0.96	31.1	32	6.5
0.95	32.5	32	6.5
0.95	32.5	32	6.5
0.93	31.3	32	6.5
0.93	31.1	32	6.5
0.95	32.9	32	6.5
0.93	33.5	32	6.5
0.95	33.6	32	6.5
0.93	30.9	32	6.5
0.94	33.2	32	6.5
0.96	32.3	32	6.5
0.94	31.9	32	6.5
0.95	30.5	32	6.5
0.94	30.7	32	6.5
0.94	34.1	32	6.5
0.95	33.4	32	6.5
0.93	33.2	32	6.5
0.94	31.7	32	6.5
0.94	32.1	32	6.5
0.93	33.5	32	6.5
0.94	31.8	32	6.5
0.94	32.4	32	6.5

0.93	49.6	28	4	0.91	78.8	32	1.5	0.96	33.5	32	6.5	0.96	33.1	32	6.5
0.93	49.2	28	4	0.91	78.7	32	1.5	0.96	31.4	32	6.5	0.96	32.3	32	6.5
0.95	50.4	28	4	0.9	78.1	32	1.5	0.94	33.5	32	6.5	0.95	31.2	32	6.5
0.9	50.7	28	4	0.92	78.4	32	1.5	0.93	33.9	32	6.5	0.93	31	32	6.5
0.93	50.3	28	4	0.84	80.4	32	1.5	0.94	34.3	32	6.5	0.92	32.5	32	6.5
0.9	50.2	28	4	0.83	79.2	32	1.5	0.94	34.3	32	6.5	0.94	32.5	32	6.5
0.94	48.4	28	4	0.9	78	32	1.5	0.94	32.8	32	6.5	0.96	31.6	32	6.5
0.94	50.2	28	4	0.92	77.4	32	1.5	0.95	31.2	32	6.5	0.96	33.1	32	6.5
0.92	49.3	28	4	0.91	81	32	1.5	0.92	32.9	32	6.5	0.95	31.9	32	6.5
0.93	49.8	28	4	0.89	78	32	1.5	0.93	33.1	32	6.5	0.94	32.6	32	6.5
0.92	50.5	28	4	0.89	79.9	32	1.5	0.94	34.1	32	6.5	0.94	32.4	32	6.5
0.94	50.1	28	4	0.9	77.9	32	1.5	0.95	31.4	32	6.5	0.95	32.5	32	6.5
0.93	50.1	28	4	0.91	78.5	32	1.5	0.95	32.2	32	6.5	0.93	33.9	32	6.5
0.93	49.4	28	4	0.9	78.8	32	1.5	0.92	34.6	32	6.5	0.94	32.5	32	6.5
0.93	50	28	4	0.88	81.5	32	1.5	0.95	32.3	32	6.5	0.93	35	32	6.5
0.93	49.4	28	4	0.82	80	32	1.5	0.93	32.5	32	6.5	0.96	31.1	32	6.5
0.9	50.1	28	4	0.89	84.8	32	1.5	0.95	32.9	32	6.5	0.94	32.9	32	6.5
0.93	49.2	28	4	0.9	79	32	1.5	0.94	34.7	32	6.5	0.94	31.9	32	6.5
0.93	49.9	28	4	0.86	85.4	32	1.5	0.97	33.4	32	6.5	0.95	31.6	32	6.5
0.9	50.2	28	4	0.86	85.3	32	1.5	0.94	38.5	32	6.5	0.96	33.3	32	6.5
0.92	50.6	28	4	0.85	85.2	32	1.5	0.95	35.3	32	6.5	0.94	32.4	32	6.5
0.94	51.4	28	4	0.91	78.9	32	1.5	0.95	34.1	32	6.5	0.95	32.3	32	6.5
0.93	50	28	4	0.86	86.9	32	1.5	0.93	34.5	32	6.5	0.95	32.6	32	6.5
0.92	50.3	28	4	0.88	82.9	32	1.5	0.93	33.4	32	6.5	0.94	29.4	32	6.5
0.94	49.4	28	4	0.87	80.1	32	1.5	0.94	33.3	32	6.5	0.96	31	32	6.5
0.93	50.9	28	4	0.82	81	32	1.5	0.94	32.5	32	6.5	0.95	32.6	32	6.5
0.93	50.5	28	4	0.88	78.7	32	1.5	0.94	34.1	32	6.5	0.95	30.9	32	6.5
0.93	50.8	28	4	0.91	81.7	32	1.5	0.95	33.1	32	6.5	0.95	32.4	32	6.5
0.93	50.4	28	4	0.92	77.9	32	1.5	0.93	33.9	32	6.5	0.93	32.5	32	6.5
0.92	50.1	28	4	0.89	79	32	1.5	0.95	33.5	32	6.5	0.93	32	32	6.5
0.93	50.5	28	4	0.86	81.3	32	1.5	0.95	31.8	32	6.5	0.94	32.8	32	6.5
0.9	50.5	28	4	0.9	81.6	32	1.5	0.94	31.7	32	6.5	0.95	33.4	32	6.5
0.93	51.6	28	4	0.92	76.9	32	1.5	0.95	34.1	32	6.5	0.95	32.8	32	6.5
0.92	49	28	4	0.92	77.4	32	1.5	0.94	33.8	32	6.5	0.94	33	32	6.5
0.93	51.1	28	4	0.81	79.4	32	1.5	0.94	33.2	32	6.5	0.95	33.9	32	6.5
0.91	49.6	28	4	0.91	79	32	1.5	0.95	33.1	32	6.5	0.93	33.1	32	6.5
0.91	49.2	28	4	0.82	80.3	32	1.5	0.93	34.2	32	6.5	0.97	33	32	6.5
0.93	49.7	28	4	0.85	79.9	32	1.5	0.94	32.8	32	6.5	0.92	33.2	32	6.5
0.92	51.2	28	4	0.88	79	32	1.5	0.95	33.2	32	6.5	0.96	33.1	32	6.5
0.91	49.7	28	4	0.91	77.8	32	1.5	0.95	32.7	32	6.5	0.94	32.7	32	6.5
0.89	50.3	28	4	0.88	75.2	32	1.5	0.93	32.2	32	6.5	0.94	32.9	32	6.5
0.93	48.8	28	4	0.9	87.8	32	1.5	0.93	32.8	32	6.5	0.95	31.3	32	6.5
0.93	49.1	28	4	0.8	88.4	32	1.5	0.95	33.6	32	6.5	0.94	32	32	6.5
0.94	49.7	28	4	0.92	77.5	32	1.5	0.92	32.7	32	6.5	0.93	33.4	32	6.5
0.92	49.3	28	4	0.9	77.8	32	1.5	0.93	34.1	32	6.5	0.93	32.3	32	6.5
0.92	51.5	28	4	0.87	72.8	32	1.5	0.95	34.8	32	6.5	0.95	27.3	32	6.5
0.92	50.5	28	4	0.91	79.3	32	1.5	0.93	33.7	32	6.5	0.94	32.7	32	6.5
0.92	49.8	28	4	0.89	78.8	32	1.5	0.92	33.5	32	6.5	0.94	30.3	32	6.5
0.94	49.6	28	4	0.82	72.2	32	1.5	0.93	33.1	32	6.5	0.93	31.8	32	6.5
0.93	49.4	28	4	0.91	78.7	32	1.5	0.95	33.6	32	6.5	0.94	32.1	32	6.5
0.93	49.8	28	4	0.91	78.8	32	1.5	0.92	33.1	32	6.5	0.94	31.5	32	6.5
0.92	50.4	28	4	0.91	77.9	32	1.5	0.97	32.2	32	6.5	0.94	32.6	32	6.5
0.88	49	28	4	0.83	80.4	32	1.5	0.96	34	32	6.5	0.94	34.5	32	6.5
0.91	49.2	28	4	0.87	79.8	32	1.5	0.95	32.5	32	6.5	0.95	32.6	32	6.5
0.93	49.2	28	4	0.9	78.9	32	1.5	0.94	32.5	32	6.5	0.95	33.5	32	6.5
0.93	47.3	28	4	0.85	78.7	32	1.5	0.94	33.9	32	6.5	0.96	33.3	32	6.5
0.93	50.9	28	4	0.88	73.8	32	1.5	0.93	34	32	6.5	0.94	34.7	32	6.5
0.93	49.7	28	4	0.91	77.8	32	1.5	0.95	34.1	32	6.5	0.96	32.2	32	6.5
0.93	50.3	28	4	0.86	80.5	32	1.5	0.93	33	32	6.5	0.94	33.3	32	6.5
0.92	49.1	28	4	0.92	79.1	32	1.5	0.94	33.4	32	6.5	0.96	32.9	32	6.5
0.92	50	28	4	0.92	76.9	32	1.5	0.97	32.9	32	6.5	0.93	30.3	32	6.5
0.91	50.5	28	4	0.9	79.2	32	1.5	0.95	33.4	32	6.5	0.95	33.9	32	6.5
0.93	49.6	28	4	0.81	78.9	32	1.5	0.95	31.4	32	6.5	0.94	32.9	32	6.5
0.92	49	28	4	0.92	79.5	32	1.5	0.93	33.6	32	6.5	0.94	32.5	32	6.5
0.92	50.1	28	4	0.91	78.9	32	1.5	0.95	32.3	32	6.5	0.96	32.1	32	6.5
0.93	48.8	28	4	0.92	78.7	32	1.5	0.94	32.1	32	6.5	0.92	32.7	32	6.5
0.93	49.9	28	4	0.89	83.5	32	1.5	0.94	34.4	32	6.5	0.97	31.3	32	6.5
0.93	50.6	28	4	0.92	78.1	32	1.5	0.96	32.6	32	6.5	0.95	31.9	32	6.5
0.94	49.8	28	4	0.9	79	32	1.5	0.94	31.7	32	6.5	0.92	31.5	32	6.5
0.93	50.4	28	4	0.89	79.1	32	1.5	0.95	32.8	32	6.5	0.94	32.5	32	6.5
0.9	49.8	28	4	0.89	77.2	32	1.5	0.94	32.9	32	6.5	0.93	31.8	32	6.5
0.9	50.8	28	4	0.91	78.1	32	1.5	0.94	31.7	32	6.5	0.94	30.6	32	6.5
0.9	52.5	28	4	0.92	76.3	32	1.5	0.93	35.1	32	6.5	0.96	32.6	32	6.5
0.93	50.1	28	4	0.88	79.4	32	1.5	0.93	33.7	32	6.5	0.96	33.9	32	6.5
0.92	51.8	28	4	0.85	78.7	32	1.5	0.94	33.2	32	6.5	0.95	31.7	32	6.5

0.93	50.8	28	4
0.93	50	28	4
0.93	48.5	28	4
0.91	51.4	28	4
0.91	50	28	4
0.88	51.3	28	4
0.94	47.8	28	4
0.91	48.9	28	4
0.94	51	28	4
0.92	52.9	28	4
0.92	50.2	28	4
0.93	52.3	28	4
0.92	51.5	28	4
0.92	48.6	28	4
0.92	52.9	28	4
0.93	52.9	28	4
0.93	48.9	28	4
0.92	48.7	28	4
0.92	50.4	28	4
0.93	49.2	28	4
0.92	50.2	28	4
0.93	49.7	28	4
0.94	48.9	28	4
0.93	49.8	28	4
0.93	48.9	28	4
0.92	49.6	28	4
0.92	48.7	28	4
0.92	49.7	28	4
0.9	50.9	28	4
0.93	48.6	28	4
0.93	50.3	28	4
0.93	49.3	28	4
0.93	50.7	28	4
0.91	49.8	28	4
0.93	50	28	4
0.92	49.3	28	4
0.9	50	28	4
0.93	50.4	28	4
0.94	49.5	28	4
0.88	52.2	28	4
0.93	49.9	28	4
0.92	50.3	28	4
0.92	50	28	4
0.92	49.6	28	4
0.93	50.9	28	4
0.92	52.5	28	4
0.93	51	28	4
0.93	50.4	28	4
0.93	50.1	28	4
0.93	50.3	28	4
0.92	51.4	28	4
0.93	50.9	28	4
0.93	52.2	28	4
0.9	49.9	28	4
0.92	49.9	28	4
0.94	49.1	28	4
0.93	49.6	28	4
0.92	49.7	28	4
0.89	51.6	28	4

0.92	78.1	32	1.5
0.9	79.4	32	1.5
0.91	77.9	32	1.5
0.9	79.2	32	1.5
0.88	78.5	32	1.5
0.92	75.7	32	1.5
0.92	77.2	32	1.5
0.9	78.6	32	1.5
0.88	77.4	32	1.5
0.89	78.8	32	1.5
0.91	77.6	32	1.5
0.91	78.2	32	1.5
0.91	78.8	32	1.5
0.92	78.6	32	1.5
0.9	78.3	32	1.5
0.92	78.8	32	1.5
0.92	78.6	32	1.5
0.91	78.1	32	1.5
0.87	79.3	32	1.5
0.91	76.5	32	1.5
0.86	78.2	32	1.5
0.84	79.2	32	1.5
0.86	78.8	32	1.5
0.88	78.8	32	1.5
0.91	78	32	1.5
0.87	82.4	32	1.5
0.92	77.6	32	1.5
0.87	84.8	32	1.5
0.91	77	32	1.5
0.8	82.5	32	1.5
0.91	79.3	32	1.5
0.8	80.8	32	1.5
0.91	78.7	32	1.5
0.92	78.6	32	1.5
0.92	79	32	1.5
0.88	80.9	32	1.5
0.84	80.2	32	1.5
0.83	84.2	32	1.5
0.87	81	32	1.5
0.89	78.6	32	1.5
0.82	79.8	32	1.5
0.9	78.1	32	1.5
0.8	80.8	32	1.5
0.91	78.8	32	1.5
0.84	79.6	32	1.5
0.91	78.5	32	1.5
0.92	77.1	32	1.5
0.91	80.4	32	1.5
0.91	78.4	32	1.5
0.88	79.1	32	1.5
0.88	78.7	32	1.5
0.91	78.5	32	1.5
0.9	80	32	1.5
0.86	78.7	32	1.5
0.86	76.2	32	1.5
0.81	79.8	32	1.5
0.87	78.1	32	1.5
0.89	79.4	32	1.5
0.84	79.7	32	1.5

0.95	33.1	32	6.5
0.92	34.7	32	6.5
0.93	34.2	32	6.5
0.95	33.9	32	6.5
0.95	32.9	32	6.5
0.95	32.3	32	6.5
0.93	32.5	32	6.5
0.96	29.3	32	6.5
0.93	30.2	32	6.5
0.92	33.3	32	6.5
0.95	35.4	32	6.5
0.94	32.8	32	6.5
0.95	34.8	32	6.5
0.92	34.6	32	6.5
0.94	34	32	6.5
0.94	34.6	32	6.5
0.92	34.4	32	6.5
0.94	34.5	32	6.5
0.96	33.5	32	6.5
0.95	32.5	32	6.5
0.95	33.4	32	6.5
0.96	32.1	32	6.5
0.95	36.6	32	6.5
0.94	34.5	32	6.5
0.93	32.8	32	6.5
0.93	34.1	32	6.5
0.94	33.1	32	6.5
0.94	31.3	32	6.5
0.94	32.2	32	6.5
0.92	33.5	32	6.5
0.93	33.3	32	6.5
0.96	31	32	6.5
0.93	33	32	6.5
0.96	31.5	32	6.5
0.93	35.2	32	6.5
0.94	30.1	32	6.5
0.94	33.5	32	6.5
0.93	32.6	32	6.5
0.93	31.5	32	6.5
0.93	34	32	6.5
0.97	33.6	32	6.5
0.94	33.8	32	6.5
0.94	32.7	32	6.5
0.93	31.4	32	6.5
0.94	33.8	32	6.5
0.94	34.8	32	6.5
0.95	32.3	32	6.5
0.96	33.1	32	6.5
0.93	33.7	32	6.5
0.93	33.7	32	6.5
0.93	33.1	32	6.5
0.95	33.3	32	6.5
0.95	34.1	32	6.5
0.95	33.4	32	6.5
0.94	32.6	32	6.5
0.94	36.2	32	6.5
0.94	33.3	32	6.5
0.93	31.7	32	6.5
0.92	32.5	32	6.5

0.93	33.1	32	6.5
0.92	32.1	32	6.5
0.95	33.3	32	6.5
0.93	32.8	32	6.5
0.93	31.1	32	6.5
0.94	31	32	6.5
0.93	32.9	32	6.5
0.92	33.1	32	6.5
0.96	32.3	32	6.5
0.95	34	32	6.5
0.94	33	32	6.5
0.95	33.1	32	6.5
0.96	33.8	32	6.5
0.93	29.4	32	6.5
0.95	33.8	32	6.5
0.94	29.8	32	6.5
0.95	32.9	32	6.5
0.93	33.5	32	6.5
0.96	33.1	32	6.5
0.93	33.6	32	6.5
0.95	35.2	32	6.5
0.95	32.6	32	6.5
0.95	34.3	32	6.5
0.94	32.9	32	6.5
0.94	33.3	32	6.5
0.95	34.5	32	6.5
0.94	33.4	32	6.5
0.94	33.1	32	6.5
0.94	33.8	32	6.5
0.92	31.4	32	6.5
0.97	33.2	32	6.5
0.94	31.1	32	6.5
0.93	34	32	6.5
0.96	33.6	32	6.5
0.94	33.3	32	6.5
0.93	35.2	32	6.5
0.93	34.3	32	6.5
0.95	33.7	32	6.5
0.95	33.4	32	6.5
0.94	32.6	32	6.5
0.94	32.8	32	6.5
0.95	32.6	32	6.5
0.95	32.7	32	6.5
0.94	34.1	32	6.5
0.95	33.1	32	6.5
0.95	33.5	32	6.5
0.94	30.6	32	6.5
0.93	33.8	32	6.5
0.94	34.7	32	6.5
0.93	35.2	32	6.5
0.96	34.8	32	6.5
0.97	30.2	32	6.5
0.94	36.7	32	6.5
0.95	32.9	32	6.5
0.92	32.9	32	6.5
0.94	32.7	32	6.5

Bibliography

[1] National Academies Press, Radioisotope Power Systems: An Imperative for Maintaining U.S. Leadership in Space Exploration, 2009.

[2] Commonly Asked Questions About Radioisotope Power Systems - Space Batteries, Idaho National Laboratory, 2005.

[3] M.K. A. Duncan, Properties and Behavior of Pu-238 Relevant to Decontamination of Building 235-F, Savannah River Nuclear Solutions, 2009.

[4] M.B. Reed, M.T. Swanson, T. Gillett, Reactor On - Thematic Study of Savannah River's Five Reactor Areas, New South Associates, 2010.

[5] Office of Oversight, T. Rollow, Type A Accident Investigation of the March 16, 2000 Plutonium-238 Multiple Intake Event at the Plutonium Facility Los Alamos National Laboratory, U.S. Department of Energy, Office of Environment, Safety, and Health, 2000.

[6] Department of Energy, Germantown, MD. National Nuclear Security Administration, Type B Accident Investigation of the August 5, 2003 Plutonium-238 Multiple Uptake Event at the Plutonium Facility, Los Alamos National Laboratory, New Mexico, Technical Information Center Oak Ridge Tennessee, 2003.

[7] United States, Report of an Investigation into Deterioration of the Plutonium Fuel Form Fabrication Facility (PuFF) at the DOE Savannah River Site, U.S. Dept. of Energy, Office of Nuclear Safety ; Available to the public from the National Technical Information Service, Washington, D.C., Springfield, VA, 1991.

[8] Nuclear Battery - Thermocouple Type First Quarterly Report January 1, 1957 to March 31, 1957, U. S. Army Signal Engineering Laboratory, 1957.

[9] R. Shor, R.H. Lafferty, P.S. Baker, Strontium-90 Heat Sources, Oak Ridge National Laboratory, 1971.

[10] G. Bennett, E.W. Johnson, American Institute of Aeronautics and Astronautics, Dayton, Ohio, 2003.

[11] G.A. Burney, P.K. Smith, Controlled PuO_2 Particle Size from Pu(III) Oxalate Precipitation, Savannah River Laboratory, 1984.

[12] P.K. Smith, G.A. Burney, D.T. Rankin, D.F. Bickford, R.D. Sisson, in:, Berkeley, CA, 1976.

[13] D.T. Rankin, G.A. Burney, Williamsburg, VA, 1974, pp. 1061–1065.

[14] G. Silver, Plutonium Oxalates as Sources of Plutonium Dioxide, Los Alamos National Laboratory, 1990.

[15] V.K. Rao, I.C. Pius, M. Subbarao, A. Chinnusamy, P.R. Natarajan, J. Radioanal. Nucl. Chem. 100 (1986) 129.

[16] J.A. Porter, A.E. Symonds, Precipitation of Plutonium(III) Oxalate and Calcination to Plutonium Dioxide, Savannah River Laboratory, 1965.

[17] S.G. Abrahamson, J Inorg Nucl Chem 29 (1966) 842.

[18] R.A. Kent, LASL Fabrication Flowsheet for GPHS Fuel Pellets, Los Alamos Scientific Laboratory, 1979.

[19] M. Borland, S. Frank, P. Lessing, D.F. Bickford, R. Cannon, K. Chidester, T. Wheeler, B. Cowell, B. Patton, J. Brown, J. Huling, A. Duncan, L. Seward, W. West, Ida. Natl. Lab. INLEXT-08-14017 (2008).

[20] J.W. Congdon, Physical Behavior of Pu-238 Oxide, Westinghouse Savannah River Company, 1996.
[21] A.S. Icenhour, Transport of Radioactive Material by Alpha Recoil, Oak Ridge National Laboratory, 2005.
[22] A.L. Serandour, N. Tsapis, C. Gervelas, G. Grillon, M. Frechou, J.R. Deverre, H. Benech, E. Fattal, P. Fritsch, J.L. Poncy, Radiat. Prot. Dosimetry 127 (2007) 472.
[23] D.E. Ferguson, Chemical Technology Division Annual Progress Report for Period Ending May 31, 1968, Oak Ridge National Laboratory, 1968.
[24] P.A. Haas, C.C. Haws, F.G. Kitts, A.D. Ryon, in:, Oak Ridge National Laboratory, Turin, Italy, 1967.
[25] P.A. Haas, W.J. Lackey, Improved Size Uniformity of Sol-Gel Spheres by Imposing a Vibration on the Sol in Dispersion Nozzles, Oak Ridge National Laboratory, 1973.
[26] M.H. Lloyd, E.J. Kosiancic, Investigation of Denitration of High-Nitrate Plutonia Sols by Baking, Oak Ridge National Laboratory, 1966.
[27] R.G. Wymer, Laboratory and Engineering Studies of Sol-Gel Processes at Oak Ridge National Laboratory, Oak Ridge National Laboratory, 1968.
[28] J.P. McBride, Laboratory Studies of Sol-Gel Processes at the Oak Ridge National Laboratory, Oak Ridge National Laboratory, 1967.
[29] R.G. Wymer, Preliminary Studies of the Preparation of UO_2 Microspheres by a Sol-Gel Technique, Oak Ridge National Laboratory, 1965.
[30] P.A. Haas, Sol-Gel Preparation of Spheres: Design and Operation of Fluidized Bed Columns, Oak Ridge National Laboratory, 1969.
[31] P.A. Haas, W.D. Bond, M.H. Lloyd, J.P. McBride, Gatlinburg, Tennessee, 1966.
[32] R.G. Wymer, Sol-Gel Processes at Oak Ridge National Laboratory: Development, Demonstration, and Irradiation Tests, Oak Ridge National Laboratory, 1973.
[33] D.D. Sood, J. Sol-Gel Sci. Technol. 59 (2011) 404.
[34] D.E. Ferguson, Chemical Technology Division Annual Progress Report for Period Ending May 31, 1968, Oak Ridge National Laboratory, 1968.
[35] Mound Laboratory Isotopic Power Fuels Programs: January-March, 1967, Mound Laboratory, 1967.
[36] D.L. Plymale, W.H. Smith, The Preparation of Plutonium-238 Dioxide Microspheres by the Sol-Gel Process, Mound Laboratory, 1968.
[37] D.L. Prosser, SNAP-27 Radioisotopic Heat Source Summary Report, Mound Laboratory, 1969.
[38] J.A. Phillips, S.G. Nagley, E.L. Shaber, Nucl. Eng. Des. 251 (2012) 261.
[39] S.G. Nagley, C.M. Barnes, D.L. Husser, M.L. Nowlin, W.C. Richardson, (2010).
[40] C.M. Barnes, W.C. Richardson, D. Husser, M. Ebner, Fourth Int. Top. Meet. High Temp. React. Technol., American Society of Mechanical Engineers, 2008, pp. 177–188.
[41] J.A. Phillips, C.M. Barnes, J.D. Hunn, Proc. HTR 2010 (2010).
[42] J.L. Collins, Production of Depleted UO_2 Kernels for the Advanced Gas-Cooled Reactor Program for Use in TRISO Coating Development, Oak Ridge National Laboratory, 2004.
[43] J.L.C. Rodney D. Hunt, Radiochim. Acta - RADIOCHIM ACTA 92 (2004) 909.
[44] D. Knighton, Preliminary Operational Safety Report for the Task 5.6 Thermoelectric Generator, Martin Company, Baltimore, Maryland, 1960.
[45] Application of Nuclear Power Supplies to Space Systems, Sigma Corporation, 1960.

[46] High-Temperature Radioisotope Thermoelectric Generator for Space Applications, Radio Corporation of America, 1964.
[47] G.P. Dix, D. Knighton, Preliminary Operational Safety Report for the Task 5.6 Thermoelectric Generator, Martin Company, 1960.
[48] R.T. Carpenter, Astronaut. Aerosp. Eng. (1963) 68.
[49] USA. Department of Energy Ohio Field Office. Source Evaluation Board, SEB, Processes and Characteristics of Major Isotopes Handled at Mound, Monroe, OH, 2002.
[50] A.I. Hoffman, Transit RTG Program Report Number 1, TRW Systems Group, 1970.
[51] Mound Laboratory Isotopic Power Fuels Programs: January-March 1971, Mound Laboratory, 1971.
[52] T.K. Keenan, R.A. Kent, R.N.R. Mulford, Data Sheets for PMC Radioisotopic Fuel, Los Alamos Scientific Laboratory, 1972.
[53] E.W. Johnson, Multi-Hundred Watt Heat Source Technology-II, Mound Laboratory.
[54] Advanced Planetary Probe Study - Final Technical Report, Jet Propulsion Laboratory, 1966.
[55] L.B. Gnagey, R.E. Vallee, (1966).
[56] C.W. Whitmore, G. Drenker, E.W. Williams, Multi-Hundred Watt Radioisotope Thermoelectric Generator Program LES 8/9 Program MJS Program, General Electric Space Division, 1975.
[57] Multi-Hundred Watt Radioisotopic Thermoelectric Generator Program - Part I, General Electric Space Division, 1973.
[58] G.L. Bennett, J.J. Lombardo, R.J. Hemler, G. Silverman, C.W. Whitmore, W.R. Amos, E.W. Johnson, A. Schock, R.W. Zocher, T.K. Keenan, Proc. 4th Int. Energy Convers. Eng. Conf., 2006, pp. 26–29.
[59] W.J. Maraman, General-Purpose Heat Source Project, Space Nuclear Safety Program, and Radioisotopic Terrestrial Safety Program, Los Alamos Scientific Laboratory, 1979.
[60] E.C. Snow, R.W. Zocher, General-Purpose Heat Source Development Phase I - Design Requirements, Los Alamos Scientific Laboratory, 1978.
[61] R.J. Hemler, General Purpose Heat Source Task Group Final Report, General Electric, 1979.
[62] E.C. Snow, R.W. Zocher, I.M. Grinborg, L.E. Hulbert, General-Purpose Heat Source Development Phase II - Conceptual Designs, Los Alamos Scientific Laboratory, 1978.
[63] GPHS-RTGs In Support of the Cassini RTG Program - Final Technical Report, Lockheed Martin, 1998.
[64] G.L. Bennett, 4th Int. Energy Convers. Eng. Conf. Exhib. IECEC, 2006, pp. 26–29.
[65] D.F. Bickford, D.T. Rankin, Fabrication of Granule and Pellet Heat Sources from Oxalate-Based $^{238}PuO_2$, Savannah River Laboratory, 1975.
[66] D.H. Taylor, Report of Iridium/$^{238}PuO_2$ Compatibility Test, Savannah River Laboratory, 1983.
[67] D.F. Bickford, D.T. Rankin, P.K. Smith, Berkeley, CA, 1976.
[68] C.T. Liu, S.A. David, Weld Metal Grain Structure and Mechanical Properties of Iridium Alloy DOP-26, Oak Ridge National Laboratory, 1982.
[69] R. Bechtel, (2010).
[70] P.K. Smith, D.F. Bickford, D.T. Rankin, Mat Res Bull 12 (1977) 589.
[71] G.B. Ulrich, 12th Symposium on Space Nuclear Power and Propulsion, Albuquerque, NM, 1995.

[72] O.J. Wick, Plutonium Handbook, Gordon and Breach, New York, 1967.
[73] S.M. Thein, P.J. Bereolos, Thermal Stabilization of $^{233}UO_2$, $^{233}UO_3$, and $^{233}U_3O_8$, Oak Ridge National Laboratory, 2000.
[74] A.I.Y. Tok, F.Y.C. Boey, Z. Dong, X.L. Sun, J. Mater. Process. Technol. 190 (2007) 217.
[75] B. Djuričić, S. Pickering, J. Eur. Ceram. Soc. 19 (1999) 1925.
[76] Z. Guo, F. Du, Z. Cui, Mater. Chem. Phys. 113 (2009) 53.
[77] J.-G. Li, T. Ikegami, Y. Wang, T. Mori, J. Am. Ceram. Soc. 85 (2002) 2376.
[78] L. De Almeida, S. Grandjean, N. Vigier, F. Patisson, Eur J Inorg Chem 31 (2012) 4986.
[79] D.L. Clark, Los Alamos Sci. 26 (2000) 364.
[80] D.L. Clark, S.S. Hecker, G.D. Jarvinen, M.P. Neu, Chem. Actin. Trans. Elem., Springer, 2006, pp. 813–1264.
[81] F.J. Miner, J.R. Seed, Chem. Rev. 67 (1967) 299.
[82] L.L. Martella, M.T. Saba, G.K. Campbell, Laboratory-Scale Evaluations of Alternative Plutonium Precipitation Methods, Rockwell International, 1984.
[83] Savannah River Laboratory Monthly Report - ^{238}Pu Fuel Form Processes - October 1972, Savannah River Laboratory, 1972.
[84] P.E. Teaney, $^{238}PuO_2$ Fines Generation in Radioisotopic Heat Sources, Mound Laboratory, 1983.
[85] Savannah River Laboratory Monthly Report - ^{238}Pu Fuel Form Processes - November 1972, Savannah River Laboratory, 1972.
[86] G.A. Burney, J.W. Congdon, Direct Fabrication of $^{238}PuO_2$ Fuel Forms, Savannah River Laboratory, 1982.
[87] R.L. Folger, ^{238}Pu Fuel Form Processes Quarterly Report - January-March 1980, Savannah River Laboratory, n.d.
[88] R.L. Folger, ^{238}Pu Fuel Form Processes Quarterly Report - January-March 1981, Savannah River Laboratory, 1981.
[89] I. Grenthe, J. Drożdżyński, T. Fujino, E.C. Buck, T.E. Albrecht-Schmitt, S.F. Wolf, Chem. Actin. Trans. Elem., Springer, 2006, pp. 253–698.
[90] International Atomic Energy Agency, Significance of Mineralogy in the Development of Flowsheets for Processing Uranium Ores., International Atomic Energy Agency, Vienna, 1980.
[91] R. Gupta, V.M. Pandey, S.R. Pranesh, A.B. Chakravarty, Hydrometallurgy 71 (2004) 429.
[92] E.H.P. Cordfunke, J Inorg Nucl Chem 24 (1962) 303.
[93] P.C. Debets, B.O. Loopstra, J Inorg Nucl Chem 25 (1963) 945.
[94] E.V. Garner, J. Inorg. Nucl. Chem. 21 (1961) 380.
[95] J. Kašpar, P. Fornasiero, M. Graziani, Catal. Today 50 (1999) 285.
[96] M. Zinkevich, D. Djurovic, F. Aldinger, Solid State Ion. 177 (2006) 989.
[97] K. Eguchi, T. Setoguchi, T. Inoue, H. Arai, Solid State Ion. 52 (1992) 165.
[98] R. Chi, Z. Li, C. Peng, H. Gao, Z. Xu, Metall. Mater. Trans. B 37 (2006) 155.
[99] R.D. Abreu, C.A. Morais, Miner. Eng. 23 (2010) 536.
[100] M. Hirano, Y. Fukuda, H. Iwata, Y. Hotta, M. Inagaki, J. Am. Ceram. Soc. 83 (2000) 1287.
[101] M.J. Godinho, R.F. Gonçalves, L.P. S Santos, J.A. Varela, E. Longo, E.R. Leite, Mater. Lett. 61 (2007) 1904.

[102] M.Y. Cui, J.X. He, N.P. Lu, Y.Y. Zheng, W.J. Dong, W.H. Tang, B.Y. Chen, C.R. Li, Mater. Chem. Phys. 121 (2010) 314.
[103] Z. Guo, F. Du, G. Li, Z. Cui, Inorg. Chem. 45 (2006) 4167.
[104] F. Hrizi, H. Dhaouadi, F. Touati, Ceram. Int. 40 (2014) 25.
[105] K. Gao, Y.-Y. Zhu, D.-Q. Tong, L. Tian, Z.-H. Wang, X.-Z. Wang, Chin. Chem. Lett. (2013).
[106] H.P. Nawada, P. Sriramamurti, K.V. Govindan Kutty, S. Rajagopalan, R.B. Yadav, P.R. Vasudeva Rao, C.K. Mathews, J. Nucl. Mater. 139 (1986) 19.
[107] H.S. Kim, C.Y. Joung, B.H. Lee, J.Y. Oh, Y.H. Koo, P. Heimgartner, J. Nucl. Mater. 378 (2008) 98.
[108] J.C. Marra, A.D. Cozzi, R.A. Pierce, J.M. Pareizs, Cerium as a Surrogate in the Plutonium Immobilized Form.pdf, Westinghouse Savannah River Company, 2001.
[109] J.A.D. Stockdale, W.D. Bostick, D.P. Hoffman, H.T. Lee, Surrogate Formulations for Thermal Treatment of Low-Level Mixed Waste, Part I: Radiological Surrogates, Oak Ridge National Laboratory, 1994.
[110] C. Shapiro, K. Garcia, J. Beller, in:, Baltimore, Maryland, 1993, pp. 10.3.1–10.3.16.
[111] A. Raraz, B. Mishra, W.A. Averill, Application of Surrogate Materials in Process Study of Actinides, Rocky Flats Plant, 1993.
[112] I.S. Golovnin, At. Energy 89 (2000) 627.
[113] D.G. Kolman, Y. Park, M. Stan, R.J. Hanrahan, D.P. Butt, An Assessment of the Validity of Cerium Oxide as a Surrogate for Plutonium Oxide Gallium Removal Studies, Los Alamos National Laboratory, Los Alamos, NM, LA-UR-99-491, 1999.
[114] S. Rossignol, Y. Madier, D. Duprez, Catal. Today 50 (1999) 261.
[115] C. Laberty-Robert, J.W. Long, E.M. Lucas, K.A. Pettigrew, R.M. Stroud, M.S. Doescher, D.R. Rolison, Chem. Mater. 18 (2006) 50.
[116] P.S. W. Huang, Solid State Ion. 100 (1997) 23.
[117] A. Trovarelli, Catal. Rev.-Sci. Eng. 38 (1996) 439.
[118] J.A. Montoya, E. Romero-Pascual, C. Gimon, P. Del Angel, A. Monzón, Catal. Today 63 (2000) 71.
[119] C.E. Hori, H. Permana, K.Y.S. Ng, A. Brenner, K. More, K.M. Rahmoeller, D. Belton, Appl. Catal. B Environ. 16 (1998) 105.
[120] M. Thammachart, V. Meeyoo, T. Risksomboon, S. Osuwan, Catal. Today 68 (2001) 53.
[121] M. Alifanti, B. Baps, N. Blangenois, J. Naud, P. Grange, B. Delmon, Chem. Mater. 15 (2003) 395.
[122] T.L. Metroke, R.L. Parkhill, E.T. Knobbe, Prog. Org. Coat. 41 (2001) 233.
[123] R. Di Maggio, L. Fedrizzi, S. Rossi, P. Scardi, Thin Solid Films 286 (1996) 127.
[124] R.L. Nelson, J.D.F. Ramsay, J.L. Woodhead, J.A. Cairns, J.A.A. Crossley, Thin Solid Films 81 (1981) 329.
[125] L.S. Kasten, J.T. Grant, N. Grebasch, N. Voevodin, F.E. Arnold, M.S. Donley, Surf. Coat. Technol. 140 (2001) 11.
[126] F. Czerwinski, J.A. Szpunar, J. Sol-Gel Sci. Technol. 9 (1997) 103.
[127] T. Adschiri, K. Kanazawa, K. Arai, J. Am. Ceram. Soc. 75 (1992) 1019.
[128] Y. Hakuta, S. Onai, H. Terayama, T. Adschiri, K. Arai, J. Mater. Sci. Lett. 17 (1998) 1211.
[129] C. Tyrsted, K.M. Ørnsbjerg Jensen, E.D. Bøjesen, N. Lock, M. Christensen, S.J.L. Billinge, B. Brummerstedt Iversen, Angew. Chem. Int. Ed. 51 (2012) 9030.

[130] M. Hirano, E. Kato, J. Am. Ceram. Soc. 82 (1999) 786.
[131] P.-L. Chen, I.-W. Chen, J. Am. Ceram. Soc. 76 (1993) 1577.
[132] H.I. Chen, H.Y. Chang, Solid State Commun. 133 (2005) 593.
[133] M. Hirano, E. Kato, J. Am. Ceram. Soc. 79 (1996) 777.
[134] K. Kaneko, K. Inoke, B. Freitag, A.B. Hungria, P.A. Midgley, T.W. Hansen, J. Zhang, S. Ohara, T. Adschiri, Nano Lett. 7 (2007) 421.
[135] J.S. Lee, S.-C. Choi, Mater. Lett. 58 (2004) 390.
[136] N.-C. Wu, E.-W. Shi, Y.-Q. Zheng, W.-J. Li, J. Am. Ceram. Soc. 85 (2002) 2462.
[137] H. Wang, J.-J. Zhu, J.-M. Zhu, X.-H. Liao, S. Xu, T. Ding, H.-Y. Chen, Phys. Chem. Chem. Phys. 4 (2002) 3794.
[138] M.L. Dos Santos, R.C. Lima, C.S. Riccardi, R.L. Tranquilin, P.R. Bueno, J.A. Varela, E. Longo, Mater. Lett. 62 (2008) 4509.
[139] A. Bonamartini Corradi, F. Bondioli, A.M. Ferrari, T. Manfredini, Mater. Res. Bull. 41 (2006) 38.
[140] A.J. Hill, 200 Area Technical Manual - Part SP - Processing of Np-237 and Pu-238, Savannah River Laboratory, 1961.
[141] W.L. Poe, A.W. Joyce, R.I. Martens, Ind. Eng. Chem. Process Des. Dev. 3 (1964) 314.
[142] G.A. Burney, Winter Meeting of the American Nuclear Society, San Francisco, CA, 1983.
[143] C.H. Bloomster, Neptunium Target Element Fabrication, Pacific Northwest Laboratories, 1967.
[144] D.T. Rankin, W.R. Kanne Jr, M.R. Louthan Jr, D.F. Bickford, J.W. Congdon, Prep. US Dep. Energy Contract No -ACO9-96SR18500 Westinghouse Savannah River Co. Savannah River Site Aiken SC 29808 (2000) 179.
[145] A.J. Hill, Processing of Np-237 and Pu-238, Savannah River Laboratory, 1961.
[146] T. Todd, R. Herbst, B. Mincher, S. Frank, J. Law, J. Swanson, in:, 2006.
[147] M.E. Pansoy-Hjelvik, M. Reimus, G. Silver, M.L. Remerowski, A. Ecclesine, G. Alletzhauser, J. Brock, J. Nixon, P. Moniz, K.B. Ramsey, L. Foltyn, G. Jarvinen, G. Purdy, Albuquerque, NM, 2001.
[148] C.B. Chadwell, T.C. Elswick, Neutron Emission Rate Reduction in PuO_2 by Oxygen Exchange, Mound Laboratory, 1971.
[149] D.L. Plymale, The Exchange of Isotopiccally Enriched Oxygen with $^{238}PuO_2$ Sol-Gel Microspheres, Mound Laboratory, 1968.
[150] Savannah River Laboratory Monthly Report - ^{238}Pu Fuel Form Processes - April 1974, Savannah River Laboratory, 1974.
[151] W.J. McDowell, F.G. Seeley, M.T. Ryan, Penetration of HEPA Filters by Alpha Recoil Aerosols, Oak Ridge National Laboratory, 1976.
[152] W.R. Harris, B.R. Kokenge, G.C. Marsh, Decommissioning of the Special Metallurgical Building at Mound Laboratory, Mound Laboratory, 1974.
[153] M.T. Sautman, D.L. Burnfield, (2010).
[154] R.J. Grimm, FAMS Decommissioning End-State Alternative Evaluation, Savannah River Company, 2006.
[155] P.S. Winokur, Recommendation 2012-1 to the Secretary of Energy - Savannah River Site Building 235-F Safety, (2012).
[156] P.A. Haas, S.D. Clinton, A.T. Kleinsteuber, Can. J. Chem. Eng. (1966).

[157] E.H. Dewell, Gel-Addition Process Chemical Studies - Quarterly Progress Report No. 9, Babcock & Wilcox, 1969.
[158] Mound Laboratory Isotopic Power Fuels Programs: October-December 1966, Mound Laboratory, 1967.
[159] B.C. Finney, P.A. Haas, Sol-Gel Process - Engineering-Scale Demonstration of the Preparation of High-Density UO2 Microspheres, Oak Ridge National Laboratory, 1972.
[160] Mound Laboratory Isotopic Power Fuels Programs: April-June 1967, Mound Laboratory, 1967.
[161] A.C. Merrington, E.G. Richardson, Proceeedings Phys. Soc. 59 (1947).
[162] J.B.W. Kanij, A.J. Noothout, O. Votocek, Proc. Panel Sol-Gel Process Fuel Fabr., International Atomic Energy Agency, Vienna, 1973.
[163] P.A. Haas, Am. Inst. Chem. Eng. 21 (1975) 383.
[164] P.A. Haas, Ind. Eng. Chem. Res. 31 (1992) 959.
[165] N. Kumar, R.K. Sharma, V.R. Ganatra, S.K. Mukerjee, V.N. Vaidya, D.D. Sood, Nucl. Technol. 96 (1991) 169.
[166] V.R. Ganatra, N. Kumar, S. Suryanarayana, Y.R. Bamankar, N. Reghu, V.N. Vaidya, S.K. Mukerjee, J. Radioanal. Nucl. Chem. 275 (2008) 515.
[167] C. Ganguly, Bull. Mater. Sci. 16 (1993) 509.
[168] Fuel Chemistry Division Progress Report for 1988, Bhabha Atomic Research Institute, 1988.
[169] R.V. Pai, S.. Mukerjee, V.. Vaidya, J. Nucl. Mater. 325 (2004) 159.
[170] V.N. Vaidya, S.K. Mukherjee, J.K. Joshi, R.V. Kamat, D.D. Sood, J. Nucl. Mater. 148 (1987) 324.
[171] S. Suryanarayana, N. Kumar, Y.R. Bamankar, V.N. Vaidya, D.D. Sood, J. Nucl. Mater. 230 (1996) 140.
[172] R.V. Pai, J.V. Dehadraya, S. Bhattacharya, S.K. Gupta, S.K. Mukerjee, J. Nucl. Mater. 381 (2008) 249.
[173] K. Verfondern, H. Nabielek, J.M. Kendall, Nucl. Eng. Technol. 39 (2007) 603.
[174] R.G. Wymer, Chemical Technology Division Progress Report for the Period April 1, 1983, to March 31, 1985, Oak Ridge National Laboratory, 1985.
[175] E. Zimmer, C. Ganguly, J. Borchardt, H. Langen, J. Nucl. Mater. 152 (1988) 169.
[176] J.L. Collins, M.H. Lloyd, S.E. Shell, Control of Urania Crystallite Size by HMTA-Urea Reactions in the Internal Gelation Process for Preparing (U, Pu)O_2 Fuel Kernels, Oak Ridge National Laboratory, 2005.
[177] J.L. Collins, M.H. Lloyd, R.L. Fellows, Effects of Process Variables on Reaction Mechanisms Responsible for ADUN Hydrolysis, Precipitation, and Gelation in the Internal Gelation Gel-Sphere Process, Oak Ridge National Laboratory, 1984.
[178] V.N. Vaidya, J. Sol-Gel Sci. Technol. 46 (2008) 369.
[179] N. Kumar, R.V. Pai, J.K. Joshi, S.K. Mukerjee, V.N. Vaidya, V. Venugopal, J. Nucl. Mater. 359 (2006) 69.
[180] J.L. Collins, A. Chi, Determination of Ideal Broth Formulations Needed to Prepare Hydrous Cerium Oxide Microspheres Via the Internal Gelation Process, Oak Ridge National Laboratory, 2009.
[181] G. Benay, F. Hubert, G. Modolo, Radiochim. Acta 96 (2008).
[182] T. Arima, K. Idemitsu, K. Yamahira, S. Torikai, Y. Inagaki, J. Alloys Compd. 394 (2005) 271.

[183] K. Idemitsu, T. Arima, Y. Inagaki, S. Torikai, M.A. Pouchon, J. Nucl. Mater. 319 (2003) 31.
[184] J.L. Collins, J.S. Watson, Economic Evaluation for the Production of Sorbents and Catalysts Derived from Hydrous Titanium Oxide Microspheres Prepared by the HMTA Internal Gelation Process, Oak Ridge National Laboratory, 2000.
[185] J.L. Collins, Experimental Methodology for Determining Optimum Process Parameters for Production of Hydrous Metal Oxides by Internal Gelation, Oak Ridge National Laboratory, 2005.
[186] F.W. v. d. Brugghen, A.J. Noothout, M.E.A. Hermans, J.B.W. Kanij, O. Votocek, in:, Sol-Gel Process. React. Fuel Cycles, Oak Ridge National Laboratory, Gatlinburg, Tennessee, 1970.
[187] M.H.L. J. L. Collins, R.L. Fellows, Radiochim. Acta 42 (1987) 121.
[188] P.A. Haas, J.M. Begovich, A.D. Ryon, J.S. Vavruska, Ind. Eng. Chem. Prod. Res. Dev. 19 (1980) 459.
[189] C.M. King, R. Bruce King, A. Ronald Garber, M.C. Thompson, B.R. Buchanan, MRS Online Proc. Libr. 180 (1990) null.
[190] R.C. Warner, J Biol Chem 142 (1942) 705.
[191] E.H.P. Cordfunke, J Inorg Nucl Chem 34 (1972) 531.
[192] M.H. Lloyd, K. Bischoff, K. Peng, H.-U. Nissen, R. Wessicken, J. Inorg. Nucl. Chem. 38 (1976) 1141.
[193] R.D. Hunt, F.C. Montgomery, J.L. Collins, J. Nucl. Mater. 405 (2010) 160.
[194] V. Baran, K. Štamberg, M. Tympl, J. Kinzelová, J. Nucl. Mater. 58 (1975) 59.
[195] A. Kumar, J. Radhakrishna, N. Kumar, R.V. Pai, J.V. Dehadrai, A.C. Deb, S.K. Mukerjee, J. Nucl. Mater. 434 (2013) 162.
[196] K. Suresh Kumar, H.. Nawada, N.. Bhat, J. Nucl. Mater. 321 (2003) 263.
[197] M.C. Burrell, D.A. Lee, Analysis of UO_3 Gel Microsphere Decomposition Products by Mass Spectrometry, Dept. of Energy, Oak Ridge National Laboratory, 1979.
[198] K.S. Kumar, N.. Bhat, Spectrochim. Acta. A. Mol. Biomol. Spectrosc. 60 (2004) 513.
[199] J. Wegener, Production of Cerium Oxide Microspheres by an Internal Gelation Sol-Gel Process, Master of Science, Texas A&M, 2008.
[200] P.C. Stevenson, W.E. Nervik, The Radiochemistry of the Rare Earths, Scandium, Yttrium, and Actinium, National Academy of Sciences National Research Council Nuclear Series, Livermore, CA, 1961.
[201] C. Serra, N. Berton, M. Bouquey, L. Prat, G. Hadziioannou, Langmuir 23 (2007) 7745.
[202] P.B. Umbanhowar, V. Prasad, D.A. Weitz, Langmuir 16 (2000) 347.
[203] J.I. Langford, A.J.C. Wilson, J. Appl. Crystallogr. 11 (1978) 102.
[204] S.E. Stein, Mass Spectra, NIST Mass Spec Data Center, National Institute of Standards and Technology.
[205] J.E. Selle, J.J. English, P.E. Teaney, J.R. McDougal, The Compatibility of $^{238}PuO_2$ with Various Refractory Metals and Alloys: Interim Report, Mound Laboratory, 1970.
[206] E.M. Cramer, Performance of Multihundred-Watt-Fueled Sphere Assemblies in the Safety Verification Test, Los Alamos Scientific Laboratory, 1976.
[207] Multi-Hundred Watt Radioisotope Thermoelectric Generator Program - 1976-1977 Annual Report/Final Report for the Voyager Program, General Electric, 1977.
[208] C.T. Liu, H. Inouye, Development and Characterization of an Improved Ir-0.3% W Alloy for Space Radioisotopic Heat Sources, Oak Ridge National Laboratory, 1977.

[209] C.G. McKamey, E.H. Lee, G.B. Ulrich, J.L. Wright, E.P. George, Grain Growth Behavior of DOP-26 Iridium Clad Vent Set Cups Used in Radioisotope Thermoelectric Generators, Oak Ridge National Laboratory, 2002.
[210] C.L. White, R.E. Clausing, L. Heatherly, Metall. Trans. A 10A (1979) 683.
[211] C.T. Liu, H. Inouye, A.C. Schaffhauser, Metall. Trans. A 12A (1981) 993.
[212] C.L. White, C.T. Liu, Acta Metall. 29 (1981) 301.
[213] L.D. Schulte, J.M. Espinoza, K.B. Ramsey, G.H. Rinehart, G.L. Silver, G.M. Purdy, G.D. Jarvinen, in:, Space Technol. Appl. Int. Forum, Albuquerque, NM, 1998.
[214] T.K. Keenan, R.A. Kent, R.N.R. Mulford, M.W. Shupe, Data Sheets for PPO Radioisotopic Fuel, Los Alamos Scientific Laboratory, 1973.
[215] G.H. Rinehart, Lightweight Radioisotope Heater Unit (LWRHU) Production for the Cassini Mission, Los Alamos National Laboratory, 1996.
[216] R.L. Deaton, C.J. Wiedenheft, Preparation of UO_2 and $^{238}PuO_2$ Fuel Pellets for a Small Heat Source, Oak Ridge National Laboratory, 1974.
[217] Materials Safety Data Sheet - Cyanuric Acid.
[218] J.P. Chen, K. Isa, J Mass Spectrom Soc Jpn 46 (1998) 299.
[219] T. Nakagawa, H. Matsuoka, M. Sawa, M. Hirota, M. Miyake, M. Katsura, J. Nucl. Mater. 247 (1997) 127.
[220] V.N. Fokin, E.E. Fokina, B.P. Tarasov, Russ. J. Inorg. Chem. 55 (2010) 1536.
[221] V.N. Fokin, E.E. Fokina, B.P. Tarasov, I.I. Korobov, S.P. Shilkin, in:, Ukraine, 2001, pp. 314–315.
[222] D.E. Peterson, R.N.R. Mulford, Analysis of Carbon Monoxide Production in Multihundred-Watt Heat Sources, Los Alamos Scientific Laboratory, 1976.
[223] E.W. Johnson, The Behavior of Oxygen Partial Pressure Over Slightly Substoichiometric Plutonia at 1410 K, Mound Laboratory, 1982.
[224] T. Howe, R.C. O'Brien, C.M. Stoots, The Woodlands, Texas, 2012.
[225] A.S. Utada, L.-Y. Chu, A. Fernandez-Nieves, D.R. Link, C. Holtze, D.A. Weitz, Mrs Bull. 32 (2007) 702.
[226] C. Clanet, J.C. Lasheras, J. Fluid Mech. 383 (1999) 307.
[227] B. Ambravaneswaran, S.D. Phillips, O.A. Basaran, Phys. Rev. Lett. 85 (2000).
[228] B. Ambravaneswaran, H. Subramani, S. Phillips, O. Basaran, Phys. Rev. Lett. 93 (2004).
[229] C. Cramer, P. Fischer, E.J. Windhab, Chem. Eng. Sci. 59 (2004) 3045.
[230] R.L. Folger, ^{238}Pu Fuel Form Processes Bimonthly Report - May/June 1979, Savannah River Laboratory, 1980.
[231] G.T. Seaborg, The Transuranium Elements, 1st Edition, Yale University, 1958.
[232] B.R. Munson, D.F. Young, T.H. Okiishi, Fundamentals of Fluid Mechanics, 5th Edition, Wiley, 2006.
[233] Silicone Fluid KF-96 Performance Test Results, (2012).
[234] J.N. Lee, C. Park, G.M. Whitesides, Anal. Chem. 75 (2003) 6544.